A Genetic Algorithm Approach for Three-Phase Harmonic Mitigation Filter Design

Zubi, Hazem

Award date:
2013

Awarding institution:
University of Bath

A Genetic Algorithm Approach for Three-Phase Harmonic Mitigation Filter Design

Hazem M. Zubi

A thesis submitted for the degree of Doctor of Philosophy

University of Bath

Department of Electronic and Electrical Engineering

February 2013

Abstract

In industry, adjustable speed drives (ASDs) are widely employed in driving AC motors for variable speed applications due to the high performance and high energy efficiency obtained in such systems. However, ASDs have an impact on the power quality and utilisation of AC power feeds by injecting current harmonics and causing resonances, additional losses, and voltage distortion at the point of common coupling. Due to these problems, electric power utilities have established stringent rules and regulations to limit the effects of this distortion. As a result, efficient, reliable, and economical harmonic mitigation techniques must now be implemented in practical systems to achieve compliance at reasonable cost.

A variety of techniques exist to control the harmonic current injected by ASDs, and allow three-phase AC-line-connected medium-power systems to meet stringent power quality standards. Of these, the broadband harmonic passive filter deserves special attention because of its good harmonic mitigation and reactive power compensation abilities, and low cost. It is also relatively free from harmonic resonance problems, has relatively simple structural complexity and involves considerably less engineering effort when compared to systems of single tuned shunt passive filters or active filters and active rectifier solutions.

In this thesis, passive broadband harmonic filters are investigated. In particular, the improved broadband filter (IBF) which has superior overall performance and examples of its application are increasing rapidly. During this research project, the IBF operating principle is reviewed and its design principles are established. As the main disadvantage of most passive harmonic filters is the large-sized components, the first proposed design attempts to optimize the size of the filter components (L and C) utilized in the existing IBF topology. The second proposed design attempts to optimize the number and then the size of filter components resulting in an Advanced Broadband passive Filter (ABF) novel structure.

The proposed design methods are based on frequency domain modelling of the system and then using a genetic algorithm optimization technique to search for

optimal filter component values. The results obtained are compared with the results of a linear searching approach.

The measured performance of the optimal filter designs (IBF and ABF) is evaluated under different loading conditions with typical levels of background voltage distortion. This involves assessing input current total harmonic distortion, input power factor, rectifier voltage regulation, efficiency, size and cost. The potential resonance problem is addressed and the influence of voltage imbalance on performance is investigated. The assessment is based on analysis, computer simulations and experimental results. The measured performance is compared to various typical passive harmonic filters for three-phase diode rectifier front-end type adjustable speed drives.

Finally, the broadband filter design's effectiveness and performance are evaluated by involving them in a standard IEEE distribution network operating under different penetration levels of connected nonlinear total loads (ASD system). The study is conducted via detailed modelling of the distribution network and the linked nonlinear loads using computer simulations.

To my parents,

who always support me in all aspects of my life

to my wife

for her patience and support in my study

to my children

for their sacrifice

and

to our new beloved home country

Libya

Acknowledgements

First of all, I would like to thank the almighty ALLAH for his mercy, endless support and grace, which enabled me to complete this work.

I would like to thank Dr. Rod Dunn, Prof. Raj Aggrawal and Dr. Francis Robinson for their support and guidance throughout this thesis.

I am grateful to Mr Andy Matthews, Mr Neil Deacon and Mr Michael Thomas the EE department technicians for their assistance on the experimental part of this work.

I am also grateful to my colleague Mr Tony Gee and all other friends in University of Bath for all the help they gave me throughout my study.

Finally I would like to dedicate this work to my parents, my father Mohamed and my mother Afaf for their encouragements throughout my education life, and to my wife Nahla for her support and sacrifice, and my children Malak, Basma, Lujayn and Mohamed for their patience during my study. Their love, care and encouragement has given me a great inner strength to success.

The Libyan secretariat of higher education is highly appreciated for its financial support during my study period. I am also grateful to the culture affairs supervisors in the Libyan embassy in London for their help.

Declaration

This research draws upon the author's earlier work at MSc level presented in 2005. The previous study has been extended, updated and used to explore new designing methods and structures for an improved broadband passive filter to be utilized in harmonic mitigation for 6-pulse diode rectifier front end applications. Furthermore, results from the former study have been used for a full comparative investigation with the original outcomes of this work.

The updated literature review is presented in chapter one and the basis material describing filter operating concepts and modelling analysis are introduced in chapter two. The rest of the thesis, however, is devoted to the expansion of the original work and new material.

Contents

List of Figures

List of Tables

List of Abbreviations

ABF	Advanced Broadband Filter
AI	Artificial Intelligence
ANN	Artificial Neural Network
ASD	Adjustable Speed Drives
CSI	Current Source Inverter
DSP	Displacement Power Factor
ΔV_o	Voltage Regulation
ES	Expert System
GA	Genetic Algorithm
IBF	Improved Broadband Filter
PCC	Point of Common Coupling
PF	Power Factor
PWM	Pulse Width Modulation
SA	Simulated Annealing
SCR	Short Circuit Ratio
STSF	Single Tuned Shunt Filter
TDD	Total Demand Distortion
THDi	Total Harmonic Distortion
THD_V	Total Harmonic Voltage Distortion
UPS	Uninterruptible Power Supplies
VSI	Voltage Source Inverter

List of Symbols

α	the line current no-load to full-load ratio
β_1	fundamental stiffness factor
C_{dc}	DC-link capacitor
C_f	filter capacitor
f_p	parallel resonant frequency
f_s	series resonant frequency
φ	displacement angle between the fundamental line-voltage and line-current components
I	rms total value of the line current
I_{dc}	mean value of the full-load DC-link current
I_{f1}	rms value of the full-load shunt filter current fundamental component
I_h	rms value of the line-current harmonic components
I_L	rated demand of the fundamental current component
I_n	harmonic current of the order n
I_{NL}	rms value of the no-load fundamental component line current
I_R	full-load fundamental frequency current value
I_{Rect1}	rms value of the rectifier current fundamental component
I_{sc}	short circuit current at the nonlinear load input
I_1	rms value of the fundamental current component
L_{ac}	AC line reactor
L_{dc}	DC-link inductor
L_f	filter reactor
L_i	input reactor
L_L	load inductor
L_o	output reactor
L_s	source reactor
P_{dc}	rated DC output power
P_R	rated line power
R_d	damping resistor
R_L	load resistor
R_s	source resistor
V_{dc}	mean value of the full-load DC output voltage

V_{LL}	rms value of the line-to-line supply voltage
V_{LR}	rated line-to-line voltage
V_n	harmonic voltage of the order n
$V_{O\text{-}FL}$	full-load rms value of the filter fundamental component output voltage
$V_{O\text{-}NL}$	no-load rms value of the filter fundamental component output voltage
V_P (FL)	rms value of the full-load node voltage fundamental component
V_P (NL)	rms value of the no-load node voltage fundamental component
Vs	AC supply voltage
V_1	rms value of the rated utility phase voltage fundamental component
ω_e	line radial frequency
ω_p	parallel resonance value in rad/sec
ω_s	series resonance value in rad/sec
Z_f	shunt filter impedance at fundamental frequency
Z_i	input impedance at fundamental frequency
Z_L	Total load side impedance as seen from the AC line side
Z_n	harmonic impedance of the order n
Z_T	Total input impedance as seen from the AC line side

1 INTRODUCTION AND LITERATURE REVIEW

1.1 Introduction

The growing importance of power electronics in saving energy of electrical apparatus by more efficient use of electricity has been clearly visible. For instance, the application of cost effective AC/DC and DC/AC power converter circuits is common in all industry. They enhance the overall performance, efficiency, and reliability of industrial processes. These power converter circuits are widely used in single and three-phase diode/thyristor rectifiers, for DC power supplies, Adjustable Speed Drives (ASD), Uninterruptible Power Supplies (UPS), and for household and industrial appliances [1]. It has been estimated that roughly 15% – 20% of electricity consumption can be saved by extensive application of power electronics. According to Electric Power Research Institute (EPRI) estimate, 60% – 65% of generated electricity in the USA and Europe is consumed in motor drives, and majority of these drives are for pumps and fan [2, 3],[4],[5]. Fig. 1.1 shows the estimated industrial motor use by application worldwide [6]. As variable speed drives reduce energy consumption and decrease pollutant emission levels to environment while increasing productivity, their proliferation is inevitable. A recent study by the European Copper Institute showed that an electricity saving potential of some 200 billion KWh/year exists. This translates into a reduction of 100 million tons of CO2 emissions from industries in the European Union. Around the world it is roughly estimated that 3.2% of the world's electricity total generation (approx. 500 billion KWh) can be saved and 250-420 million tons of CO2 emissions can be avoided [7].

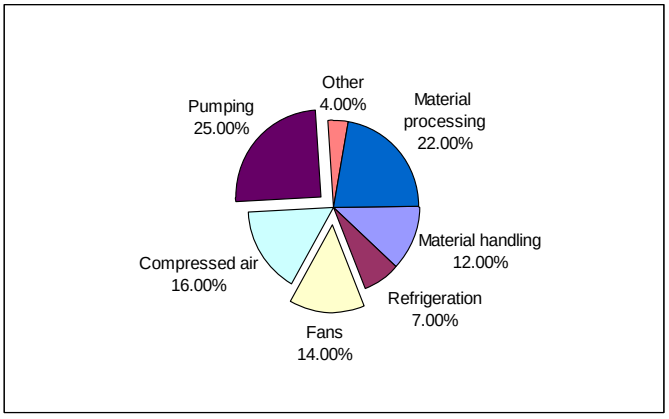

Fig. 1.1 Estimated industrial motor use by application worldwide; taken from [6].

For variable speed applications, ASDs are widely employed in driving induction and permanent magnet motors due to the high static and dynamic performance obtained in such systems. Low starting torque, high energy efficiency and high motion quality, low maintenance and moderate initial cost, etc. are the positive attributes of the ASDs. Consequently, the world market for ASDs had grown and is still growing rapidly (10% per year for AC drives) [8] . Table 1.1 shows numbers from different markets of development in adjustable speed drives. In the last 15 years the market has doubled (in value) with approximately 10% annual growth each 7th year [7].

Table 1.1 World market development in adjustable speed drives (Billion Euros) for lower voltage up to 160kW; taken from [7]

Market	1991 Billion €s	2002 Billion €s	Annual growth % (approximate)
Europe	0.44	1.08	7.7%
North America	0.40	0.72	5.0%
Japan	0.49	0.73	3.4%
Rest of world	0.27	0.96	11.1%
Total	**1.60**	**3.49**	**6.7%**

The power converters utilized in ASDs are AC/DC converter (rectifier) connected to DC/AC inverter. Until the beginning of the 21st century the DC/AC inverter has been shifting between Current Source Inverters (CSIs) and Voltage Source Inverters (VSIs). Of all the modern power electronics converters, the Voltage Source Inverter (VSI) is perhaps the most widely utilized DC/AC conversion topology with commonly used Pulse Width Modulation (PWM) methods [9].

The PWM-VSI comprises six power semiconductor switches with anti-parallel freewheel diodes. It converts a fixed DC voltage to three-phase AC voltages with controllable frequency (speed) and magnitude. Typically, a rectifier bridge transforms the AC three-phase line supply voltages to DC voltage in the AC motor drive applications. To control the motor shaft speed/position/torque, the VSI interfaces the DC source with the AC motor. Usually, the rectifier DC voltage is connected to a capacitive filter with/without DC-link reactor. As a consequence of the familiar advantages of the 6-pulse diode rectifier (low cost, robustness, high

energy efficiency and consistency), it is still the most used front-end topology for ASDs. Fig. 1.2 and Fig. 1.3 show the main configuration of PWM-VSI drive with a 6-pulse diode rectifier front end excluding or including the DC-link reactor, respectively.

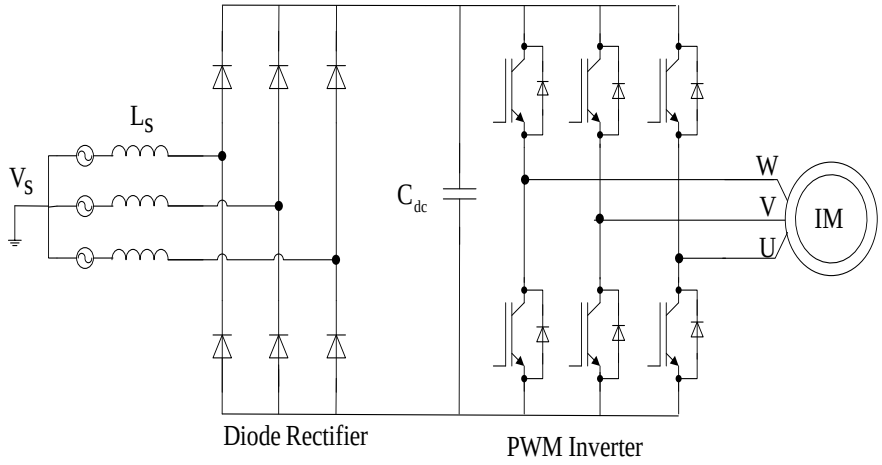

Fig. 1.2 The main configuration of PWM-VSI diode bridge rectifier front-end AC drive excluding DC-link reactor.

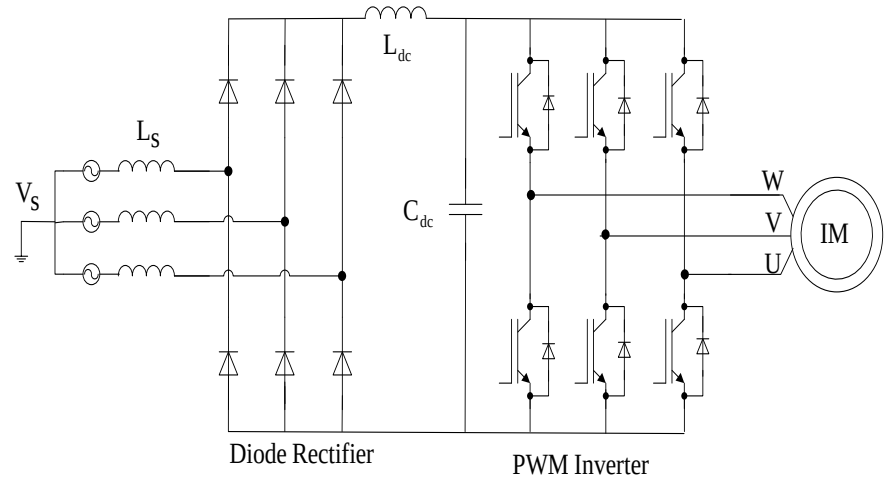

Fig. 1.3 The main configuration of PWM-VSI diode bridge rectifier front-end AC drive including DC-link reactor.

With sinusoidal supply voltages, the line commutated diode bridge rectifiers exhibit nonlinear load characteristics and draw distorted (non-sinusoidal) currents. Fig. 1.4 illustrates the typical waveform of the input line current and Fig. 1.5 shows the corresponding harmonic spectrum. Generated current harmonics have an order of

2p±1, where p is the number of pulses in the rectifier output DC voltage. The first dominant four harmonics are (5^{th}, 7^{th}, 11^{th} and 13^{th}), as shown in the harmonic spectrum (Fig. 1.5).

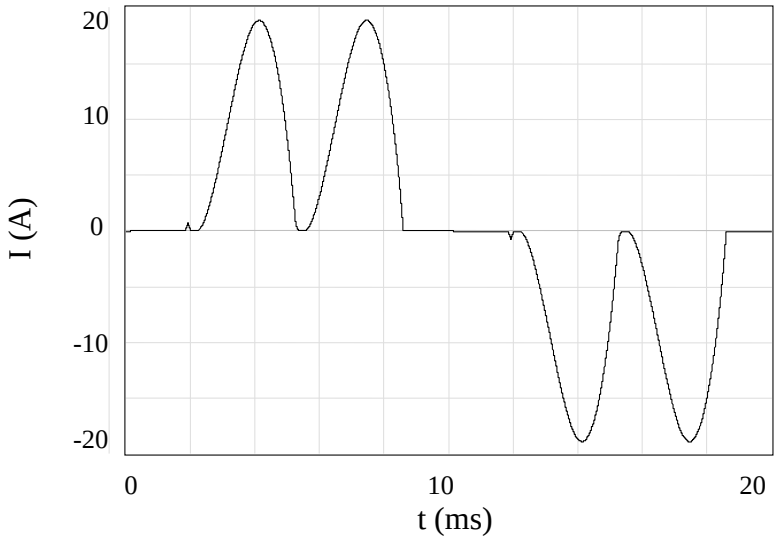

Fig. 1.4 Diode bridge rectifier front-end ASD system: Line current waveform.

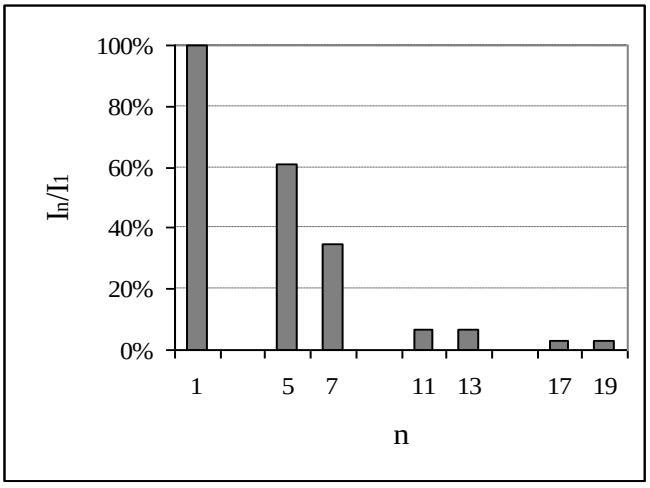

Fig. 1.5 Diode bridge rectifier front-end ASD system: Line current harmonic spectrum.

Due to the wide spread connection of such nonlinear systems in industrial distribution networks , the previously identified harmonic currents pollute the supply systems and, consequently, increase the harmonic voltage level within the networks, as shown in Fig. 1.6 [10].

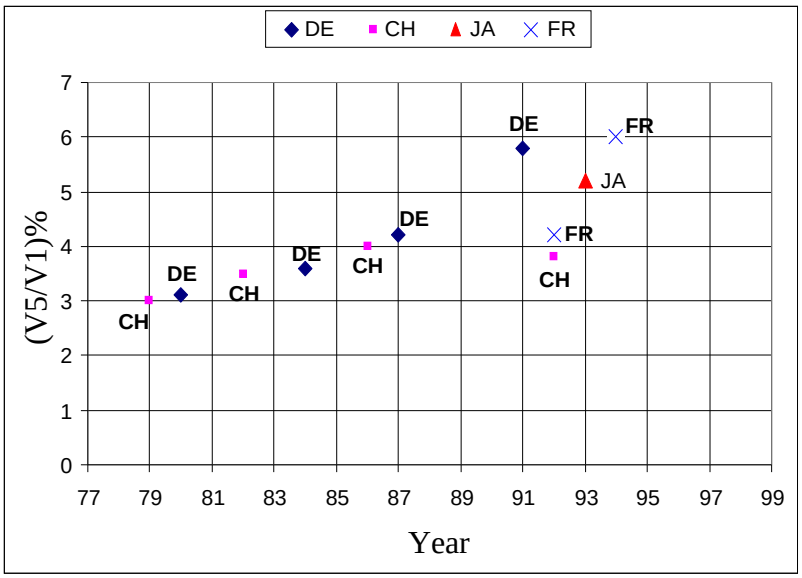

Fig. 1.6 Increase of the 5th harmonic voltage levels since 1979 measured in Germany (DE), Switzerland (CH), Japan (JA) and France (FR); taken from [10].

There are other nonlinear loads that inject harmonic currents to the feeding distribution networks. Nevertheless, compared to the full bridge diode rectifier, these harmonic sources load systems have a limited impact on the overall electrical power system. These harmonic sources are:

1. Arc furnaces.
2. Saturated magnetic devices, such as transformers.
3. Rotating machines.
4. Controlled rectifiers (e.g. thyristor 6-pulse rectifiers).

In practice, a voltage drop occurs in the supply impedance as the generated harmonic currents circulate and flow from the non-linear load to the supply system. As shown in Fig. 1.6, this harmonic voltage drop results in a distorted supply sine waveform voltage that increases its harmonic voltage content. The harmonic voltage (V_n) of the order n can be defined by:

$$V_n = Z_n \times I_n \tag{1.1}$$

where Z_n is harmonic impedance of the order n and I_n is the injected harmonic current of the order n.

Actually, the harmonic impedance itself is frequency dependent in a non-linear manner. Additionally, estimating the harmonic current generated by the diode bridge rectifier simple topology is a complicated task. This is due to the effect of various practical factors that may affect the current harmonic generation values (line impedance, operating loading conditions, DC-link filtering passive elements values and any utilized AC line reactors). Of these common factors, the substantial influence is usually caused by the line impedance. Less harmonic current distortion can be tolerated with large line impedance while higher harmonic currents can be allowed to appear in the line with low line impedance. On the other hand, high harmonic voltage distortion is usually encountered by the large line impedance. Moreover, the harmonic current distortion of the diode rectifier can also be affected by supply voltage pre-distortion and/or unbalance. This feature adds to the complexity of the harmonic distortion prediction of generated by the diode bridge rectifier.

Various undesirable effects on the power system distribution networks and their components can result from the injected current harmonics and the increased harmonic voltage levels problem. In addition, these side-effects can disturb other linear and nonlinear loads connected to the same Point of Common Coupling (PCC), shown in Fig.1.7. The PCC is a point where the voltage harmonic levels are usually determined and assessed to monitor the harmonic distortion and protect other existing customers connected at same feeder.

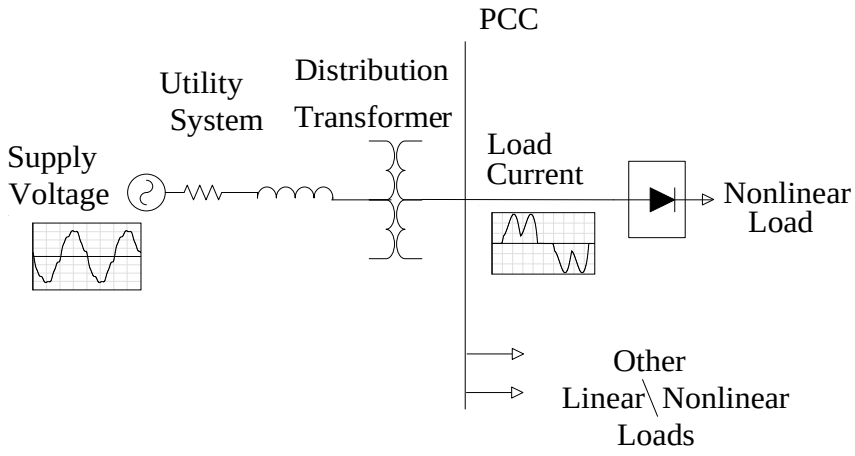

Fig. 1.7 Definition of the point of common coupling (PCC).

One major undesirable effect is the losses increment in the power system and its series connected equipment (transformers, wiring, etc.) as the injected current harmonics increase the rms value of the current. Additionally, these harmonic currents also interact unfavourably with most parallel connected equipment (power factor correction capacitors, and core-loss effects of transformers and motors) causing extra losses, overheating and overloading. As a result, affected equipment will be subjected to possible damages that can reduce their expected successful operation lifetime.

Another well-known negative effect is the injected current harmonics interference with telecommunication lines and errors in power metering. Also, they cause harmonic resonance or amplification in the utility distribution system as generated current harmonics circulate in the system and do not provide active power to the load.

Lastly, some power system equipment is subjected to mal-functioning. This is due to the fact that, the existence of a high level of harmonic voltage distortion changes the sinusoidal shape of the supply voltage waveform, typically at the peak and zero-crossing points, which some equipment, for example thyristor rectifiers, detect and use.

Therefore, the IEEE 519 recommended harmonic standard was introduced as a guideline in 1981 in north America, and revised in 1992 [11]. The IEEE Standard 519-1992 proposes to limit harmonic current injection from end users so that the harmonic voltage levels on the overall power system will be acceptable. The approach set recommended limits for both users and utility ends. For individual end users, the standard limits the level of harmonic current injected at the PCC. This is the quantity that the end users have control over. Recommended limits are provided for both individual harmonic components and the total distortion indices. Total Harmonic Distortion (THD) is commonly used indices for measuring the harmonic content of a waveform and may be applied to either voltage or current. The current THDi is given by

$$THD_i = \frac{\sqrt{\sum_{n=2}^{N} I_n^2}}{I_1}.100\% \quad (1.2)$$

where the I_n is the rms value of the current harmonics and I_1 is the rms value of the fundamental current component. However, this can be often misleading. For instance, many ASD's will exhibit high input current THDi values when they are operating at very light-loads. This is not critical because the magnitude of harmonic current is low, even though its relative distortion is high. To account for the loading effect for characterizing the harmonic currents in a consistent fashion, the IEEE Standard 519-1992 defines an additional term, the Total Demand Distortion (TDD). This term is the same as THDi except that the distortion is expressed as a percentage of rated fundamental load current rather than of the fundamental current magnitude at the instant of measurement. TDD is therefore given by

$$TDD_i = \frac{\sqrt{\sum_{n=2}^{N} I_n^2}}{I_L}.100\% \quad (1.3)$$

where the I_n is the rms value of the current harmonics and I_L is the rated demand of the fundamental current component. Therefore, IEEE Standard 519-1992 recommended harmonic current limits, shown in Table 1.2, is expressed in terms of current TDD, rather than current THDi. The I_{sc}/I_L ratio is the short circuit ratio (SCR) at PCC. As I_L is previously defined, I_{sc} is the short circuit current available at the input of the nonlinear load. The short circuit ratio defines the TDD limit that applies to a distribution transformer output, and therefore to the loads connected to it.

Table 1.2 IEEE 519 harmonic current limits*; taken from [11]

I_{SC}/I_L	<11	11≤h<17	17≤h<23	23≤h<35	35≤h	TDD%
<20	4.0	2.0	1.5	0.6	0.3	5.0
20-50	7.0	3.5	2.5	1.0	0.5	8.0
50-100	10.0	4.5	4.0	1.5	0.7	12.0
100-1000	12.0	5.5	5.0	2.0	1.0	15.0
>1000	15.0	7.0	6.0	2.5	1.4	20.0

*Higher levels of harmonic current generation are allowed for higher values of SCR because a single customer has less impact on the system voltage distortion

For the utility, since the harmonic voltage distortion on the utility system arises from the interaction between distorted load currents and the utility system impedance, the utility is mainly responsible for limiting the voltage distortion at the PCC. The IEEE Standard 519-1992 recommended harmonic voltage limits, shown in Table 1.3, are given for the maximum harmonic components and for the voltage THD. These values are expressed as the percentage of the fundamental voltage. For systems below 69 kV, the voltage THDi should be less than 5% provided that the system resonances do not coincide with harmonic frequencies present in the load currents. Therefore, to comply with these limitations, utilization of efficient, reliable, and economical harmonic mitigation technique is mandatory.

Table 1.3 Voltage distortion limits; taken from [11]

Bus Voltage at PCC	Maximum Individual Harmonic Component %	Maximum THDv%
69kV and Below	3.0	5.0
69.001kV Through 161kV	1.5	2.5
161.001kVand Above	1.0	1.5

Note: High-voltage systems can have up to 2.0% THDv where the cause is an HVDC terminal that will attenuate by the time it is tapped for a user.

1.2 **Harmonic Mitigation Techniques**

Generally, for three-phase rectifier ASDs system the well-known harmonic mitigation techniques can be categorized as shown in Fig. 1.8. Reducing the overall line current THDi to maintain the current sinusoidal waveform characteristics is the major role of these harmonic mitigation methods.

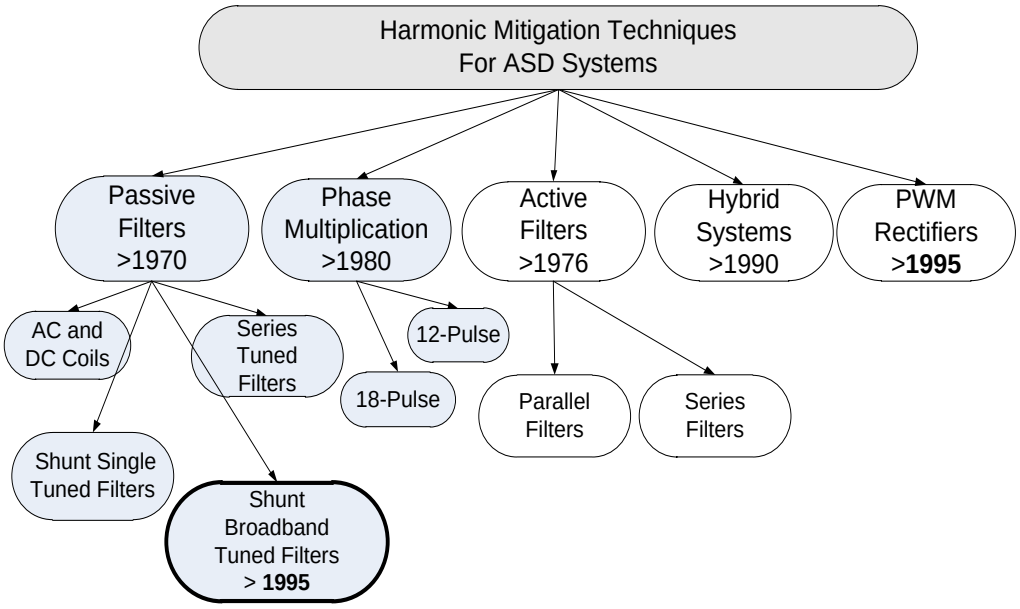

Fig. 1.8 Classification of common harmonic mitigation techniques for ASD systems.

1.2.1 Passive Filters

In passive harmonic filters, preventing the circulation of the unwanted harmonic currents in the power system can be achieved by the usage of a high series impedance to block them (series filter concept) or by diverting the harmonic currents to a low impedance shunt path (shunt filter concept).

Series passive filters can be purely inductive type or LC tuned type. AC line reactor filter and DC-link inductor filter are the two purely inductive type filters. AC line reactors offer a considerable magnitude of inductance that alters the shape or form factor the current waveform drawn by the rectifier bridge. They make the current waveform less peaky and discontinuous, resulting in lower current harmonics. To maximize the input reactance while minimizing AC voltage drop both AC line reactors and DC-link inductance (choke), shown in Fig. 1.9, can be combined. The DC-link inductance is electrically present after the diode rectifier and before the DC bus capacitor and it performs very similar to the three-phase AC line reactors. Since the DC inductor and capacitor often account for a significant portion of cost and size of the total converter, their proper selection and design is very important to achieve a cost and/or size optimized converter design while meeting the system performance

requirement [12]. Both AC line and DC-link inductance insertion methods provide a limited amount of THDi reduction that is not sufficient to comply with the IEEE 519 standards.

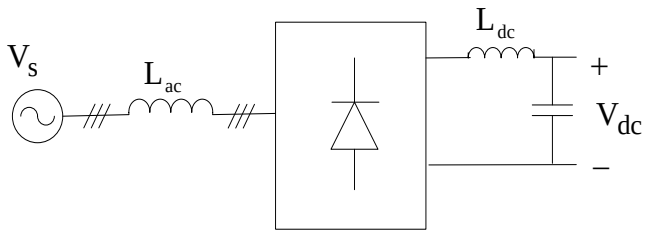

Fig. 1.9 AC line reactor and DC line inductance based passive filtering.

The tuned series passive filter type is shown in Fig. 1.10. The filter consists of parallel inductance (L_f) and capacitance (C_f) that are tuned to provide high impedance at a selected harmonic frequency. The high impedance then attenuates the flow of harmonic current at the tuned frequency only. At fundamental frequency, the filter is designed to yield low impedance, thereby allowing the fundamental current to flow. For blocking multiple harmonics, multiple series filters are needed. They must be designed to carry the full rated load current as they are connected in series to full line voltage. Therefore, they can create significant losses at the fundamental frequency. In contrast, shunt passive filters carry only a fraction of the current that a series filter must carry. Given the higher cost of a series filter, and the fact that shunt filters may supply reactive power at the fundamental frequency, the most practical approach usually is the use of shunt filters.

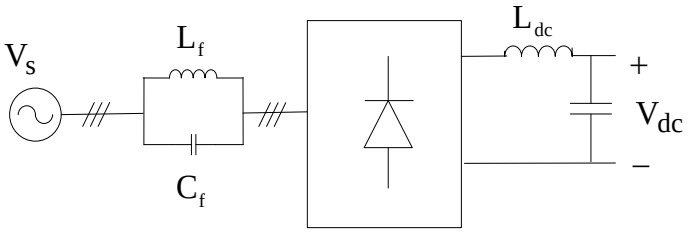

Fig. 1.10 Tuned series passive filter type.

A shunt filter, shown in Fig. 1.11, offers very low impedance path at the frequency to which it is tuned and it shunts most of the harmonic current at that frequency. The

most common shunt filter types are the single tuned and high-pass (2^{nd} order) filters. The layout of these practical shunt filter types is shown in Fig. 1.12 [13].

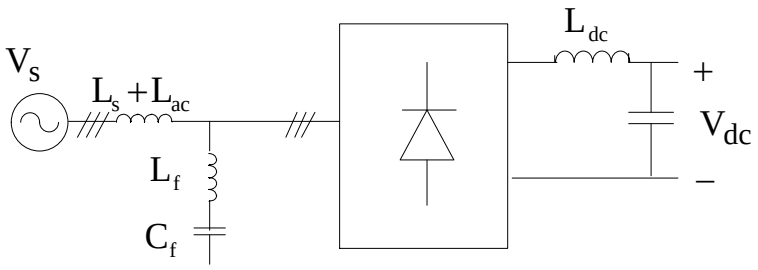

Fig. 1.11 Shunt passive filter type

In ASD systems and other rectifier applications, in particular at increasing power ratings (above several tens of kilowatts), shunt filters are frequently utilized for harmonic reduction. The single tuned filter is probably the most common shunt filter in use [14]. It shows very low impedance at the frequency to which it is tuned with the respect to the effective line impedance. As a result it diverts the flow of the rectifier harmonic current through its path. Harmonic suppression is achieved provided that the effective line impedance is considerably higher than the shunt filter impedance at the harmonic frequency.

Single tuned shunt filters also improve the total power factor by supplying reactive power to the load at the fundamental frequency and by reducing the harmonic distortion factor. Typically, basic diode bridge rectifier has a high displacement power factor (DPF > 0.97). However, adding AC line smoothing reactors will increase the commutation time between diodes and deteriorate the DPF value.
Generally, a single tuned shunt filter can only attenuate a single harmonic current component. This may not be adequate to filter all the problematic current harmonics effectively. Therefore, for a wide range generated harmonics a single tuned filter must be individually designed for each harmonic current component to be suppressed.

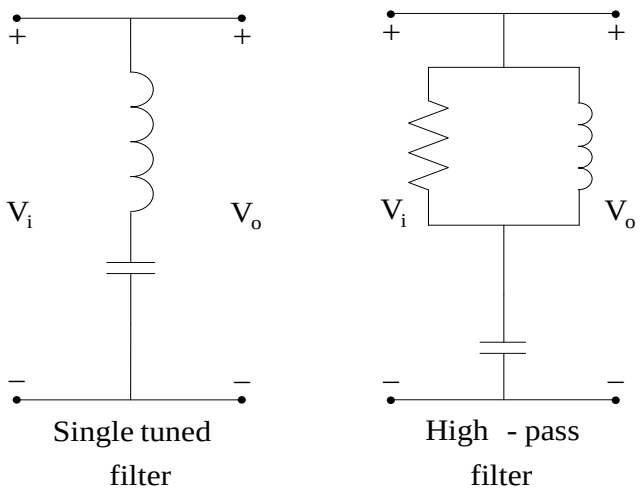

Fig. 1.12 Common shunt passive filter configurations.

In practice the tuned filters are employed for at most a few dominant harmonics. Filtering must begin with the highest harmonic frequency to be filtered and the utilization of the filters for the lower frequency harmonics is necessary to avoid parallel resonance related over-voltages at the lower harmonic frequency. Therefore, filtering the dominant 7^{th} harmonic would require a 7^{th} harmonic filter along with the 5^{th} harmonic filter. In ASD systems below megawatt levels 5^{th} and 7^{th} harmonic filtering is sufficient (higher order harmonic filtering is cost prohibitive also), while at higher power the 11^{th} and 13^{th} harmonics may be considered.

The filter performance depends on the source impedance value which is usually not accurately known and can vary with system changes. Instability may occur due to parallel resonance of the filter components with the source impedance. The filter effectiveness is highly affected by the source stiffness. The more the source impedance the more current harmonic suppression is gained. For stiff systems (low source impedance) the design also may require the addition of large AC line reactors to achieve the required THDi performance criteria. Therefore, single tuned filters are not suitable for changing system conditions. Once installed, they are rigidly in place. Neither the tuning frequency nor the size of the filter can be changed easily. Outage of a parallel branch can totally alter the resonant frequency, resulting in overvoltage/overcurrent stressing of filter components [15], [16]. Most of all, the THDi value is usually difficult to decrease to less than 10% with an economical filtering system size, and that means the tuned filter approach does not give IEEE

519 compliant in most cases. These main disadvantages have been the driving force behind the development of the low-pass broadband filters. Moreover, due to the recent development in magnetic materials and technology these new types of passive harmonic filters were possible to develop with more practical components size and economical cost. In addition, even in non-ideal supply voltage (e.g. unbalance, voltage pre-distortion) these types of harmonic filters may give total harmonic current distortion (THDi) values of less than 10%.

Unlike the shunt and series filters that have a narrow band of harmonic suppression, broadband filters have a wider range of harmonics suppression capability. Broadband filters employ a combination of the two passive techniques, with a high series impedance to block the undesired current harmonics (from flowing through the grid) and a low shunt impedance path to divert their flow through the shunt filter. Therefore, the low-pass broadband filtering method is an ideal approach to block the harmonic currents at multiple (widespread) frequencies. The rectifier current components with frequencies below the filter cut-off frequency can pass to (from) the AC line. However, current components with frequencies above the cut-off frequency are filtered out. Practically, broadband filters are designed to achieve a cut-off frequency that is less than the first dominant harmonic frequency minimizing the resonance phenomena risk.

Low-pass broadband filters (LPF) can be in different structures; shown in Fig. 1.13, the basic LC [17], [18] the improved LLCL [19], [20], [21] and a modified LLCCL type [22]. They are tuned to a low cut-off frequency such that only fundamental component will pass from the input to the output. Therefore, they are called low-pass broadband filters. All shown low-pass broadband filters use only one shunt filter to suppress all the harmonics. On the contrary, classical shunt filters are tuned to a single harmonic frequency to be suppressed and multiple stages are used to suppress all injected current harmonics. The improved broadband (LLCL) filter type has less filter components than the modified (LLCCL) filter and superior performance than the basic (LC) filter.

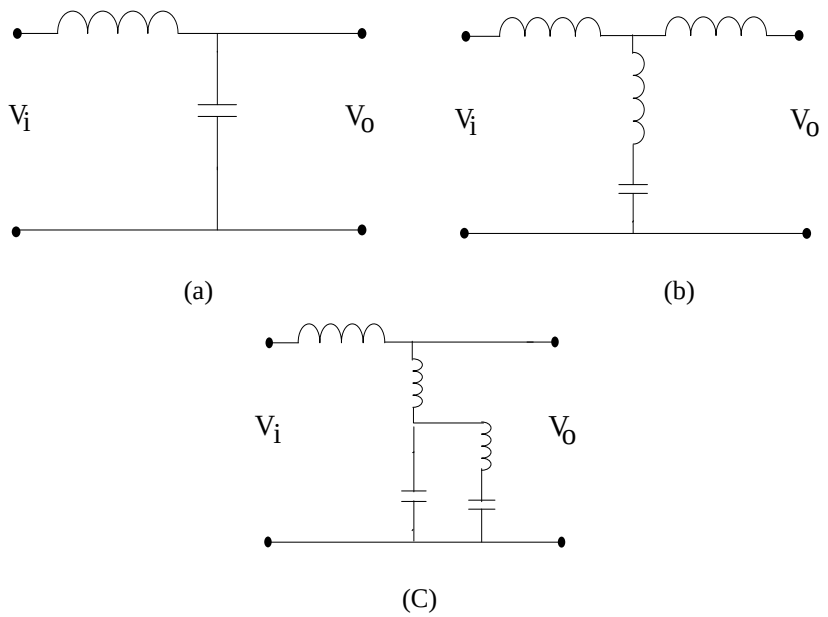

Fig. 1.13 Low-pass broadband filter configurations (a): Basic (LC) type, (b): Improved (LLCL) type, (c): Modified (LLCCL) type.

1.2.2 Phase Multiplication Systems

Phase multiplication technique is based on increasing the pulse number for the converter. This increases the lowest harmonic order for the converter and reduces the size of the passive filter needed to filter out the current harmonics. A 12-pulse converter ideally has the lowest harmonic order of 11 (5^{th} and 7^{th} current harmonics are theoretically non-existent). Similarly, an 18-pulse converter has the lowest harmonic order of 17. However, a 12-pulse converter, shown in Fig. 1.14, needs two 6-pulse bridges and two sets of 30^{o} phase shift AC inputs and an 18-pulse converter needs three 6-pulse bridges and three sets of 20^{o} phase shift AC inputs. Many different topologies exist for the phase shift achievement. In general, the phase multiplication technique is effective to reduce low order current harmonics as long as there is a balanced load on each of the converters. However, the need for added transformers with multiple windings increases their size, reduces the energy efficiency, and increases the cost. These factors are the main topology drawbacks [23] [24].

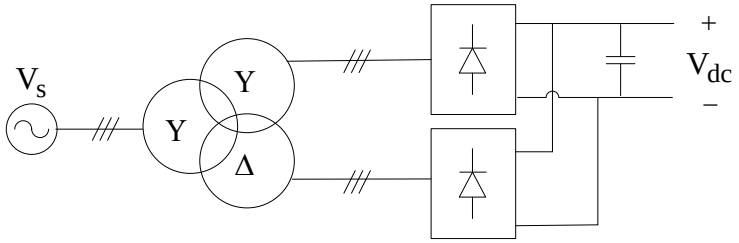

Fig. 1.14 Twelve pulse rectifier system configuration.

1.2.3 Active Harmonic Compensation Systems

Active harmonic compensation (filtering) method is relatively a new method for eliminating current harmonics from the line. Active filters give good system performance and current harmonics reduction. They are more adaptive, maintain good harmonic attention and line power factor correction across a wide range of rectifier load current. However, they are based on sophisticated power electronics systems and thus they are much more expensive than passive filters [25], [16] and are still avoided in most applications due to their high cost and complexity [26].

In active filters the basic idea is to inject to the line equal magnitudes of the current/voltage harmonics generated by the nonlinear load and with 180 degrees phase angle difference so they cancel each other.

Active filters can be classified based on converter type, topology, and number of phases. The converter type can be either Current Source Inverters (CSI) or Voltage Source Inverter (VSI). CSI-based active filters employ an inductor as the energy storage device. VSI-based active filters used a capacitor as the energy storage device. The topology can be shunt, series, or a combination of both. The third classification is based on the number of phases, such as two-wire (single-phase) and three- or four-wire (three-phase) systems [27]. Three-phase active filters are used for high-power nonlinear loads such as ASD AC/DC converters. Active filters of many configurations have been introduced and improved. Shown in Fig. 1.15, are the fundamental configurations [28]. Of all various configurations, the parallel active filter using the voltage source inverter topology accompanied by high performance current regulation methods is the most frequently employed type. For harmonic

compensation, the parallel active filter employs the instantaneous reactive power theory or synchronous frame transformation based compensation technique.

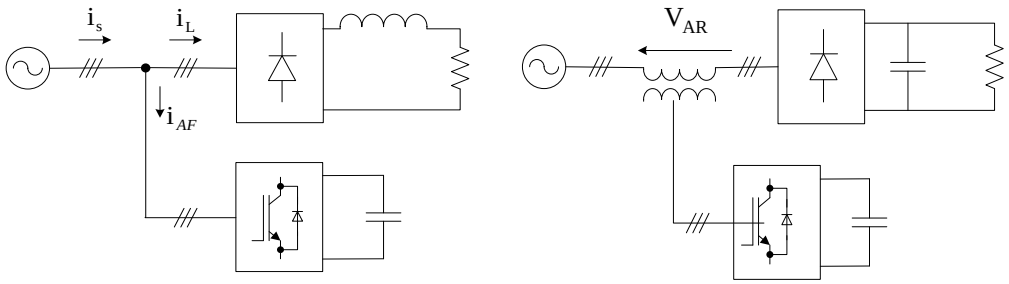

(a) (b)

Fig. 1.15 Active filter fundamental system configurations:
(a) Shunt active filter, (b) Series active filter.

1.2.4 Hybrid Systems

Hybrid active filters, as shown in Fig. 1.16, combine active and passive filters in various configurations [28]. The main purpose of hybrid active filters is to substantially reduce the rating of the VSI inverter system and hence initial costs and to improve efficiency. They are also used to improve the compensation characteristics of passive filters and reduce any series or parallel resonance due to supply or load, respectively. Practically, more viable and cost-effective hybrid filter topologies have been developed than stand-alone active filters. They enable the use of significantly small rating active filters that is less than 5% of the load KVA compared to stand-alone parallel (25-30%) or series active filter solutions [29]. Usually, with shunt passive filter combinations shown in Fig. 1.16, the passive filter is tuned up to a specific frequency to suppress the corresponding harmonic and decrease the power rating of the active filter.

Another typical combination is of a series active filter and a series passive filter. High fundamental component current through the series active filter and the fundamental component voltage across the shunt active filter are problematic. High initial cost, high running cost and complexity are major drawbacks of the active harmonic filtering techniques.

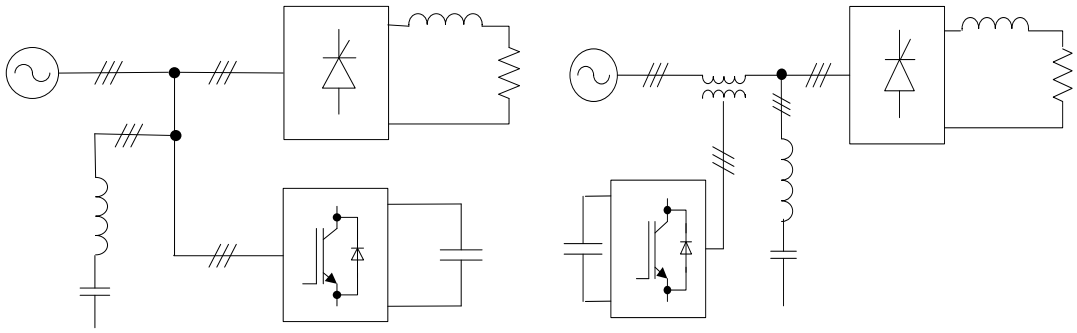

(a) (b)

Fig. 1.16 Hybrid active filters common configurations: (a) Shunt active filter and shunt passive filter, (b) Series active filter and shunt passive filter.

1.2.5 PWM Rectifiers

The three-phase boost type (ac-dc) PWM rectifier has superior performance compared to conventional diode or thyristor bridge rectifiers. Under balanced supply voltages conditions, it can draw sinusoidal current at near unity power factor while maintaining a high quality DC output voltage with a small filter capacitor. However, designing a proper controller for it is generally a challenging task [30]. For PWM-Voltage Source Rectifiers (PWM-VSR) benefits like power regeneration, low harmonic distortion, unity power factor, and controlled DC-link can be obtained. They are often used in applications where substantial regenerative operating mode activities are required. PWM-VSR operation principle is based on direct sinusoidal current generation, whereas the active filter is based on load harmonic compensation. However, the system and control complexity and high cost are the main drawback that makes it impractical in many applications [31].

1.3 Thesis Motivation

From the previous background, USA market survey and as shown in Fig. 1.17, it is concluded that most of the reviewed filtering techniques have common drawbacks of higher design complexity, higher cost (rectifier type and ASD cost dependent estimation) or most likely lower effectiveness compared to passive filtering techniques [32]. Consequently, the passive harmonic filtering techniques, to a large

extent, are still the most commonly used techniques for current harmonic mitigation of 6-pulse front-end diode/thyristor rectifier applications [33], [34]. Several recent papers deal with the passive harmonic filter placement in the power system issues [35], [14], [36] . As the active harmonic filters remain costly and problematic, passive filtering solutions will continue finding applications. As a result high performance passive or hybrid (active and passive) filters must be developed to meet the increasingly strict power quality requirements of the modern technology era. Thus, enhanced passive filter topologies involving better performance, smaller size, higher efficiency, reduced noise, and most importantly lower cost have to be developed and research in this area is a necessity of the modern power quality era.

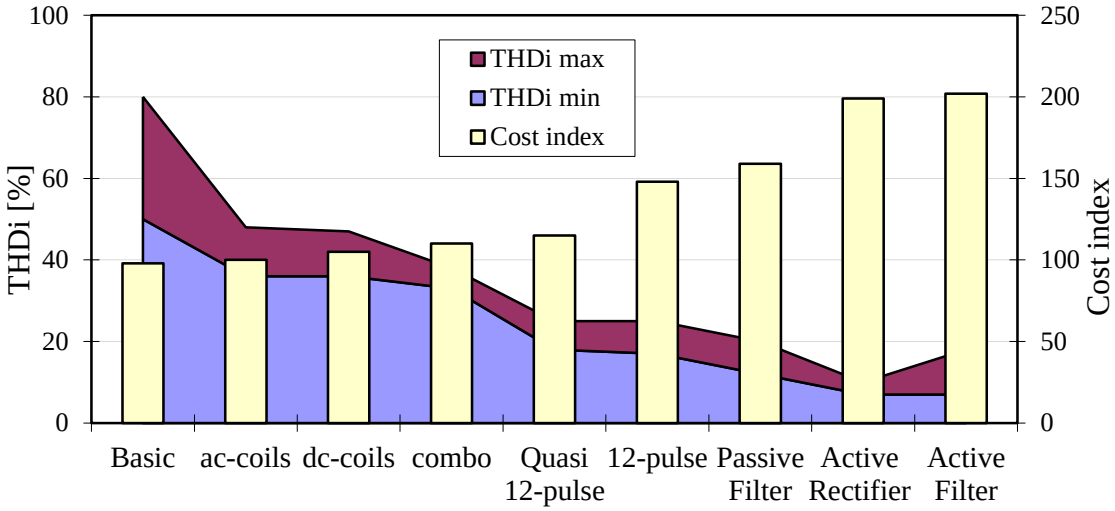

Fig. 1.17 Cost-benefit of harmonic reduction techniques for three-phase ASDs [32].

In this research project the emphasis is put on the passive harmonic filtering technique, in particular the improved broadband passive filter (IBF) topology. The filter has superior overall performance and its applications have been increasing rapidly. These low-pass passive filters (LPF) are capable to comply with IEEE Standard 519-1992 recommendations. Other harmonic standards such as; (IEC 61000 series and G5/4-1) that recommend similar current and voltage harmonic limits on power system networks are applied in Europe.

In practice, the IEEE Standard 519-1992 is a one document publication that has more stringent recommendations. On the other hand, the low-pass broadband filters were

patent and operating performance was assessed according to the IEEE Standard 519-1992. Recently, most of the commercial broadband filters data sheets are illustrating the filter effectiveness that can comply with this harmonic standard recommendation. Therefore, IEEE Standard 519 is more common to be used for broadband passive filters assessment process. This will also ensure complying with other harmonic standards.

As harmonic distortion problems are more common at end-users facilities than on the utility supply system, and the highest voltage distortion levels occur close to harmonic sources, the focus in this study will be complying with the harmonic recommendations at the end user side where most non-linear loads are located in the network.

The low-pass broadband filters are capable of minimizing the undesirable effects of harmonic distortion in electrical power systems (as shown in Fig. 1.18) [37]. As the figure reveals, minimizing the power system losses and the total rms drawn current (consequently the KVA generated) can be achieved by reducing the total harmonic distortion (THD%) in the system to levels below 10%. The higher current distortion values in the system, the higher total rms current in the cables and loading equipment causing extra heat and losses in the system. As a result, the low-pass broadband filters effectively contribute in reducing the CO2 emissions caused by variable speed drives applications by reducing the extra KVA generation caused by harmonic distortion (as shown in Fig. 1.19) [37].

However, the design process for determining the IBF parameters is complex. With input, output power quality requirements and filter efficiency, cost and size requirements, there are a number of conflicting constraints to be optimized which complicate the design process and impede reaching the most effective design. At the present time, there are few publications on IBF design. Available material, filter manufacturer datasheets, does not give parameters and only provides performance data [20]. One linear optimization searching method for the filter values was introduced in [19]. The linear nature of this searching method could be considered as

the main drawback. This is due to the fact that linear method can be easily trapped in local optima.

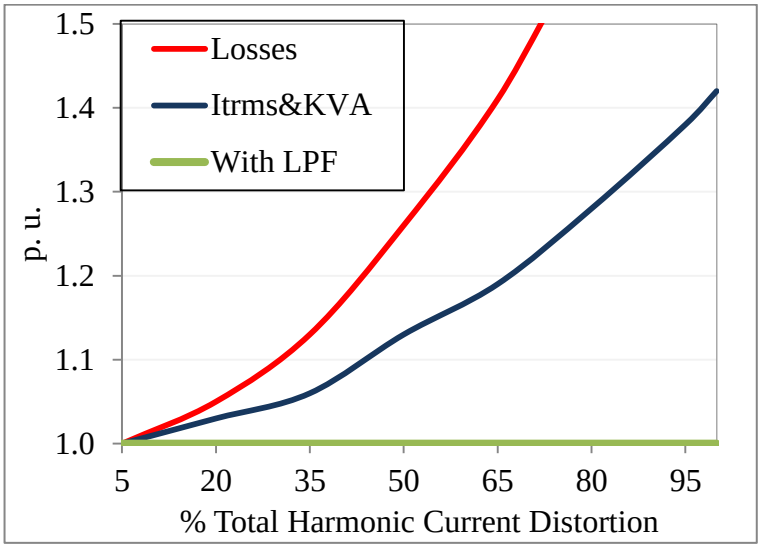

Fig. 1.18 Total harmonic distortion undesirable effect in electrical systems[37].

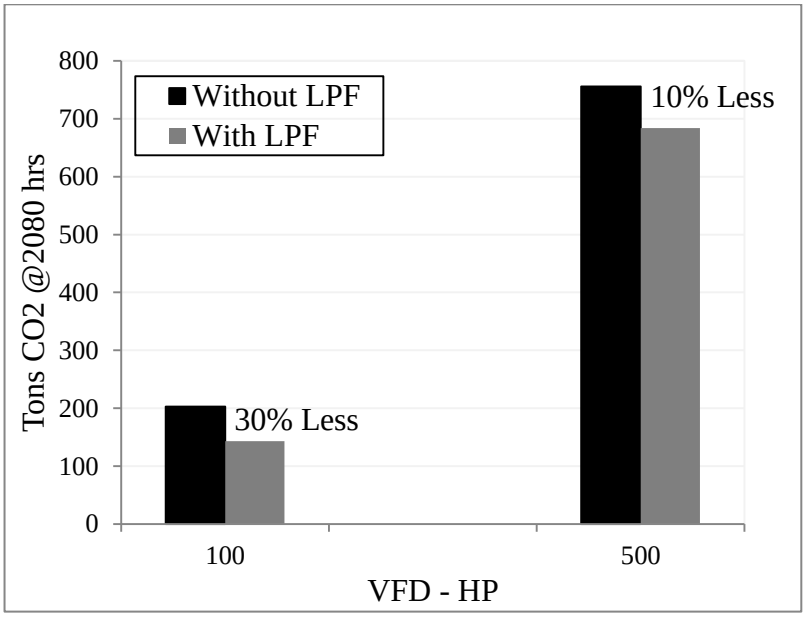

Fig. 1.19 Reduction VFD systems CO2 emissions by using LPF[37].

Mathematical optimization methods have been used over the years in designing conventional shunt passive filters [38], [39], [40], [41], [15], [16]. However, for IBF topology, the filter values cannot be easily obtained by these design methods. This is due to multi-objective, discontinuous nature of the solution space. Taking into consideration the fact that the optimal solution cannot be simply achieved by

conventional mathematical optimization techniques, it has been essential to use an optimization technique with a robust searching capability.

1.4 **Thesis Objectives**

The first major aim of this research project is to develop a design method, by using the Genetic Algorithm (GA) searching technique, to find the optimized filter component values of the improved broadband passive harmonic (IBF) filter. This filter is used to mitigate current harmonics caused by three-phase bridge rectifiers front-end applications (such as motor drives), in order to comply with the IEEE standard 519-1992, improve line power factor and reduce the well-known undesirable effects of current harmonics in power system distribution networks. The GA has strong searching features ability and has been recently used for passive filter design for single-phase and three-phase rectifier front-end applications [42], [12], [43].

In view of the fact that the main disadvantage of the passive harmonic filters is the large-size components, the suggested design method will attempt to minimize the size of the existing IBF filter components (L and C) utilized.

The second key aim of this thesis is to propose a design process that will challenge to reduce the number (and size) of the IBF filter components utilized. This attempts in achieving a novel Advance Broadband Filter (ABF) structure with less components, lower cost and size, while maintaining the same IBF power quality constraints design criteria level (if not improved).

The completed broadband passive harmonic filters IBF and ABF designs will be evaluated via computer simulations and accuracy of the results will be proven through experimental work. In addition, explanation of the IBF and ABF design approach theoretical limitations and practical implementation restrictions is provided. Furthermore, both broadband passive harmonic designed filters (IBF and ABF) performance will be compared with conventional passive filters. The comparison involves the input current total harmonic distortion, input power factor, rectifier voltage regulation, energy efficiency, filter component values and the passive filter

size, and cost. The parallel/series harmonic resonance problem related issues will be addressed and unbalanced operation performance will be investigated. The comparison is based on analysis and computer simulation. Studies and thier findings are confirmed experimentally.

The final aim includes testing the proposed broadband passive filters effectiveness in a typical distribution system under various nonlinear load penetration level in the network.

The research objectives of this research project can be summarized at:

1. Review and analyse the theoretical background of the IBF and ABF configurations design and operating principles.
2. Develop a design method of the improved broadband passive filter by using the Genetic Algorithm to optimize the size (cost) of the existing IBF topology components.
3. Evaluate the optimized IBF performance characteristics via analysis, detailed computer simulation and laboratory experiments.
4. Propose a novel advanced broadband filter (ABF) structure by reducing the number of filter components utilized in the IBF structure (if possible).
5. Optimize the size of the new ABF components using the Genetic Algorithm.
6. Estimate the ABF performance characteristics via analysis, detailed computer simulation and laboratory experiments.
7. Provide ABF performance comparison with IBF and other typical passive filters.
8. Assess the proposed IBF and ABF topologies effectiveness in a standard distribution network.

1.5 **Thesis Organization**

The thesis is structured in seven chapters. This first chapter presents the thesis subject and motivation. It describes the related engineering drawbacks of the

inevitable proliferation of ASD systems in industry in order to save electrical energy consumption and reduce CO2 emissions. The main disadvantage of the current harmonic distortion caused by such systems is reviewed and the well-known undesirable side effects encountering the distribution networking is revised. Furthermore, this chapter presents a literature review of the major harmonic mitigation techniques solving ASD application harmonic problems.

The second chapter describes and reviews the low-pass broadband filter topologies along with the IBF operating principles. It also reviews the ASD frequency domain modelling method and the linear searching approach for the IBF parameters design.

The third chapter briefly investigates mathematical optimization algorithms and common artificial intelligence optimization algorithms used in solving complex power system, nonlinear problems. It also provides comparisons of the discussed methods.

The fourth chapter illustrates the GA implementation process in designing the IBF filter and compares the results with the linear design method previously defined. ASD performance simulation results utilizing the IBF optimal design parameters are presented for various power ratings and compared with typical passive filters performance. Finally, a 5.5kW ASD system using an IBF prototype is designed, built and tested in the laboratory. ASD experimental performance evaluation and comparison with simulation results are provided.

In the fifth chapter, the new structure of the ABF and the corresponding DC-link inductor selection method is explained. Furthermore, in a similar organization of the previous chapter, the GA implementation process in designing the ABF filter is presented along with the results comparison with the linear design method. ASD performance simulation new results utilizing the ABF optimal design parameters are presented for various power ratings and compared with different passive filters performance. Finally, a 5.5kW ASD system using an ABF

prototype is designed, built and tested in the laboratory. ASD experimental performance evaluation and relationship with simulation results are detailed.

The sixth chapter describes the effectiveness assessment process of the broadband filters IBF and ABF, designed in the thesis, connected and operating in a standard IEEE distribution network. This involves different levels of nonlinear loads (ASD systems) penetration in the network.

The seventh and final chapter summarizes the research stages, outcomes and delivers several concluding observations. Future work recommendations for thesis related topics are also presented in this last chapter.

1.6 **Statement of Contribution**

The major novelty in this project involves:

1. Providing a theoretical background and design analysis of the broadband harmonic filters being introduced into commercial ASD products.

2. Providing a novel design method using the GA searching technique to optimize the size (cost) of the existing IBF structure filter components.

3. Investigating the new design of the optimized IBF topology performance characteristics via a comprehensive analysis, detailed simulation and experimental studies.

4. Developing a new ABF structure by reducing the number of the IBF filter components utilized in conjunction with optimizing the size.

5. Providing a new design method using the GA searching technique to optimize the size (cost) of the novel ABF structure filter components.

6. Investigating the new design of the optimized ABF topology performance characteristics via a comprehensive analysis, detailed simulation and experimental studies.

7. Providing a detailed quantitative and qualitative performance comparison of the proposed broadband filters with the conventional passive filters.

8. Investigating the designed broadband filters effectiveness under different harmonic distortion levels in power system distribution networks.

2 BROADBAND HARMONIC PASSIVE FILTER DESIGN

2.1 Introduction

In the previous chapter, the common passive filtering methods used for ASD harmonic mitigation were presented and their general performance attributes were discussed. Among the passive harmonic filters different topologies, the low-pass broadband filtering method is a more practical approach to mitigate the harmonic currents at several frequencies. The basic structure (LC) broadband filter has superior performance to the other filtering methods discussed. It is effective in suppressing the rectifier current harmonics, simple and free of harmonic resonance problems. However, the simple structure of the filter comes with a serious drawback which is the rectifier terminal over-voltages. As a result, the Improved Broadband Filter (IBF) has been developed in order to overcome the deficiency of the LC filter and obtain superior overall performance characteristics.

In this section the IBF topology is under investigation. The filter construction, operating principle and behaviour analysis are described. Finally, the same design method using the linear approach presented in my M.Sc. thesis [44] is briefly described and will form the basis of the new design method which uses a genetic algorithm approach in an attempt to reduce the IBF filter component size and cost while maintaining the achieved performance (if not improved).

2.2 Improved Broadband Filter (IBF) Topology and Its Operating Principles

The basic LC broadband filter, shown on Fig. 2.1(a), involves a simple structure with relatively large components [44]. The filter is free of the harmonic resonance problem. However, in particular at no-load the filter output voltage becomes

excessive that may lead to rectifier or filter failure [18]. Also the power factor is largely leading at all load conditions. Trade-off relations between input current THDi% and power factor are strong. Thus, the filter does not yield overall a satisfactory performance. To overcome the deficiency of the LC broadband filter, the improved broadband LLCL filter (IBF), shown on Fig. 2.1(b), has been developed such that the basic LC filter problems are eliminated [20], [21]. As shown in Fig. 2.1(b), splitting the 25% L filter of the simple LC broadband filter into two elements (L_i and L_f) the filter input-to-output behaviour is altered. Further, a 3-5% smoothing reactor (L_o) is inserted between the rectifier terminals and the filter output terminals. Filter capacitors C_f are usually delta connected and damping resistors R_d are connected to C_f (shown later in the system equivalent circuits) to damp the voltage/current peaks during line-side switching transients.

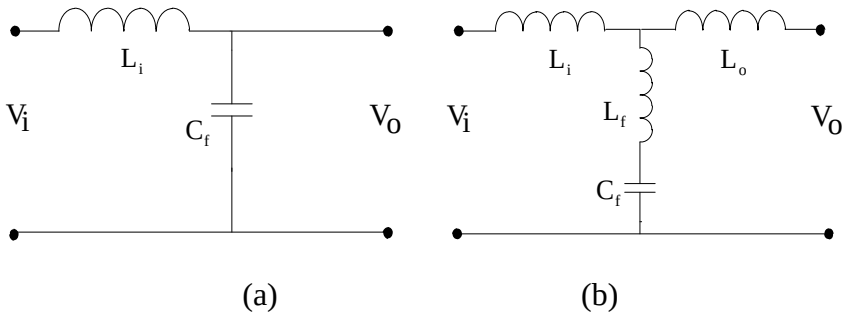

Fig. 2.1 Broadband filter configurations (a): LC type, (b): LLCL type.

At the rectifier current dominant harmonic frequencies components, with a suitable design, the large AC three-phase input reactor (L_i) exhibits high impedance over a wide-ranging frequency and provides a high impedance ratio as shown in Fig. 2.2, with respect to the single shunt filter impedance. In consequence, all the rectifier current harmonics will be blocked by the line and diverted to pass through the single shunt filter. Not only does L_i block the current harmonic flow from the rectifier to the AC line, but it also minimizes the effect of the line voltage harmonics on the rectifier (i.e. provides harmonic isolation between the source and the rectifier) and on the shunt filter. Therefore, L_i suppresses the current harmonic flow either way.

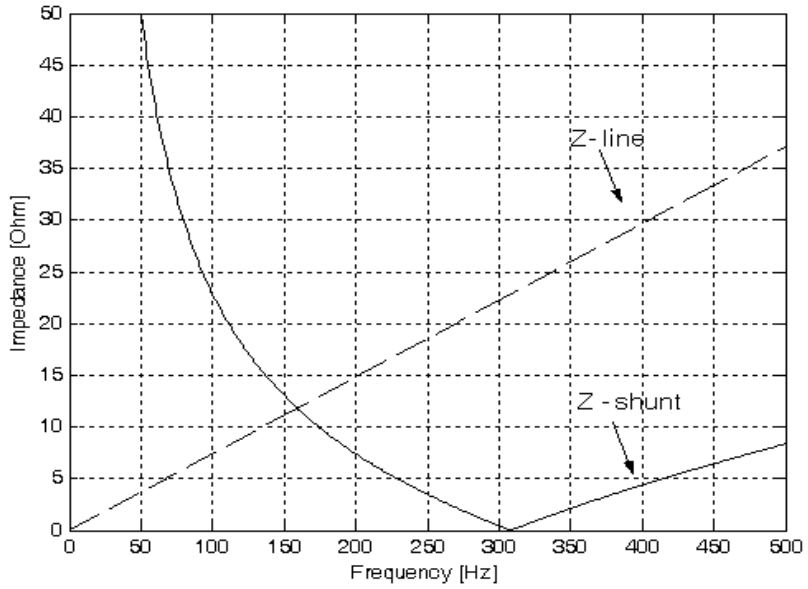

Fig. 2.2 Typical line and shunt branch impedances of IBF.

The filter parallel-resonant frequency f_p involving L_i-L_f-C_f is defined in the following.

$$f_p = \frac{1}{2\pi\sqrt{(L_i + L_f)C_f}} \tag{2.1}$$

The parallel-resonant frequency is selected between the fundamental frequency and the first dominant rectifier current harmonic which is the 5^{th} harmonic such that harmonic resonance related overvoltage stresses are avoided. The filter capacitor C_f improves the input power factor while L_f is partitioned with L_i such that there is no overvoltage at the rectifier terminals (unlike the LC filter) and no-load to full-load filter output voltage change is confined within a specified range (< 5%).

Filter components L_f and C_f are connected in series to provide very low series impedance to the dominant rectifier current harmonics and short circuit them through its path. The series resonant frequency f_s is defined in the following.

$$f_s = \frac{1}{2\pi\sqrt{L_f C_f}} \tag{2.2}$$

The output reactor (L_o) is a current smoothing reactor that makes the rectifier current waveform less discontinuous, resulting in lower current harmonics. It reduces the rectifier current THDi significantly (4% L_o reduces the THDi by 50%); and, hence, produces less harmonic current/voltage stress on the shunt branch components L_f and C_f, leading to smaller, lower cost and more efficient filter structure.

2.3 **Improved Broadband Filter (IBF) Design Using Linear Method**

In the IBF design procedure there are five filter component values (L_i, L_f, L_o, C_f, and R_d) that must be determined. With various power quality requirements and operating constraints such as; resonance risk and no-load input current (I_{NL}) limitations, along with filter efficiency, cost and size, the design is limited. Therefore, the design process is a complicated duty.

The power quality design indices considered in the design are the input current THDi%, input power factor, and filter output voltage (rectifier input voltage) regulation, which are all defined in the following.

$$\mathrm{THD_i} = \frac{\sqrt{\sum_{h=2}^{N} I_h^2}}{I_1}.100\% \tag{2.3}$$

$$\mathrm{PF} = \frac{I_1}{I} \times \cos\varphi \tag{2.4}$$

$$\Delta V_o = \frac{V_{O\text{-}NL} - V_{O\text{-}FL}}{V_{O\text{-}NL}}.100\% \tag{2.5}$$

In (2.3) and (2.4), I_1 is the line-current fundamental component, I_h terms are the line-current harmonic components, and I is the line current, all rms values. In (2.4), φ is the displacement angle between the fundamental phase-voltage and line-current

components. In (2.5), $V_{O\text{-}NL}$ is the no-load filter output voltage and $V_{O\text{-}FL}$ is its full-load value, both fundamental frequency and rms values.

First, in the design (as previously explained), the first parameter L_o is selected as 4% reactor [13].

$$\omega_e L_o = 4\% \times Z_b = 4\% \times \frac{V_R}{I_R} = 4\% \times \frac{V_{LL}^2}{P_R} \tag{2.6}$$

In the above equation, ω_e is the line radial frequency and Z_b is system base impedance. V_R and I_R are the rated phase voltage and current. V_{LL} and P_R are the rated line-to-line voltage and power respectively. This mathematical definition can be achieved assuming lossless system and the rated ASD power P_R is equal to the DC link power P_{dc} (Section 2.3.2 and Appendix A shows more details). With this choice, the rectifier full-load current waveform becomes well defined (practically its shape is independent of power ratings). Therefore, the rectifier current fundamental component and the dominant harmonic current components ratios can be approximated as shown in Table 2.1. Closed form formula calculation of the remaining filter component values (L_i, L_f, C_f, and R_d) based on a required performance indices (2.3), (2.4), and (2.5) involves extremely complex mathematics (if possible at all).

Therefore, for a given set of design constraints (fs, fp, I_{NL}, THDi%, PF and ΔV_o%), the design problem is progressed in two steps. First, for selected fs, fp and I_{NL} practical values, approximate filter parameter (L_i, L_f, C_f, and R_d) values can be obtained by employing analytical formulas.

Second, these initial values are utilized in the detailed frequency domain model of the rectifier and the filter system such that accurate filter values are calculated in a computer program. For the frequency domain model, the system equations are evaluated in a MATLAB [45] code that increments (decrements) the parameters linearly (in this stage) until optimal results are obtained. It is observed that the first step which provides the approximate filter parameter values is essential in reducing

the total calculation time to obtain accurate results. In the following section, the approximate filter parameter estimation method will be reviewed and the accurate design method will follow.

Table 2.1 Rectifier current ratios

Current ratios (%)	I (%)
I_1/I_1	100
I_5/I_1	34
I_7/I_1	9.5
I_{11}/I_1	7
I_{13}/I_1	3.5
Higher order terms	neglected

2.3.1 Initial Filter Parameters Calculation Method

The filter component values Li, Lf and Cf are initially calculated in a closed form formula. Due to the strong trade-off that exist between steady-state and dynamic conditions the damping resistor (Rd) selection is complex. A computer simulation approach has been utilized through a detailed procedure to optimize its value. The selection process is neglected at this stage and will be presented in Appendix B.

For the remaining filter component values, analytical formulas can be obtained by selecting a suitable and approximate range of the parallel resonance frequency (fp), series resonance frequency (fs), and the no-load to full-load line current fundamental components ratio (α). Selection of the series resonant frequency value f_s depends on the rectifier current harmonic content while the parallel resonance frequency (f_p) can be selected to avoid harmonic resonance amplification risk as it comes closer to the first dominant harmonic component (5^{th}). The no-load line current (I_{NL}) should be significantly less than the full-load line current (typically about α <50%). Meanwhile lower α values imply smaller filter capacitors that may not be able to absorb the wide range of harmonic current components.

Based on given ASD power rating information the full-load DC-link current can be calculated. The full-load DC-link current mean value for a basic 6-pulse diode bridge rectifier with no AC in line reactors is given by

$$I_{dc} = \frac{P_{dc}}{V_{dc}} = \frac{P_{dc}}{\left(\frac{3\sqrt{2}}{\Pi}\right) \times V_{LL}} = \frac{P_{dc}}{1.35 \times V_{LL}} \tag{2.7}$$

where P_{dc} is the rated DC output power (the rated ASD power P_R with the assumption of lossless power conversion) and V_{LL} is the line-to-line rms supply voltage.

With the 4% Lo typical AC reactor selection (excluding the IBF) the rectifier current fundamental component (I_{Rect1}) rms value will be related to the DC-link current mean value by a simulation based defined fundamental stiffness factor β_1 (0.79). Theoretically, this factor can be estimated by the Fourier series analysis for a quasi-square rectifier current waveform (approx. 0.78).

$$I_{Rect1} = \beta_1 \times I_{dc} \tag{2.8}$$

Similarly, the non-sinusoidal rectifier current rms value (I_{Rrms}) (for the 4% Lo selected AC reactor) can be also related to the DC-link current mean value by a simulation based defined rms stiffness factor β_{rms} (0.84). Both stiffness factors β_1 and β_{rms} were investigated for various filter types and various rectifier current waveform shapes at different power ratings by means of computer simulations and compared to its value for the quasi-square rectifier current waveform [19] (Shown in Appendix C).

In IBF, if the filter is assumed to be lossless, the utility side power factor near unity, the rectifier side voltage rms value equal to the rated line voltage, and the diode rectifier displacement power factor being unity, then a power balance equation involving the fundamental components can be written. With the design completed

and the results obtained, it will be shown that all these assumptions are acceptable for the purpose of initial parameter calculation.

The first result of such assumptions is that the rectifier full-load current fundamental component (I_{Rect1}) is equal to the line full-load current fundamental component (I_{Line1}) as a low-pass filter. Therefore, using equations 2.7 and 2.8, for a given power rating and line-to-line supply voltage, the line full-load current fundamental component (I_{Line1}) can be estimated. On the other hand, the no-load fundamental line current can be estimated with the assumption that there is no harmonic injected from the load at no-load operating condition. Therefore, the no-load total rms value is equal to the no-load fundamental value. Moreover, the damping resistor Rd is considered open circuit (high impedance) with respect to filter reactors at 50 Hz. Then, the rms fundamental no-load line current is given by

$$I_{NL} = \frac{V_1}{Z_f + Z_i} \tag{2.9}$$

where V_1 is the rated utility phase voltage fundamental component rms value, Z_f is the shunt filter impedance (L_f, C_f) and Z_i is the input impedance, both at the fundamental frequency. Using the equations (2.7), (2.8) and (2.9), the line current no-load to full-load ratio can be as follows

$$\propto = \frac{\left[\frac{V_1}{Z_f + Z_i}\right]}{\left[\beta_1 \times \frac{P_R}{1.35 \times V_{LL}}\right]} \tag{2.10}$$

and defining the magnitude of Z_f and Z_i in terms of L_i, L_f and C_f components in equation (2.10), result in

$$\propto = \frac{\left[\frac{V_1}{\left|\omega_e\left(L_i + L_f\right) - \frac{1}{\omega_e C_f}\right|}\right]}{\left[\beta_1 \times \frac{P_R}{1.35 \times V_{LL}}\right]} \tag{2.11}$$

where ω_e is the fundamental electrical angular velocity (rad/sec). The L_i, L_f, and C_f filter values are separated and defined depending on the operating conditions and design constraints in (2.12).

$$\left|\omega_e\left(L_i + L_f\right) - \frac{1}{\omega_e C_f}\right| = \frac{V_1 \times 1.35 \times V_{LL}}{P_R \times \beta_1 \times \propto} = \frac{0.78 \times (V_{LL})^2}{P_R \times \beta_1 \times \propto} \tag{2.12}$$

Based on (2.1) and (2.2), equations (2.13) and (2.14) define the parallel and series resonance values in rad/sec, respectively.

$$\omega_p^2 = \frac{1}{(L_i + L_f)C_f} \tag{2.13}$$

$$\omega_s^2 = \frac{1}{L_f C_f} \tag{2.14}$$

Utilizing (2.14), equation (2.13) is rewritten in (2.15) and consequently in (2.16)

$$\omega_p^2 = \frac{1}{\left(L_i C_f\right) + \left(\frac{1}{\omega_s^2}\right)} \tag{2.15}$$

$$L_i \times C_f = \left(\frac{1}{\omega_p^2} - \frac{1}{\omega_s^2}\right) \tag{2.16}$$

According to (2.14) and (2.16) the L_f and L_i are defined in terms of C_f for a selected ω_s and ω_p values, in (2.17) and (2.18), respectively.

$$L_f = \frac{1}{\omega_s^2 \times C_f} \tag{2.17}$$

$$L_i = \frac{1}{C_f}\left(\frac{1}{\omega_p^2} - \frac{1}{\omega_s^2}\right) \tag{2.18}$$

Substituting L_i and L_f with their equivalents from (2.17) and (2.18) in equation (2.12), the C_f is finally given by

$$C_f = \frac{P_R \times \beta_1 \times \alpha}{0.78 \times (V_{LL})^2}\left[\frac{1}{\omega_e} - \frac{\omega_e}{\omega_p^2}\right] \tag{2.19}$$

At this stage the approximate filter design method formulas are complete. The equations must be executed in the order of (2.19), (2.18) and (2.17). The parameters involved in the equations must be carefully selected in order to make the initial parameter calculations accurate enough for the purpose of reducing the number of calculations required in the accurate design method.

Selection of the series resonant frequency value f_s (ω_s) depends on the rectifier current harmonic content, and therefore depends on the rectifier current waveform stiffness. The series resonant frequency f_s is selected in the vicinity of the two most dominant current harmonic (5^{th} and 7^{th}) frequencies. For the considered 4% Lo current waveform case with the known harmonic components (Table 2.1), which is the most frequently encountered case in practice, the tuning frequency should be selected much closer to the 5^{th} harmonic which is the most dominant harmonic. In this case, for example, a series resonant frequency of 275 Hz can be selected.

The parallel resonance frequency (f_p) can be selected in a wide range of 150 – 200 Hz. For higher frequency values (>200 Hz) there is a harmonic resonance amplification risk as f_p comes closer the fifth (dominant) harmonic and lower frequency range (<150 Hz) results in very large filter component values (greater than Table 2.2 filter parameter results for 150Hz selection) rendering the design cost prohibitive.

To restrict the f_p value, based on the approximate method, filter parameter calculation and a simple performance estimation study is conducted. The performance estimation

involves harmonic equivalent circuits. The rectifier along with L_o is modelled as a current source. Therefore, the input performance of the calculated filter values could be predicted (approximately). The equivalent circuit approach based performance prediction will be discussed in the next section. However, the method will be utilized here for the purpose of aiding the parallel resonant frequency selection. Shown in Table 2.2, the results illustrate the relation between the parallel resonant frequencies, filter component values, and input power quality. A 4% L_o is assumed and the rectifier current harmonics ratios are assumed to be the same as shown in Table. 2.2. For the upper half of f_p range (175-200 Hz), for all α values, the line THD_i% is high (up to 11.4%) and/or the line displacement power factor is low (<0.97). Therefore, the lower range (150-162 Hz) results in more reasonable line side performance ($THD_i \leq 5.1\%$ and/or DPF>0.92). Consequently, 150 Hz is selected as the initial value range of parallel resonant frequency as there is no rectifier current harmonic in this range under balanced three-phase voltage source and the possibility of exciting resonance is practically non-existent. It will be proved later in the thesis that the ASD using the broadband filter has minimum sensitivity of the unbalance voltage supply operating condition and practically does not initiate third current harmonic (I_3) in the system.

The no-load line current should be significantly less than the rated line current (typically about α<50%). However α <50% implies small a filter capacitor ($C_{f\Delta} < 15$ μF) and result in very large L_i (>23%) for the selected f_s and f_p values. Therefore, α is selected as 0.5.

Given the power ratings of an ASD and its current stiffness information (if not given, it can be assumed as soft current source), with the series and parallel resonant frequencies as selected above, and α as 0.5, the initial filter component values can be calculated from (2.19), (2.17), and (2.18). For example, for 50 Hz ASD applications with 5.5 kW and 55 kW power ratings, 275 Hz series resonant frequency and 150 Hz parallel resonant frequency, the calculated approximate filter component values are illustrated in Table 2.3. The flow chart of the MATLAB code constructed for the approximate method is shown in Fig. 2.3 [14].

Table 2.2 Filter initial parameters for 5.5 kW ASD system with soft source (f_s=275Hz)

f_p (Hz)	α	$C_{f\Delta}$ (μF)	L_f (mH)	L_f (%)	L_i (mH)	L_i (%)	Line THD_i(%)	Line DPF
150	0.6	22.2	5.0	6.6	11.9	15.6	4.0	0.94
	0.5	**18.5**	**6.0**	**7.9**	**14.2**	**18.7**	**4.0**	**0.97**
	0.4	14.8	7.5	9.9	17.8	23.3	4.0	0.99
162	0.6	22.6	4.9	6.5	9.3	12.2	5.1	0.92
	0.5	18.8	5.9	7.8	11.2	14.6	5.1	0.95
	0.4	15.1	7.4	9.7	14.0	18.3	5.1	0.98
175	0.6	23.0	4.9	6.4	7.2	9.4	6.6	0.91
	0.5	19.1	5.8	7.6	8.6	11.2	6.6	0.94
	0.4	15.3	7.3	9.6	10.7	14.1	6.6	0.97
200	0.6	23.4	4.8	6.3	4.2	5.6	11.4	0.89
	0.5	19.5	5.7	7.5	5.1	6.7	11.4	0.92
	0.4	15.6	7.2	9.4	6.4	8.3	11.4	0.96

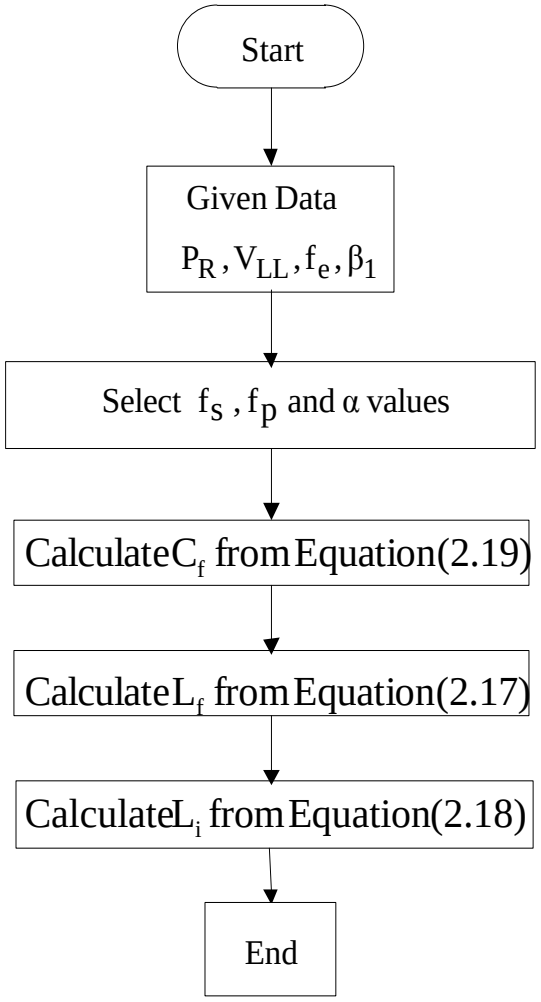

Fig. 2.3 Approximate IBF initial parameters determination method flowchart.

Table 2.3 Initial IBF filter component values for various power rating ASDs (f_s=275 Hz, f_p=150 Hz and α=0.5)

P_R (kW)	5.5	55
L_{ij} (mH)	14.2	1.40
L_{fj} (mH)	6.0	0.60
$C_{fj\Delta}$ (μF)	18.5	185

2.3.2 Accurate Computational Method

The evaluation of the filter performance indices (THDi%, PF and ΔV_o%), for a given values for set of parameters Li, Lf and Cf of Table 2.3, will be through an approximate design method. The approach is based on utilizing accurate filter-ASD system equivalent circuits (in the frequency domain) and evaluating the filter performance for the given set of parameters. Therefore, the whole drive system must be modelled accurately. For steady-state performance investigation, the frequency domain model of the total system involving the AC line, the broadband filter, and the rectifier is established. At steady-state the ASD is modelled with equivalent impedance or current source elements, depending on the frequency considered. Fig. 2.4 and Fig. 2.5 show the fundamental frequency model and the harmonic model of the system at full-load (rated power), while Fig. 2.6 demonstrates the no-load fundamental component model.

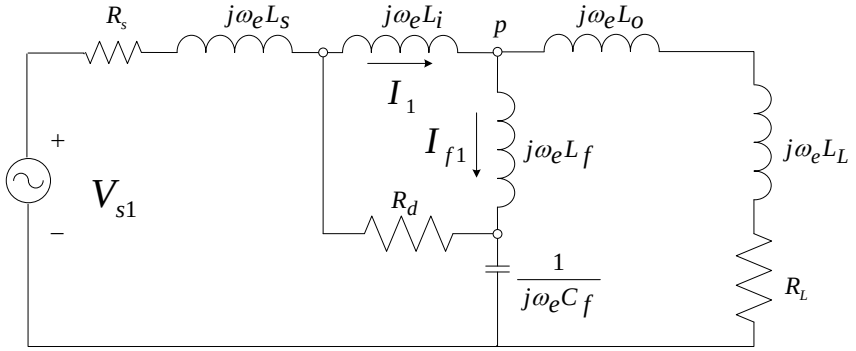

Fig. 2.4 Full-load fundamental frequency model of the ASD system.

In the fundamental frequency equivalent circuit, the ASD is reflected to the AC side of the rectifier as an R-L impedance circuit. Since the DC bus capacitor of an ASD is typically very large and decouples the inverter dynamics from the rectifier side, the drive (DC bus capacitor, inverter, motor load, etc.) is modelled with an equivalent DC resistor [46]. This DC resistor, DC bus capacitor, and rectifier are all reflected to the filter side as the equivalent load resistor R_L and inductor L_L. Assuming that the diode rectifier has unity displacement power factor and the rectifier is lossless, the fundamental component power AC and DC sides can be equated and equivalent load resistor value is found. It is also assumed that the filter is lossless and its terminal

voltage is equal to the nominal voltage. The rectifier commutation effect and output voltage drop are represented with L_L which has been found empirically [44] (Appendix A). These parameters are defined as follows:

$$R_L = \frac{V_{LL}^2}{P_R} \tag{2.20}$$

$$L_L \cong L_i + L_0 \tag{2.21}$$

In the harmonic equivalent circuit of Fig. 2.5, the rectifier side is modelled with a harmonic current source and the grid is represented with a harmonic voltage source. The grid voltage harmonics are selected depending on the utility grid properties. The rectifier current harmonic ratios are chosen from Table 2.1, and the harmonic currents are found by multiplying the harmonic current ratio with the fundamental component current. For each harmonic frequency, the effect of the line-voltage harmonics and rectifier-current harmonics on the circuit is found by superimposing the magnitude (pessimistic approach) of the resulting voltages (or currents). The simplified approach yields satisfactory results [44].

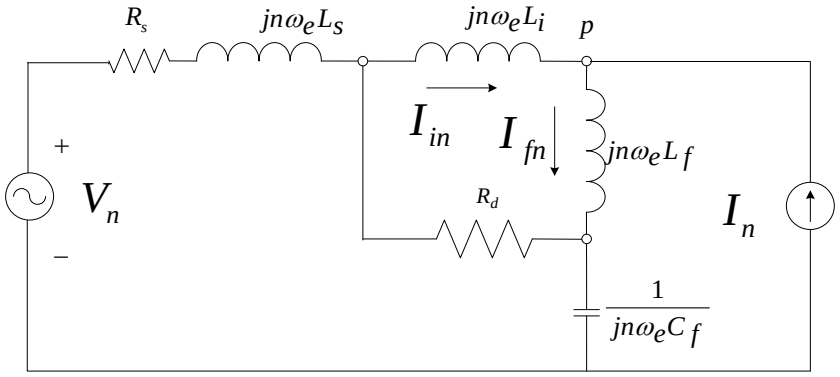

Fig. 2.5 Full-load harmonic frequency model of the ASD system.

With the rectifier and its nonlinear behaviour replaced by linear circuit elements and sources, the steady-state equivalent circuit becomes a linear circuit where closed form calculations and analysis can be made. With all the parameters defined, the circuit can be completely analysed and performance predicted. The damping resistor

Rd is neglected in the steady-state conditions. Its selection criteria are related to transient conditions and are explained in Appendix C.

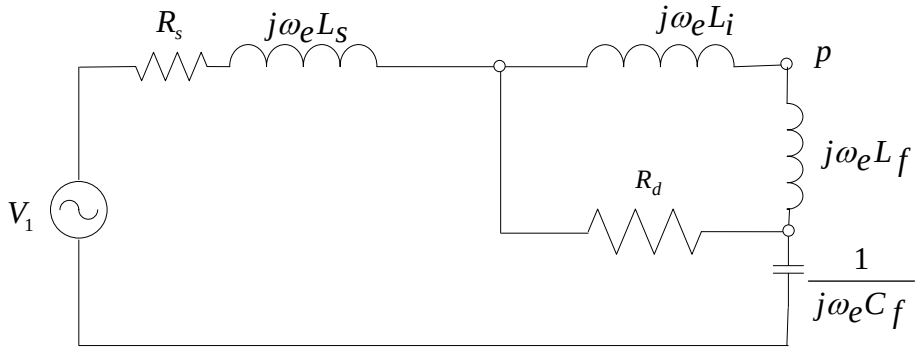

Fig. 2.6 No-load fundamental frequency model of the ASD system.

Utilizing the ASD system equivalent circuits, the mathematical equations needed to calculate the performance of the system for a given set of filter values becomes possible. Thus, the filter component values can be incremented/decremented in the appropriate direction for meeting the given performance criteria in order to find more accurate (optimal) filter values than the approximate ones found in the previous section. The line current THDi value, given in (2.3), is found by calculating the values of the current harmonics injected to the line I_n for a known I_{FL} fundamental component rms value (I_1) and the current harmonics ratios (rectifier stiffness). Calculating the total line and the shunt filter equivalent impedance ratio at each dominant harmonic frequency, the I_n values and then the corresponding line current THD_i% is calculated at full-load.

Calculating the line power factor value at full-load requires the line displacement power factor (DPF) information (cos φ). This is achieved by utilizing the fundamental frequency model, shown in Fig. 2.4. The line PF is calculated by (2.4) assuming that the I_1/I ratio is near unity for a low line THD_i% value design criteria <10 %. Therefore, it is assumed that the line total power factor is practically equal to the input displacement power factor for the assigned low line current THDi% levels (PF≈DPF) in all related analysis throughout the study. Thus, the input displacement power factor angle φ becomes equal to the angle of the input impedance Z_T (impedance seen from the AC line side) at the fundamental frequency. As a result

DPF (cos φ) is calculated. The line current full-load fundamental component rms value I_1 is calculated by the following equation.

$$I_1 = \frac{V_1}{Z_T} \tag{2.22}$$

To calculate the output voltage regulation (ΔV_o %) at the filter node (P), the V_P(NL) and V_P(FL) are calculated using the drive system fundamental frequency equivalent circuits for both loading conditions. At full-load, based on Fig. 2.4 equivalent circuit, the shunt filter current I_{f1} is found as

$$I_{f_1} = \frac{Z_L}{Z_L + Z_f} \times I_1 \tag{2.23}$$

where Z_L is the total load side impedance (involving L_o, L_L, and R_L) and Z_f is the filter impedance (L_f, C_f) both at the fundamental frequency. Consequently, the full-load node voltage fundamental component rms value is given by

$$V_p(FL) = I_{f_1} \times Z_f \tag{2.24}$$

At no-load, based on the equivalent circuit in Fig. 2.6, the node voltage fundamental component rms value is given by

$$V_P(NL) = \frac{V_1}{Z_f + Z_i} \times Z_f = I_{NL} \times Z_f \tag{2.25}$$

where Z_i is the total input impedance (involving Li and the utility line impedance). Finally the output voltage regulation at node P (ΔV_o %) is calculated by (2.5).

Based on the obtained drive system equivalent circuit formulas (2.22-2.25), and for a given set of performance constraints defined previously, the filter values L_i, L_f, and C_f are precisely calculated in MATLAB M-file based computer program that implement the obtained formulas for a given ASD and power system parameters. The algorithm involves an incremental parameter variation procedure.

Since the approximate method gives the first estimate of the values, the optimal filter values are within the proximity of these initial values. Therefore, by linearly incrementing the values and scanning the three dimensional parameter space, the performance is sequentially calculated and the values yielding poor performance are discarded until a sufficiently good performance is obtained that can meet the proposed power quality design criteria. The flow chart of the MATLAB code constructed for the accurate proposed method is shown in Fig. 2.7.

The main advantage of this linear approach of scanning the filter component values space solution, depending on the initial estimated values, is the low number of iterations needed to obtain the optimal parameters. However, the linear nature of this searching method could be considered as the major drawback. This is due to the fact that linear method can be easily trapped in local optima. Therefore, it is necessary to employ more efficient algorithms that may result in a globally optimal filter component values with less size and cost. Consequently, more robust optimization method can be utilized in an attempt to improve the design method results.

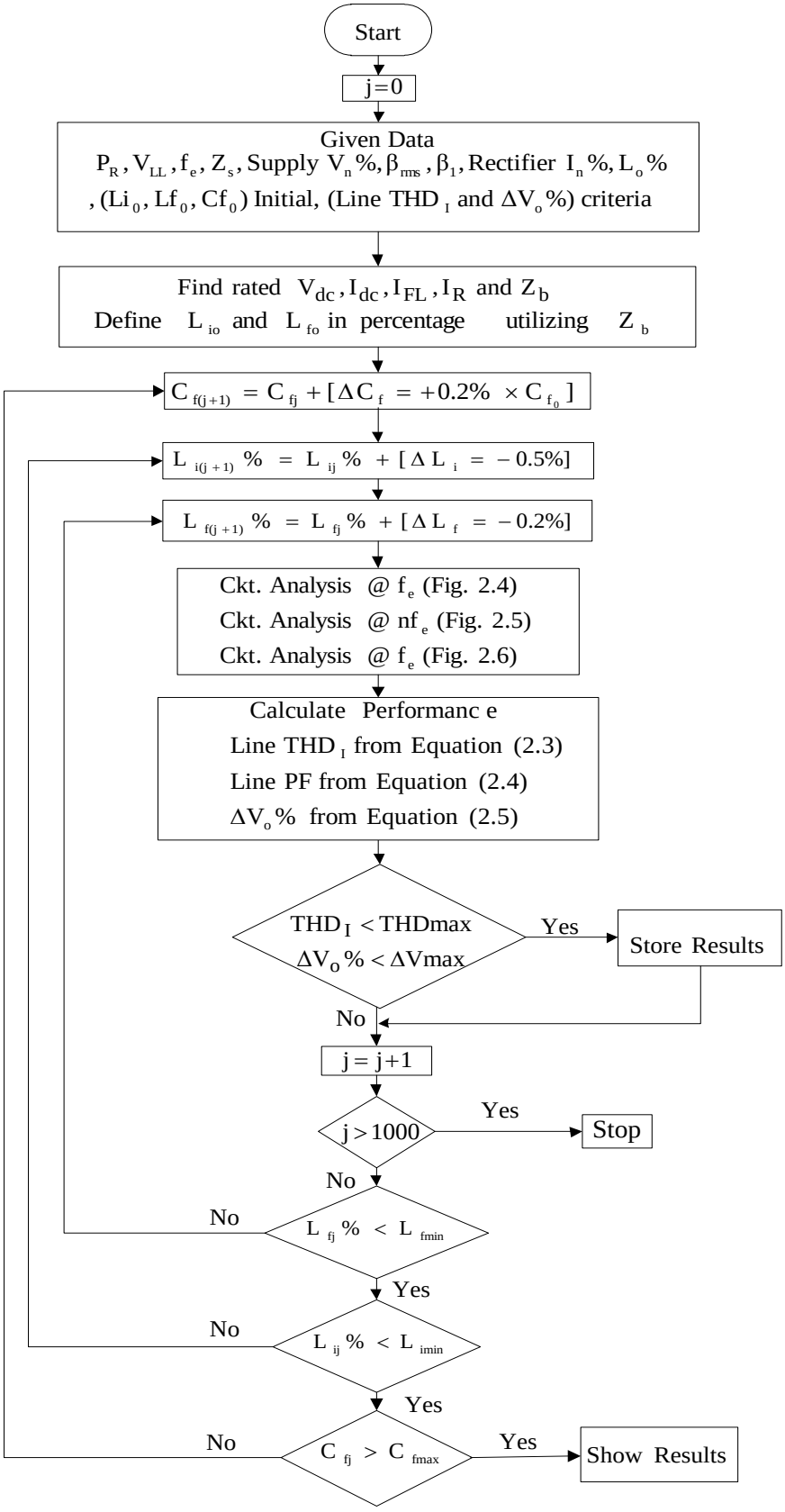

Fig. 2.7 Accurate IBF parameter determination method flowchart.

2.4 **Summary**

In this chapter the improved broadband filter topology has been shown, its operating principle explained, and the linear design method has been reviewed. The design approach is based on a filter-ASD system frequency domain equivalent circuits and evaluating the filter performance for the given set of parameters. The method replaced the nonlinear behaviour of the rectifier by linear circuit elements and sources. Consequently, the steady-state equivalent circuit becomes a linear circuit for which closed form analysis can be performed. With all the parameters defined, the circuit can be provisionally analysed and approximate performance predicted.

The next chapter involves optimization techniques investigation and provides comparisons among the discussed methods in order to select a suitable one to improve the filter design results.

3 OPTIMIZATION TECHNIQUES

3.1 Introduction

Power systems optimization problems are very difficult to solve because of the complex and nonlinear nature of these problems. It is therefore necessary to employ the most efficient optimization methods to take full advantages in simplifying the formulation and implementation of the problem. The use of optimization methods in power system associated issues have been used over the years. They introduced a valued contribution in terms of economics and operation. Generally, the optimization methods are divided into two main categories; the Mathematical Optimization and the Artificial Intelligence Optimization.

3.1.1 Mathematical Optimization Algorithms

The main objective of an optimization problem is to minimize specific effects (cost, size, energy loss, errors, etc.) or maximize others (efficiency, profit, quality, etc.), subject to some constraints. The mathematically precise optimality involved in some algorithms is considered a main advantage of such methods. Usually, several assumptions must be made in order to implement mathematical algorithms to practical power system issues. However, with these assumptions the solutions are not adequately accurate. Also the solutions found are optimum locally, while it is strongly required to be optimum globally. Therefore, it is very difficult for mathematical algorithms to deal effectively with real-word power system optimization problems. Nevertheless, there are many mature mathematical programming techniques, which are proposed to handle ordinary mathematical algorithms drawbacks. These techniques include linear programming (interior point and quadratic programming), nonlinear programming, decomposition technique, integer and mixed integer programming, dynamic programming, etc. In spite of the successes of mature mathematical programming techniques, they could not properly

deal with real-world power system problems which need the optimization technique to have the following features [47]:

1. Storing and utilizing the human knowledge to judge the solutions capability.
2. The high potential of learning and adapting from one solution point to another.
3. Maximum probability of searching most of the solution space.

3.1.2 Artificial Intelligence

Over the years, nature has been a main source of motivation and metaphors for scientific and technical developments. The obvious relation between the brain and neural network system, the camera and the eye, etc., has been well known. Similarly, the method of natural selection and evolution has motivated the development of several Artificial Intelligence (AI) techniques. They can find global optima and are capable of playing the main role in solving power system optimization problems. Recently, many AI techniques have been established such as Expert System, Neural Network, Simulated Annealing and Genetic Algorithm. They all attempt to imitate human reasoning in a way that is beyond conventional computation.

Expert System (ES) is a learning based method which can be provided by sufficient data to work out complicated problems that require human expertise. The ES has the advantages of being permanent and consistent [48]. The main disadvantages, however, are the inability to learn and adapt to new situations because of the knowledge bottleneck.

Artificial Neural Network (ANN) is also a learning-based method, imitating the network neurons and its ability to gain knowledge [49]. ANN has the following advantages; it is fast, has a high capability to learn, and is robust and able to contend with any sort of data. The ANN has some disadvantages such as continuity of producing results even though the input data is unreasonable.

Simulated Annealing (SA) is a searching technique based on the formation of crystals in solids during cooling. The main advantages of SA are its facility to deal with difficult problem, and the possible implementation even with complex systems.

On the other hand, its optima cannot be assured to be the global one. The concrete disadvantage of the SA method is the enormous computing time needed to converge to optimal solution [50]. Furthermore, SA only deals with one individual selection at each iteration rather than population based selection as in Genetic Algorithms approach [51].

A genetic Algorithm (GA) is a global searching technique based on the principle of genetics and evolution. The GA major advantages involve the ability to search from population to population rather from point to point, and the capability to deal with illustrations of the problems rather than the problem itself. This special feature makes GA easy to apply. Moreover, in GA it is difficult to stick in local optima as the solution is randomly developed [52]. The main drawback of GA is that it requires a large amount of time to converge in variety of real world power system problems.

3.2 **Genetic Algorithm**

The GA is a search mechanism based on the principle of natural selection and population genetics. An increasingly better approximation of the desired solution can be produced by applying the principal of survival of the fittest. In each generation, a new set of approximations of the solution are chosen according to fitness evaluation. The more 'fit' the approximation is, the higher likelihood it has to be selected to reproduce the next generation by using operators borrowed from natural genetics (crossover and mutation). Thus, the population of solutions is improved from one generation to the next with respect to their fitness evaluation. So, the least fit individuals are replaced with new offspring, which come from a previous generation, and which are better suited to the evolution of the environment. Fig. 3.1 shows the Genetic Algorithm Flowchart used in this work. In the first step, a set of possible random solutions is created or initial solutions range can be specified. Every solution in the population (which can also be called an individual or a chromosome) is represented by a string of numbers that in turn represent the number of variables in the problem. Every variable is encoded in a suitable coding format (binary, integer, etc.). In the second step, every chromosome is applied to the fitness function (also called the objective function) to produce an output of fitness values. In accordance

with their fitness values a probabilistic technique, such as the Roulette Wheel [53], is used to select the chromosomes ,according to their fitness score, that will contribute to the production of the next generation. The reason for this selection process is to keep the best and most fit chromosomes and increase the number of their offspring in the next generation, eliminating the least fit chromosome. Having selected the parents, the crossover process then takes place by the exchange of genetic information between the selected chromosomes in order to form two new chromosomes (also referred to as children or offspring). This helps to avoid sticking in local optima. In order to ensure that GA will search different zones of the search space, a mutation is applied by randomly selecting and changing the structure of a limited number of chromosomes. This process is repeated until all solutions converge into one optimum solution [47].

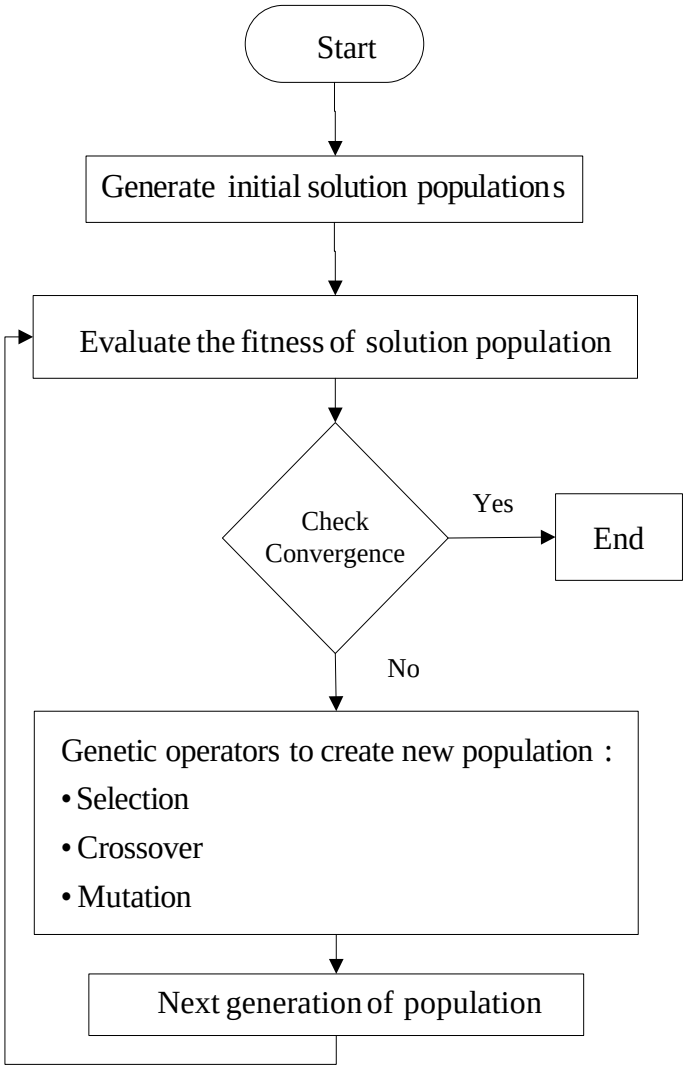

Fig. 3.1 Genetic Algorithm Flowchart

For extra clarification, the three basic operators of genetic algorithms (selection, crossover and mutation) are shown in Fig.3.2 (a, b and c) in an illustrating chromosomes with 8-bit genes, respectively. In GA, by the use of these main operators, the chromosomes in each generation are forced to evolve into a better next generation. The reproduction deals with the process of selection of the fittest chromosome individuals that get inherited in the offspring (children) in the next generation. The number of offspring that an individual selected parent will produce according to its selection rate is defined in this process. In order to avoid being trapped in local optima the crossover operator swaps the individual selected fit parents subsections to produce offspring. The crossover operator is typically applied on a high percentage of the selected parents (80% approximate). Fig. 3.2 (b) shows a common single point crossover process at point C. This implies exchanging selected parents chromosome information (genes) to the right of the point C. In mutation, as shown in Fig. 3.2 (C), a very low number of the selected parents (1% approximate) genes are altered in a random selection process (at a mutation point m) to produce new offspring. This operator is required to give the ability of searching different solution space zones.

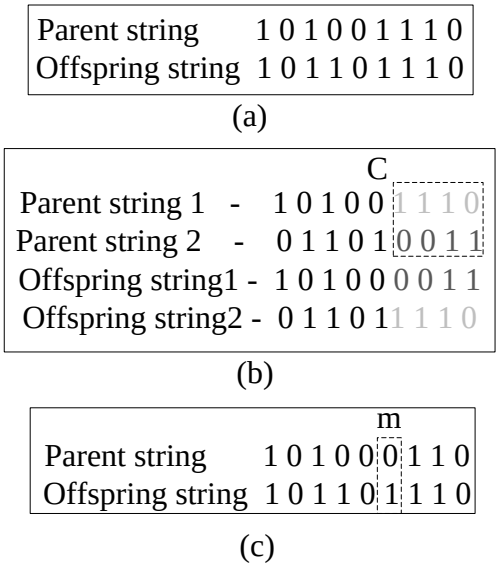

Fig. 3.2 Basic GA operators: (a) Reproduction (b) Crossover (c) Mutation

3.3 Comparison of Genetic Algorithm with Other Optimization Techniques

The majority of Artificial Intelligence techniques are very static. Their architecture is usually designed for one given specific problem that can be solved by the assigned AI method. Therefore, for any changes in the given problem the proposed technique may have difficulties to adapt and learn these amendments. Genetic algorithms were created to cope with such problems. They, in principal, are algorithms based on natural biological evolution. The structural design of systems that implement genetic algorithms is more intelligent to adapt to a wide range of problems [51].Genetic algorithm differs from conventional optimization techniques in the following aspects:

1. GA does not deal with the parameters themselves rather it operates with coded versions of the problem parameters. Specifically, GA works with the coding of a solution set and not with the solution itself.
2. GA always operates on a full population of points (strings) while almost all conventional optimization techniques search from a single point. This plays a major role to enhance the robustness of GA. It helps in avoiding local stationary point and also enhances the chance of reaching the global optimum.
3. GA uses a fitness function for evaluation rather than derivatives. Consequently, they can be applied to any kind of continuous or discrete optimization problem.
4. GA uses probabilistic transition operates rather than deterministic rules while traditional methods apply deterministic transition operates for continuous optimization.

3.4 Advantages and Limitations of Genetic Algorithm

The main advantages of genetic algorithm include [51]:

1. Explore wider solution space.
2. No mathematical restrictions on the properties of the fitness function.

3. Easy to discover global optima and resistant to becoming trapped in local optima.
4. The problem may have multi objective function.
5. Easily modified for different problems.
6. Handles large, poorly understood search spaces easily.
7. Good for multi-modal problems.
8. Very robust to difficulties in the evaluation of the objective function.
9. Requires no knowledge or gradient information about the response surface.
10. Performs very well for large-scale optimization problems and can operate in parallel to speed up processing.
11. Can be employed for a wide variety of optimization problems.
12. Its exceptional ability to be parallelized.

The limitations of genetic algorithm include [51]:

1. The problem of identifying fitness functions.
2. Premature convergence may occur.
3. The problem of choosing the various parameters such as; the size of the population, mutation rate, cross over rate, the selection method and its strength.
4. Cannot use gradients and incorporate problem's specific information easily.
5. Needs to be coupled with a local search technique.
6. Require large number of response (fitness) function evaluations.

3.5 **Summary**

In this chapter an overview on several optimization methods used in a power system related issues has been provided. Background on the Mathematical Optimization, main advantages and major disadvantages has been shown. Various Artificial Intelligence Optimization techniques have been discussed. This involved the Expert System (ES), Artificial Neural Network (ANN), Simulated Annealing (SA) and Genetic Algorithm (GA) methods. More details of the GA method and a comparison with the other optimization techniques have been presented. Finally, advantages and limitations of GA technique detailed.

The next chapter involves implementing the GA method in the IBF design, extracting the ASD system, utilizing the newly designed IBF, performance via detailed computer simulations and laboratory experiments.

4 IMPROVED BROADBAND FILTER DESIGN USING A GENETIC ALGORITHM

4.1 Introduction

The second chapter, previously presented, has discussed the operating principles and a linear design technique of the improved broadband filter (IBF) structure. The complex design process of the IBF has been noticed and the strong trade-off between the different design criteria is illustrated. Consequently, the need for a more sophisticated IBF filter component value searching technique than the linear approach has been identified in an attempt to reduce the size and the cost while maintaining or achieving better power quality performance.

Therefore, the third chapter has investigated different conventional optimization techniques that can be used for similar design problems showing the Genetic Algorithm (GA) approach preferable advantages. The GA searching technique seems to be suitable as it has recently proved robust and effective design of the conventional single tuned shunt filters (STSF) for more problematical operating conditions and special applications [46].

In this chapter, the implementation of the GA searching technique to estimate the IBF filter component values will be presented. Comparison of the GA obtained results with the previous linear method will be illustrated. Moreover, the performance of the new IBF achieved design is under focus. The study will be conducted by computer simulations through detailed modelling of the ASD system. Steady-state performance characteristics will be assessed from light-load to full-load operating conditions. ASD system utilizing the IBF operating under balanced and unbalanced supply voltage with practical voltage harmonic distortion will all be considered. Input power quality (input current THD_i% and power factor), energy efficiency filter output voltage regulation will all be evaluated.

Finally, the experimental performance characteristics of the ASD system using the GA designed IBF under various operating conditions are extracted.

4.2 **Genetic Algorithm implementation**

a) Problem Formulation

The main goal of this optimization problem is to design an improved broadband filter that yields optimal system power quality indices, smaller filter size and minimal harmonic resonance problems. The power quality indices considered in this optimization problem are THDi%, PF and ΔV_o%. The use of these factors facilitates achieving a design with acceptable filter component values. The main filter elements which dominate the design size and performance of the IBF are the inductances L_i, L_f, and the capacitance C_f.

b) Chromosome Encoding and Selection

As mentioned before, the values of the inductance, L_i, L_f, and the capacitance C_f, play a very important role in the design of the improved broadband filter and the performance of ASD system. Therefore, they are considered in the structure of the chromosomes used in this optimization problem.

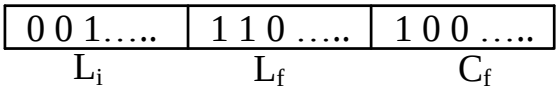

Fig. 4.1 Chromosome structure utilized in GA.

As seen in Fig. 4.1, the number of variables in each chromosome represents the values of the line inductance L_i, and filter inductance L_f, and the filter capacitance C_f, respectively. These values will be initially defined by the GA-Matlab tool box in the first generation for the whole population number selected. Consequently, the chromosome structure of the best fit and selected individuals can be altered to reproduce new offspring using the crossover and mutation GA operators on these

selected highly fitted parents. This process will reproduce new individuals, with higher expected fitness value scores, that will replace the discarded chromosomes from the previous population that have scored low fitness levels.

c) Crossover and Mutation

The crossover value specifies the fraction of the next population that are made up of crossover children, that will replace the least fit chromosomes, by changing the genetic information between the most fit parents selected (reproduction). The crossover method used in this study is a single point crossover (all data beyond a selected point in the parents chromosomes are exchanged). The mutation GA operator randomly changes the structure of limited number of chromosomes to reproduce mutated children to explore wider space solution with different zones. This replacement and reproduction process (selection, crossover and mutation) is conducted every generation of population.

Different values of crossover fraction, varying from 10% to 100%, and mutation rates, from 1% to 10%, have been used in this research project to compare the performance of the proposed GA program. A range of population sizes from 50 to 200 and different numbers of generations varying from 100 to 700 were utilized. It has been observed that higher population and/or generation sizes are not useful causing extra computation time.

A relatively wide range of GA operators was initially used until experience was gained observing their effects. It was found that an appropriate mutation rate would speed up the evolution process and shorten the searching time of GAs. High crossover fractions ($\geq 80\%$) and low mutation rates ($\leq 2\%$) applied on the selected fittest parents each generation achieve the best convergence (as shown later in Fig. 4.4 and Fig. 4.5) for 5.5kW and 55kW ASD systems, respectively, utilizing the IBF topology. In contrast, Fig. 4.2 shows a poor convergence case when the mutation rate is increased to 5% while Fig. 4.3 shows similar low convergence as the crossover fraction is reduced to 10%. These GA operators are applied to 200 generations with 100

populations for each generation. In modern computers, this computational requirement can be completed in a few minutes.

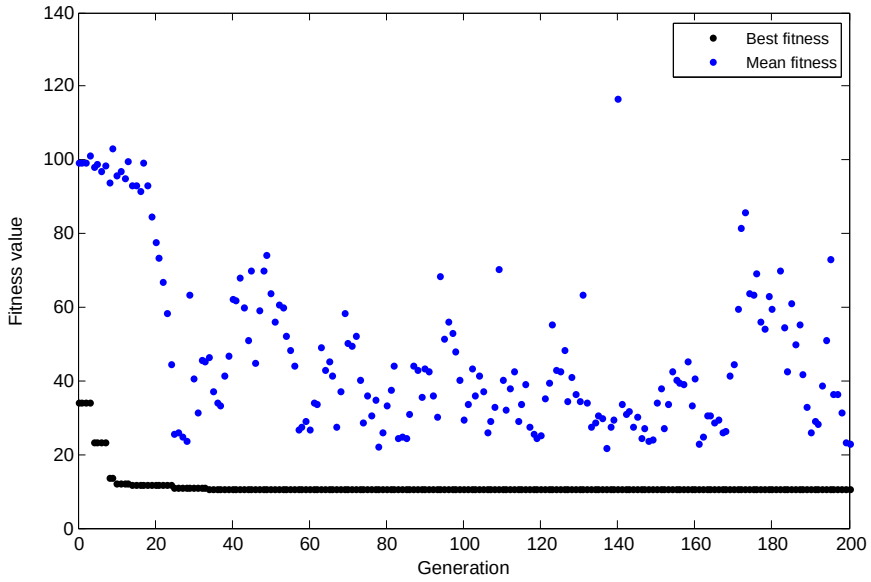

Fig. 4.2 Best and mean fitness function curves in GA for 5.5kW ASD system with high mutation rate (5%).

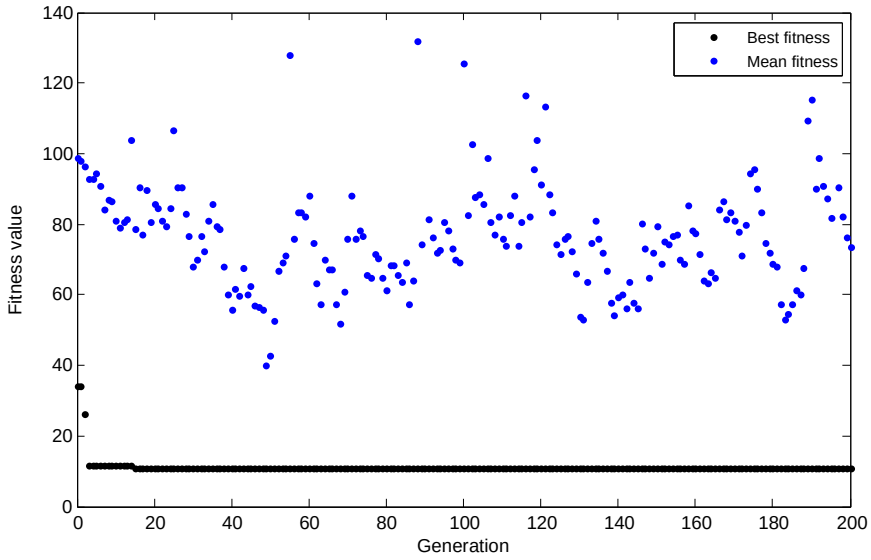

Fig. 4.3 Best and mean fitness function curves in GA for 5.5kW ASD system with low crossover fraction (10%).

d) Fitness Function

The objective of the fitness function illustrated by (4.1) in the proposed GA program is to find out the minimum line current THDi%, the minimum voltage regulation and the maximum line PF.

$$Fitness = THD\% + \Delta Vo\% + \left({}^{1}/_{PF}\right) \quad (4.1)$$

Every chromosome in the current generation will be examined by the above fitness function. To calculate the filter performance indices (THDi%, ΔV_o% and PF) in the fitness function via some mathematical models, the approximate design method described in section 2.3.2 is used.

e) Genetic Algorithm Output

For given ASD ratings and power system parameters, based on the system equivalent circuits shown in section 2.3.2, the filter-component values for L_i, L_f, and C_f are initially proposed in a GA MATLAB [45] M-file based computer program. It has been observed that initial parameter range should be obtained and specified in the GA tool box in order to achieve expected results. This is consistent with one of the GA limitations mentioned earlier in section 3.4.

The GA based program uses the system equivalent circuits derived formulas (in section 2.3.2), calculates the required impedances, then voltages, and currents followed by performance calculation (THDi%, PF, ΔV_o%). Based on the performance obtained, every set of solutions (chromosome) in the current generation will be examined by the fitness function of (4.1). Each chromosome fitness score will be normalized with the total population fitness score and a corresponding area in the roulette wheel selection method will be assigned to the chromosome (i.e. the higher the fitness score the higher the probability of being selected in the next generation). The filter component values are varied by the crossover and mutation GA operators from generation to another until the objective of the fitness function is globally optimized with suitable convergence.

The proposed design method with the GAs searching technique was evaluated for 5.5kW and 55kW ASDs power ratings. The utility line was considered to have 3% voltage THD_V. The grid impedance was considered to be negligible compared to the impedance of the input inductance L_i. The first step involves using the linear approach (described in section 2.3) to obtain IBF filter component values that can exhibits the best power quality performance criteria. Therefore, the minimum line current THDi% and voltage output regulation ΔV_o% was implemented to estimate the filter component values. The achieved results involve system power quality indices of line current THDi $\leq$ 6.75% and filter output voltage regulation $\Delta V_o \leq 4\%$ (line power factor (PF) or DPF is inherently correlated to this criteria and is expected to be > 0.98). It is noticed that no results can be obtained by the linear method for better power quality criteria. The second step, involves using the obtained filter component values by the linear method as initial parameters in the GA tool box and implementing the previously described GA operators' values, selection technique and fitness function (equation 4.1).

Fig. 4.4 shows the 5.5kW ASD power rating GA fitness curve (applying 80% crossover and 1.12% mutation reproduction rates on the selected fittest parents). The optimized solution is obtained in generation number 126 and the whole population ultimately converges toward the optimized solution. The corresponding filter values obtained are L_i (10.1mH), L_f (8.1 mH) and $C_{f\Delta}$ (16.6 µF). The resultant series resonance frequency f_s and parallel resonance frequency f_p values are 250Hz and 167Hz, respectively. Similarly, Fig. 4.5 shows the 55kW ASD power rating GA fitness curve (applying 80% crossover and 0.5% mutation reproduction rates on the selected fittest parents). The optimized solution is achieved in generation number 134 and the entire population eventually converges toward the optimized solution. The obtained filter values are L_i (1.138mH), L_f (0.75 mH) and C_f (180 µF). The resultant series resonance frequency f_s and parallel resonance frequency f_p values are 250Hz and 163Hz, respectively. It is very important to notice that in both power rating cases the f_p values show that the harmonic resonance problem risk is negligible for the system.

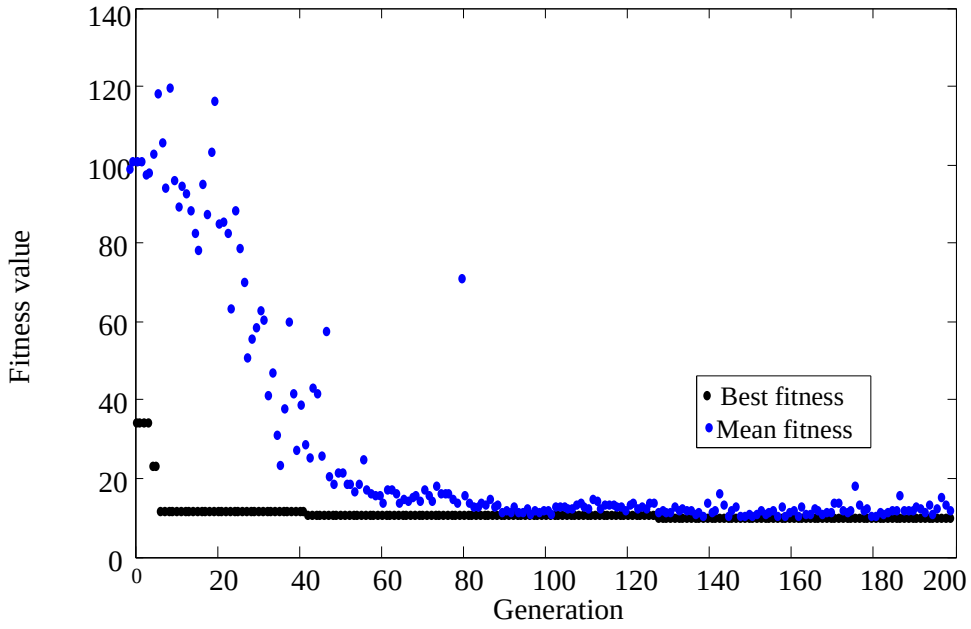

Fig. 4.4 Best and mean fitness function curves in GA for 5.5kW ASD system.

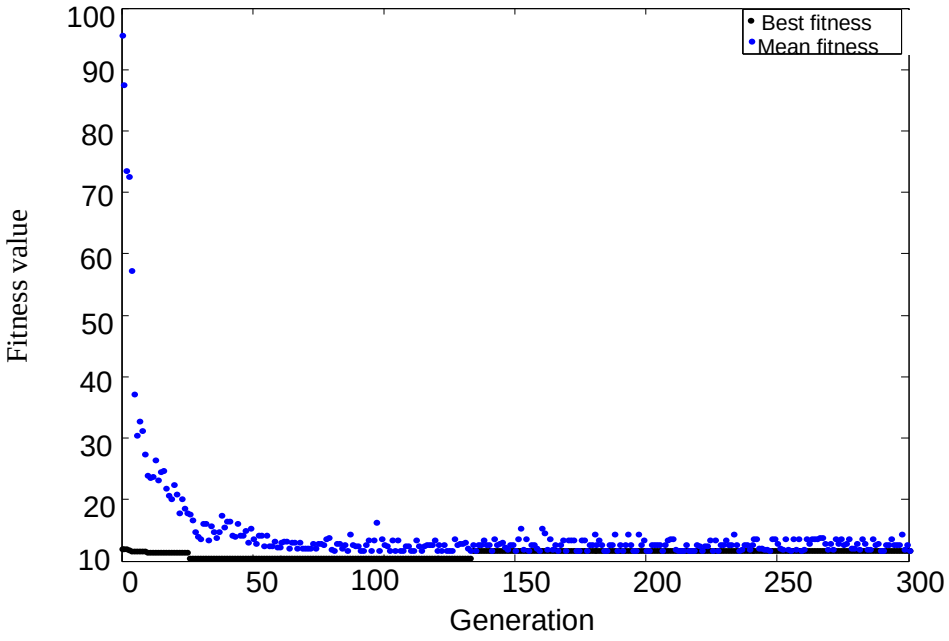

Fig. 4.5 Best and mean fitness function curves in GA for 55kW ASD system.

In order to compare between the linear approach and the GA approach results, the utilized linear method MATLAB code results for the 5.5kW and 55kW power ratings with the maximum achievable power quality indices design criteria are represented. It has been observed that no results can be obtained for better than those shown below to meet the power quality criteria. The code displays the following results:

enter the ASD rated power value in kW:5.5

enter the line current THDi limit value (THDi-max%): 6.75

enter the output voltage regulation limit value (DelVmax%): 3.75

PLEASE WAIT

Results are:

Columns 1 through 6

'Results'	'Li(mH)'	'Lf(mH)'	'Cf(µF)'	'THDi'	'DelVo'
[1]	[10.6123]	[5.9822]	[21.0297]	[6.7250]	[3.4784]
[2]	[10.6123]	[5.9822]	[21.0660]	[6.6941]	[3.4790]
[3]	[10.6123]	[5.9822]	[21.1024]	[6.6636]	[3.4796]

Columns 7 through 9

'PF'	'fp'	'fs'
[0.9663]	[155.5467]	[259.0678]
[0.9665]	[155.4124]	[258.8440]
[0.9666]	[155.2783]	[258.6208]

enter the ASD rated power value in kW:55

enter the line current THDi limit value (THDi-max%): 6.5

enter the output voltage regulation limit value (DelVmax%): 4.0

PLEASE WAIT

Results are:

Columns 1 through 6

'Results'	'Li(mH)'	'Lf(mH)'	'Cf(µF)'	'THDi'	'DelVo'
[1]	[1.1388]	[0.5982]	[208.1136]	[6.4775]	[3.9051]
[2]	[1.1388]	[0.5982]	[208.4774]	[6.4477]	[3.9058]
[3]	[1.1388]	[0.5982]	[208.8412]	[6.4182]	[3.9064]

Columns 7 through 9

'PF'	'fp'	'fs'
[0.9663]	[152.8292]	[260.4230]
[0.9665]	[152.6958]	[260.1957]
[0.9666]	[152.5627]	[259.9690]

The new IBF filter values, obtained by the GA searching method, of the 5.5kW and 55kW ASD power rating and the expected correlated system performance results are presented and compared to the linear searching method results in the next section.

4.3 **Comparison of Different Searching Methods Results**

The IBF filter component values obtained with both methods for 5.5 and 55kW power rating ASDs are shown in Table 4.1. Reductions of (5-15)% in the input inductance L_i parameter and (15-20)% in filter capacitance C_f parameter have been achieved. Consequently, the filter inductance L_f parameter will increase to keep the series resonance frequency (f_s) within its desired and effective values. Nevertheless, the value of L_f is much smaller than L_i for all power ratings. Since the input inductor is carrying the full line-current while the filter inductor is carrying only the harmonic-current components (< 50% of rms rated line value), a reduction in L_i is more valuable and results in a smaller filter size, and therefore lower cost. As the filter capacitor presents the major cost of the IBF filter topology, its considerable value reduction is also very effective in reducing the size and cost, improving the system power factor characteristics and reducing output voltage regulation from no-load to full-load. Tables 4.1 and 4.2 allow a comparison between the performances of the two searching methods.

Table 4.1 IBF component values

P_R (kW)	5.5		55	
Searching method	Linear	**GA**	Linear	**GA**
L_i (mH)	10.6	**10.1**	1.138	**0.99**
L_f (mH)	6.0	**8.1**	0.598	**0.75**
$C_{f\Delta}$ (µF)	21	**16.6**	208	**180**

Table 4.2 Performance comparison of ASD system utilizing IBF

Searching method	THD_i %	PF≈ Cosφ	ΔV_o %	fp (Hz)	fs (Hz)
Linear	6.5 – 6.75	0.95 – 0.96	3.5 - 4.0	153-156	259-260
GA	**6.0 - 6.50**	**0.98 - 0.99**	**3.0 - 3.2**	**163-167**	**250**

As the tables indicate, the GA algorithm is capable of finding smaller values for the more bulky filter components and meanwhile achieves better power quality indices.

4.4 **Computer Simulations and Performance Evaluation**

In this section, the focus will be on the performance of the selected 4% AC line reactor (Lac) and the IBF filter. A detailed model of the ASD system (rectifier, DC-link and inverter) will be utilized in the computer simulations. The steady-state performance characteristics under different operating and loading conditions (from light-load to full-load) will be investigated. Conventional voltage supply harmonics (3% THDv) along with balanced and unbalanced voltage supply conditions will be considered. Furthermore, assessing the ASD line total harmonics distortion and power factor, IBF filter energy efficiency and output voltage regulation will be conducted.

The 3% THDv considered supply voltage distortion is implemented by considering practically the first four dominant voltage harmonic components (5^{th}, 7^{th}, 11^{th} and 13^{th}) only. Lower components will have higher ratios of the fundamental component (2.2%, 1.3%, 1.1% and 0.9%), respectively. The 5^{th} and 11^{th} voltage harmonics components are negative sequence while the 7^{th} and 13^{th} voltage harmonic components are positive sequence. Therefore, the voltage harmonic components phase angles are assigned accordingly in the simulation model. The considered dominant voltage harmonics magnitudes and phase angles are modelled as voltage sources connected in series with the main voltage supply. The investigation involves two ASD power ratings (5.5 kW and 55 kW) and the corresponding supply source impedance parameters are shown in Table 4.3.

Table 4.3 Source impedance parameters for 5.5 kW and 55 kW power ratings

Power rating (kW)	5.5	55
L_s (μH)	100	10
R_s (mΩ)	50	5.0

In an attempt to increase the system modelling accuracy, the 4% AC line reactor and the IBF filter components are modelled by adding their internal resistance assuming 99% component energy efficiency concept (1% losses at rated component voltage and current). However, an equivalent load resistor connected to a switch is used to

model the inverter side. This conventional method [46] is acceptable due to the fact that the large DC bus capacitor used decouples the PWM dynamics of the drive from the rectifier side (in practice interference between the DC capacitor and PWM-INV dynamics can exist). Based on theory, the value of the rectifier DC-link capacitor is selected with minimum of 50uF/kW [12]. From the market data survey of industrial ASD products, the DC-link capacitance can vary from (75 to 360) μF/kW [54]. According to recent industrial information the 5.5kW DC-link capacitor is selected to have 1mF capacitance and, consequently, 10mF is selected for the 55kW power rating. In all cases, a 2% DC-link inductor (L_{dc}) is considered to increase the effectiveness of the filtering methods. Therefore, the L_{dc} has a 1.52mH and 0.15mH for the 5.5kW and 55kW power ratings, respectively.

The computer simulation package program Ansoft-Simplorer (student 7^{th} version, SV7) has been used for modelling [55]. The power electronic circuit simulator in the program is based on a graphic window. The computer simulation software contains a circuit schematic diagram window (ssh file), a graphic view window (view file), and the Day-postprocessor window.

The circuit is drawn and simulation parameters are given in the schematic window, while the simulation waveforms are displayed via an oscilloscope in the graphic window. Finally, data analysis means for the purpose of estimating currents and voltages values, power factor, harmonic spectrum, THDi%, etc, are provided in the Day-postprocessor window.

The trapezoidal integration method is selected in the computer simulation with a low step size in order to increase the accuracy level. The selected simulation end time ensures that the steady-state of the modelled system is reached and all calculations are carried out through this operating condition (excluding transient results) for the purpose of better accuracy results. Extra properties parameters are shown in Fig. 4.6.

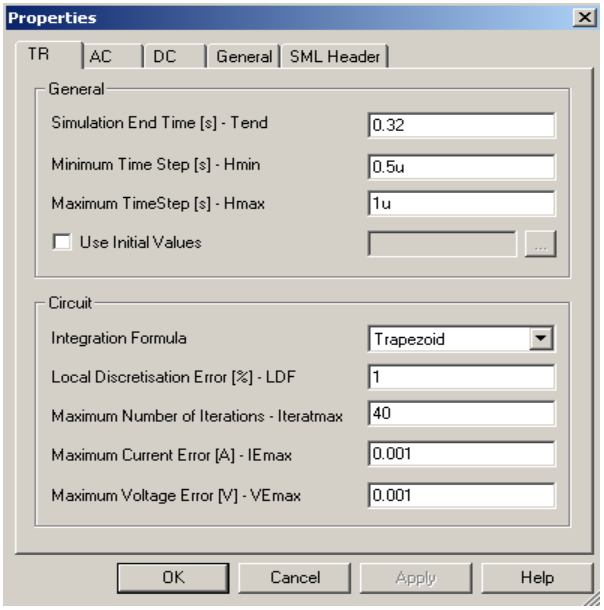

Fig. 4.6 Simulator integration method and its computational parameters.

4.4.1 AC Line Reactor Filter Based ASD System

In this section, as a preliminary step, the ASD system utilizing a three-phase 4% AC reactor (Lac) filter is under investigation. The performance analysis of the system is demonstrated under practically distorted balanced supply voltage (3% THDv). Simulation waveforms of line current and voltage along with calculated performance indices are presented. The AC line reactor filter inductance and DC load resistance implemented values in the simulation circuit for 5.5kW and 55kW power ratings are shown in Table 4.4. These parameters along with shown in Table 4.3 are implemented in the simulation circuit shown in Fig. 4.7.

Table 4.4 AC line reactor (4% Lac) filter values and load resistance values

Power rating (kW)	5.5	55
AC reactor L_{ac} (mH)	3.1	0.31
DC inductor L_{dc} (mH)	1.52	0.15
DC Capacitor C_{dc} (mF)	1.0	
Load resistor R_L (Ω)	45	4.5

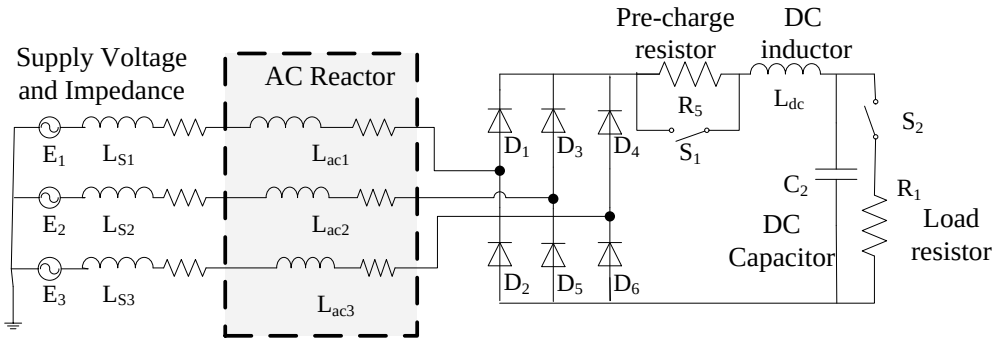

Fig. 4.7 Simulation circuit for ASD system utilizing 4%Lac filtering method.

The simulation results of the 5.5kW ASD system utilizing the 4% AC three-phase reactors are extracted and presented. The full-load line current and supply voltage simulation waveforms are shown in Fig. 4.8. While the DC side current (I_{dc}) and voltage (V_{dc}) rectifier outputs are shown in Fig. 4.9. This simple and basic filtering method can relatively smooth the line current reducing the current THDi% value to 33% and boost the line power factor to 0.93 lagging. Table 4.5 shows the full-load performance of this filtering method for both 5.5kW and 55kW ASD ratings.

However, even though that these results are improved power quality indices with respect to the basic ASD system that utilize no filtering techniques (> 80% THDi and 0.6 lagging PF), the achieved performance cannot comply with the power quality standards. Therefore, the use of more sophisticated passive filter structures is inevitable and mandatory.

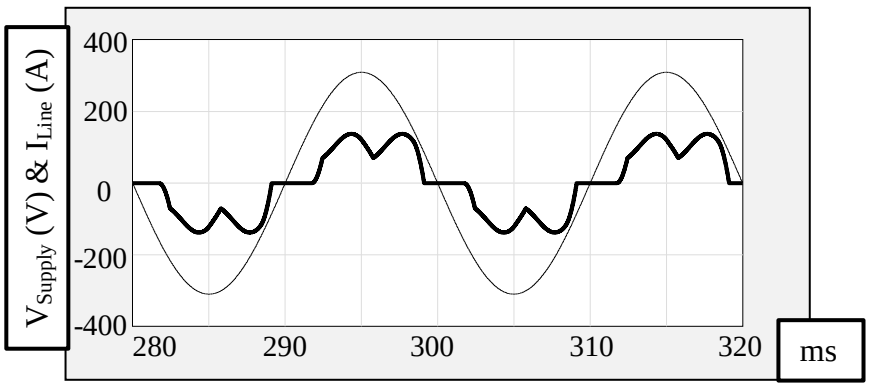

Fig. 4.8 Line current (**bold**) and supply voltage simulation waveforms at full-load for 5.5kW rated system employing 4%Lac (current scale: 10x).

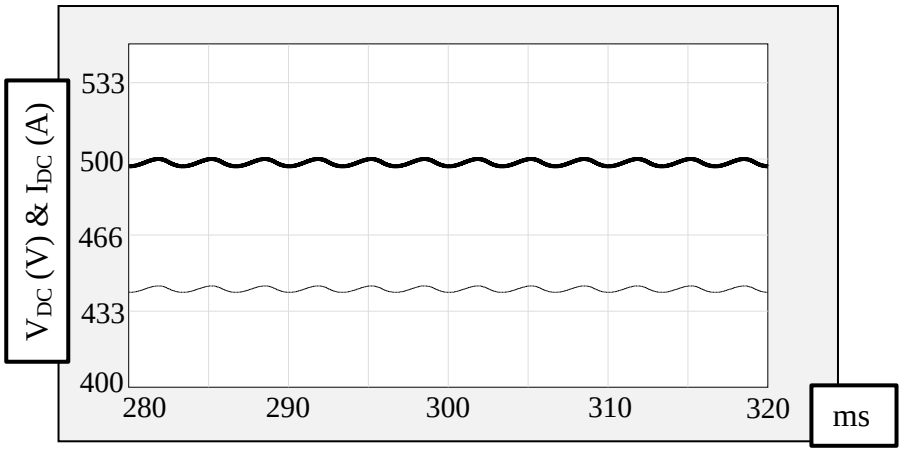

Fig. 4.9 DC load current and voltage (**bold**) simulation waveforms at full-load for 5.5kW rated system employing 4%Lac (current scale:40x).

Table 4.5 Full-load performance of 4% AC line reactor filter for 5.5kW and 55kW power ratings

Power rating (kW)	5.5	55
Line THD_i%	32.6	33.0
Line PF	0.929	0.928
Output V_{dc} (V)	498	499

4.4.2 IBF Full-Load Simulations of 5.5 kW ASD System

In this section, the ASD system utilizing the IBF filter with its new reduced filter component values obtained by the GA method, explained in section 4.2, is under investigation. The system performance is evaluated under balanced and unbalanced supply system conditions with the 3% THDv existence. The 5.5kW IBF reduced parameters shown in Table 4.1 are implemented in the simulation circuit presented in Fig. 4.7. The damping resistor (Rd) of 300 ohms resistance value (maximum) has been selected from Table C.1 (AppendixC) and implemented in the simulation circuit in order to minimize the filter power losses.

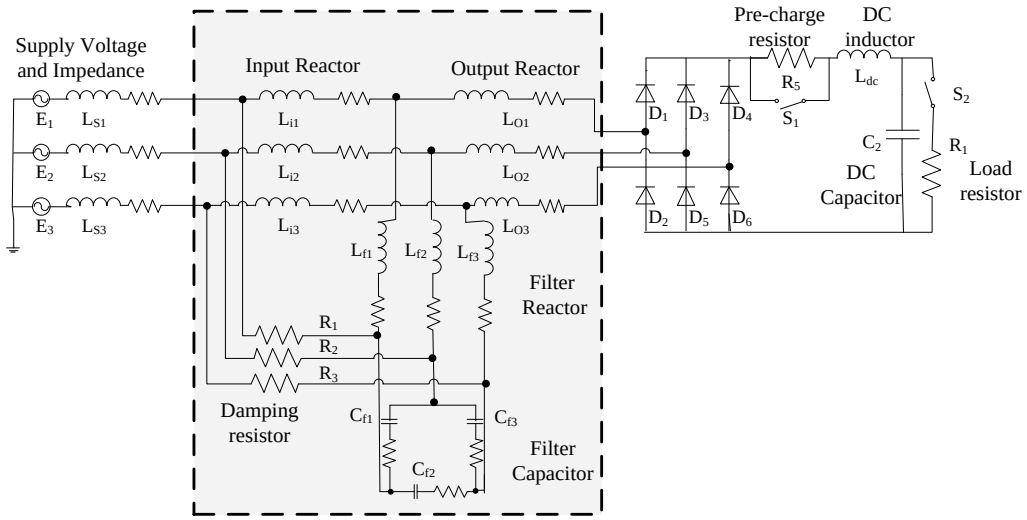

Fig. 4.10 Simulation circuit for ASD system utilizing IBF.

The simulation waveforms of the rated line current and rectifier side current are illustrated in Fig. 4.11. As the waveforms reveals, the IBF filter effect is obvious in smoothing the distorted rectifier current and preventing its harmonic components to appear in the line side. As a result, line current has a very low THDi% value (5.35%) and the rectifier side current 33% THDi value has been dramatically reduced. Moreover, Fig. 4.12 shows the rated line current and supply phase voltage simulation waveform. The line-side power factor is nearly unity (0.996) at full-load operating condition. These simulation based results verify the accuracy of the system modelling and parameter estimation procedure as they are closely linked with the analytical results shown in Table 4.2.

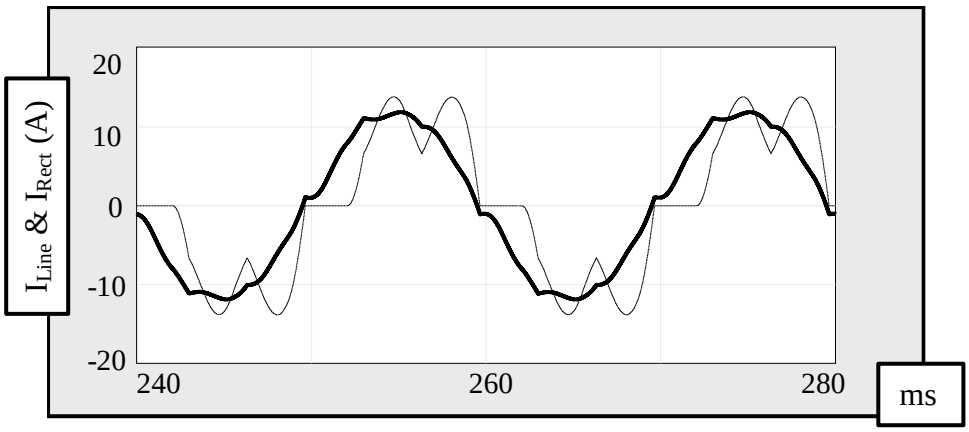

Fig. 4.11 Line (**bold**) and rectifier current simulation waveforms at full-load for 5.5kW rated system employing IBF.

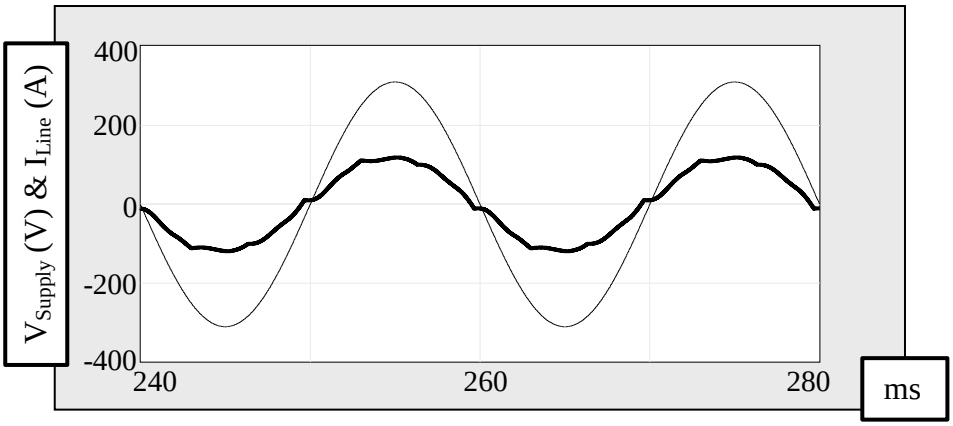

Fig. 4.12 Line current (**bold**) and supply voltage simulation waveforms at full-load for 5.5kW rated system employing IBF (current scale: 10x).

The load side simulation results are also obtained. Fig. 4.13 shows the full-load DC current and voltage waveforms with appropriate current scaling factor. The DC output voltage is 507V which is slightly higher than the 4% Lac filtering method DC output voltage (498V). This is due to the existences of the relatively large filter capacitor (C_f) that can boost the voltage and compensate the utilized line reactors (L_i and L_o) voltage drops.

Finally, the full-load filter capacitor current and voltage simulation waveforms are shown in Fig. 4.14. While the full-load rectifier current and rectifier line-to-line voltage simulation waveforms are shown in Fig. 4.15.

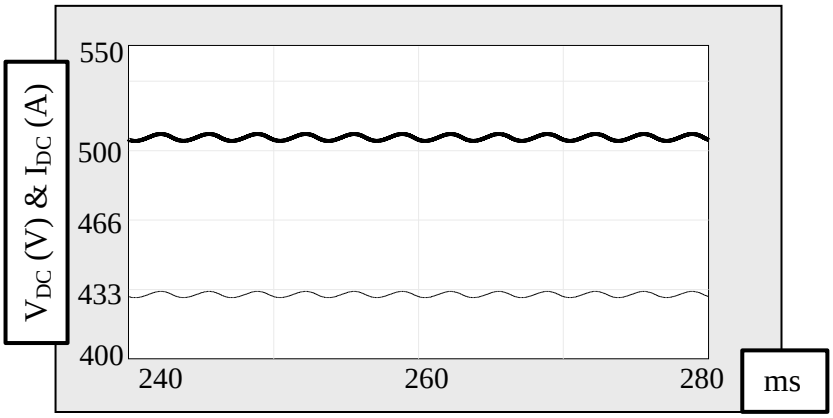

Fig. 4.13 DC load current and voltage (**bold**) simulation waveforms at full-load for 5.5kW rated system employing IBF (current scale: 40x).

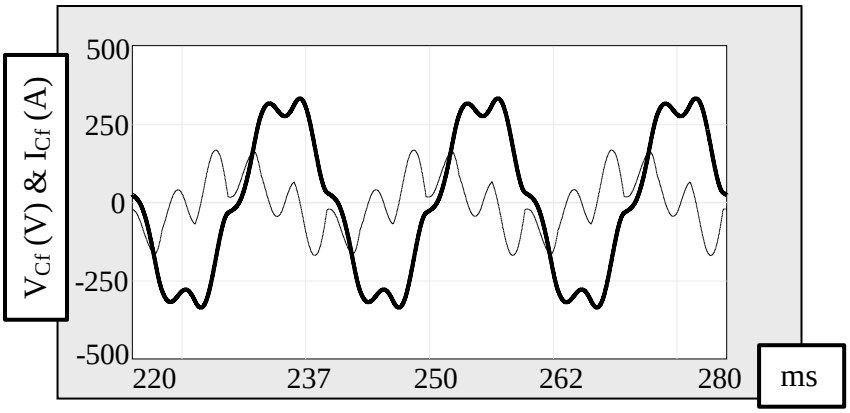

Fig. 4.14 Filter capacitor current and voltage (**bold**) simulation waveforms at full-load for 5.5kW rated system employing IBF (current scale: 20x).

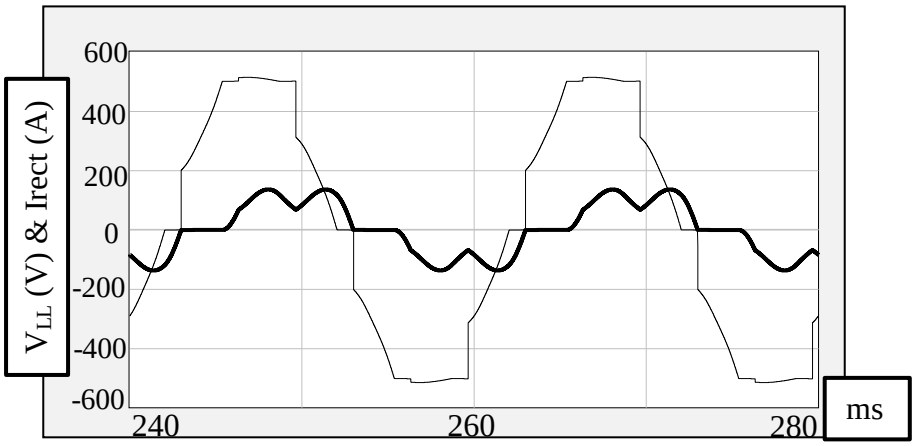

Fig. 4.15 Rectifier current (**bold**) and line-to-line voltage simulation waveforms at full-load for 5.5kW rated system employing IBF (current scale: 10x).

According to the presented simulation results, the IBF structure with its new reduced parameters (by using the GA method previously described) still has the ability to maintain its superior performance at full-load (5.35% THDi and unity PF) compared to the 4% Lac filter topology (>32% THDi and 0.93 lagging PF) or the conventional single tuned filters (>12% THDi and 0.95 lagging PF) [56].

4.4.3 IBF Light-Load Simulations of 5.5 kW ASD System

In this section, the light-load (10%) operating condition simulation results and waveforms are demonstrated. This operating condition is achieved by increasing the load resistance by a multiplication factor of 10. Fig. 4.16 shows the light-load line current and the supply phase voltage simulation waveforms. The line current has a

low THDi% value of < 10% as the filter large input reactor (L_i) isolates the filter and attenuates the supply current harmonics. However, the line power factor is quite low and leading (0.269) as a result of considerable current drawn by the filter capacitors.

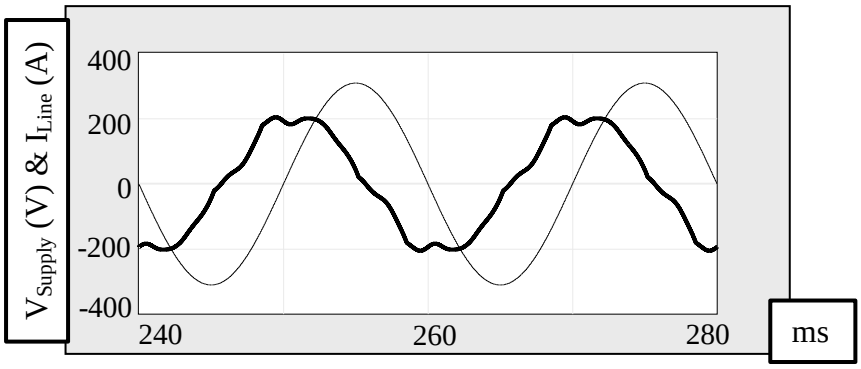

Fig. 4.16 Line current (**bold**) and supply voltage simulation waveforms at 10% load for 5.5kW rated system employing IBF (current scale: 40x).

4.4.4 IBF Full-Load Simulations of 55 kW ASD System

In this section, the 55kW power rated ASD system is under assessment process, similar to what has been described earlier, in an attempt to extract the ASD system performance characteristics at different operating conditions. The 55kW IBF obtained new optimal filter values (less in size and cost) shown in Table 4.1 are applied in the simulation circuit shown in Fig. 4.7. In addition, to maximize the IBF efficiency, the maximum damping resistor (Rd) of 40 ohms is selected from Table C.1 (Appendix C).

The full-load line current and rectifier current simulation waveforms are shown in Fig. 4.17. Similarly to the previous 5.5kW results, the 55kW ASD system draws nearly a sinusoidal line current, by installing the IBF, with very low total harmonic distortion index (5.37%). Therefore, the 55kW IBF is greatly capable to reduce the rectifier side current waveform harmonic distortion (33%) to this improved line side harmonic distortion value. On the other hand, the full-load line current and the supply phase voltage simulation waveforms are shown in Fig. 4.18. As the graph reveals, the waveforms are almost in-phase with a line power factor value of 0.992 leading. These results are also correlated with Table 4.2 presented analytical results.

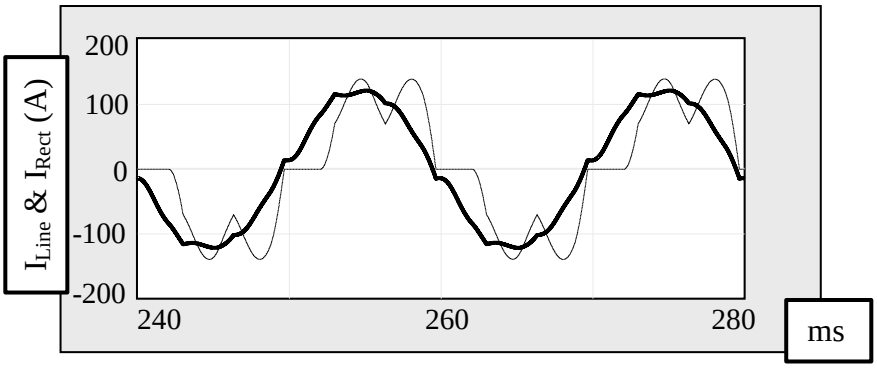

Fig. 4.17 Line (**bold**) and rectifier current simulation waveforms at full-load for 55kW rated system employing IBF.

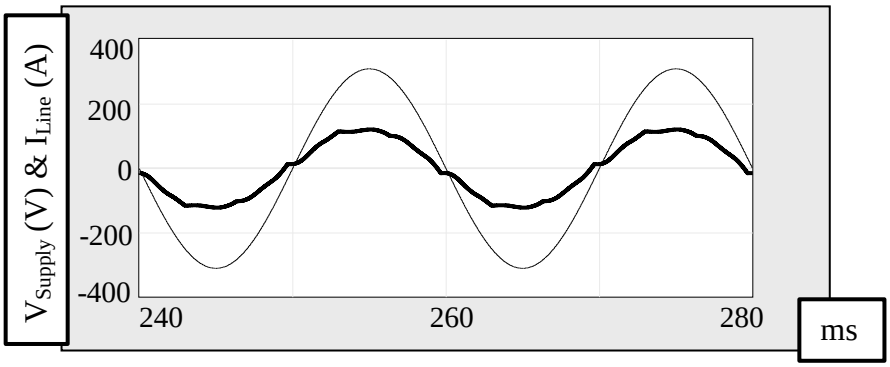

Fig. 4.18 Line current (**bold**) and supply voltage simulation waveforms at full-load for 55kW rated system employing IBF.

The rated load DC voltage and DC current simulation waveforms are shown in Fig. 4.19. Similarly, the DC output voltage (V_{dc}) is negligibly boosted by the filter capacitor to 506V with respect to the 4%Lac filter output DC voltage (498V). In addition, Fig. 4.20 shows the full-load filter capacitor current and voltage simulation waveforms. Finally, the rectifier current and rectifier line-to-line voltage simulation waveforms are shown in Fig. 4.21.

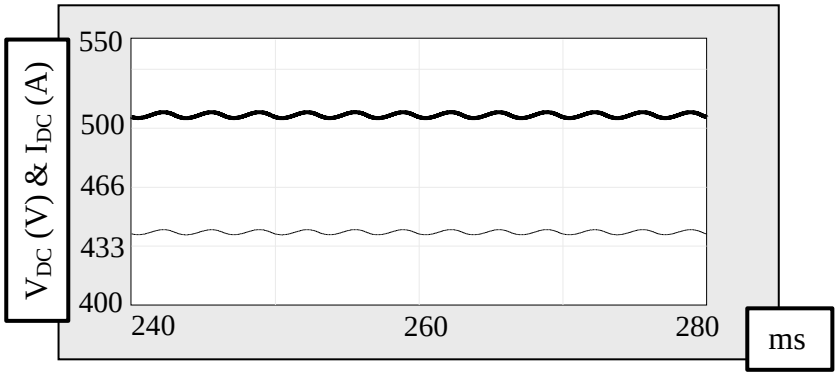

Fig. 4.19 DC load current and voltage (**bold**) simulation waveforms at full-load for 55kW rated system employing IBF (current scale: 4x).

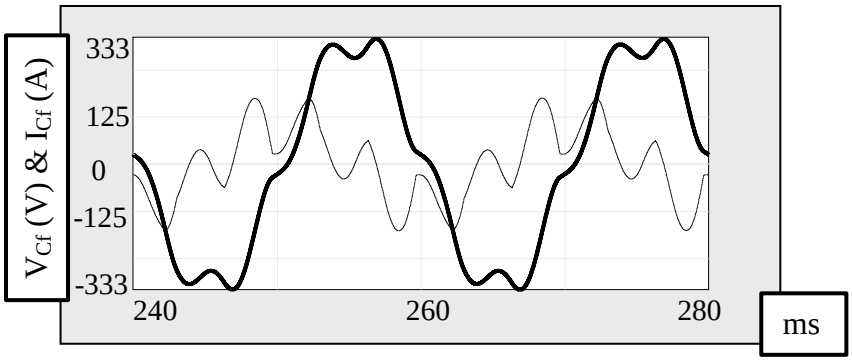

Fig. 4.20 Filter capacitor current and voltage (**bold**) simulation waveforms at full-load for 55kW rated system employing IBF (current scale:2x).

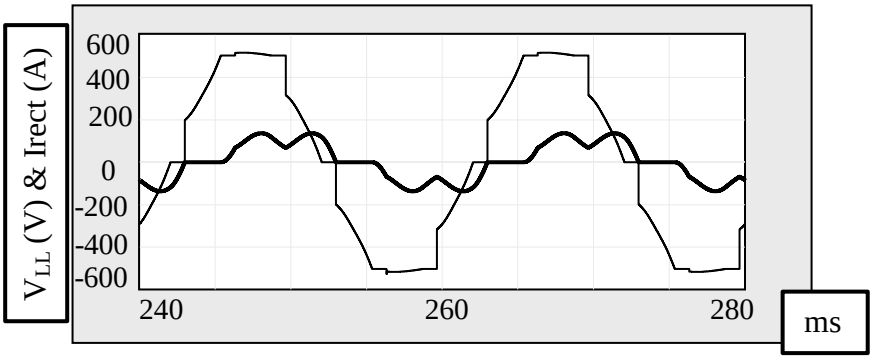

Fig. 4.21 Rectifier current (**bold**) and line-to-line voltage simulation waveforms at full-load for 55kW rated system employing IBF.

4.4.5 IBF Light-Load Simulations of 55 kW ASD System

This section illustrates the light-load (10%) operating condition simulation waveforms and results for 55 kW power rating ASD system utilizing the IBF topology. The light-load line current and the supply phase voltage simulation waveforms are shown in Fig. 4.22. The line current has a low THDi value of 8.7% at this loading condition and the filter succeeds to suppress the utility current harmonics. However, as shown in the diagram, the line power factor is very low at this light loading condition (0.247 leading).

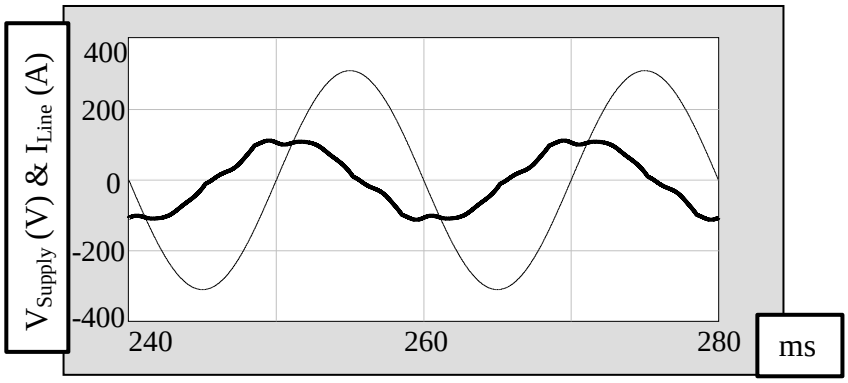

Fig. 4.22 Line current (**bold**) and supply voltage simulation waveforms at 10% load for 55kW ASD system employing IBF (current scale: 2x).

Finally, the half-load operating condition simulation study has been conducted for both ASD power ratings systems and the obtained results are shown in Appendix D.

In conclusion, the main power quality indices simulation results for the 5.5kW and 55kW ASD system at full-load utilizing the new reduced IBF filtering technique are summarized in Table 4.6. In addition, the analytical equivalent circuit's results based method are presented and compared to the computer simulation results method. It is apparent that both results are in good agreement with relatively little difference. The pessimistic approach of the effect of the line-voltage harmonics (superimposed with the rectifier-current harmonics magnitudes) considered in the analytical design approach have slightly increased the line THDi% values with respect to the simulation results where voltage harmonics components are implemented using the magnitude and phase angles.

Table 4.6 Full-load performance comparison for 5.5kW and 55kW power rating ASD systems using IBF structure based on analytical and computer simulation results

P_R(kW)	5.5			55		
Power Quality Indices@ F.L.	Line THD_i%	Line PF	ΔV_o %	Line THD_i%	Line PF	ΔV_o %
Analytical Results	6.00	0.980	3.00	6.50	0.990	3.20
Simulation Results	5.35	0.996	3.51	5.37	0.992	3.56

4.4.6 IBF Simulations Under Unbalance Supply Voltage

The last stage of evaluating the ASD system utilizing IBF performance involves the operation under unbalance supply voltage condition neglecting the voltage harmonic distortion. The assessment includes the full-load and half-load operating conditions. The three-phase lines THDi% values are examined under different supply unbalance conditions (1%, 2% and 3%) and related simulation waveforms presented. Results are investigated and compared to other common passive filtering techniques (AC line reactors and single tuned filters).

Typically, the unbalance supply voltage condition can be caused by unbalanced loading and/or faults in the distribution transformer tap-changers. Under unbalance supply condition the three-phase diode bridge rectifier tend to operate similar to a single-phase bridge rectifier as only four diodes will continue conducting with unsymmetrical conduction periods. This operating condition will introduce a third current harmonic component (I_3) in the AC-side and generates a second order voltage harmonic component (V_2) in the DC-link output voltage. Consequently, the third current harmonic introduced may increase the resonance risk and the total rms value of the line current causing extra thermal losses. On the other hand, the DC-link output voltage will contain higher voltage ripple values reducing the output DC voltage average value and decreasing the DC-link capacitance life-time.

In practice, AC motors are sensitive to supply unbalance (negative sequence components) that result in a counter-rotating magnetic field inducing unwanted current in the rotor and generating reverse torque. Large machines will have phase-negative sequence protection fitted. Smaller machines will generally operate satisfactorily with high losses and high internal temperature. Thermal protection scheme under severe unbalance supply voltage conditions (>5%) is typically needed or machines operating under an unbalance supply required to be de-rated [57].

The unbalance voltage supply definition considered in the investigation is the National Electrical Manufacturers Association of USA (NEMA) standard [58] and is given by

$$\text{Voltage unbalance} = \frac{\text{Maximum deviation from mean of } \{V_{ab}, V_{bc}, V_{ca}\}}{\text{Mean of } \{V_{ab}, V_{bc}, V_{ca}\}} \quad (4.2)$$

where the voltages utilized are the line-to-line values. Therefore, according to this definition, a 4% supply voltage value decrement is required in phase 1 to achieve a 2% supply voltage unbalance case. Consequently, to test the ASD system performance under (1%, 2% and 3%) unbalance voltage supply conditions; a corresponding (2%, 4% and 6%) voltage magnitude value reduction in phase 1 is implemented, respectively.

The three-phase supply voltage and line currents simulation waveforms at full-load of the 5.5kW IBF system under balanced and 2.0% unbalanced (at phase 1 (**bold**)) voltage supply are shown in Fig. 4.23 and 4.24, respectively. It is seen that the drawn line currents are steady and stable under both voltage supply conditions. Therefore, the 2.0% unbalance voltage supply has practically no effect in the performance of the ASD system installing the designed improved broadband filter for harmonic mitigation and power quality enhancement purposes.

For further investigation, the 5.5kW ASD system utilizing the IBF performance evaluation under other unbalance voltage supply situations at half-load condition have been also analysed. Table 4.7 shows and compares the line current THDi% results for balanced and the considered different three unbalance voltage supply case studies.

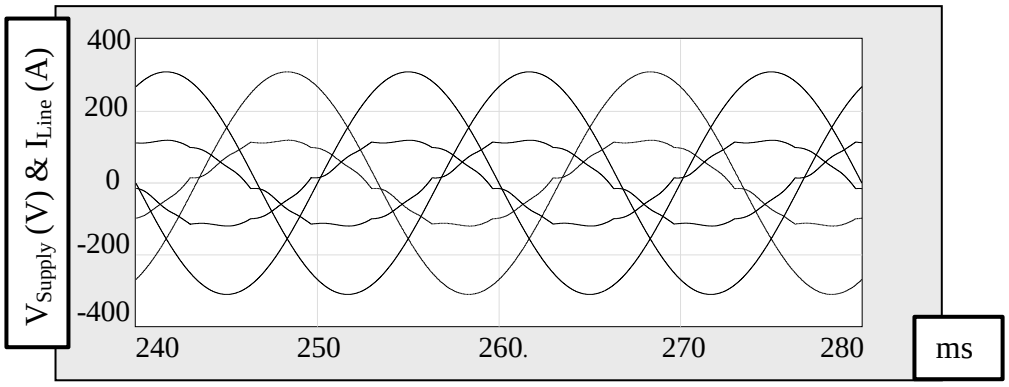

Fig. 4.23 Full-load three-phase supply voltage and current waveforms for balanced utility grid for 5.5kW ASD system utilizing IBF (current scale:10x).

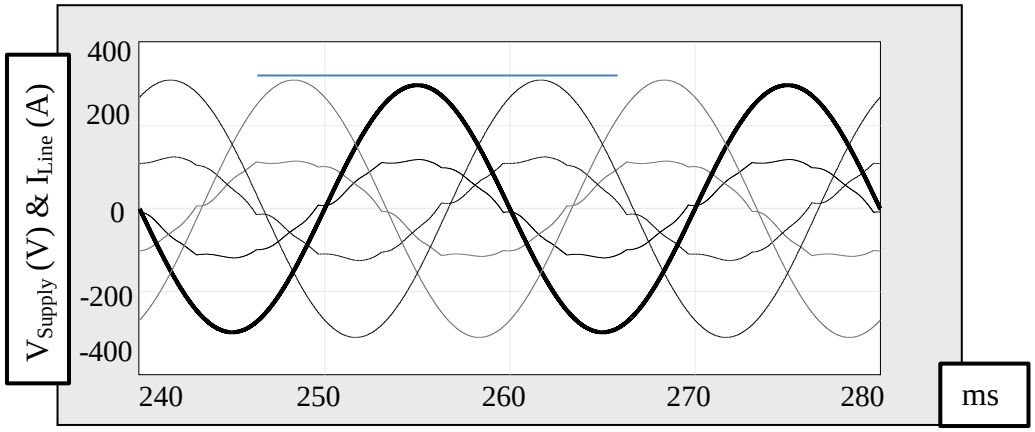

Fig. 4.24 Full-load three-phase supply voltage and current waveforms for 2.0% unbalanced utility grid for 5.5kW ASD system using IBF (current scale:10x).

As shown in the Table 4.7, the 5.5kW ASD system utilizing IBF succeeds to maintain the low and steady line current THDi% values in all phases. For example, at full-load condition the line THDi has a low values range (< 8%) even though with the maximum unbalance supply voltage considered case (3%). In addition, with this maximum 3% unbalance supply voltage the line THDi% worst case result is 12% for the half-load condition. Therefore, these results confirm the low unbalance supply voltage sensitivity of the IBF topology. This is due to the fact that the IBF structure employs a relatively large input reactor (L_i) that can keep the line current THDi% values within acceptable levels even under severe operating conditions. The IBF filter typically initiates a minimal 3rd harmonic current component (I_3) under supply voltage unbalance compared with a typical AC three-phase reactor (Lac) filtering method (e.g. 1.488% I_3 for IBF and 20% I_3 for 3% Lac at full-load operating condition with 2% unbalance supply case study for 5.5kW ASD system.)

Table 4.7 ASD 5.5kW rated system performance under unbalanced supply voltage utilizing IBF filter structure

V unbalance%	Mag (peak)	Full-load (THDi%)	Half-load (THDi%)
0	310.0	5.35	8.13
1	303.8	5.48-5.70-5.71	8.35-8.79-8.63
2*	**297.6**	**5.63-6.65-6.53**	**8.80-10.5-10.0**
3	291.4	6.08-8.3-7.9	9.48-12.9-12.0

*I_3 @ F.L. is 1.488% and @H.L. is 2.77%

Similarly, the 55kW power rated ASD system using the IBF is examined under the same different three voltage supply unbalance practical values. The balanced and 2% unbalanced three-phase supply voltage and line currents simulation waveforms at full-load are shown, respectively, in Fig. 4.25 and Fig. 4.26. The results support the previous ones and confirm the IBF ability to maintain the system low THDi% values.

Finally, Table 4.8 presents all the simulation results for the 55kW ASD system under balanced and unbalanced voltage supply three various conditions. The results involve the full-load and half-load operating situations. It is shown that the 55kW ASD system results are consistent with the 5.5kW ASD system and support the IBF ability to maintain its superior performance under normally experienced, industrial supply voltage practical imperfection circumstances.

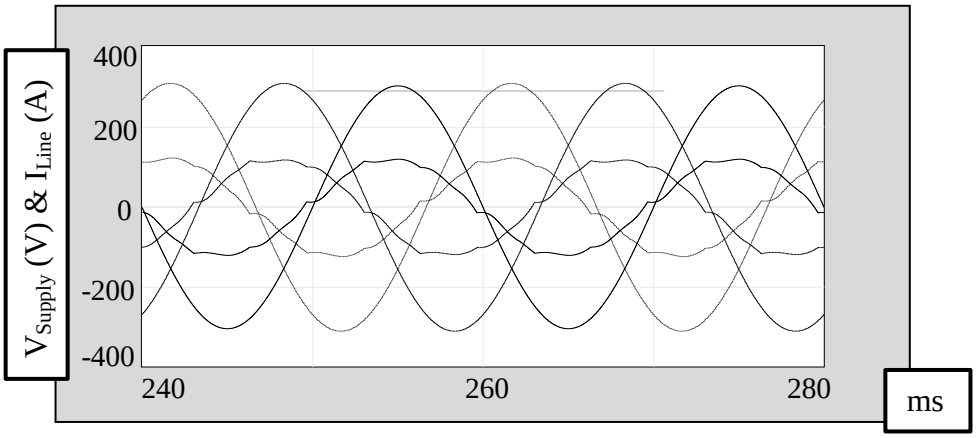

Fig. 4.25 Full-load three-phase supply voltage and current waveforms for balanced utility grid for 55kW ASD system utilizing IBF.

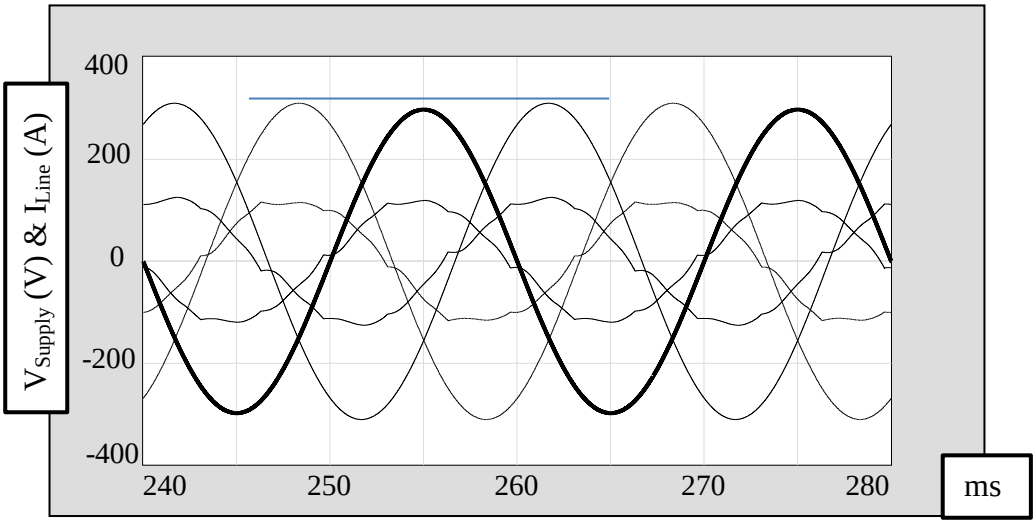

Fig. 4.26 Full-load three-phase supply voltage and current waveforms for 2.0% unbalanced utility grid for 55kW ASD system utilizing IBF.

Table 4.8 ASD 55kW rated system performance under unbalanced supply voltage utilizing IBF filter structure

V unbalance%	Mag (peak)	Full-load (THDi%)	Half-load (THDi%)
0	310.0	5.37	7.90
1	303.8	5.41-5.58-5.61	8.1-8.54-8.45
2	**297.6**	**5.65-6.70-6.62**	**8.5-10.3-9.9**
3	291.4	6.01-8.28-7.97	9.2-12.8-11.97

4.4.7 Simulation Based IBF Performance Evaluation and Comparison

In this section, the overall ASD system performance utilizing the reduced IBF structure parameters (by using GA) is presented. The main power quality indices (line-current THDi% and line power factor) along with the IBF energy efficiency load depended performance characteristics, for 5.5kW and 55kW power ratings considered, are shown in Fig. 4.27 to Fig. 4.29. Moreover, the IBF based system performance will be compared to other conventional and simpler passive filters topologies (AC reactors (Lac) and single tuned shunt filters (STSF)) [56].

As shown in Fig. 4.27 to Fig. 4.29, the IBF-based ASD system delivers high overall power quality performance under the various loading operating conditions. Over the wide loading range the line current THDi% has a satisfactory spectrum of values (<10%) with very low full-load value (5.5%), as shown in Fig. 4.27. This will allow the ASD system using the IBF filtering method to have negligible effect on the distribution network and specifically to the other loads connected at the same PCC point. This might be considered as a major improvement in terms of polluting the network.

The line power factor performance, shown in Fig. 4.28, has been improved and corrected successfully at full-load to reach its ideal value (unity). From half-load to full-load practical operating range the line power factor is still high (> 0.8) and minimize the reactive power requirement of the ASD. At no-load condition the IBF structure draw a considerable amount of capacitor current that improves the line

current THDi% at the cost of very low leading power factor value. Practically, this might be useful in networks where the reactive power compensation is highly demanded and cannot be achieved. Otherwise, the IBF topology should be primarily considered for high operating utilization inverter drive applications with the aim of avoiding poor leading PF and complications related with such operating condition.

Finally, as shown in Fig. 4.29, the IBF filter exhibits low energy losses with a high efficiency range values (> 97%) from light-load to full-load range.

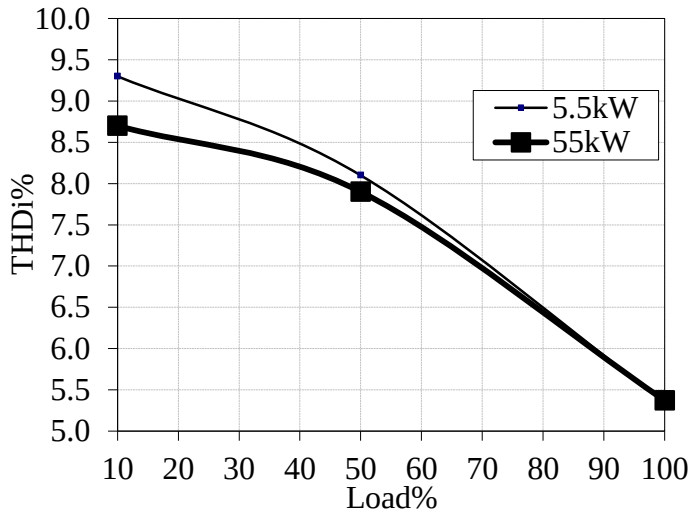

Fig. 4.27 The load current dependency of the IBF line current THDi%.

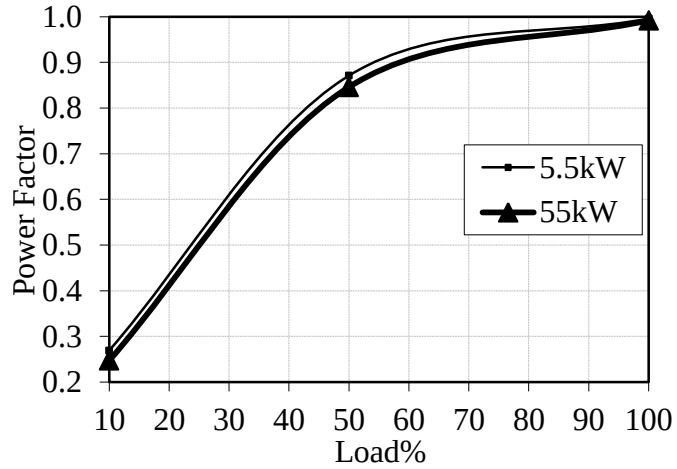

Fig. 4.28 The load current dependency of the IBF line power factor.

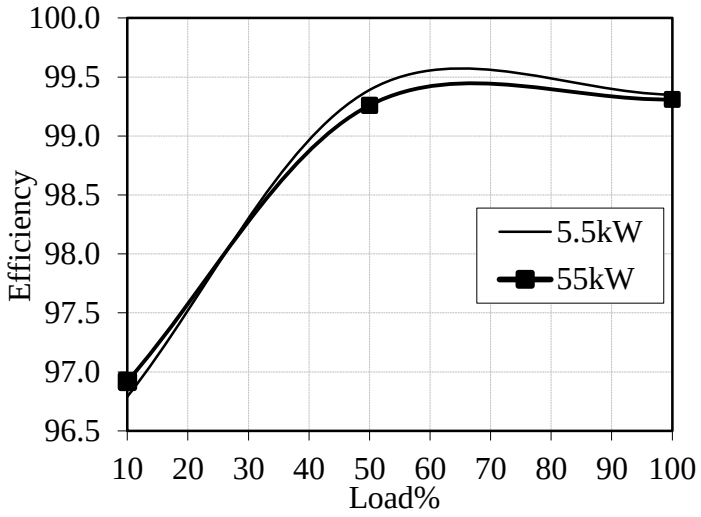

Fig. 4.29 The load current dependency of the IBF energy efficiency.

In order to clarify the IBF filter performance satisfaction, Table 4.9 shows the ASD 5.5kW system full-load main power quality simulation results of utilizing the 3%Lac, single tuned shunt filters (5^{th} and 7^{th}) along with the updated IBF results for comparison reasons [56].

As the table indicates, the IBF based ASD system has the minimum line current THDi% and achieving unity line power factor. Meanwhile the IBF topology utilizes fewer components than the STSF (5^{th} and 7^{th}) and therefore has less cost and complexity. On the other hand, the IBF based system is nearly free from any harmonic resonance risk that might cause an overvoltage excited by parallel resonance large impedance phenomena. However, the output DC bus voltage and voltage regulation (ΔV_o%) of the IBF is slightly higher than other filtering methods, but this is not considered to be a significant practical problem.

Table 4.9 ASD performance characteristics comparison utilizing various filters techniques for 5.5kW power rating under balanced 3%THDv voltage supply

Filter Type	THD_i (%) @Full-load	PF @Full-load	V_{dc} @Full-load	η(%) @Full-load	ΔV_o (%)
3%L_{ac}	36	0.92 lagging	501	>99.5	0.6
STSF	11.6	0.99 lagging	496	>99.0	2.5
IBF	5.35	0.99 leading	507	>99.0	3.5

Furthermore, based on the evaluation of the unbalanced line voltage IBF performance attributes shown in Table 4.7 and Table 4.8, the IBF filtering technique is not sensitive to the line voltage unbalance. Meanwhile the other considered conventional passive filtering topologies are more sensitive to such feeders supply voltage variations [56].

Finally, a qualitative assessment of the proposed IBF filter, three-phase AC reactor and single tuned shunt filters are considered and shown in Table 4.10 [56]. As the Table indicates, the IBF structure has the lowest line current harmonic distortion factor and is able to meet THDi requirement < 10%. The single tuned shunt filters (STSF) can be comparable to the IBF size, cost and complexity. However, the voltage unbalance sensitivity and harmonic resonance risk factors (shown in the table) strongly support the superiority of the IBF. However, as earlier mentioned, for frequent light-load range drive operation the IBF will degrade the line power factor by providing a considerable amount of capacitive reactive power to the AC line. This may lead to large reactive power bills in certain installations. Therefore, the passive filter considered (including IBF) either be switched off or bypassed during the light-load conditions or different filtering techniques should be considered for light-load (< 50% loading) dominant applications.

Table 4.10 Qualitative comparison of various common passive filters

Filter Type	L_{ac}	STSF	IBF
Total Harmonic Distortion	High	Low	***Lowest***
Voltage Regulation	Low	Low	Low
Voltage Unbalance Sensitivity	High	High	***Low***
Power Factor @ full-load	Low	High	High
Power Factor @light-load	Not an Issue	Low	Low
Cost (depending on number of filter components used)	Low	High	Medium
Size	Small	Large	Large
Structure Complexity	Low	High	Medium
Efficiency	High	Medium	Medium
Harmonic Resonance Risk	No	Yes	***No***

4.5 Experimental Results of 5.5 kW Rated ASD System and Performance Evaluation

The preceding sections demonstrated the computer simulations results and performance analysis of the ASD system under various operating conditions with use of the AC line reactor passive filter and the IBF proposed filter. In this section, the presented passive filters are examined in the lab and their experimental performances are illustrated and analysed. The steady-state performance will be assessed under various loading conditions (from no-load to full-load) with the consideration of the practical voltage supply distortion.

4.5.1 Laboratory Setup

An experimental (380 - 415)V_{LL}, 50Hz, 5.5 kW rating ASD system (three-phase 6-pulse diode rectifier) is designed and built in the laboratory utilizing both passive filters shown in the previous sections (4% AC line reactors and IBF). The ASD system tested in the lab is not an actual AC motor drive. However, a three-phase diode bridge rectifier supplying DC power to an RC load that emulates a real ASD performance is used. Table 4.11 shows the different utilized components in the setup (DC-link inductor and capacitors, limiting resistor and load resistors). The load equivalent resistor is a combination of 13 variable resistors with different specifications that are connected in series and parallel to allow the consumption of the total power delivered by the system.

Table 4.11 ASD system experimental setup parameters

Component	Specification
DC-link inductor (L_{dc})	1 piece *1.6mH
DC-link capacitors (C_{dc})	4 pieces * 1mF, 450V
Pre-charge resistor (Rpre)	1 piece * 47 Ω, 20W
Load resistor (Rload)	13 pieces (3-20 Amps) in parallel/series combinations

Fig. 4.30 shows the experimental ASD system circuit illustration. The load side consists of a set of connected variable resistors that can be used to change the loading conditions through the experiment. This variable load is connected in parallel to the DC-link capacitors combination and in series to the DC-link inductor through an automatic load switching (63A). The combination of the used four DC capacitors is equivalent to 1mF capacitor with acceptable voltage and current ratings. To limit the practical initial inrush current, a pre-charge resistor is connected to DC inductor (L_{dc}) and shorted by a manual switch. For protection purpose, a fast fuse (25A) is connected between the rectifier DC terminal and the pre-charge resistor.

The AC side of the three-phase diode full-bridge rectifier (IXYS 63A, 1200V) is connected to the proposed passive filter via three-phase fast fuses (25A). Then the passive filter under investigation is connected to the three-phase supply through a three-phase voltage variac transformer and a manual circuit breaker box, as shown in Fig. 4.30.

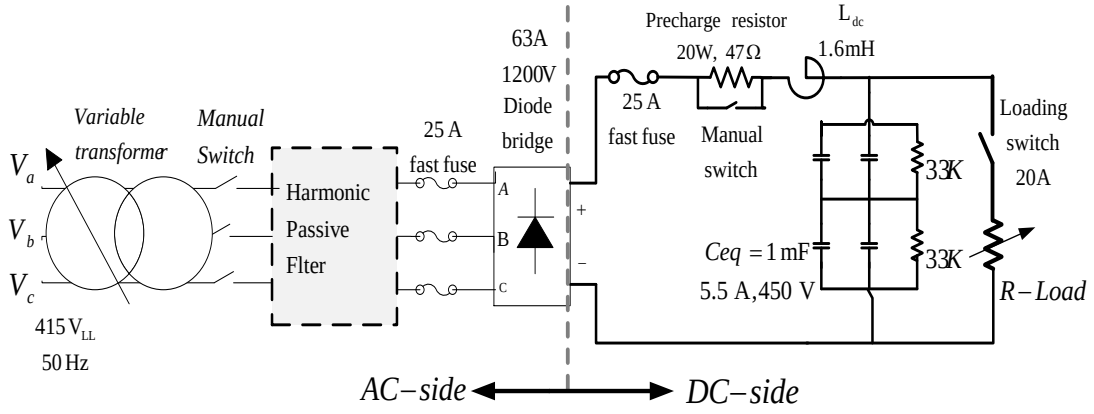

Fig. 4.30 The experimental ASD system circuit illustration.

The actual three-phase diode rectifier and the DC side components used in the laboratory are shown in Fig. 4.31. The picture shows the three-phase rectifier mounted on a heat sink with a small black fan at the back (for extra cooling). The DC-link inductor and set of capacitors are connected to the three-phase rectifier via the pre-charge resistor, as shown in the figure. The DC side components are connected to the automatic load switch. Moreover, Fig. 4.32 shows the combination of the used variable resistors that form the system load.

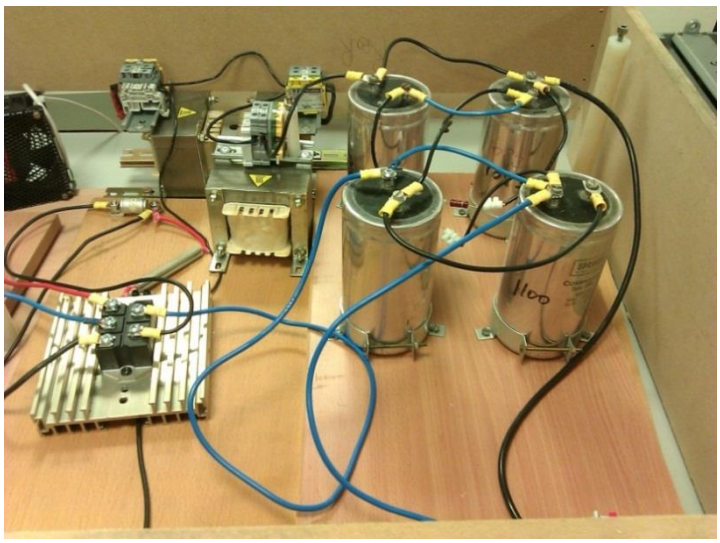

Fig. 4.31 Picture of the 5.5kW experimental three-phase rectifier and DC-link system.

Fig. 4.32 Picture of the 5.5kW experimental variable resistors loading system.

All AC side current, voltage measurements and power quality analysis are done with the NORMA 5000 power analyser, shown in Fig. 4.33 [59]. The three-phase power analyser performs a time measurement with high sampling rate value. The voltage, current and phase angle measurement error is approximately < 0.1% at the 5.5kW designed experiment current and voltage

measurement range. Consequently, the equipment estimated real power error is approximately < 0.2%. Several AC and DC conventional multi-meters and clamp-meters were also utilized for monitoring purposes.

The research laboratory line side 3-phase voltage experimental waveforms at full-load for 5.5kW rated ASD elementary system are shown in Fig. 4.34. Supply experimental data for the ASD built system without utilizing any filtering technique is shown in Fig. 4.35. The supply voltage has minor magnitude variations between the phases and a voltage harmonic distortion THDv value of 1.38%. The delivered apparent power (S) and consumed real power (PH) is also presented and reveals the amount of losses in the system due to the high current harmonic distortion (Fig. 4.37).

Fig. 4.33 Norma 5000 power analyser utilized in the experiment.

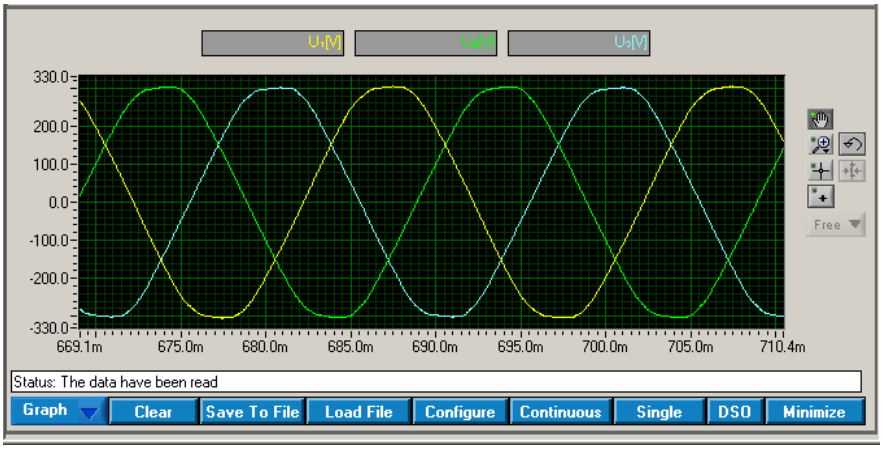

Fig. 4.34 Line side 3-phase voltage experimental waveforms at full-load for 5.5kW rated system.

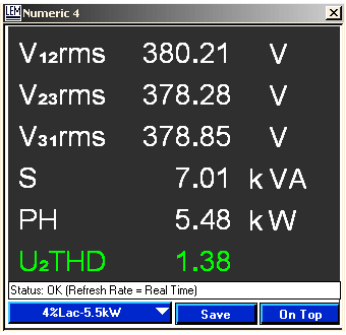

Fig. 4.35 Supply experimental data at full-load for 5.5kW rated system employing no filter (line-to-line voltage, total apparent and real power, supply voltage THDv%).

The line experimental data for the three-phase 1, 2 and 3 at full-load for 5.5kW rated system employing no filter is shown in Fig. 4.36. All phase voltages and currents rms values, real power, line current THDi%, reactive power and power factor (ʎ) are presented. The line currents have a very high harmonic distortion with THDi values >75%. Meanwhile the correlated line power factor values reach a low range of < 0.781 lagging. The line 3-phase current experimental waveforms at full-load and the corresponding harmonic spectrum are shown in Fig. 4.37 and 4.38, respectively.

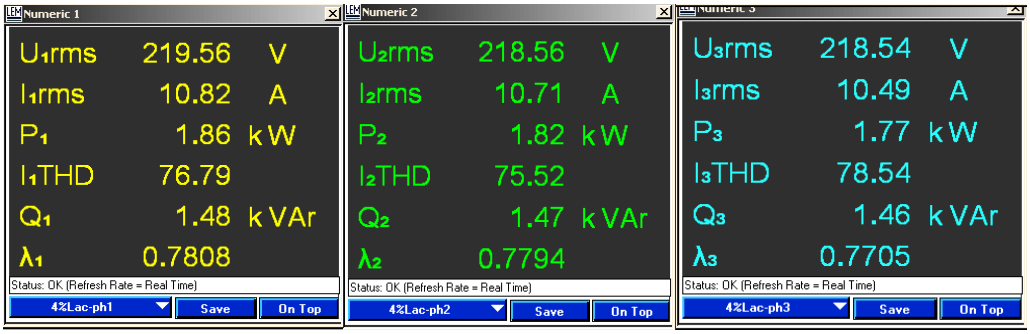

Fig. 4.36 Line experimental data for phases 1, 2 and 3 at full-load for 5.5kW rated system employing no filter (voltage V, current I, real power P, current THDi%, reactive power Q, power factor ʎ).

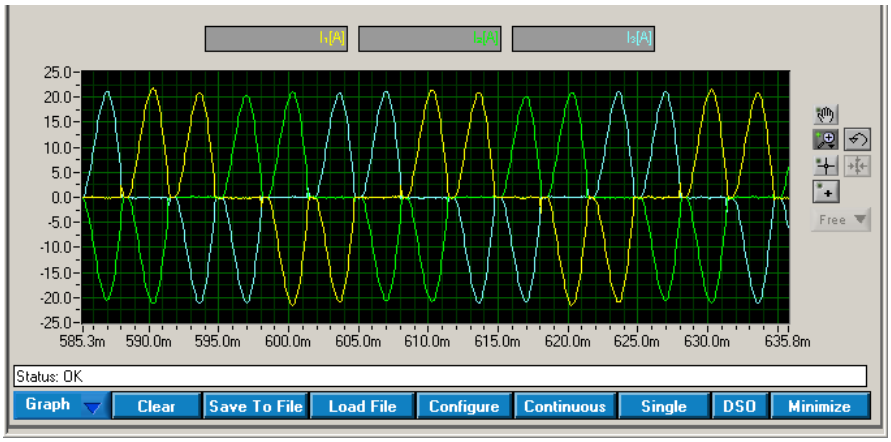

Fig. 4.37 Line 3-phase current experimental waveforms at full-load for 5.5kW rated system employing no filter.

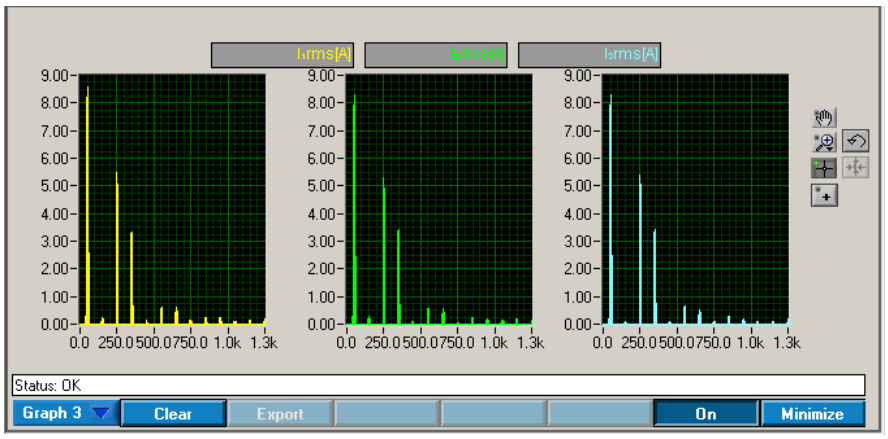

Fig. 4.38 Line 3-phase current harmonic spectrum at full-load for 5.5kW rated system employing no filter.

4.5.2 AC Line Reactor Filter Based Experimental Results

In this section, the designed 4% three-phase AC line reactors are implemented in the ASD system (as shown in Fig. 4.39). The experimental performance features of the whole system are presented. Practical current and voltage waveforms are demonstrated and investigated. The 4% Lac (3.0 mH) AC line reactors are combined with an approximate 2%L_{dc} available (1.6 mH) DC-link inductor in the DC side.

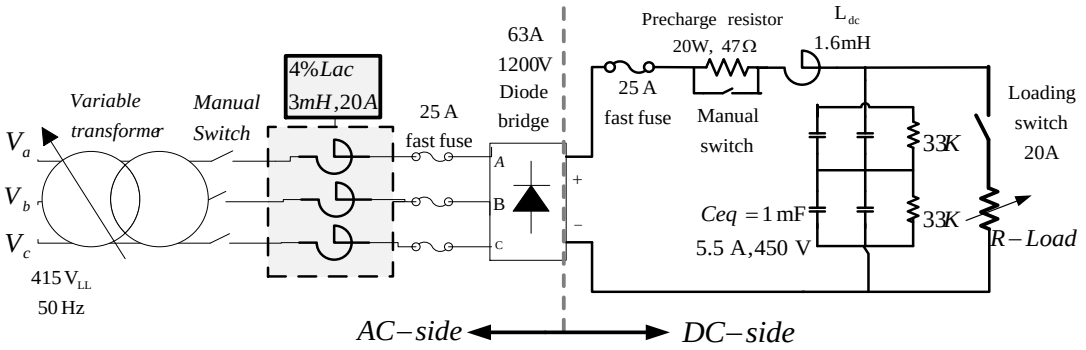

Fig. 4.39 The experimental 5.5kW ASD system setup utilizing 4% AC line reactor.

The full-load supply data is presented in Fig. 4.40. The voltage supplying the setup under investigation has 1.96% THDv value in phase 2. The line experimental data for all phases are shown in Fig. 4.41. As presented, the resultant line current THDi% values have decreased to a range of 30.6% to 33.81% and the corresponding line power factor values improved in all phases to a range of 0.91 to 0.93 (lagging) values.

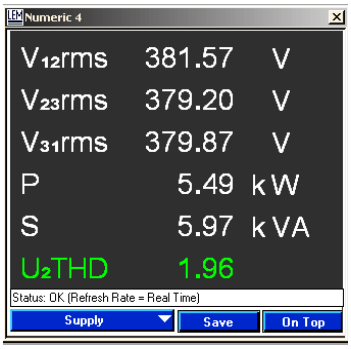

Fig. 4.40 Supply experimental data at full-load for 5.5kW rated system employing 4% L_{ac} and 2% L_{dc} (line-to-line voltage, total real and apparent power and supply voltage THD_V%).

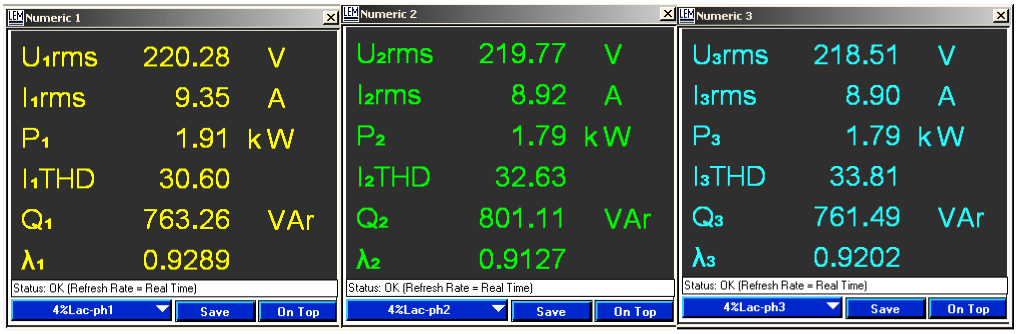

Fig. 4.41 Line experimental data for phases 1, 2 and 3 at full-load for 5.5kW rated system employing 4% L_{ac} and 2% L_{dc} (voltage V, current I, real power P, current THDi%, reactive power Q, power factor λ).

The three-phase experimental line currents waveforms at full-load for the 4% Lac and 2% L_{dc} filtering method designed for the 5.5kW ASD system are shown in Fig. 4.42. The harmonic spectrum analysis of the presented distorted currents (32.63% THDi) is shown in Fig. 4.43. The line currents still have most of the dominant harmonic components in the presented spectrum with a high 5^{th} component.

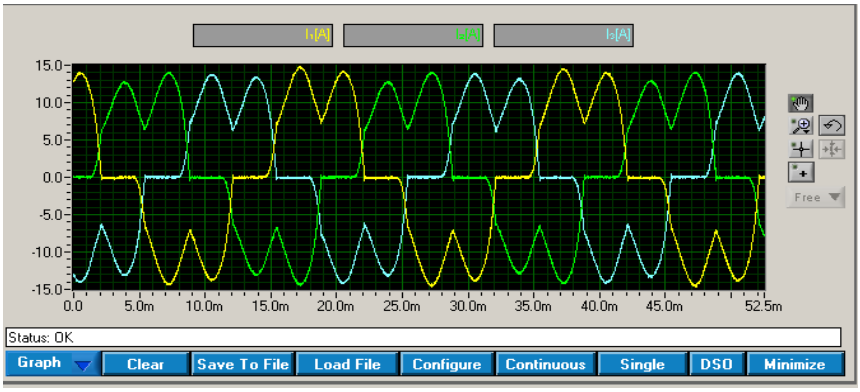

Fig. 4.42 Line 3-phase current experimental waveforms at full-load for 5.5kW rated system employing 4% L_{ac} and 2% L_{dc} filter.

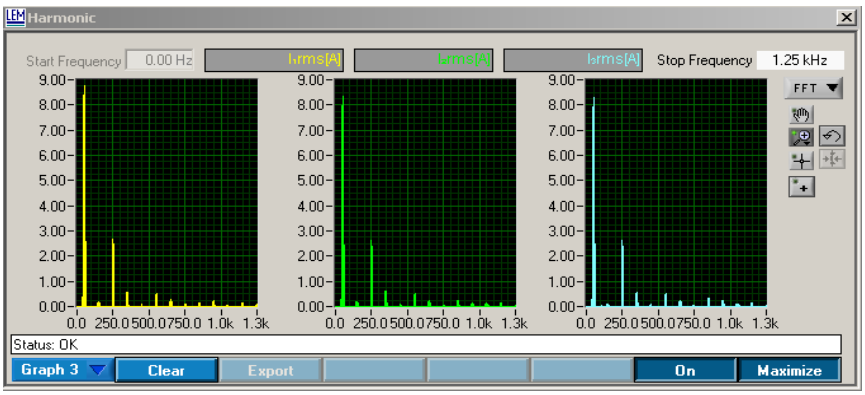

Fig. 4.43 Line 3-phase current harmonic spectrum at full-load for 5.5kW rated system employing 4% L_{ac} and 2% L_{dc} filter.

Fig. 4.44 illustrates the 5.5 kW ASD system experimental supply voltage and line current (phase 1) waveforms at full-load and zoomed-in Fig. 4.45. This power analyser measured and shown waveforms represent the 30.6% current THDi and the 0.93 lagging power factor results in phase 1. Therefore, this simple filtering method exhibits unsatisfactory power quality level and is not capable of complying with the modern harmonic standards and regulations.

The rated load DC current and voltage experimental values were measured by means of conventional DC ammeters and voltammeters (11A and 488V). The corresponding DC waveforms are not extracted due to the limited performance of the power quality analyser and other existing instruments.

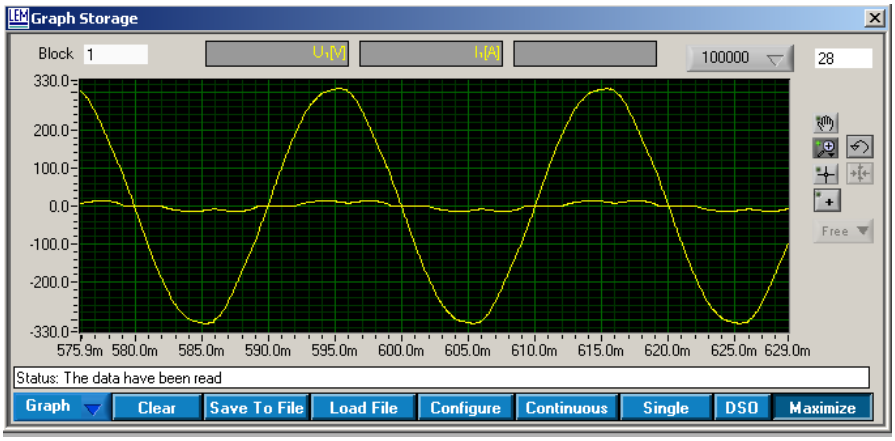

Fig. 4.44 Supply phase voltage and current experimental waveforms at full-load for 5.5kW rated system employing 4% L_{ac} and 2% L_{dc} filter.

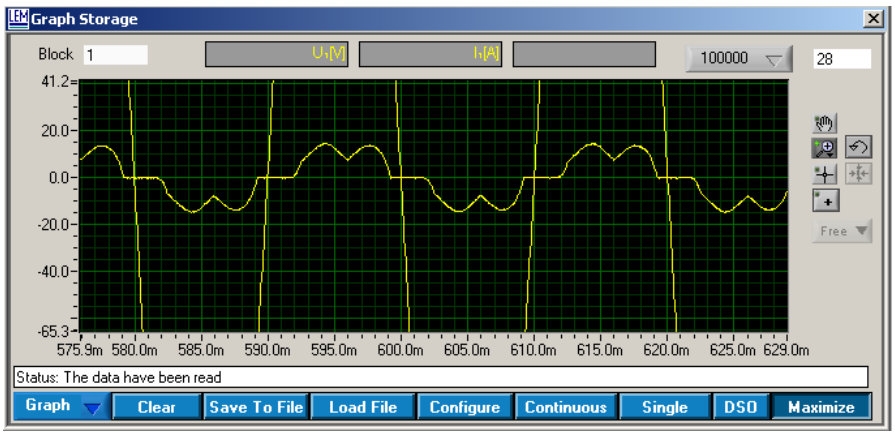

Fig. 4.45 Supply phase voltage and current experimental waveforms at full-load for 5.5kW rated system employing 4% L_{ac} and 2% L_{dc} filter (Zoomed).

4.5.3 IBF Full-Load Experimental Results

In this section the ASD system experimental performance characteristics utilizing the designed improved broadband filter (IBF) are presented. Experimental supply and rectifier side data, current and voltage waveforms are illustrated and analysed. The IBF is designed using the optimal values (shown in Table 4.1) with 10.1mH for the input reactor (L_i), 8.1mH for the filter reactor (L_f) and the filter capacitor (star connection) C_{fY} 49.8uF (16.6uF delta connection equivalent). Both used three-phase reactors were designed with their original values by a major UK company (Amethyst Designs Ltd). However, the available star connected capacitors were three large variable capacitors boxes. Each capacitors box contains seven capacitors with various capacitances values (1.0, 2.05, 3.91, 8.31, 12.14, 12.41 and 12.11 all in microfarads) connected in parallel. The selected equivalent capacitance used is set to 49.88uF which is very close to the desired filter capacitance (C_{fY} 49.8uF). The laboratory three-phase filter capacitance measured values are C_{fY1} 49.5 uF, C_{fY2} 49.0 uF and C_{fY3} 49.0 uF.

The same 4% AC output reactor (Lac 3.0 mH) is connected to the rectifier AC terminals and 2% DC inductor (L_{dc} 1.6 mH) used in the previous section experiment is connected at the rectifier DC side. The designed filter is implemented as shown in Fig. 4.46.

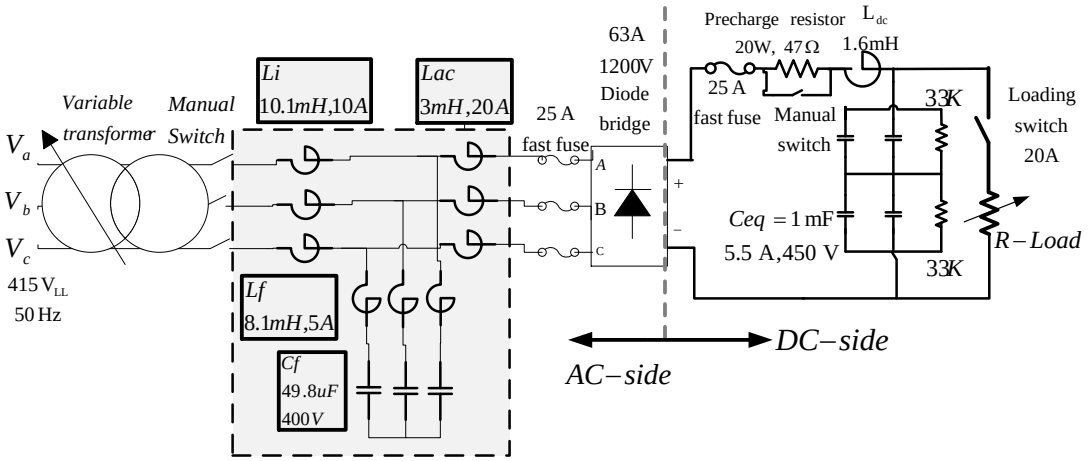

Fig. 4.46 The experimental 5.5kW ASD system setup utilizing IBF.

The NORMA 5000 power analyser has an extra three channels of measurements. These added channels were connected to the rectifier side terminals and considered as phases 4, 5 and 6. This allows additional measurements facilities at different points for further investigation. The full-load supply side and rectifier side data is presented in Fig. 4.47. On the supply side, the phase 2 voltage has an acceptable 1.91% THDv and the three-phase power delivered is 5.47kW. On the rectifier side presented measurements, the line-to-line rectifier side voltage rms values are negligibly boosted by the filter capacitor at full-load.

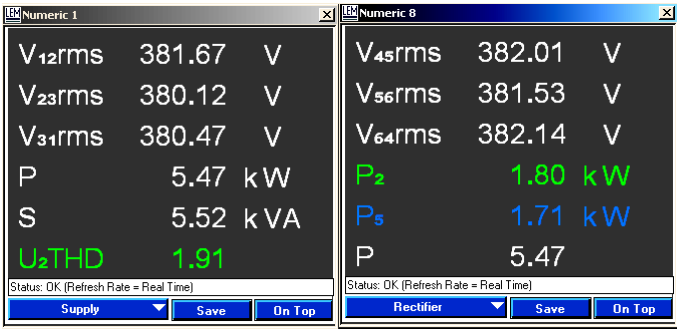

Fig. 4.47 Supply and rectifier side experimental data at full-load for 5.5kW rated system employing IBF filter (line and rectifier line-to-line voltages, total real and apparent power and supply voltage THD_V%).

The line side experimental data for all phases (1, 2 and 3) are shown in Fig. 4.48, while the rectifier side data for phases 4, 5 and 6 are shown in Fig. 4.49. The line current THDi% values have improved and dropped to a range of 5.23% to 6.44% by utilizing the IBF topology. Meanwhile a unity line side power factor values are achieved. Therefore, the filter exhibits practical ability to improve the rectifier side

distorted current (32.5% - 33.12% THDi) and low power factor conditions (0.927 – 0.932) leading (* it has been noticed that the rectifier side channels 4, 5, and 6 in this experiment add a minus sign to the reactive power Q_4, Q_5 and Q_6 indicating in a false leading current condition that conflict with the waveforms in Fig. 4.59 and the typical lagging current condition expected).

Furthermore, the slight variation of phases measured THDi and power factor are due to the unsymmetrical designed filter components, supply voltage imbalance, phases loading imbalance and measuring instruments errors.

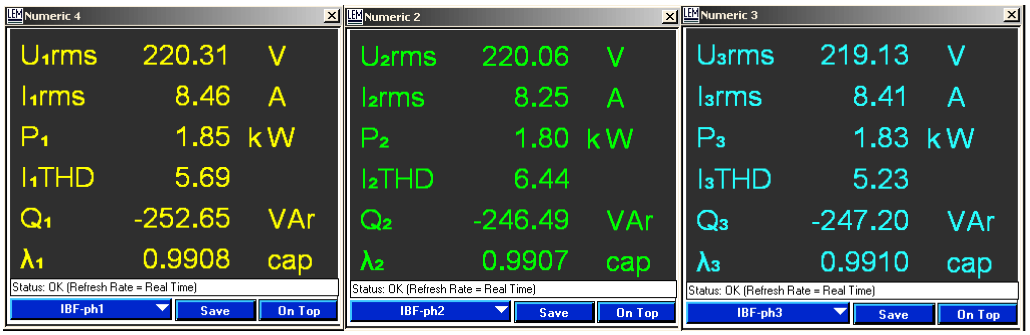

Fig. 4.48 Line side experimental data for phases 1, 2 and 3 at full-load for 5.5kW rated system employing IBF filter (voltage V, current I, real power P, current THDi%, reactive power Q, power factor ʎ).

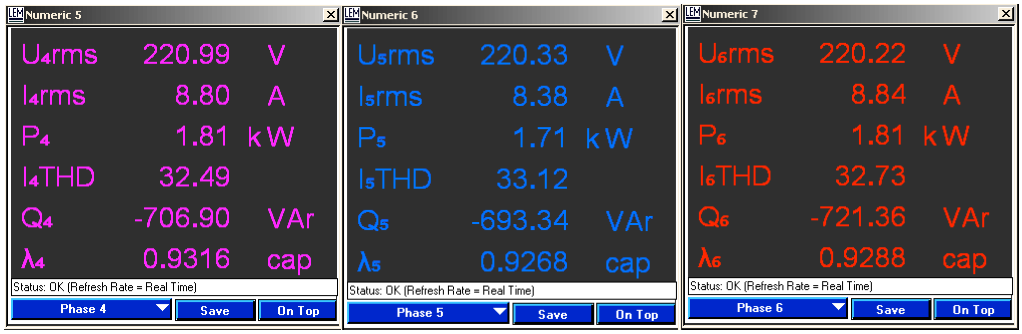

Fig. 4.49 Rectifier side experimental data for phases 4, 5 and 6 at full-load for 5.5kW rated system employing IBF filter (voltage V, current I, real power P, current THDi%, reactive power Q, power factor ʎ).*

The three-phase experimental full-load line current waveforms and their harmonic spectrum for the 5.5kW ASD system are shown in Fig. 4.50 and Fig. 4.51, respectively. While the three-phase experimental full-load rectifier side current waveforms and the associated harmonic spectrum are shown in Fig. 4.52 and Fig. 4.53, respectively. As the power analyser figures indicate, the IBF filtering method

dramatically decreases the rectifier current distortion and is able to eliminate a broad range of its harmonic components.

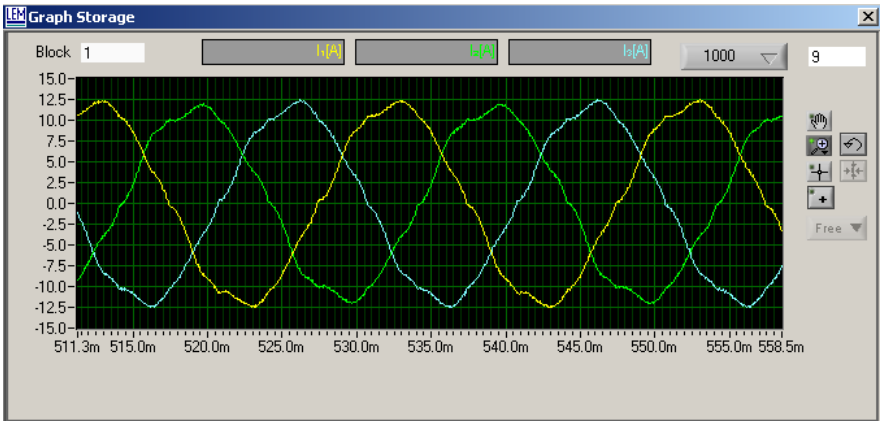

Fig. 4.50 Line side 3-phase current experimental waveforms at full-load for 5.5kW rated system employing IBF filter.

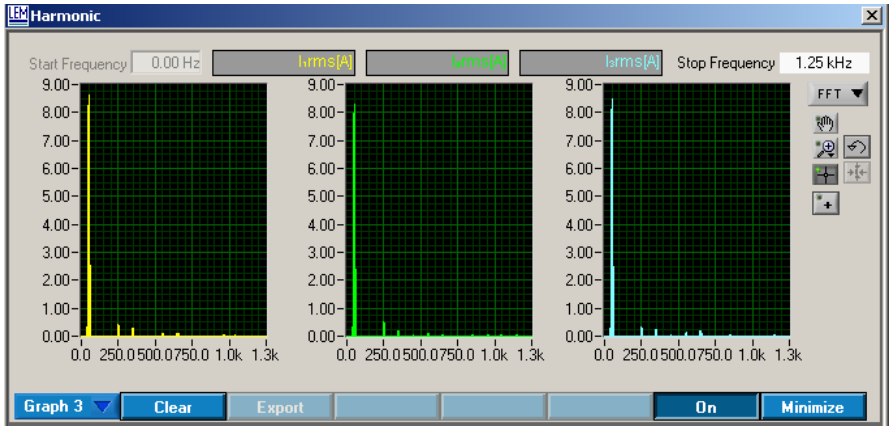

Fig. 4.51 Line side 3-phase current harmonic spectrum at full-load for 5.5kW rated system employing IBF filter.

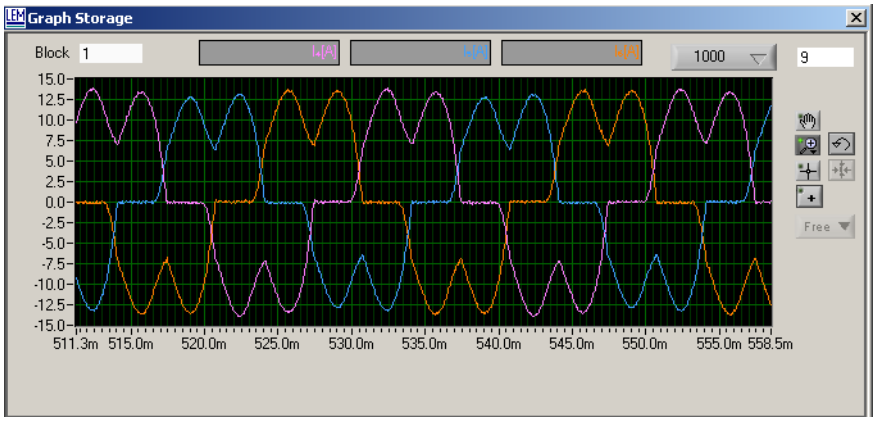

Fig. 4.52 Rectifier side 3-phase current experimental waveforms at full-load for 5.5kW rated system employing IBF filter.

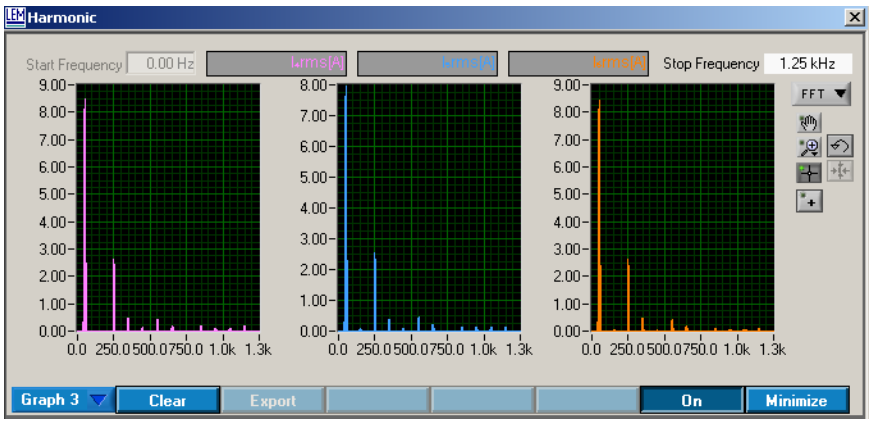

Fig. 4.53 Rectifier side 3-phase current harmonic spectrum at full-load for 5.5kW rated system employing IBF filter.

For better illustration, the phase 2 (green) line side current and phase 5 (blue) rectifier side current waveforms are shown overlapped in Fig. 4.54. While the harmonic spectrum for both currents are shown, zoomed-in, in Fig. 4.55. The effectiveness of the IBF filtering method in smoothing the line current and eliminating most of the undesired dominant harmonic components in the rectifier current is observed. The line current has a continuous less-distorted sinusoidal waveform with a very low THDi value (6.4%) for phase 2.

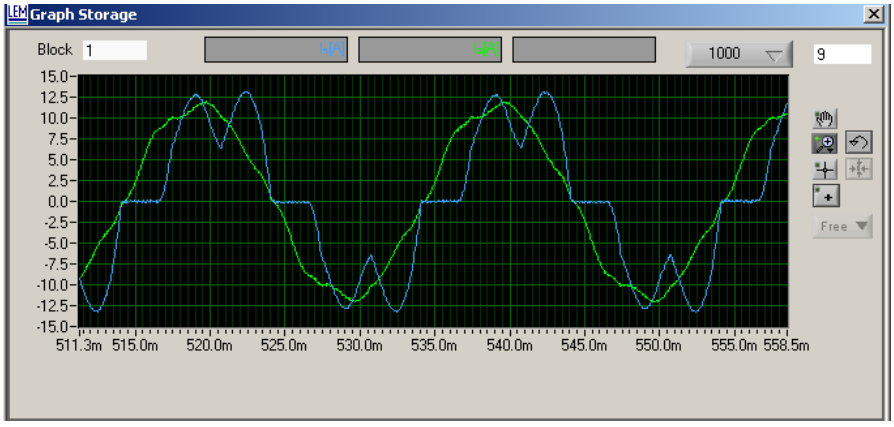

Fig. 4.54 Line and rectifier current experimental waveforms at full-load for 5.5kW rated system employing IBF filter.

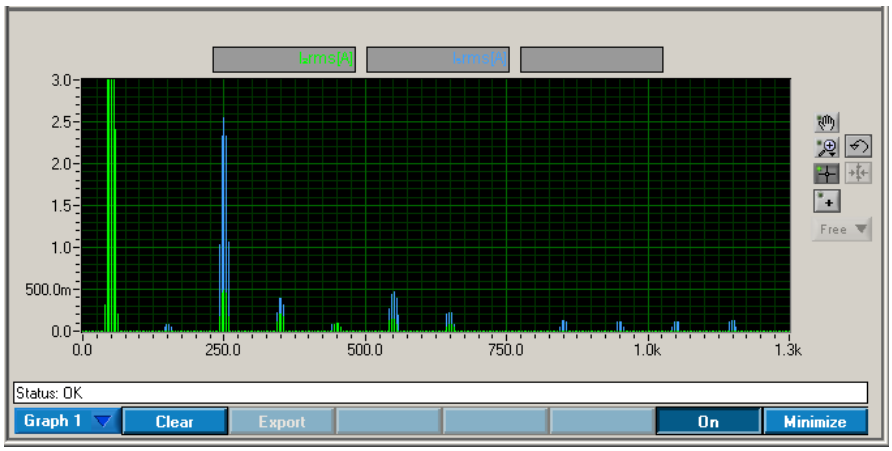

Fig. 4.55 Line and rectifier side current harmonic spectrum at full-load for 5.5kW rated system employing IBF filter (Zoomed).

The phase 1 full-load line current and supply voltage waveforms are shown in Fig. 4.56 and zoomed-in in Fig. 4.57 to investigate the displacement angle between the waveforms. Actually, as shown in both figures, the total line power factor represented is unity (0.9908 leading) and the observed phase shift is negligible. Finally, the phase 1 (yellow) full-load line current and supply voltage harmonic spectrums combined with the phase 4 (purple) rectifier current harmonic spectrum are shown in Fig. 4.58. The phase 5 full-load rectifier current and rectifier voltage waveforms are shown in Fig. 4.59. It is perceived that the rectifier current harmonics cause the rectifier voltage distortion. The rated load DC current and voltage experimental measured values are (10.6A and 500V).

As the presented experimental data reveals, the improved broadband filter structure has superior performance at full-load than the previous filtering simple technique. With only single shunt tuned filter the IBF were capable to absorb most of the harmonic components in the rectifier side distorted current and meanwhile provided the required reactive power compensation at fundamental frequency to improve the total line power factor value to unity.

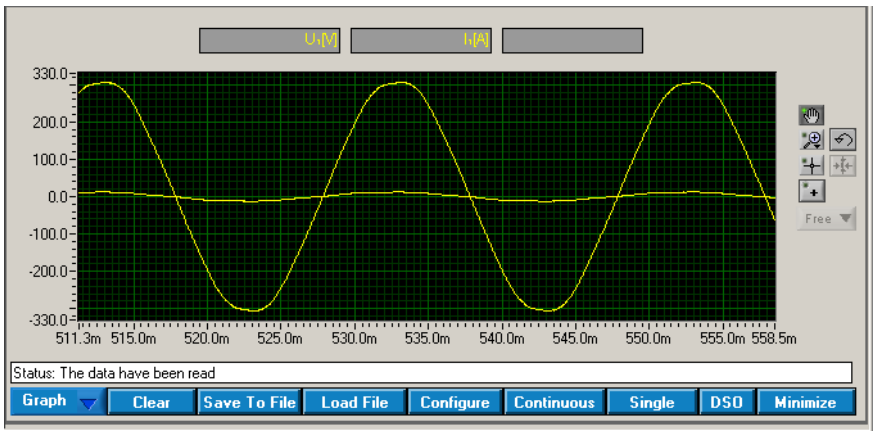

Fig. 4.56 Supply phase voltage and current experimental waveforms at full-load for 5.5kW rated system employing IBF filter.

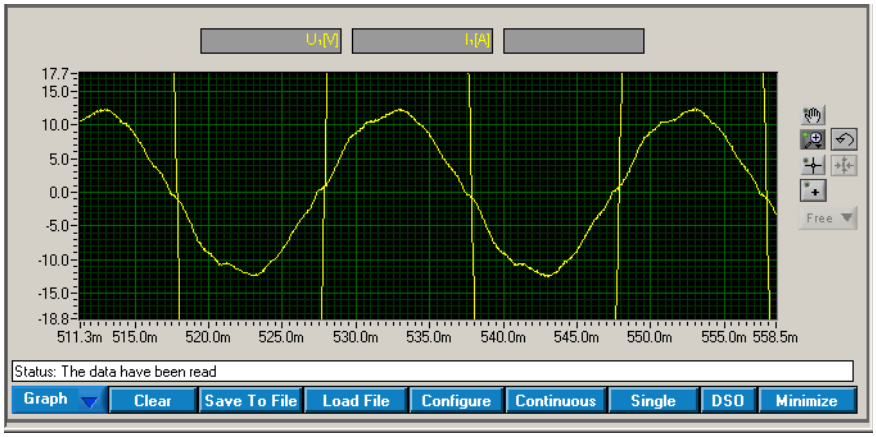

Fig. 4.57 Supply phase voltage and current experimental waveforms at full-load for 5.5kW rated system employing IBF filter (Zoomed).

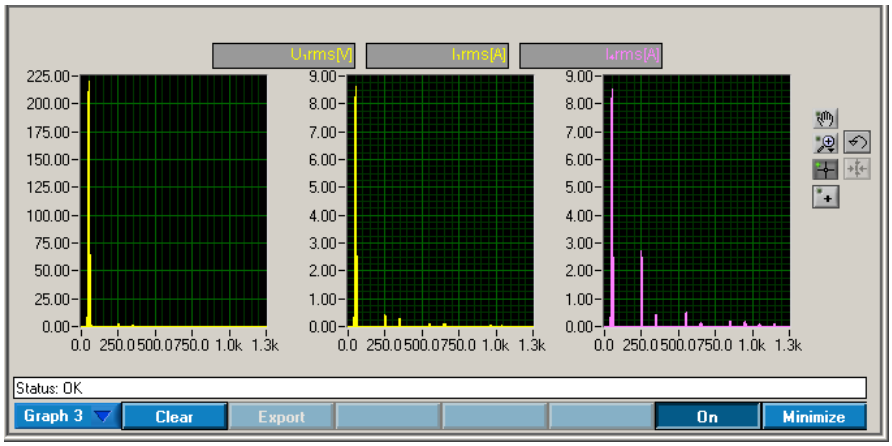

Fig. 4.58 Phase voltage, line current and rectifier current harmonic spectrum at full-load for 5.5kW rated system employing IBF filter.

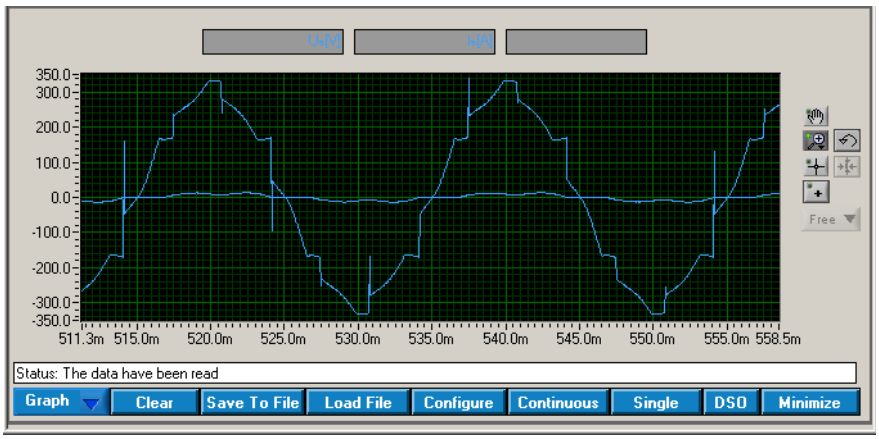

Fig. 4.59 Rectifier side phase voltage and current experimental waveforms at full-load for 5.5kW rated system employing IBF filter.

4.5.4 IBF Half-Load Experimental Results

In this section, the 5.5kW ASD system experimental results of the half-load operating condition are demonstrated. The load equivalent resistor is increased to reduce the load current and the delivered power to approximately 50% (limited by the resistors rating). The half-load supply and rectifier side data is presented in Fig. 4.60. The phase 2 supply voltage has a standard 2.11% THDv and the three-phase power delivered is 2.80kW. The increment in the line-to-line rectifier side voltage rms values is slightly higher than the previous full-load case study results due to the filter capacitance effect.

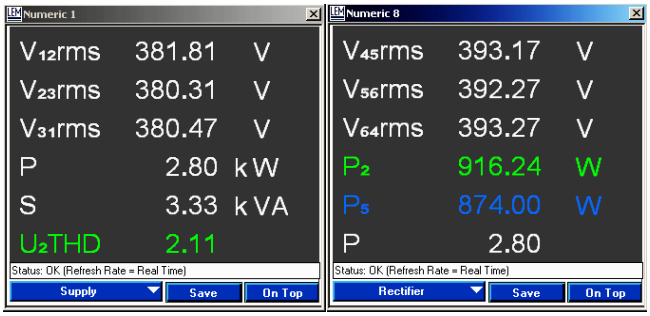

Fig. 4.60 Supply and rectifier side experimental data at 50% load for 5.5kW rated system employing IBF filter (line and rectifier line-to-line voltage, total real and apparent power and supply voltage THD_V%).

The supply side experimental data for phases 1, 2 and 3 are shown in Fig. 4.61, while the rectifier side data for phases 4, 5 and 6 are shown in Fig. 4.62. The line current THDi% values decreased from approximate 42% (rectifier side) to a low range of

5.71% to 6.98% by utilizing the IBF topology. However, the line side power factor did not improve and the IBF capacitor added extra reactive power to maintain the line power factor at 0.84 leading. These experimental results have good correlation accuracy with the simulation results presented in section 4.4.7.

Fig. 4.61 Supply side experimental data for phases 1, 2 and 3 at 50% load for 5.5kW rated system employing IBF filter (voltage V, current I, real power P, current THDi%, reactive power Q, power factor ʎ).

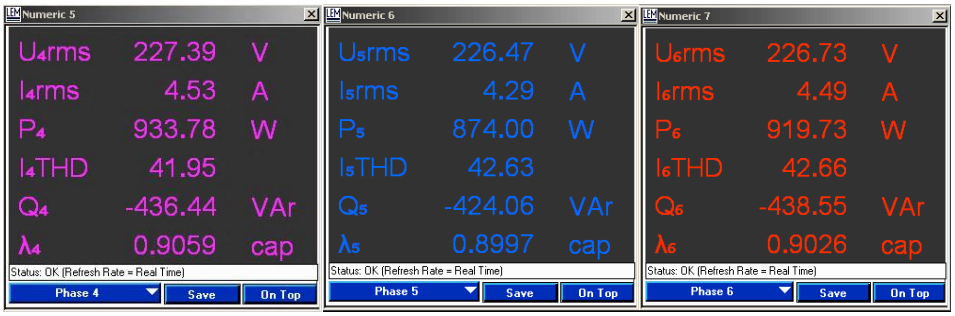

Fig. 4.62 Rectifier side experimental data for phases 4, 5 and 6 at 50% load for 5.5kW rated system employing IBF filter (voltage V, current I, real power P, current THDi%, reactive power Q, power factor ʎ).*

The three-phase experimental half-load line current waveforms and their harmonic spectrum for the 5.5kW ASD system are shown in Fig. 4.63 and Fig. 4.64, respectively. On the other hand, the corresponding three-phase experimental half-load rectifier side current waveforms are shown in Fig. 4.65 and the associated harmonic spectrum is shown in Fig. 4.66. Compared to the full-load condition results, the rectifier currents at half-load have much higher distortion (42% THDi), nevertheless, the IBF succeeded in reducing this extra level of injected harmonics and keeps the line current distortion at low range (5.8% average THDi). From the illustrated harmonic spectrum of the line and rectifier currents, the IBF ability at the half-load operating condition to eliminate a wide range of current harmonic components is obvious.

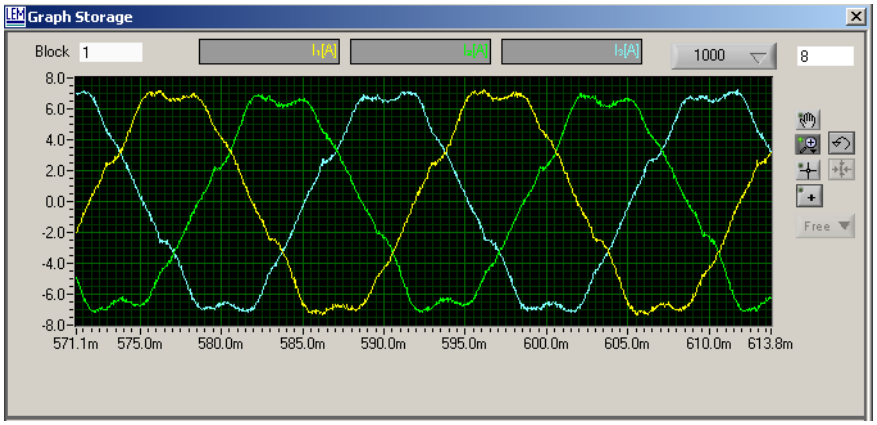

Fig. 4.63 Line side 3-phase current experimental waveforms at 50% load for 5.5kW rated system employing IBF filter.

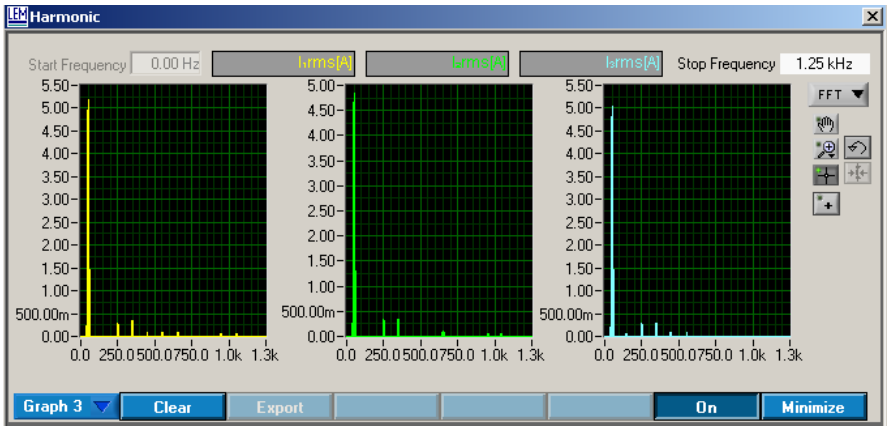

Fig. 4.64 Line side 3-phase current harmonic spectrum at 50% load for 5.5kW rated system employing IBF filter.

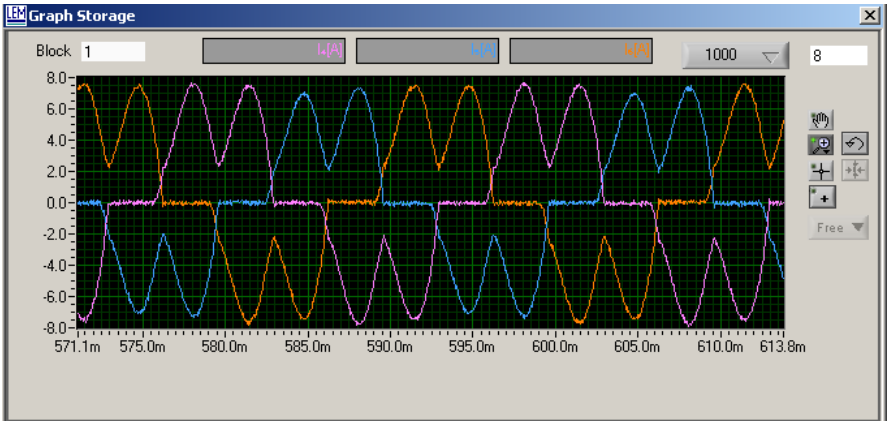

Fig. 4.65 Rectifier side 3-phase current experimental waveforms at 50% load for 5.5kW rated system employing IBF filter.

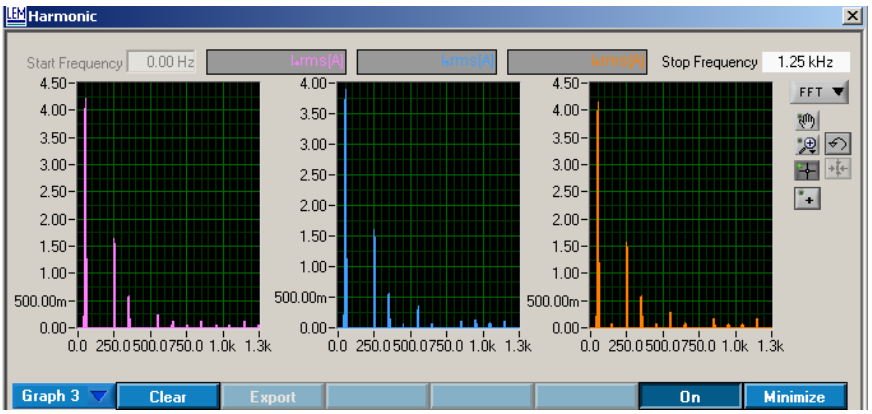

Fig. 4.66 Rectifier side 3-phase current harmonic spectrum at 50% load for 5.5kW rated system employing IBF filter.

The phase 2 line side current and phase 5 rectifier side current waveforms, and their harmonic spectrums are shown superimposed in Fig. 4.67 and Fig. 4.68, respectively. The IBF improved the discontinuity of the polluted rectifier current to an uninterrupted semi-sinusoidal clean line current. As a result, the rectifier current first two dominant current harmonics (5^{th} and 7^{th}) components (blue) are highly suppressed by the IBF in the line side (green) as shown in Fig. 4.68.

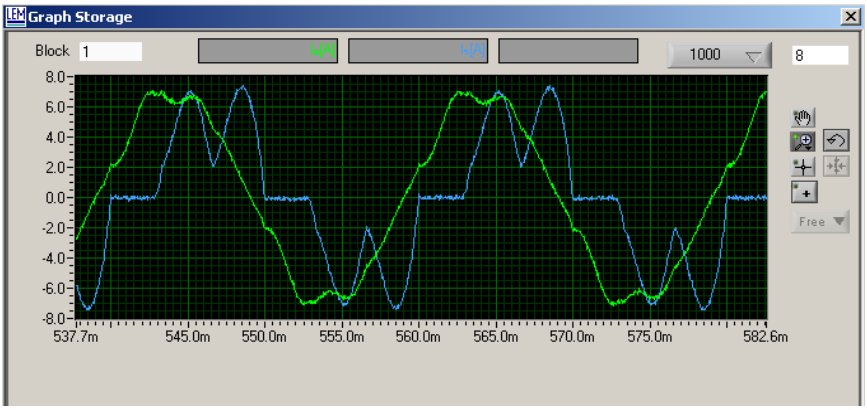

Fig. 4.67 Line and rectifier current experimental waveforms at 50% load for 5.5kW rated system employing IBF filter.

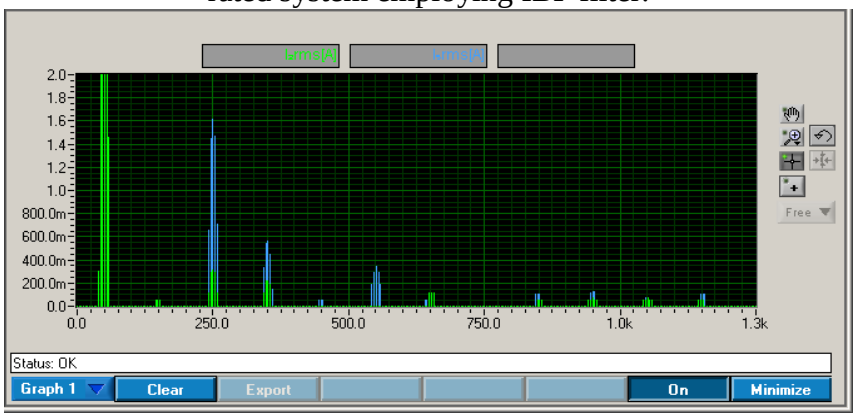

Fig. 4.68 Line and rectifier side current harmonic spectrum at 50% load for 5.5kW rated system employing IBF filter (Zoomed).

To examine the displacement angle between the line current and the supply voltage, phase 1 related waveforms are shown in Fig. 4.69. Moreover, due to the voltage and current scale large difference, a closer view to the same waveforms is shown in Fig. 4.70 to clarify the condition. The leading power factor condition of the line current (approx. 0.84) is observed. The rated load DC current and voltage experimental measured values are (5.3A and 520V).

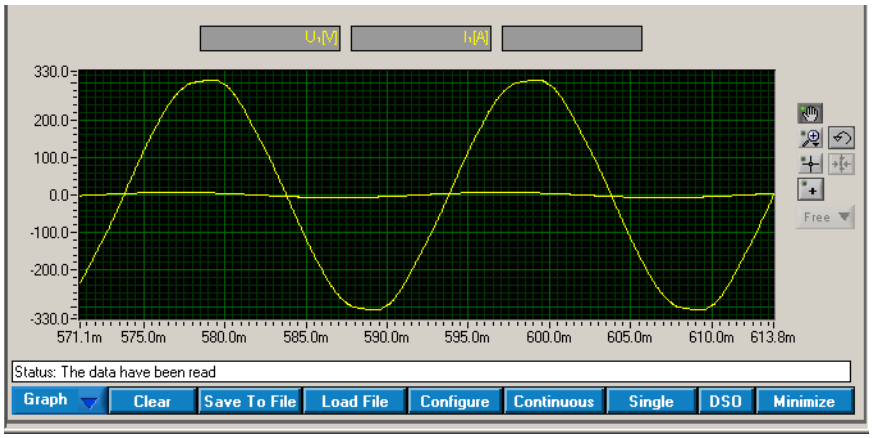

Fig. 4.69 Supply phase voltage and current experimental waveforms at 50% load for 5.5kW rated system employing IBF filter.

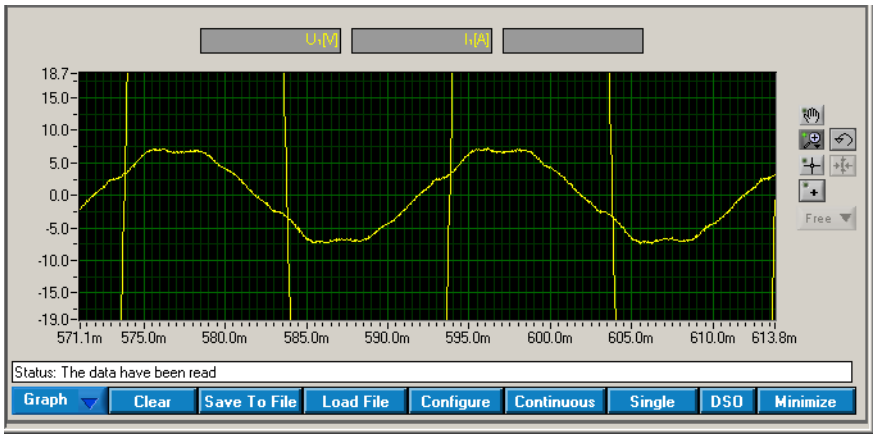

Fig. 4.70 Supply phase voltage and current experimental waveforms at 50% load for 5.5kW rated system employing IBF filter (Zoomed).

4.5.5 IBF No-Load Experimental Results

In this section, the experimental results of the 5.5kW ASD system at no-load operating condition are presented. The loading switch (shown in Fig. 4.46) is kept open during the test and, therefore, the set of the load resistors are not connected to

the system. The no-load supply side and rectifier side data is presented in Fig. 4.71. The line to line voltages at the rectifier side are increased to 402V rms value. From the full-load supply and rectifier side experimental data shown in Fig. 4.47 (depending on the measurement accuracy) the filter no-load to full-load output voltage regulation (ΔV_o (%)) value is about 4.9%. This is a stable improved broadband filter output voltage.

Fig. 4.71 Supply and rectifier side experimental data at no- load for 5.5kW rated system employing IBF filter (line and rectifier line-to-line voltage, total real and apparent power and supply voltage THD_V%).

The no-load line side experimental data for phases 1, 2 and 3 are shown in Fig. 4.72. The line currents in all phases have a low THDi% (< 10%) with a very poor leading power factor condition. Meanwhile, the rectifier side results data for phases 4, 5 and 6 are shown in Fig. 4.73 with no power consumption situation.

Fig. 4.72 Line side experimental data for phase 1, 2 and 3 at no- load for 5.5kW rated system employing IBF filter (voltage V, current I, real power P, current THDi%, reactive power Q, power factor Λ).

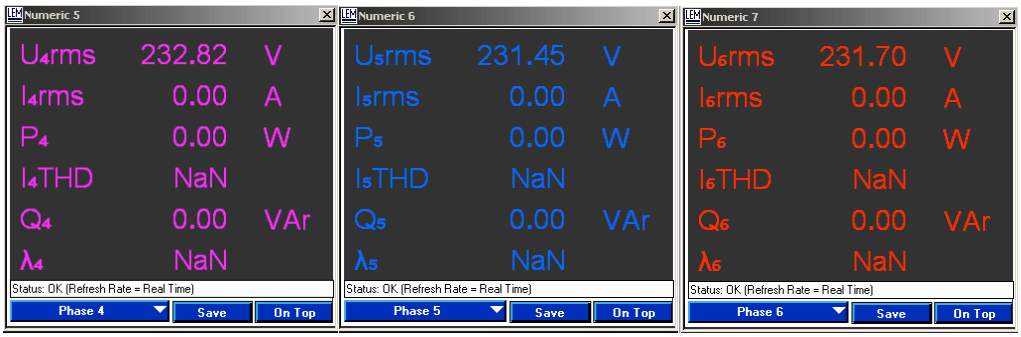

Fig. 4.73 Rectifier side experimental data for phase 4, 5 and 6 at no-load for 5.5kW rated system employing IBF filter (voltage V, current I, real power P, current THDi%, reactive power Q, power factor ʎ).

The related three-phase power analyser experimental no-load line (capacitor) current waveforms and their harmonic spectrum for the 5.5kW ASD system are shown in Fig. 4.74 and Fig. 4.75, respectively. The three-phase power analyser experimental no-load rectifier side current waveforms are shown in Fig. 4.76. The line currents have a considerably low THDi% values range from 7.54% to 9.17% with minimum 5^{th} harmonic component and no other dominant harmonic components (7^{th}, 11^{th} and 13^{th}) in their spectrum. The rectifier side has practically no current drawn at no-load condition.

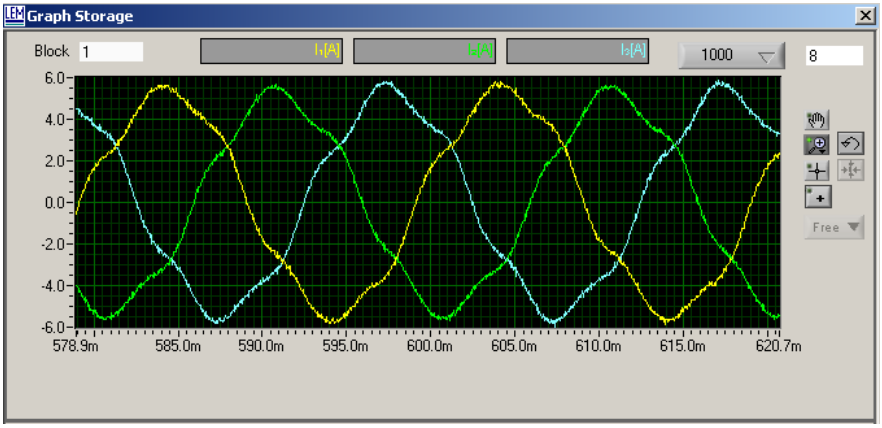

Fig. 4.74 Line side 3-phase current experimental waveforms at no-load for 5.5kW rated system employing IBF filter.

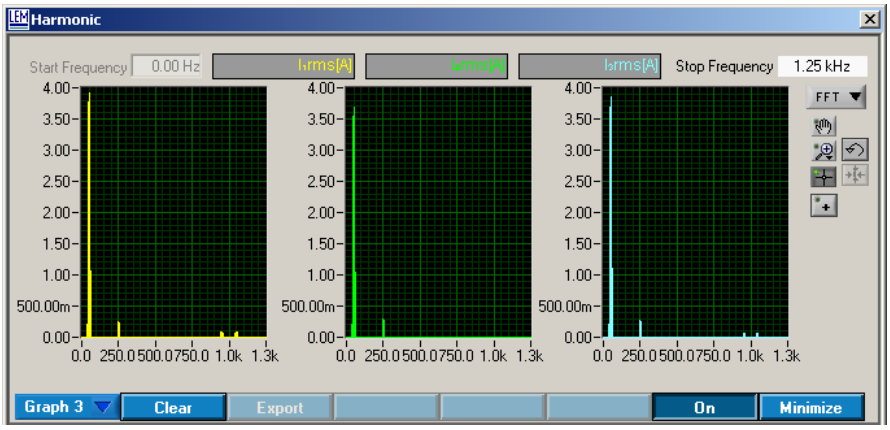

Fig. 4.75 Line side 3-phase current harmonic spectrum at no-load for 5.5kW rated system employing IBF filter.

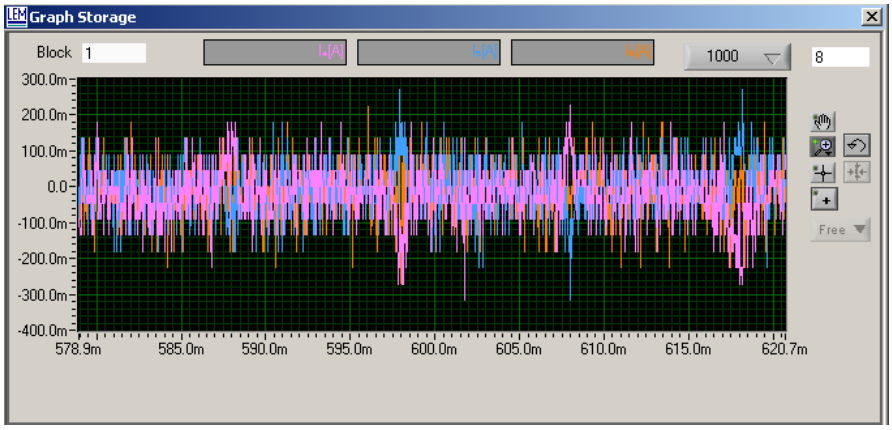

Fig. 4.76 Rectifier side 3-phase current experimental waveforms at no-load for 5.5kW rated system employing IBF filter.

Finally, the phase 1 (yellow) no-load line current and supply voltage harmonic spectrums combined with the phase 4 (purple) rectifier current harmonic spectrum are shown in Fig. 4.77. Practically, the supply voltage and the line side current have insignificant harmonic voltage and current components that can interact and cause any undesirable effects to other loads connected at the same PCC point in the distribution network. On contrary, the poor leading line power factor condition between the supply voltage and the line current (phase 1) is shown in Fig. 4.78. This is considered as the major limitation for the IBF filtering topology usage.

Fig. 4.79 shows the no-load current waveform at the rectifier side (zero value) and the rectifier side smooth phase voltage as a result of the non-existence of any distorted rectifier current. The rated load DC current and voltage experimental measured values are (0.0A and 565V).

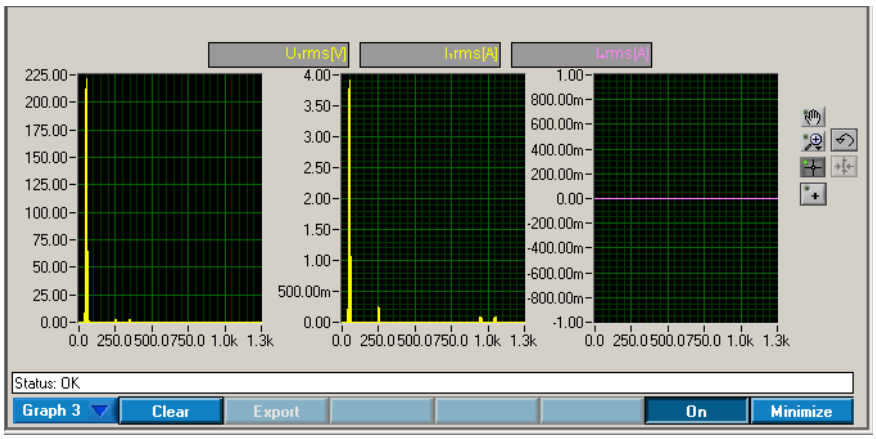

Fig. 4.77 Phase voltage, line current and rectifier current harmonic spectrum at no-load for 5.5kW rated system employing IBF filter.

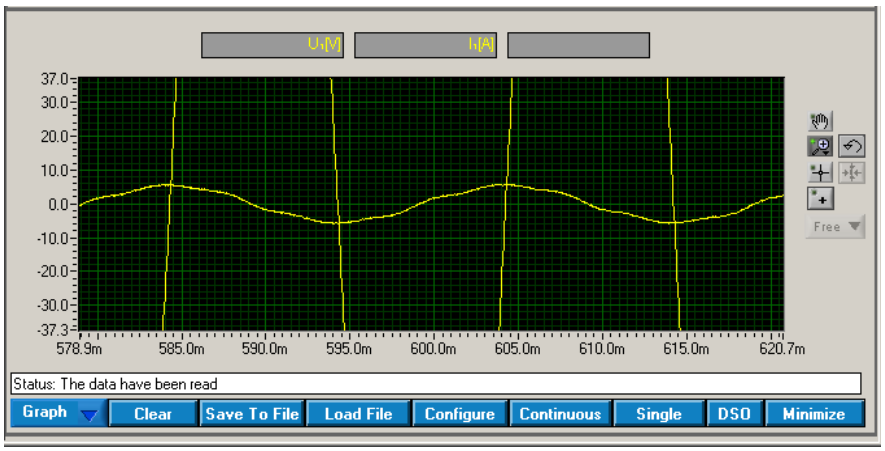

Fig. 4.78 Supply phase voltage and current experimental waveforms at no-load for 5.5kW rated system employing IBF filter (Zoomed).

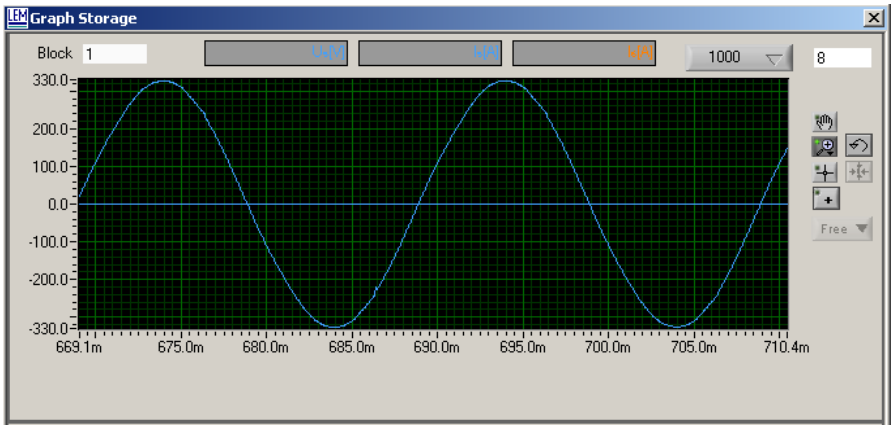

Fig. 4.79 Rectifier phase voltage and current experimental waveforms at no-load for 5.5kW rated system employing IBF filter.

Finally, the laboratory prototype built ASD system using the IBF was also examined with 75% and 60% loading conditions. The associated experimental measured results and waveforms are shown in Appendix E (sections E.1 and E.2).

4.5.6 Experimental Based Performance Evaluation of the IBF

In this section the improved broadband filter (IBF) overall experimental performance features are found. Data information has been used from no-load to full-load in five consecutive steps (0%, 50%, 60%, 75% and 100%) operating conditions and the performance characteristic resultant curves are presented. The improved broadband filter line current THDi% range (minimum to maximum) values are shown in Fig. 4.80. As the curve reveals, the ASD system using the IBF filtering topology has an overall low current distortion in the drawn input current. The input current THDi% load dependent values can comply with the standard harmonic regulations of any modern power quality criteria.

It has been observed the asymmetry of the power analyser measured line current THDi values as well as other values through all loading conditions investigated. This can be due to the accuracy measurements, supply voltage imbalance, phases loading imbalance and three-phase reactors manufacturer tolerance. In an attempt of measuring the IBF designed input and filter three-phase inductance, it has been found that phase 2 input inductor has less inductance value than the other phases. This difference will also contribute in the experiments measured results asymmetry between phases.

The line power factor and energy efficiency (including the power analyser shunt resistors) performance characteristics, from no-load to full-load, are shown in Fig. 4.81 and Fig. 4.82, respectively. As the curve in the Fig. 4.81 specify, the IBF based ASD system has a unity power factor at full-load condition and high values over the 50% loading situations. However, from no-load to about half-load operating range the line power factor has a limited range of values. This is major limitation that should be considered and, therefore, ASD drives with low duty cycle should consider disconnecting the IBF filter during the specified low loading condition

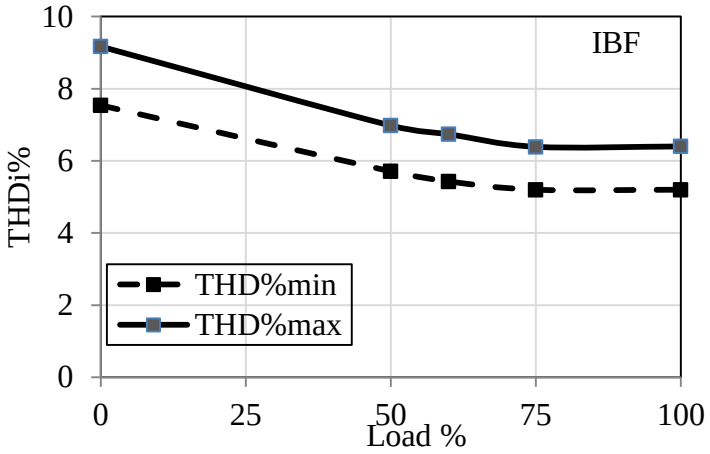

Fig. 4.80 The experimental line current THD_i% range from no-load to full-load for a 5.5kW ASD system utilizing the IBF structure.

The energy efficiency curve of the ASD system including the power analyser (Norma 5000) shunt resister box (shown in Fig. 4.82) has a relative low overall efficiency values. This is due to the Norma TRIAX-SHUNT resistors losses used to measure the current in the system by measuring the voltage drop across these precision resistors (connected between the three-phase voltage supply variac and the power analyser). Furthermore, power analyser accuracy limits and the laboratory line voltage variation may affect the efficiency estimation. Therefore, it is highly expected (as simulation results reveal) that the IBF filter individually should have a considerably higher energy efficiency values from half-load to full-load conditions (> 98%).

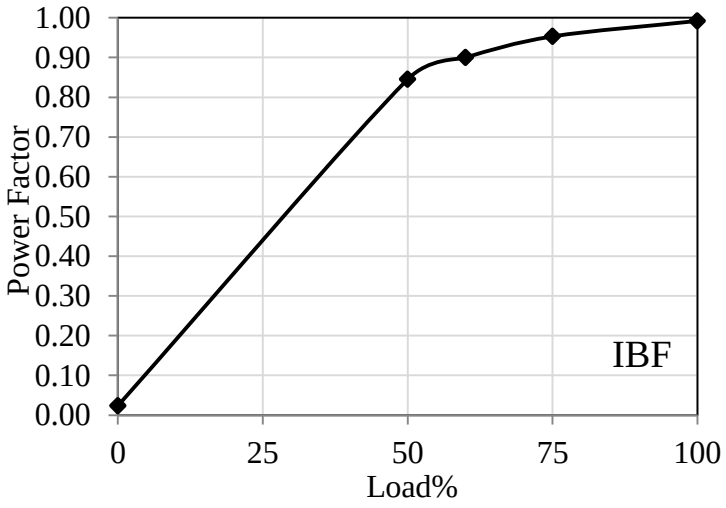

Fig. 4.81 The experimental line power factor from no-load to full-load for a 5.5kW ASD system utilizing the IBF structure.

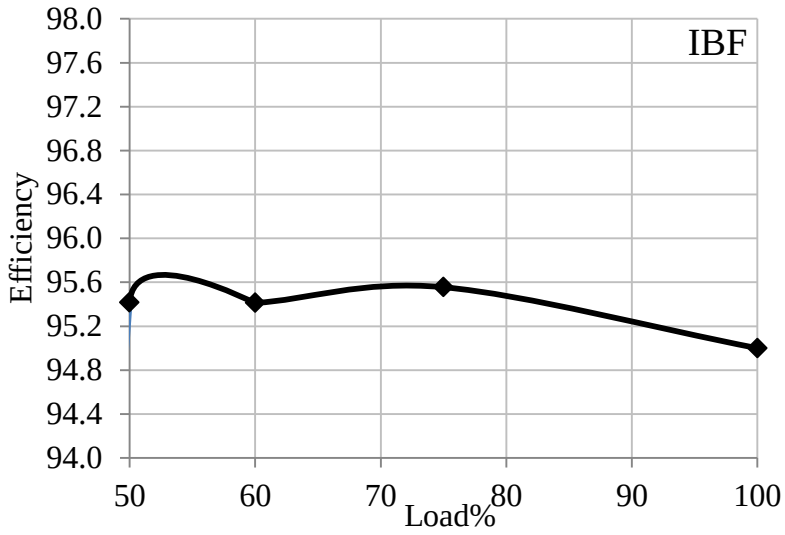

Fig. 4.82 The experimental IBF structure energy efficiency from half-load to full-load for a 5.5kW ASD system (including the power analyser shunt resistors).

Finally, the designed 5.5kW IBF laboratory prototype has been tested under 400V supply voltage. The full-load and no-load experimental measured results and waveforms are shown in Appendix E (sections E.3 and E.4). The IBF superior performances are maintained.

4.6 **Summary**

In this chapter, the GA implementation process in designing the IBF filter has been explained. This involved the problem formulation, chromosome encoding and selection of all GA operators. Fitness function and the GA results have been shown. The comparison with the linear searching method results reveals the advantage of the GA technique in optimizing the filter component values.

The performance of the optimized IBF structure has been discussed. The steady-state performance characteristics at various operating (loading) points were in focus. Balanced and unbalanced utility grid with and without voltage harmonic distortion operating conditions were considered. Furthermore, the main power quality parameters (line current THDi% and power factor, filter output voltage regulation (ΔV_o %)) and energy efficiency attributes have been investigated. The computer

simulation based study supports the theoretical performance prediction and illustrates the accuracy of the IBF filter parameter optimization method.

Finally, the laboratory performance characteristics of a 5.5 kW power rated ASD system utilizing the 4% AC reactor filter type and the optimized IBF configuration have been studied. The ASD steady-state performance characteristics from no-load to full-load operating conditions were considered. Similarly, investigation of the main power quality parameters (line current THD_i%, power factor, and filter output voltage regulation (ΔV_o %)) and energy efficiency attributes have been conducted.

The attained experimental results also supports the simulation results achieved and the superior complete performance of IBF based ASD systems has been validated and topology limitations agreed.

Extra detailed simulation and experimental results comparison will be presented in the conclusion chapter (final chapter).

The next chapter illustrates a new suggested reduced advanced broadband filter structure design, simulation and experimental performances results.

5 ADVANCED BROADBAND FILTER DESIGN

5.1 Introduction

In the previous chapter, the improved broadband filter (IBF) designs have been shown to give superior overall performance and proposed applications are increasing [21], [60], [61]. Compared to multi-stage single tuned shunt filters (STSF), the IBF has reduced sensitivity to line-voltage disturbance and unbalance, and is without harmonic resonance problems. Furthermore, the line current THDi% is significantly better, and the power factor may be close to unity [56].

In this chapter, based on the IBF success, a study that proposes a new advanced broadband filter (ABF) design which further reduces the number of utilized filter components, size (cost) and demonstrates its satisfactory performance for ASD applications is presented. The modified IBF structure is developed by eliminating the filter output smoothing AC reactor (L_o), normally connected at the rectifier side, which introduces a novel advanced broadband filter (ABF) structure. Similarly, the ABF design is performed using genetic algorithm (GA) at different power ratings to optimize the frequency-domain model of the system. In order to validate the effectiveness of the GA method in sizing components, a comparison of the filter components given by a linear design method is presented. Finally, the performance of an ABF applied to an ASD system is evaluated, and its successful performance is confirmed by analytical means, detailed computer simulations and lab experiments.

For better clarification, the basic IBF broadband filter structure is shown again on Fig. 5.1(a). Previous performance and experimental investigations (chapter 4) have shown that the IBF has very low input current THDi (<10%) over the full operating range, near unity power factor at full-load, and confirmed the improved input power quality of ASD systems line-connected via IBFs. The advanced broadband filter (ABF), shown on Fig. 5.1(b), has been developed, in this study, to explore the possibility of excluding the use of the 3-phase 4% smoothing AC reactor (L_o).

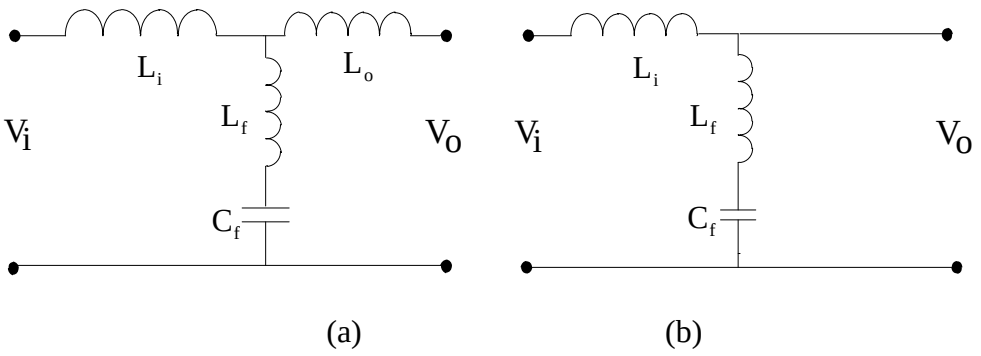

Fig. 5.1 Broadband filter configurations (a): Basic IBF, (b): Proposed ABF.

Consequently, the rectifier-side line current will be less heavily smoothed and, hence, contains higher levels of current at the dominant harmonics. This will lead to different filter characteristics and overall system performance under various operating conditions.

With an appropriate ABF design, the large input reactor (L_i) provides high impedance relative to the shunt filter impedance over a wide frequency range, which includes the dominant rectifier-current harmonics, and gives a high impedance ratio as shown in Fig. 5.2. In consequence, the rectifier-current harmonics will be impeded by the line and diverted through the shunt filter. Not only does L_i block the harmonic-current flow from the rectifier to the AC line, but it also minimizes the effect of the line-voltage harmonics on the rectifier (i.e. provides harmonic isolation between the source and the rectifier) and on the shunt filter. Therefore, L_i suppress harmonic-current flow either way (reduces line current THDi%).

The ABF filter parallel-resonant frequency f_p involving L_i-L_f-C_f is defined by equation 2.1 (similar to IBF). The parallel-resonant frequency is selected between the fundamental frequency and the first dominant rectifier current harmonic which is the 5^{th} harmonic such that harmonic resonance related overvoltage stresses are avoided. The filter capacitor C_f improves the input power factor (PF), while L_f is partitioned with $L_{i,}$ such that there is no overvoltage at the rectifier terminals and light-load to full-load filter output voltage change (ΔV_o%) is confined within a specified range.

Filter components L_f and C_f are connected in series to provide very low series impedance to the dominant rectifier current harmonics and short circuit them through

its path. The series resonant frequency f_s is defined in equation 2.2. Filter capacitors C_f are usually delta connected and damping resistors R_d are connected to C_f (similarly to IBF structure) to damp the voltage/current peaks during line-side switching transients.

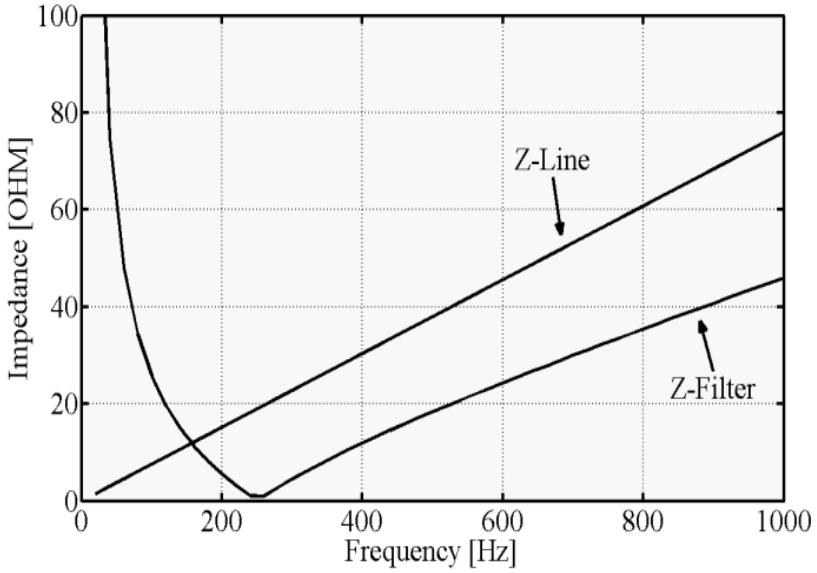

Fig. 5.2 Line and shunt branch impedances of ABF (5.5 kW system).

Therefore, this new ABF structure should have nearly the same IBF attributes in improving the overall ASD system power quality performance. However, eliminating the rectifier side three-phase smoothing reactor (with minimum built-in DC inductor 2% L_{dc} existence) will result in highly distorted rectifier drawn current, as shown in Fig. 1.4 and Fig. 1.5. This polluted current has very high harmonic components (5^{th} >60%, 7^{th} >35%, 11^{th} >8% and 13^{th} >8%) that may overstress the ABF filter components and prevent it from achieving the expected performance characteristic. Therefore, extra built-in DC inductor filter utilization may be mandatory in order to achieve satisfactory ASD performance while keeping the proposed filter components parameters, size and cost comparable to the successful IBF structure.

The design of the single-phase DC-link inductor is, therefore, re-considered in order to reduce this highly distorted rectifier current stress on the filter components and compensate the three-phase AC reactor loss (L_{ac}) in the new ABF topology.

5.2 **DC-link Inductor Selection Method**

In order to reduce the rectifier-current harmonic components, an extra DC-link inductor built into an ASD may be used to give a similar effect as the AC smoothing reactors. The DC-inductor is, when compared to AC reactors, smaller in size, lower in cost and operates at higher efficiency (fewer losses). Also, it causes no reduction of the DC-link voltage, and even reduces its ripple. The DC-link inductor is, therefore, more effective in reducing harmonic current levels and, hence, reducing the current stress on the DC-link capacitor (ensuring longer lifetime). The rectifier in-rush current and input current THDi values are reduced. Therefore, DC-link inductors are usually included inside many commercial drives, particularly at higher power ratings [12], [62].

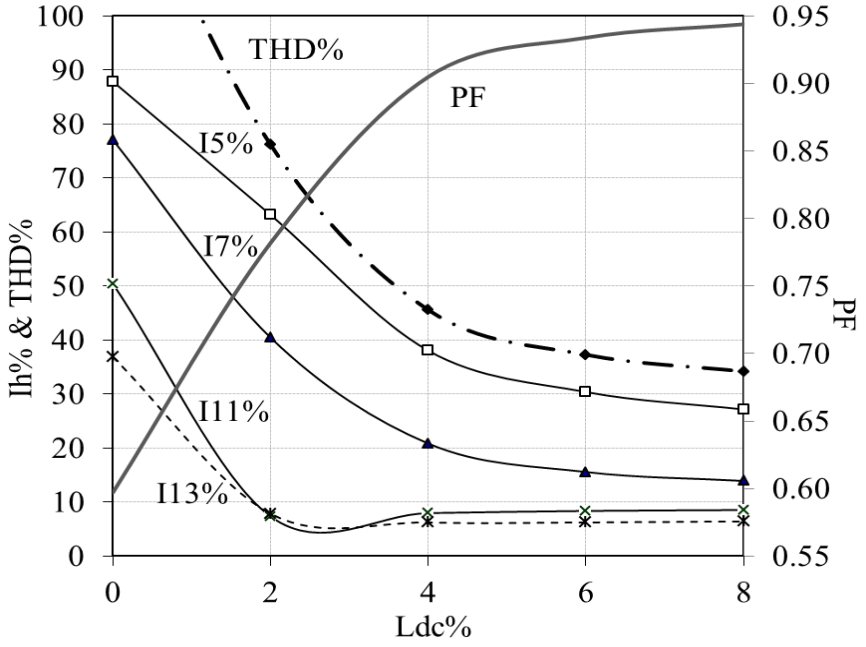

Fig. 5.3 Rectifier current THDi%, PF and dominant harmonic components for various range of DC-link inductor filter type.

Fig. 5.3 shows the effect of utilizing a range of DC-link inductor values, with no AC-side added reactors, on ASD system performance. This involves the rectifier current THDi% and the dominant harmonic component's percentage (I5%, I7%, I11% and I13%) along with the power factor all at the full-load operating condition. It is noticeable, as the figure reveals, that increasing the DC-link inductance decreases the

rectifier current THDi% and its harmonic contents, meanwhile improving the rectifier side PF. This reduction is huge (almost halving the values) at the 3% L_{dc} compared with no filter (0% L_{dc}) values. However, this rapid reduction rate is less for DC-link inductance values between (4% and 6%). Above 6% DC-link inductance the harmonic currents are almost constant. Therefore, it may be argued that the optimal value of the DC-link inductance is in the range of 4-6 %.

A further investigation was conducted to select a DC-link inductance value within the specified range. This involved the DC-link inductor capability to smooth the rectifier current waveform and reduce the most dominant harmonics compared with utilizing the smoothing three-phase and single-phase combination reactors (4% L_o and 2% L_{dc}) in the basic IBF structure. It is shown in Fig.5.4 that this IBF smoothing combination has a greater effect in reducing the rectifier side current harmonics with overall THDi% value of 33%, while the 4% L_{dc} and 6% L_{dc} inductors has less capability with total THDi% values of 45% and 37%, respectively. It is apparent that most current harmonic components have the lowest percentage values with the IBF smoothing structure.

However, it is clear from the figure that only the 6% L_{dc} inductor has a special ability to also minimize the most dominant harmonic component (I5). Therefore, this special characteristic will favour the use of the 6% L_{dc} DC-link inductor in the new ABF structure in order to reduce the most problematic harmonic current component in ASD systems. This will result in less stress in the ABF AC-side filter components and will give an opportunity to achieve almost the same basic IBF overall performance while keeping the ABF filter size comparable.

Finally, as shown in Fig.5.5, the DC output voltage reduction caused by the 6% L_{dc} DC-link inductor is negligible compared with the reduction caused by the smoothing combination in the basic IBF (4% L_o and 2% L_{dc}).

Therefore, the new ABF filter structure will contain the input reactor L_i, filter reactor Lf and the filter capacitor Cf along with 6%L_{dc} built-in single-phase DC-link

inductor drive system or an equivalent existing three-phase AC reactor 3-5%Lac (used by the customer).

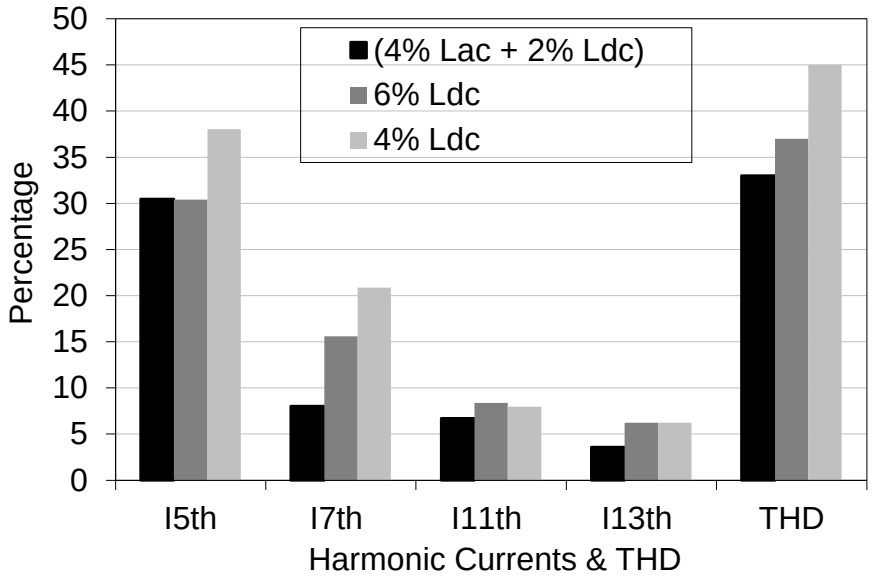

Fig. 5.4 Rectifier current dominant harmonic components and THDi for ASD system utilizing different filters.

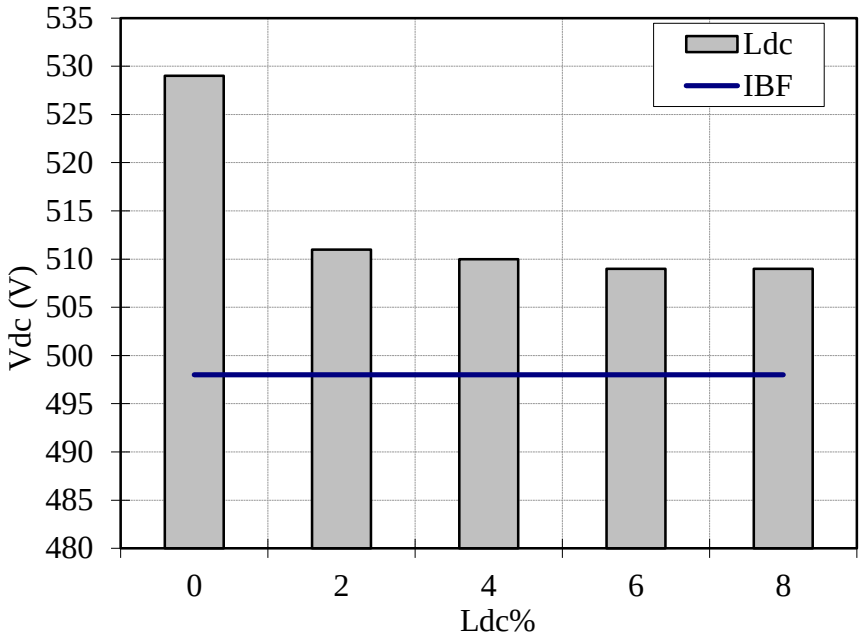

Fig. 5.5 DC rectifier output voltage mean values for ASD system using the IBF smoothing combination (4%Lac and 2%L_{dc}) and various range of DC-link inductor filter type.

Similar to the IBF, the process of optimizing the ABF design is complex. Because of the need to consider input and output power quality requirements, filter efficiency, cost and size, there are a number of conflicting constraints to be optimized which complicate the design process and obstruct reaching the most effective design. Therefore, the same IBF design procedure using the linear method then the GA method is proposed for the ABF design. The similar system modelling equivalent circuits shown in Fig 2.4 to Fig. 2.6 are utilized by assuming that the AC output reactor (L_o) has a zero inductance value in Fig. 2.4 ($L_o \rightarrow 0.0$). Similar, elimination will be done in equation 2.21 as follows:

$$L_L \cong [L_i + (L_o \rightarrow o)] \tag{5.1}$$

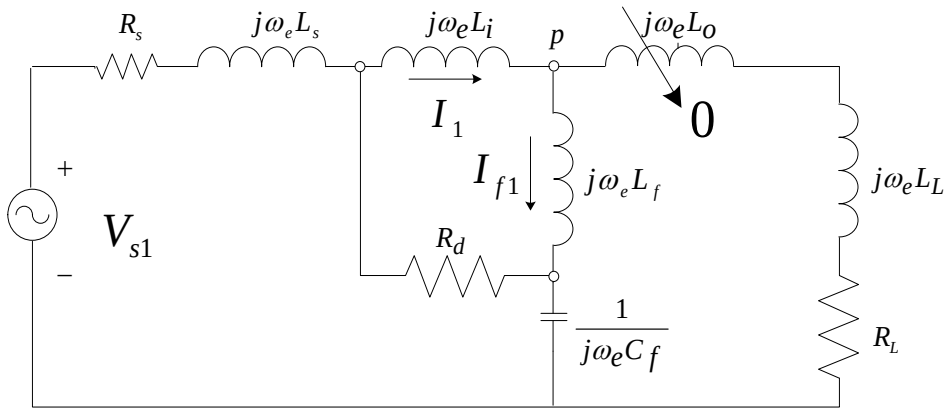

Fig. 5.6 Full-load fundamental frequency model of the ASD system.

5.3 **Linear Method Implementation**

Similarly, in order to compare between the linear approach and the GA approach results, the utilized linear method MATLAB code results for the 5.5kW and 55kW power ratings with the maximum achievable power quality indices design criteria (implementing the 6%L_{dc} DC-link filter associated harmonic current spectrum) are represented. It has been observed that no results can be obtained for better power quality criteria than the shown below. The code displays the following results:

L_{dc} (mH) = 4.56

enter the ASD rated power value in kW:5.5

enter the line current THDi limit value (THDi-max%): 6.5

enter the output voltage regulation limit value (DelVmax%): 4.0

PLEASE WAIT

Columns 1 through 9

'Results'	'Li(mH)'	'Lf(mH)'	'Cf(µF)'	'THDi'	'DelVo'	'PF'	'fp'	'fs'
[1]	[12.94]	[5.98]	[20.9]	[6.49]	[3.91]	[0.953]	[146.2]	[259.97]
[2]	[12.94]	[5.98]	[20.9]	[6.47]	[3.91]	[0.953]	[146.1]	[259.74]
[3]	[12.94]	[5.98]	[20.9]	[6.46]	[3.91]	[0.952]	[145.9]	[259.52]

enter the ASD rated power value in kW:55

enter the line current THDi limit value (THDi-max%): 6.5

enter the output voltage regulation limit value (DelVmax%): 4.0

PLEASE WAIT

Columns 1 through 9

'Results'	'Li(mH)'	'Lf(mH)'	'Cf(µF)'	'THDi'	'DelVo'	'PF'	'fp'	'fs'
[1]	[1.294]	[0.5982]	[208.8]	[6.49]	[3.91]	[0.952]	[146.2]	[259.96]
[2]	[1.294]	[0.5982]	[209.2]	[6.47]	[3.91]	[0.953]	[146.0]	[259.74]
[3]	[1.2939]	[0.5982]	[209.7]	[6.46]	[3.91]	[0.952]	[145.9]	[259.29]

In a similar approach, these linear method results will be used for comparison with the GA method results and, meanwhile, are utilized as initial values in the GA approach. This will help to obtain feasible results that can reduce the ABF components parameters and, therefore, reduce its bulky passive components while maintaining a satisfactory ASD system performance under various operating condition.

5.4 **Genetic Algorithm Implementation**

For given ASD ratings and power system parameters, based on the system equivalent circuits, the filter-component values for L_i, L_f, and C_f are initially proposed in a GA MATLAB M-file based computer program. The initial range of values is estimated by the linear design method previously explained. Similarly, the program implements

modified equivalent circuits derived formulas, calculates the impedances, then voltages, and currents followed by performance calculation (THDi%, PF, ΔV_o%). Based on the performance obtained, every set of solutions (chromosomes) in the current generation will be examined by the same fitness function given in 4.1. The filter component values are varied until the objective of the fitness function is met with suitable convergence. Similarly to the IBF case study, it was also observed that an appropriate mutation rate would speed up the evolution process and shorten the searching time of GAs. High crossover fractions ($\geq$ 80%) and low mutation rates ($\leq$ 1.5%) applied on the selected fittest parents of each generation to achieve the best convergence for this specific design problem.

Fig. 5.7 shows the 5.5kW ASD power rating GA fitness curve (80% crossover and 1.0% mutation rates). It illustrates that the optimized solution is obtained in generation number 13 and the whole population ultimately converges towards it. The corresponding 5.5kW ASD power rating filter values obtained are L_i (12.1mH), L_f (7.8 mH) and $C_{f\Delta}$ (17.3 µF). The corresponding series resonance frequency f_s and parallel resonance frequency f_p values are 250Hz and 156Hz, respectively. The f_p value shows that the harmonic resonance problem risk is negligible for the system.

Similarly, Fig. 5.8 shows the 55kW ASD power rating GA fitness curve (100% crossover and 0.1% mutation rates). The optimized solution is achieved in generation number 12 and the entire population eventually converges toward the optimized solution. The obtained filter values are L_i (1.20mH), L_f (0.79 mH) and $C_{f\Delta}$ (168 µF). The resultant series resonance frequency f_s and parallel resonance frequency f_p values are 250Hz and 157Hz, respectively. It is very important to notice that in both power rating cases the f_p values show that the harmonic resonance problem risk is insignificant.

The new ABF filter component values, obtained by the GA searching method, of the 5.5kW and 55kW ASD power rating and the expected correlated system performance results are presented in the next section. Furthermore, comparison with the linear searching method results is illustrated.

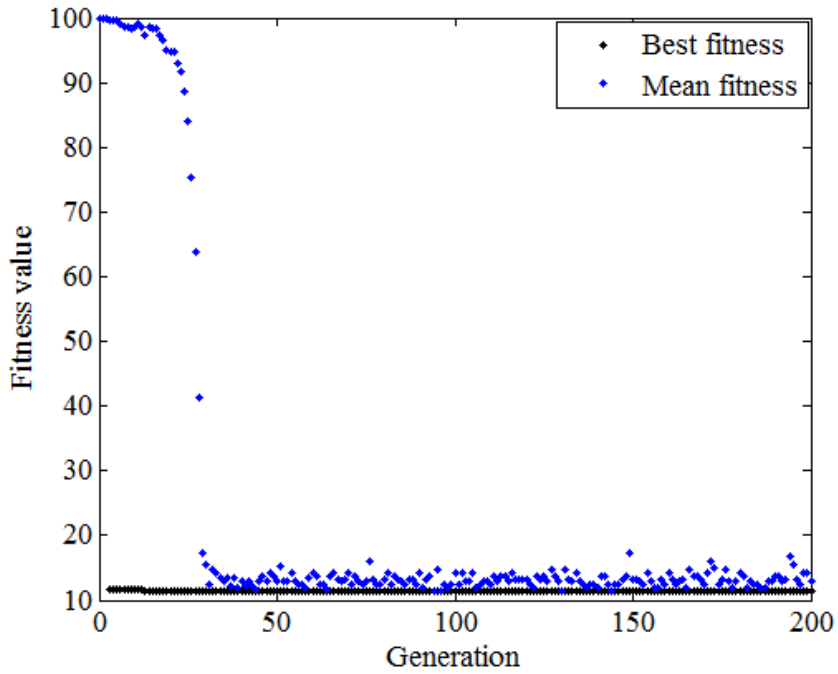

Fig. 5.7 Best and mean fitness function curves in GA for 5.5kW ASD system.

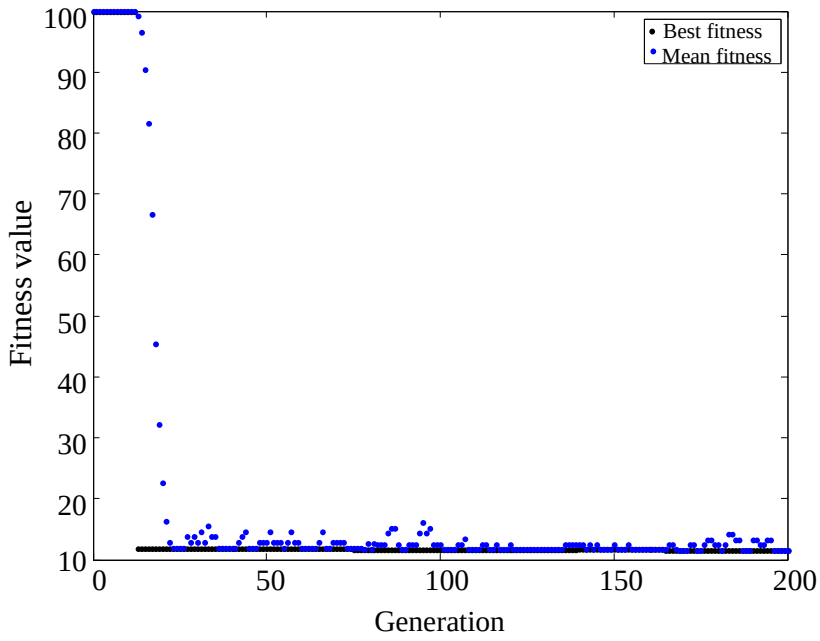

Fig. 5.8 Best and mean fitness function curves in GA for 55kW ASD system.

5.5 **Comparison of Different Searching Methods Results**

The ABF filter component values achieved with both searching methods (linear and GA) for 5.5 and 55kW power rating ASDs are shown in Table 5.1. Reductions of

(6.5 -7.0) % in the input inductance L_i parameter and (17-20) % in filter capacitance C_f parameter have been accomplished. Consequently, and essentially, the filter inductance L_f parameter will increase to preserve the series resonance frequency (f_s) within its preferred operative value. This involves keeping it closer to the dominant harmonic current component ($I5^{th}$). However, the value of L_f is still much smaller than L_i for both power ratings. Furthermore, the filter inductor is designed to carry only the harmonic-current components (< 50% of rms rated line value) and, therefore, is compact in size. On the other hand, the input inductor is carrying the full line-current and any reduction in L_i parameter results in considerably reduced filter size and cost.

Usually the filter capacitor is the most expensive part in the ABF filter and about 20% capacitance reduction is very effective in decreasing the cost and size, improving the system power factor characteristics, and reducing output voltage regulation from light-load to full-load. Table 5.1 shows a comparison between the obtained filter component values of the two searching methods, while Table 5.2 demonstrates a comparison of the analytically estimated system performance.

Table 5.1 ABF component values

P_R (kW)	5.5		55	
Searching method	Linear	**GA**	Linear	**GA**
L_i (mH)	12.94	**12.10**	1.290	**1.20**
L_f (mH)	5.98	**7.80**	0.598	**0.79**
$C_{f\Delta}$ (µF)	20.9	**17.3**	208.8	**168**

Table 5.2 Performance comparison of ASD system utilizing ABF

Searching method	THD_i (%)	PF≈Cosφ (leading)	ΔV_o (%)	fp (Hz)	fs (Hz)
Linear	6.5	0.95	3.9	146	259-260
GA	**6.9**	**0.98 - 0.99**	**3.3 - 3.5**	**156-157**	**250**

As Table 5.1 and Table 5.2 show, the GA algorithm is an effective method of finding smaller ABF filter components values which are capable to achieve higher input

power factor, lower voltage regulation and practically the same input current THDi% values with respect to the linear approach results.

5.6 Computer Simulations and Performance Evaluation

In this section, a similar detailed model of the ASD system (rectifier, DC-link and inverter) for computer simulation will be utilized to extract the steady-state performance characteristics under different operating and loading conditions. This will involve the ASD system using the 6% DC-link inductor individually and along with the new proposed ABF filter. Operation performance under balanced and unbalanced voltage supply conditions will be investigated with the assumption of practical voltage supply harmonics (3% THDv) existence (implementing the same dominant voltage harmonic components shown in section 3.4 in the simulation circuit).

Additionally, evaluating the ABF filter energy efficiency and output voltage regulation ΔV_o (%), ASD line total current harmonics distortion (THDi%) and power factor (PF) will be in focus.

The computer simulation based investigation involves 5.5 kW and 55 kW ASD power ratings. The same supply source impedance parameters for both power ratings, shown in Table 4.3, are used.

5.6.1 DC-link Inductor Filter Based ASD System

In this preliminary investigation, and for comparison reasons, the ASD system performance characteristics utilizing only the selected single-phase 6% DC-link inductor filtering type are presented. The line current and voltage simulation waveforms are illustrated.

Table 5.3 shows the implemented values of the 6% DC-link inductance, DC-link capacitance and DC load resistance in the simulation circuit for 5.5kW and 55kW power ratings. These parameters along with source impedance parameters, shown in Table 4.3, are implemented in the simulation circuit shown in Fig. 5.9.

Table 5.3 DC-link inductor (6% L_{dc}) filter value and load resistance values

Power rating (kW)	5.5	55
DC inductor L_{dc} (mH)	4.6	0.46
DC Capacitor C_{dc} (mF)	1.0	10
Load resistor R_L (Ω)	47	4.7

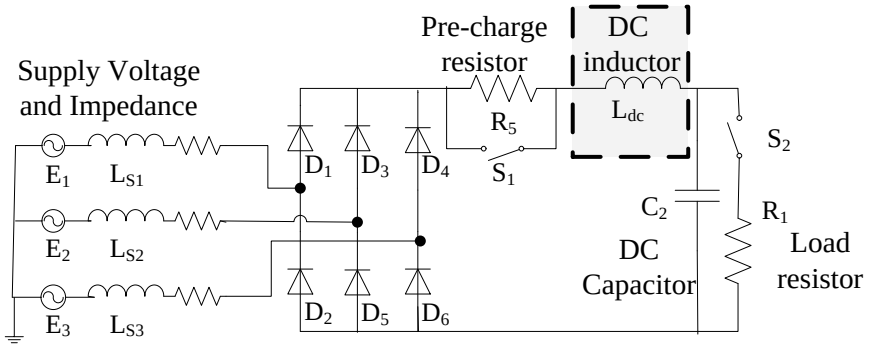

Fig. 5.9 Simulation circuit for ASD system utilizing DC-Link inductor (L_{dc}).

Fig. 5.10 shows the full-load line current and supply voltage simulation waveforms for 5.5kW rated system. The line current THDi value is 37.6% while the line power factor value is 0.934 lagging. Fig. 5.11 shows the DC current (I_{dc}) and voltage (V_{dc}) rectifier full-load outputs simulation waveforms for 5.5kW rated system.

Table 5.4 shows the full-load performance of this filtering method for both 5.5kW and 55kW ASD ratings. As the table indicates, the single-phase 6% L_{dc} built-in inductor will smooth the drawn rectifier current and result in minimum voltage drop in the output DC voltage. However, this line current THDi% and power factor attained performance cannot comply with conventional power quality regulations. Therefore, along with the ABF filter topology the ASD system should improve the overall performance.

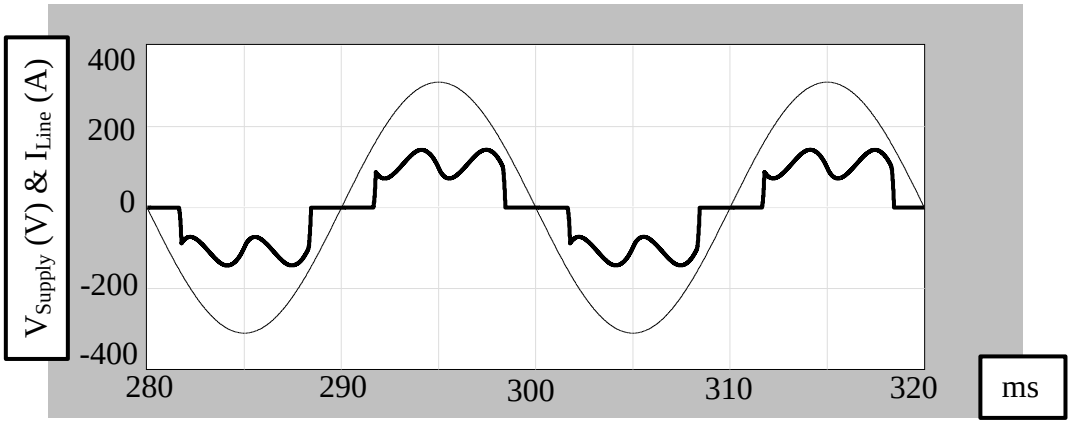

Fig. 5.10 Line current (**bold**) and supply voltage simulation waveforms at full-load for 5.5kW rated system employing 6%L_{dc} (current scale: 10x).

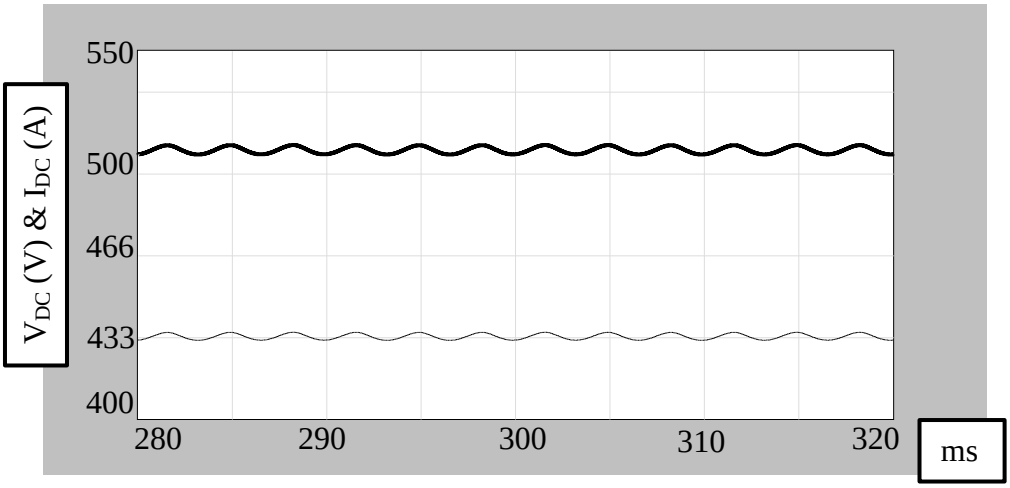

Fig. 5.11 DC load current and voltage (**bold**) simulation waveforms at full-load for 5.5kW rated system employing IBF (current scale: 40x).

Table 5.4 Full-load performance of 6% L_{dc} filter for 5.5kW and 55kW power ratings

Power rating (kW)	5.5	55
Line THD_i%	37.6	37.4
Line PF	0.934	0.932
Output V_{dc} (V)	509	508

5.6.2 ABF Full-Load Simulations of 5.5 kW ASD System

In this section, simulation based performance of the ASD system utilizing the proposed ABF filter with its final optimized filter component values estimated by the GA process are explored. Similarly, the ASD system performance is estimated under

both balanced and unbalanced supply system conditions along with the practical 3% THDv voltage harmonics distortion existence.

Table 5.1 shows the 5.5kW ABF confined parameters that are implemented in the simulation circuit presented in Fig. 5.12. The same maximum damping resistor (Rd) of 300 ohms resistance value has been applied in the simulation circuit in order to minimize the filter power losses at steady-state operating conditions.

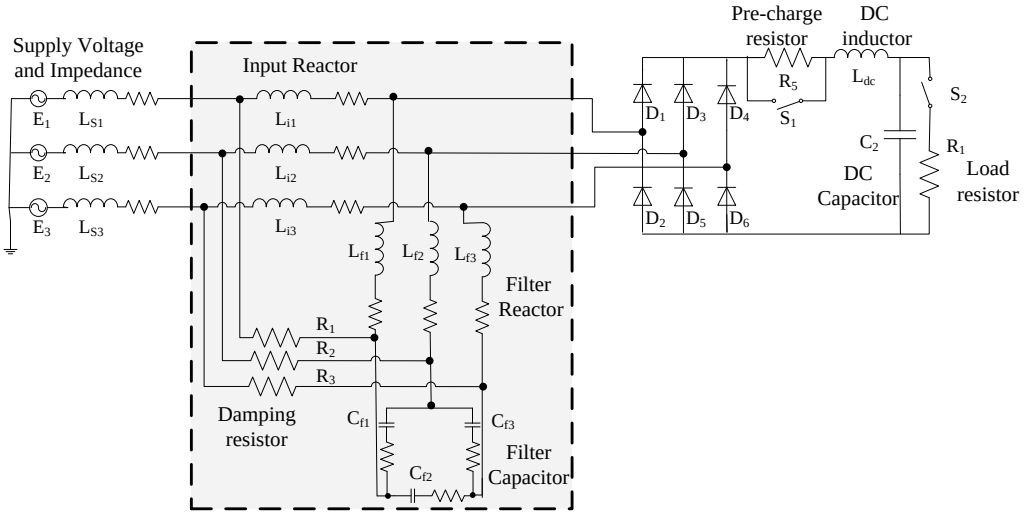

Fig. 5.12 Simulation circuit for ASD system utilizing ABF.

Fig. 5.13 demonstrates the full-load line current and rectifier current simulation waveforms. The rectifier side current THDi% high value (37%) has been successfully decreased to a very low THDi% value (5.20%) in the line side current. This nearly sinusoidal line current waveform confirm the ability of the ABF structure to block the injected harmonic current components from the nonlinear bridge rectifier converter and short them through the single filter shunt path.

Additionally, Fig. 5.14 shows the full-load line current and supply phase voltage simulation waveform. The line power factor is 0.984 leading at full-load operating condition. It is noticed that the ABF filter exhibits slightly less line power factor value than the IBF filter. This is due to the less inductive reactor components used in the ABF structure and the marginally higher filter designed capacitance parameter utilized. These simulation based results are closely linked with the analytical results

shown in Table 5.2 (similar to IBF results correlation level) and, therefore, support the good accuracy level of the system modelling and parameter estimation technique.

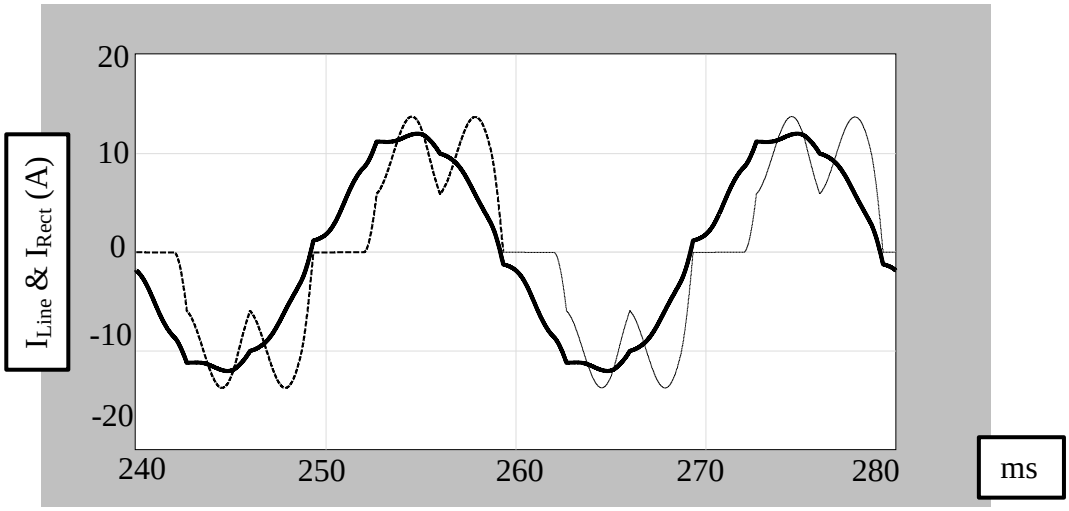

Fig. 5.13 Line (**bold**) and rectifier current simulation waveforms at full-load for 5.5kW rated system employing ABF.

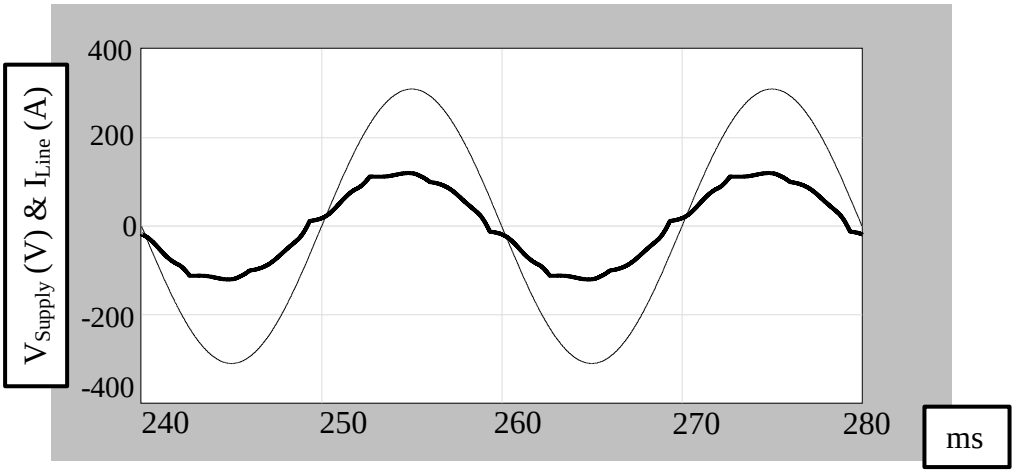

Fig. 5.14 Line current (**bold**) and supply voltage simulation waveforms at full-load for 5.5kW rated system employing ABF (current scale: 10x).

Fig. 5.15 shows the full-load DC current and voltage waveforms with suitable current scaling factor. The ABF DC output voltage is 526V which is slightly higher than the IBF DC output voltage (508V). Even though both broadband filter structures have almost the same capacitor size, this small increment is mainly due to the elimination of the output reactor 4%Lac voltage drop used in the IBF configuration. Lastly, Fig. 5.16 shows the filter capacitor current and voltage simulation waveforms

and Fig. 5.17 shows the rectifier current and rectifier line-to-line voltage simulation waveforms, both at full-load operating condition.

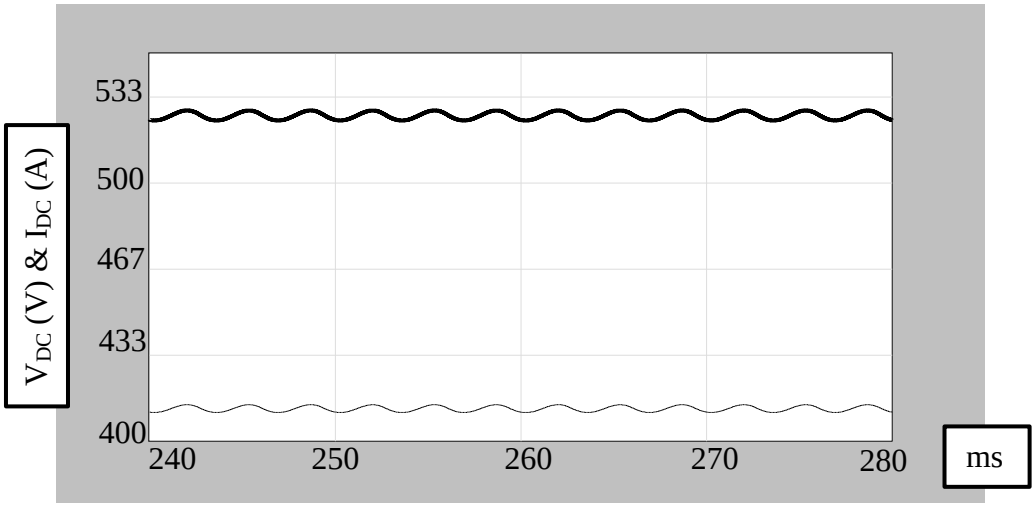

Fig. 5.15 DC load current and voltage (**bold**) simulation waveforms at full-load for 5.5kW rated system employing ABF (current scale: 40x).

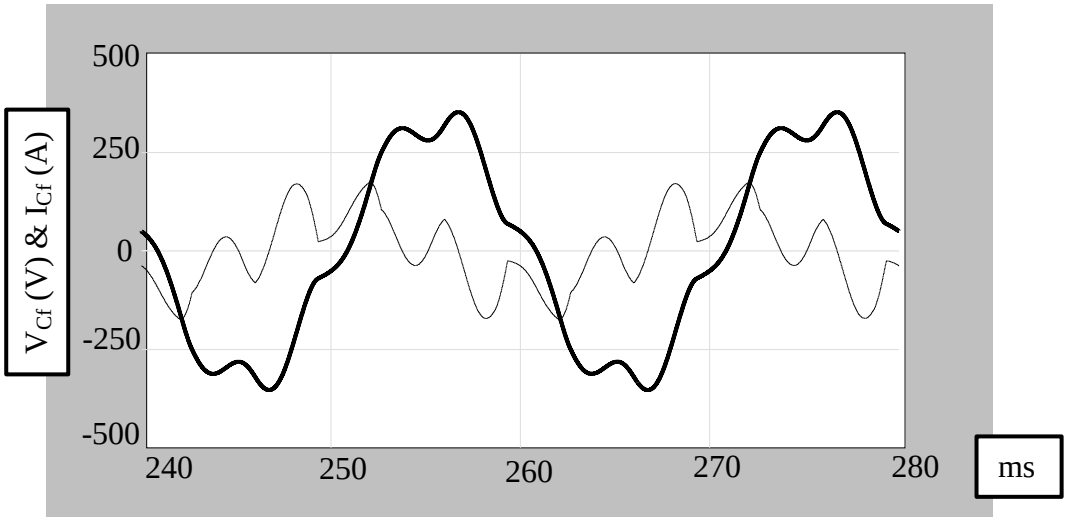

Fig. 5.16 Filter capacitor current and voltage (**bold**) simulation waveforms at full-load for 5.5kW rated system employing ABF (current scale: 20x).

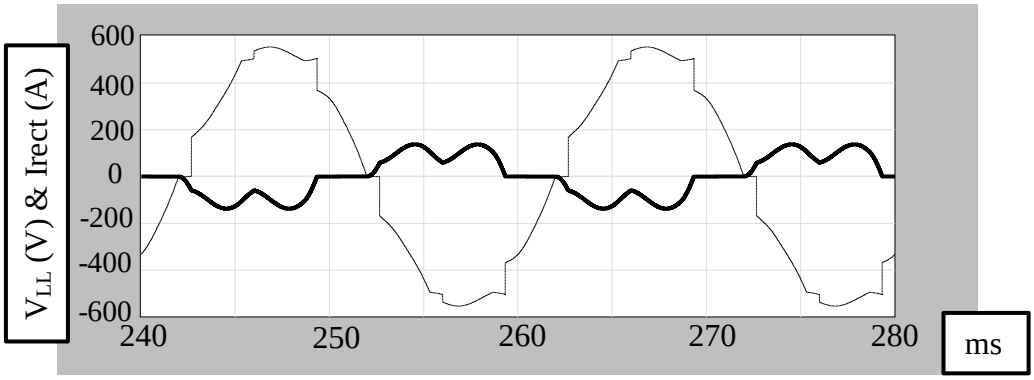

Fig. 5.17 Rectifier current (**bold**) and line-to-line voltage simulation waveforms at full-load for 5.5kW rated system employing ABF (current scale: 10x).

These illustrated simulation waveforms and the corresponding power quality results at steady-state full-load operating condition support the good ability of the ABF new reduced structure to comply with harmonic control standard regulations in modern distribution network systems. Therefore the ABF achieved a considerable success in maintaining good and satisfactory ASD system performance (compared to the IBF usage) with the use of less broadband filter components and the expenses of maximizing the single-phase built-in DC-link inductor.

5.6.3 ABF Light-load Simulations of 5.5 kW ASD System

Similarly, the ASD using the ABF filter simulation results and waveforms operating at light-load condition (10%) are revealed in this section. This operating condition is achieved by increasing the load resistance by a multiplication factor of 10. The light-load line current and the supply phase voltage simulation waveforms are shown in Fig. 5.18. The ABF filter, with its relatively large designed isolating input AC three-phase reactor (L_i), succeeds to block the supply current harmonics and preserve the line current low THDi (7.4%) value. However, this drawn light-load filter capacitor current provide extra reactive power compensation at fundamental frequency and result in very low leading line power factor (0.246). This simulation result validates the need to consider this main limitation (previously concluded from the IBF light-loading results) in applying such broadband passive filters during light-load drive conditions.

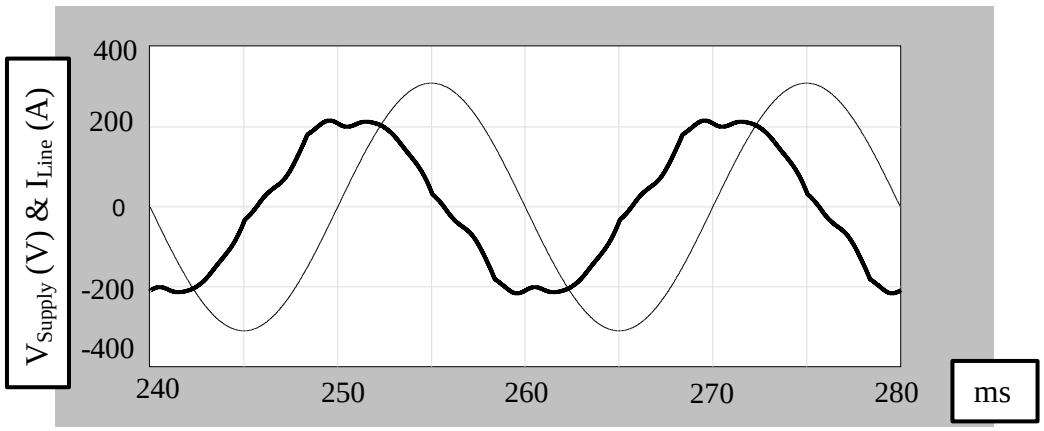

Fig. 5.18 Line current (**bold**) and supply voltage simulation waveforms at light-load for 5.5kW rated system employing ABF (current scale:40x).

5.6.4 ABF Full-Load Simulations of 55 kW ASD System

To confirm the obtained ASD simulation results performance attributes, the 55kW power rated ASD system simulation model is under focus. The 55kW ABF estimated GA filter component (less in values, design size and cost) shown in Table 5.1 are applied in the same simulation circuit shown in Fig. 5.12. Moreover, to achieve maximum ABF efficiency at steady-state, similarly, the maximum damping resistor (Rd) of 40 ohms is selected from Table A.1.

Fig. 5.19 shows the full-load line current and rectifier current simulation waveforms. The illustrated smooth line current has a very low THDi value of 5.25%, while the rectifier current shown waveform has high THDi value of 37%. This result approves the ABF ability to suppress the rectifier current harmonics and prevent them from appearing in the supply side. Furthermore, the full-load line current and the supply phase voltage simulation waveforms are shown in Fig. 5.20. The drawn line current has a high power factor value of 0.985 leading.

Similarly these 55kW ASD simulation findings are in good correlation with Table 5.2 analytical estimated results.

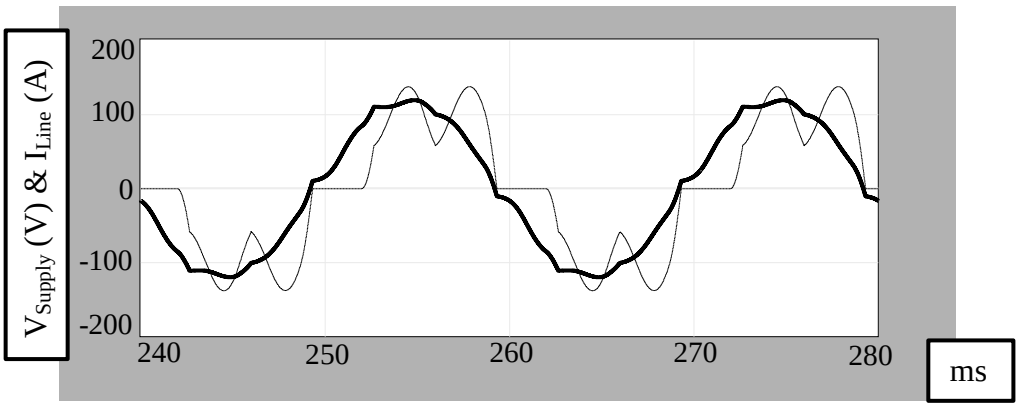

Fig. 5.19 Line (**bold**) and rectifier current simulation waveforms at full-load for 55kW rated system employing ABF.

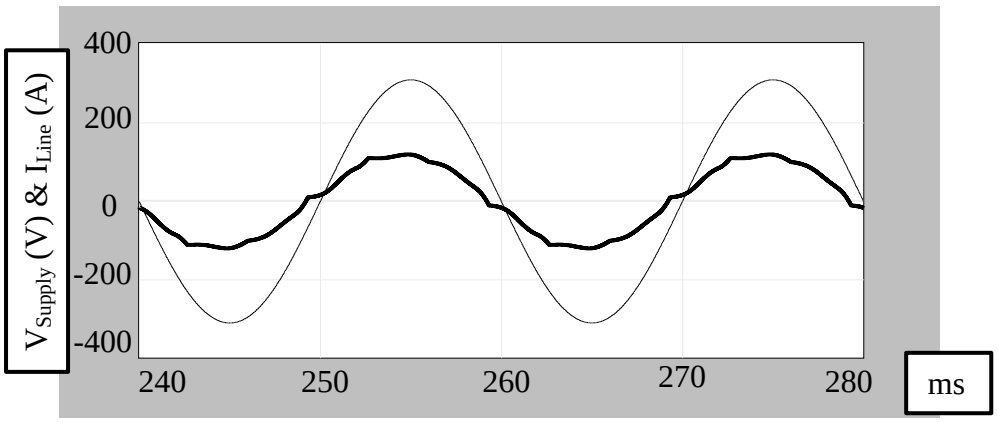

Fig. 5.20 Line current (**bold**) and supply voltage simulation waveforms at full-load for 55kW rated system employing ABF.

Fig. 5.21 displays the full-load DC current and voltage waveforms with suitable current scaling factor. Fig. 5.22 shows the filter capacitor current and voltage simulation waveforms and Fig. 5.23 shows the rectifier current and rectifier line-to-line voltage simulation waveforms, both at full-load operating condition.

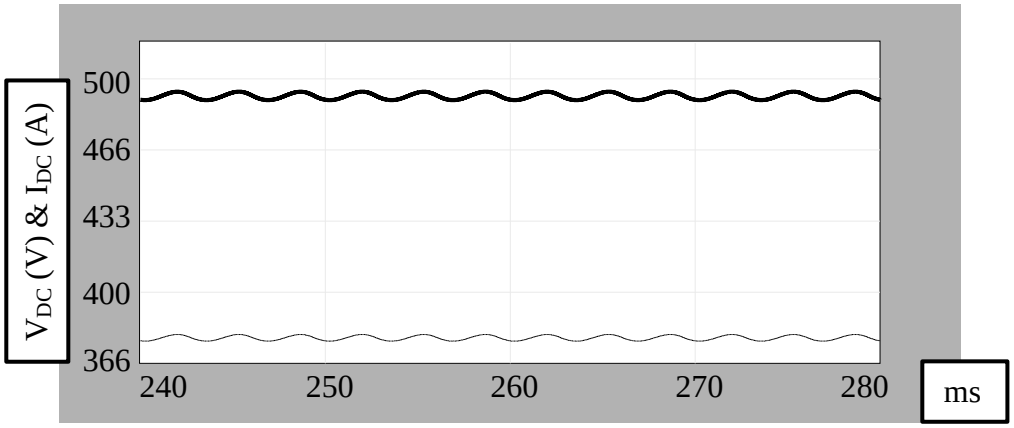

Fig. 5.21 DC load current and voltage (**bold**) simulation waveforms at full-load for 55kW rated system employing ABF (current scale: 4x).

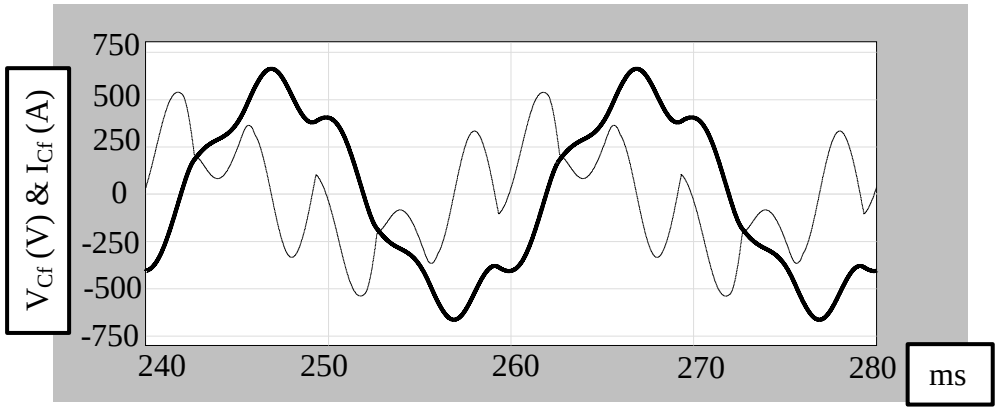

Fig. 5.22 Filter capacitor current and voltage (**bold**) simulation waveforms at full-load for 55kW rated system employing ABF (current scale:4x).

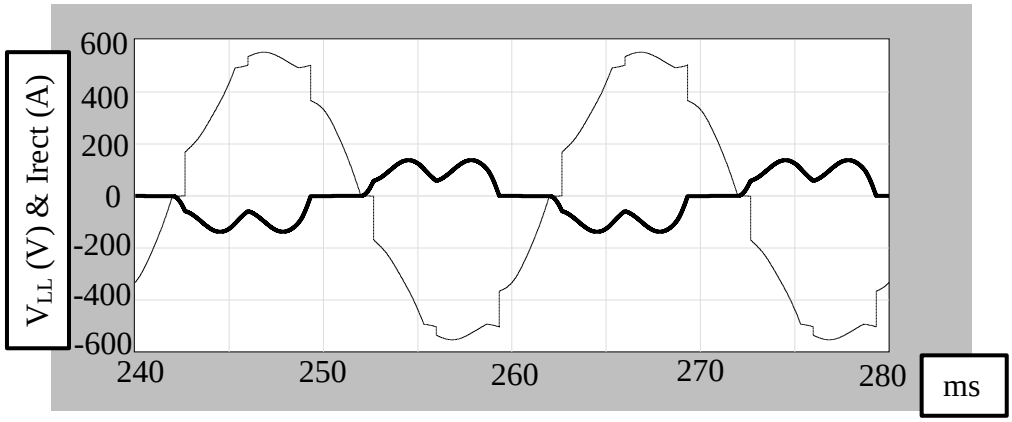

Fig. 5.23 Rectifier current (**bold**) and line-to-line voltage simulation waveforms at full-load for 55kW rated system employing ABF.

5.6.5 ABF Light-Load Simulations of 55 kW ASD System

Similarly, this section shows the ASD using the ABF filter simulation results and waveforms under light-load condition (10%). The light-load line current and the supply phase voltage simulation waveforms are shown in Fig. 5.24. The line current is smooth and has low THDi value (7.6%). Nevertheless, this drawn capacitive current result in very low leading line power factor (0.25).

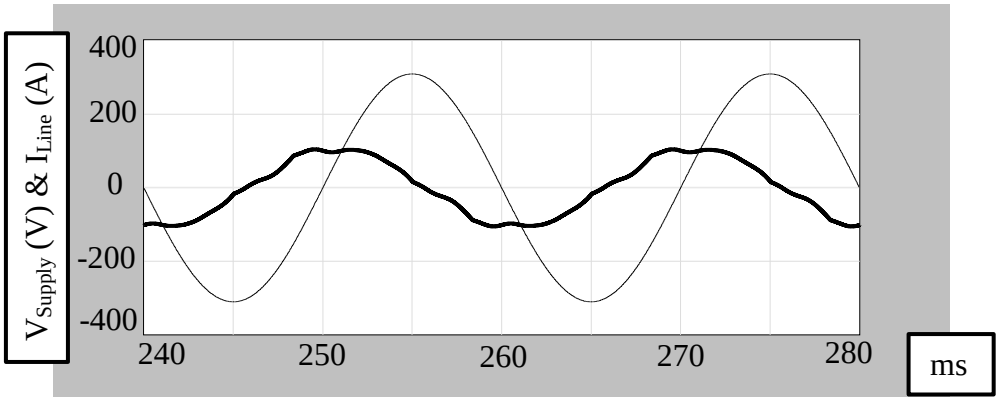

Fig. 5.24 Line current (**bold**) and supply voltage simulation waveforms at light-load for 55kW ASD system employing ABF (current scale:10x).

Finally, the half-load operating condition study has been conducted for both ASD power ratings systems utilizing the ABF designed filter and the obtained simulation waveform results are shown in Appendix F.

In summary, the main power quality indices simulation results for the 5.5kW and 55kW ASD system at full-load utilizing the new reduced ABF filtering technique are summarized in Table 5.5. In addition, the analytical equivalent circuit's results based method are presented and compared to the computer simulation results method. It is apparent that both results are in good correlation with an acceptable accuracy range. However, similarly, the analytical line THDi% results have marginally larger values due to the considered pessimistic approach of the effect of the line-voltage harmonics (superimposed with the rectifier-current harmonics magnitudes) in the Matlab m-file design code.

Table 5.5 Full-load performance comparison for 5.5kW and 55kW power rating ASD systems using ABF structure based on analytical and computer simulation results

P_R(kW)	5.5			55		
Power Quality Indices@ F.L.	Line THDi%	Line PF	ΔV_o %	Line THDi%	Line PF	ΔV_o %
Analytical Results	6.90	0.980	3.30	6.90	0.990	3.50
Simulation Results	5.20	0.984	2.92	5.25	0.985	3.00

5.6.6 ABF Simulations Under Unbalance Supply Voltage

The final step, likewise, involves assessing the ASD system performance employing ABF under unbalance supply voltage condition disregarding the voltage harmonic distortion. The ASD performance estimation includes the full-load and half-load operating conditions. Under the same supply unbalance definition (section 4.4.6) and considered conditions range (1%, 2% and 3%), the three-phase lines current simulation waveforms and the estimated THDi% values are presented.

Fig. 5.25 shows the three-phase supply voltage and line currents simulation waveforms at full-load of the 5.5kW ABF system under balanced voltage supply, while Fig. 5.26 shows the same variables waveforms under 2.0% unbalanced voltage supply at phase 1 (**bold**). It is observed that the line currents in both cases have nearly similar and undistinguishable waveform characteristics.

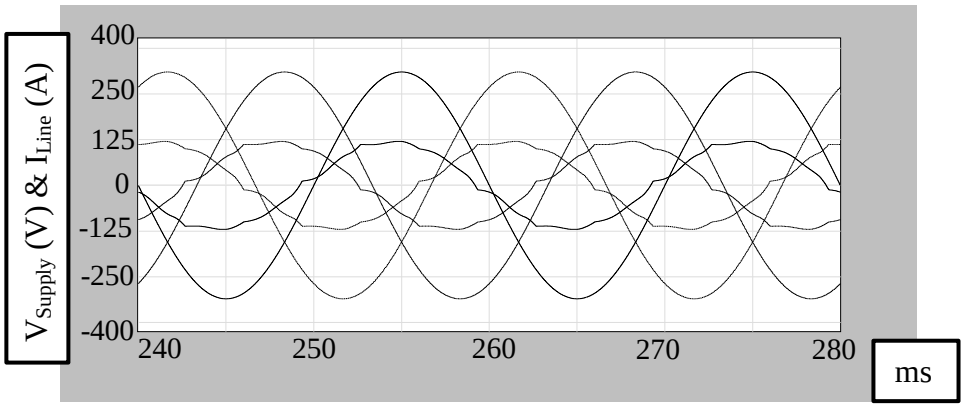

Fig. 5.25 Full-load three-phase supply voltage and current waveforms for balanced utility grid for 5.5kW ASD system utilizing ABF (current scale: 10x).

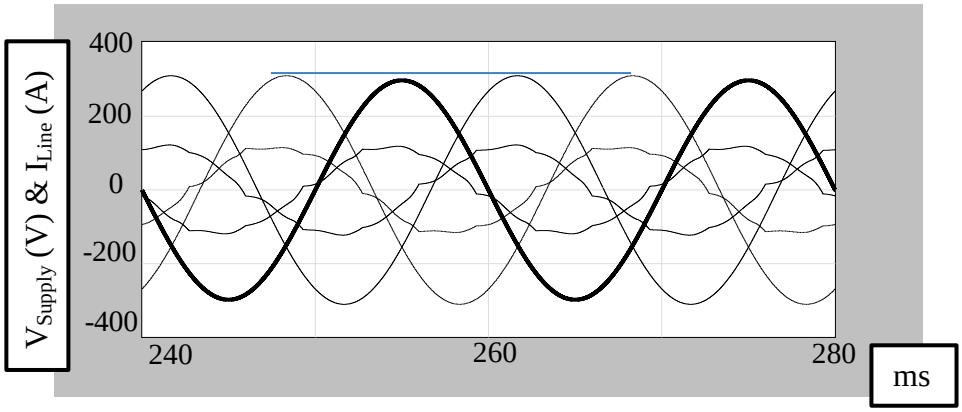

Fig. 5.26 Full-load three-phase supply voltage and current waveforms for 2.0% unbalanced utility grid for 5.5kW ASD system utilizing ABF (current scale: 10x).

In addition, half-load operating condition performance assessment of the 5.5kW ASD system using the ABF under the assigned unbalance voltage supply situations has been also examined. Table 5.6 illustrates and compares the line current THDi% results for balanced and the three unbalance voltage supply given case studies.

As Table 5.6 reveals, the 5.5kW ASD system using ABF is able to preserve the low and steady line current THDi% values in the three-phase under all voltage supply unbalance conditions. For instance, at full-load condition, the line THDi has low values range (< 7.5%) despite the maximum 3% unbalance supply voltage applied case. In addition, for half-load condition, with this implemented maximum unbalance supply voltage the line THDi maximum value reached 11.3%. These results support the low sensitivity advantage of the broadband filters to unbalance supply voltage variations. Similar to the IBF, the ABF filter usually initiates a negligible 3rd harmonic current component (I_3) under supply voltage unbalance compared to a typical AC three-phase reactor (Lac) filtering technique (e.g. 1.614% I_3 for ABF and 20% I_3 for 3% Lac at full-load operating condition with 2% unbalance supply case study for 5.5kW ASD system.)

Table 5.6 The full-load line THDi% for 5.5kW ASD system using ABF under different voltage supply unbalanced conditions

Supply voltage unbalance%	Magnitude (peak)	Full-load (THDi%)	Half-load (THDi%)
0	310.0	5.20	7.00
1	303.8	5.31-5.43-5.45	7.32-7.70-7.68
2*	**297.6**	**5.57-6.31-6.25**	**7.80-9.22-9.08**
3	291.4	5.96-7.60-7.38	8.54-11.3-11.0

*I^{3rd} @ F.L is 1.614% and @H.L is 2.77%

Correspondingly, the 55kW power rated ASD system full-load performance using the ABF is also studied under the same various three voltage supply unbalance practical values. The balanced and 2% unbalanced three-phase supply voltage and line currents simulation waveforms at full-load are shown in Fig. 5.27 and Fig. 5.28, respectively. Moreover, Table 5.7 shows the line current THDi% values for full-load and half-load operating condition under the various unbalance supply voltage conditions. In conclusion, the table validates the low sensitivity characteristic of the ABF filter structure to grid voltage unbalance variations.

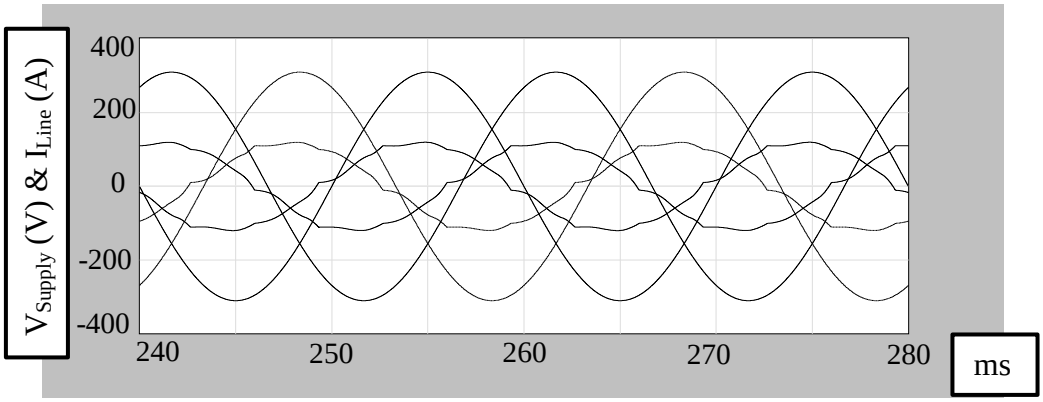

Fig. 5.27 Full-load three-phase supply voltage and current waveforms for balanced utility grid for 55kW ASD system utilizing ABF.

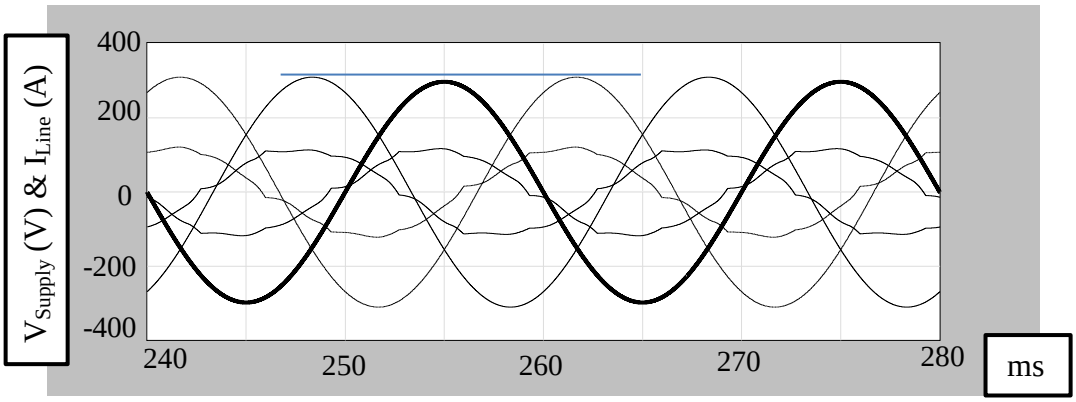

Fig. 5.28 Full-load three-phase supply voltage and current waveforms for 2.0% unbalanced utility grid for 55kW ASD system utilizing ABF.

Table 5.7 The full-load line THDi% for 55kW ASD system using ABF under different voltage supply unbalanced conditions

Supply voltage unbalance%	Magnitude (peak)	Full-load (THDi%)	Half-load (THDi%)
0	310.0	5.3	7.3
1	303.8	5.59-5.71-5.71	8.5-8.6-8.7
2	**297.6**	**5.85-6.5-6.4**	**9.1-10.3-10.1**
3	291.4	6.2-7.7-7.5	10.0-12.4-12.0

5.6.7 Simulation Based Performance Evaluation and Comparison

The ABF line-current THDi% and line total power factor performance characteristics, from light-load to full-load, are shown in Fig. 5.29 and Fig. 5.30 for the power ratings considered. From nearly 50% load to full-load, over a wide range the ABF based system provides high overall power quality performance. The input-

current THDi% is at an acceptable level over the full operating range. The ABF based drive is substantially improved in terms of the harmonic injection to the connected AC network, making the drives impact on the connected power system and other users in the vicinity of the PCC absolutely minimal. The power factor approaches unity at rated load and thus the ABF filter aids minimizing the reactive power requirement of the drive. The energy efficiency of the filter is high (>99.0%) from half-load to full-load, as shown in Fig. 5.31.

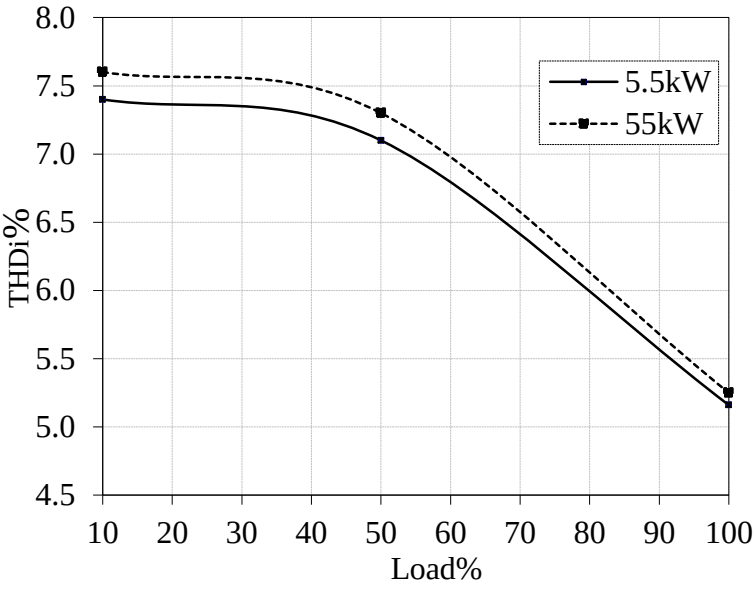

Fig. 5.29 The load current dependency of the ABF line current THDi%.

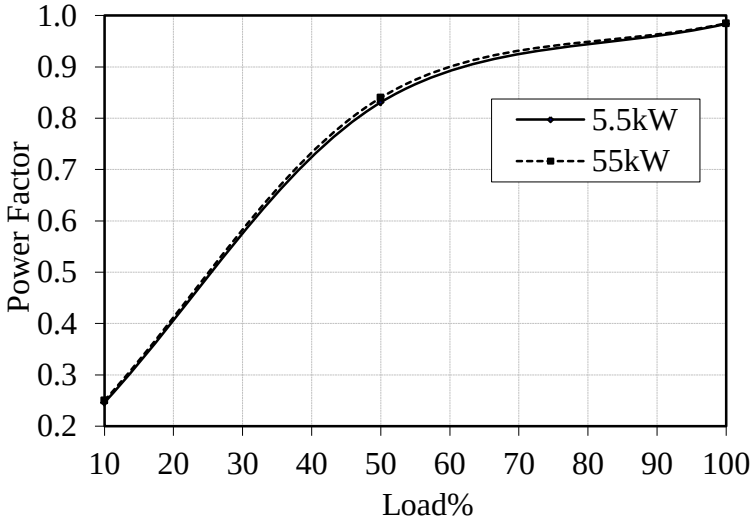

Fig. 5.30 The load current dependency of the ABF line power factor (leading).

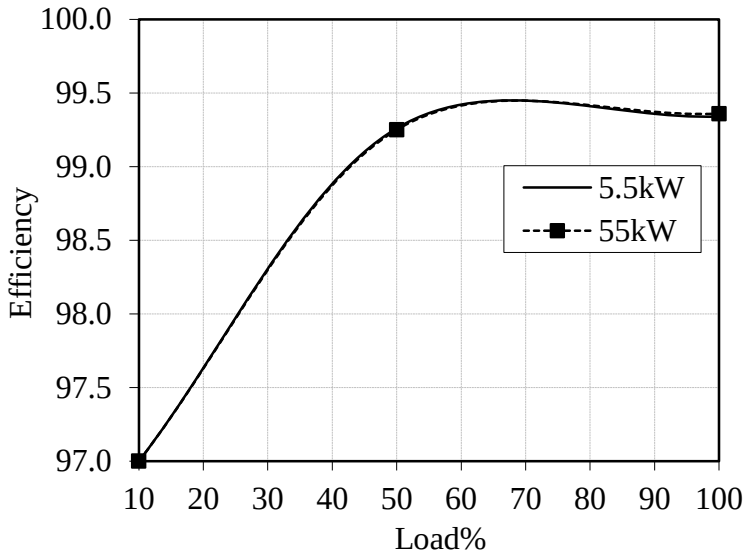

Fig. 5.31 The load current dependency of the ABF energy efficiency.

The ABF performance characteristics under unbalanced AC supply are obtained. Table 5.6 and Table 5.7 summarize the full-load and half-load operating performance of the 5.5kW and 55kW rated ASD, respectively, under conditions of increasing line-voltage unbalance. As the table indicates, good ABF performance is maintained, and the line-current THDi increase is relatively small. Additionally, the line voltage harmonic distortion has minimal effect on the ABF based system due to the large utilized L_i. Therefore, the ABF is relatively insensitive to line voltage unbalance and harmonic distortion.

In conclusion, the ABF new structure has succeed to maintain the IBF topology performance with less utilized components at the expense of maximizing the built-in DC-link inductor. Furthermore, the ABF new topology is comparable to the conventional passive harmonic filters in a similar IBF attribute that has been shown in Table 4.10 with an extra advantage of less complex structure, size and cost. On the other hand, these presented performances are possibly achievable provided that the existence of the 6% DC-link built-in inductor in the drive side.

5.7 Experimental Results of 5.5 kW Rated ASD System and Performance Evaluation

In the previous sections (5.6.1 to 5.6.5) the computer simulation results and performance analysis of the ASD system at several loading conditions utilizing the built-in 6% DC-link inductor and the ABF filtering method was presented. In this section, the several experiments carried out to examine the performance of the presented passive filters are explained and investigated.

The focus is on the steady-state performance of the 5.5kW ASD system utilizing the assigned passive filters at different loading conditions (from no-load to full-load) taking into account the applied voltage supply distortion in a distribution network. The same lab setup explained in section 4.5.1 (shown in Fig. 4.30) is designed and used in the laboratory experiments.

5.7.1 DC-link Inductor Filter Based Experimental Results

In the first experiment, presented in this section, the single-phase 6% DC-link inductor is designed and implemented in the ASD system as shown in Fig. 5.32 below. The same power analyser equipment (Norma 5000) is used to measure the required data and obtain the real current and voltage waveforms in the ASD system.

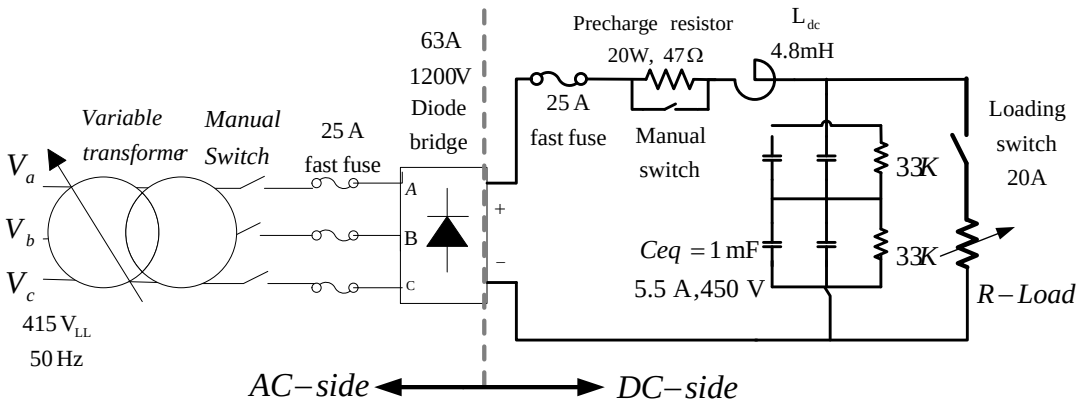

Fig. 5.32 The experimental 5.5kW ASD system setup utilizing 6% DC-link inductor.

The full-load operating condition supply data (line-to-line voltage, total real and apparent power, and supply voltage THD_V%) is presented in Fig. 5.33. While the line three-phase obtained results (phase voltage V, phase current I, phase real power P, phase current THDi, phase reactive power Q, phase power factor ʎ) for the designed 5.5kW ASD system are shown in Fig. 5.34. The lines current have a considerable amount of harmonic distortion and the associated THDi% values range from 38.1% to 43%). Accordingly, the power analyser estimated total power factor values of the system are low (0.90 – 0.93) lagging. However, compared to the ASD performance with no filtering method committed (Fig. 4.36) the single-phase 6% L_{dc} has a remarkable effectiveness. The selected DC inductor succeeded to reduce the lines THDi% from 75.5% to 44.9% and to improve the total power factor from 0.78 to 0.90 lagging (phase 2 results).

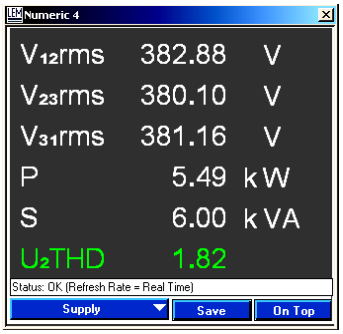

Fig. 5.33 Supply experimental data at full-load for 5.5kW rated system employing 6% L_{dc} filter (line-to-line voltage, total real and apparent power, and supply voltage THD_V%).

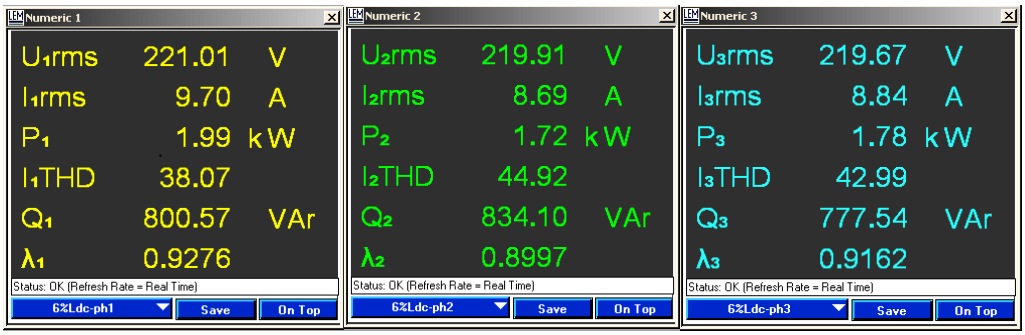

Fig. 5.34 Line experimental data for phases 1, 2 and 3 at full-load for 5.5kW rated system employing 6% L_{dc} filter (voltage V, current I, real power P, current THDi%, reactive power Q, power factor ʎ).

Shown in Fig. 5.35, the line 3-phase current experimental waveforms at full-load for 5.5kW rated system engaging 6% L_{dc} filter while their harmonic spectrum

components (up to 1.3 kHz) are shown in Fig. 5.36. The produced results indicate the distortion level in the line currents waveforms and the high harmonic components existence that may cause a number of undesirable effects in the drive and the feeding network adjacent connected loads (distorting PCC voltage, increasing losses and operating temperature, interference, enhancing the resonance risk…etc.).

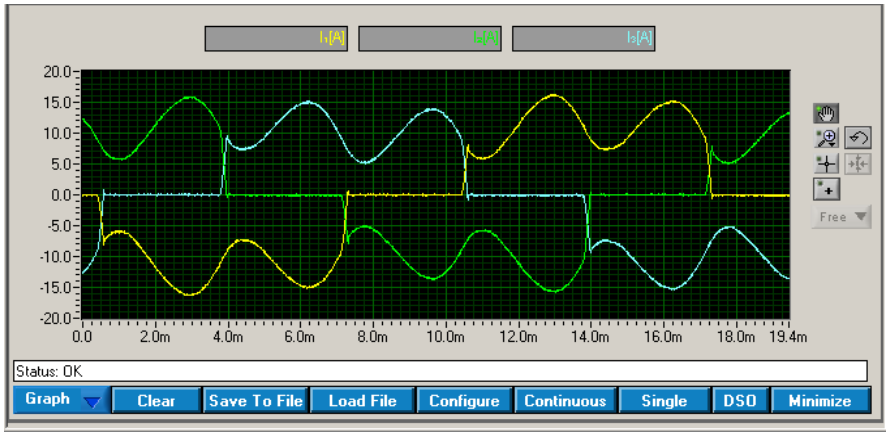

Fig. 5.35 Line 3-phase current experimental waveforms at full-load for 5.5kW rated system employing 6% L_{dc} filter.

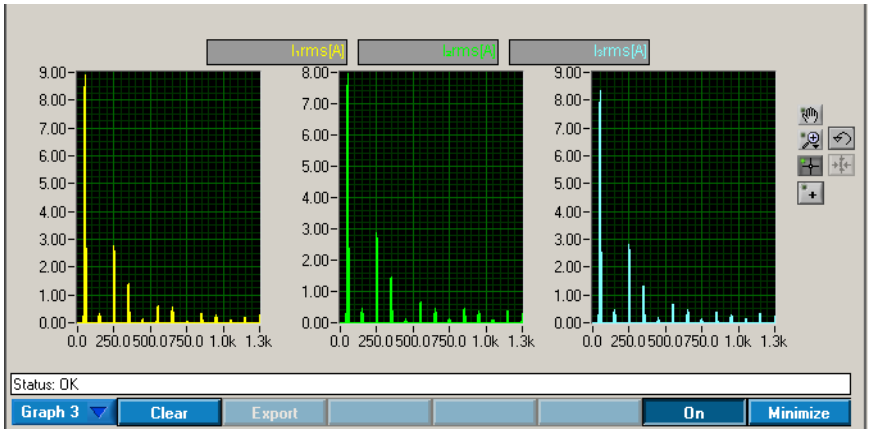

Fig. 5.36 Line 3-phase current harmonic spectrum at full-load for 5.5kW rated system employing 6% L_{dc} filter.

The full-load supply (phase 2) voltage and current experimental waveforms are shown in Fig. 5.37 and a zoomed-in view in Fig.5.38. Further to the current high harmonic factor specification, the displacement phase shift between the phase voltage and phase current presented is clearly noticeable. Therefore, the ASD system has relatively low power factor range value (< 0.93 lagging). The rated load DC current and voltage experimental measured values are (10.7A and 506V).

In conclusion, these findings show the overall unsatisfactory performance of the case study and further support the need of an extra filtering type in order to comply with the power systems harmonic regulations and standards. On the other hand, the produced experimental results are consistent with the simulation results shown in section 5.6.1 which proof the good accuracy of system modelling and analysis.

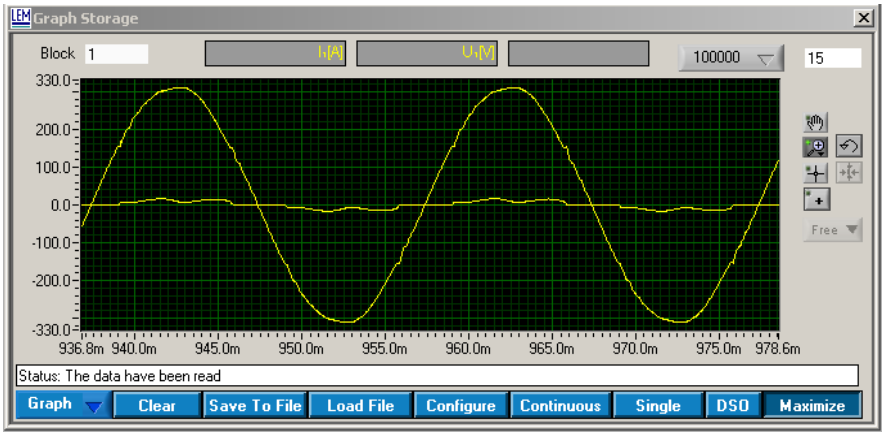

Fig. 5.37 Supply phase voltage and current experimental waveforms at full-load for 5.5kW rated system employing 6% L_{dc} filter.

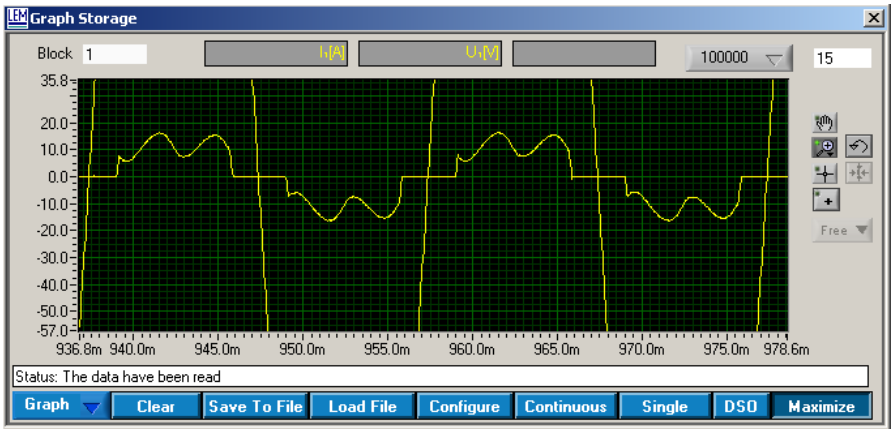

Fig. 5.38 Supply phase voltage and current experimental waveforms at full-load for 5.5kW rated system employing 6% L_{dc} filter (Zoomed).

5.7.2 ABF Full-Load Experimental Results

From the earlier observation and in order to achieve an acceptable level of overall ASD system performance, implementation of the ABF structure is involved and examined. The full range of operating conditions (from no-load to full-load) is considered to present the experimental performance of the system. Current and

voltage measured data and extracted waveforms at both sides (line and rectifier) are investigated.

The ABF reduced elements (three components only) is designed using the optimal component parameters shown in Table 5.1 (L_i = 12.1mH, L_f = 7.8mH and $C_{f\Delta}$ = 17.3µF). The filter capacitance is star connected and the equivalent capacitance value is utilized (Cf_Y 51.9µF). The three-phase input reactors (Li) and the filter reactors (L_f) where designed with their original values by the same manufacturing company based in UK (Amethyst Designs Ltd). Meanwhile the same filter capacitor boxes are utilized and set to their maximum values (Cf_Y 51.98µF). The laboratory three-phase capacitance measured values are C_{fY1} 51.0 uF, C_{fY2} 50.0 uF and C_{fY3} 50.0 uF.

In the DC side the built 6%L_{dc} inductor (4.8mH) utilized in the previous experiment is connected at the rectifier DC side. The designed filter is implemented as shown in Fig. 5.39. The ABF filter components (with equivalent practical capacitors) photo in the lab is shown in Fig. 5.40.

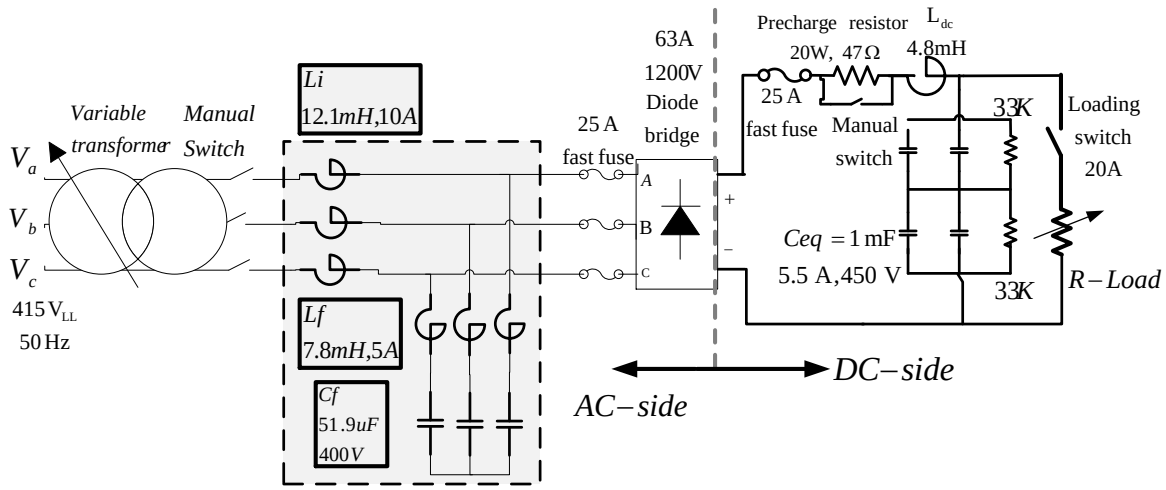

Fig. 5.39 The experimental 5.5kW ASD system setup utilizing ABF.

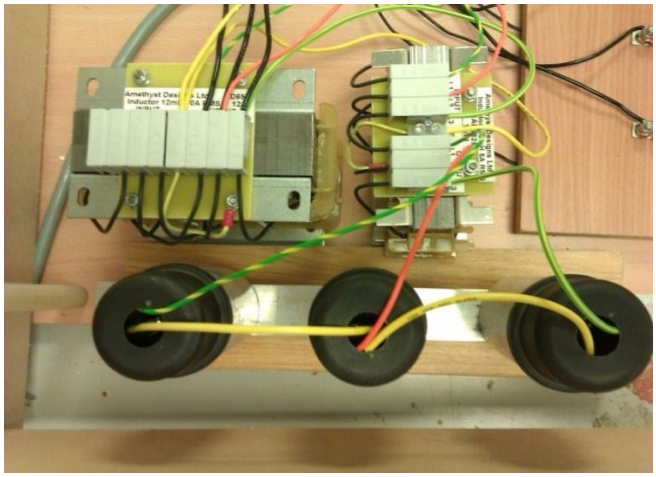

Fig. 5.40 Picture of experimental ABF system for 5.5kW ASD rating.

With the same 6-channels in the power analyser all current and voltage measurements and data estimation is conducted. The full-load data is presented in, Fig. 5.41, for both sides (supply and rectifier). The three-phase power supplied is 5.51kW while phase 2 voltage, on the line side, has a low harmonic distortion (1.58% THDv). On the rectifier side obtainable measurements, the phase real power estimated values of phase 2 and phase 5 are presented. These values will be utilized to estimate the ABF filter energy efficiency at full-load condition (section 5.7.4). Due to the elimination of the output AC reactor (4%Lac) used in the IBF structure (no voltage drop), the line-to-line rectifier side voltage rms values are stably increased.

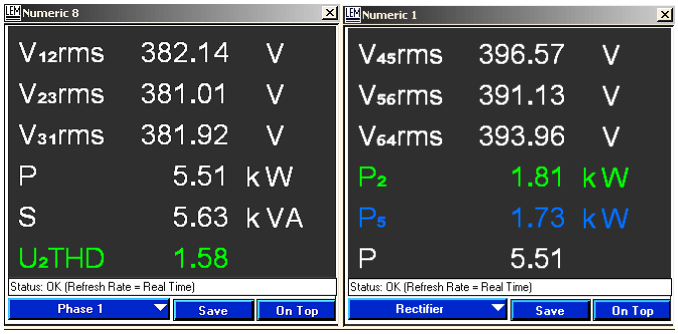

Fig. 5.41 Supply and rectifier side experimental data at full-load for 5.5kW rated system employing ABF filter (line and rectifier line-to-line voltage, total real and apparent power and supply voltage THD_V%).

The line side experimental data for all phases (1, 2 and 3) are shown in Fig. 5.42. The three-phase line currents have very low range of THDi% power analyser estimated values (4.53% to 5.01%) by the ABF topology implementation. Moreover, the ASD

designed system has a high line side leading power factor calculated values (0.975 to 0.983). The rectifier side data for phases 4, 5 and 6 are shown in Fig. 5.43. Before the filtering effect, the three-phase rectifier currents have a considerable undesired amount of harmonic distortion (> 31% THDi) and relatively poor lagging power factor (< 0.94) as presented. Hence, the new ABF filter structure shows, in a practical environment, the capability to reduce the rectifier side current distortion and increase the power factor at the line side to acceptable and satisfactory values.

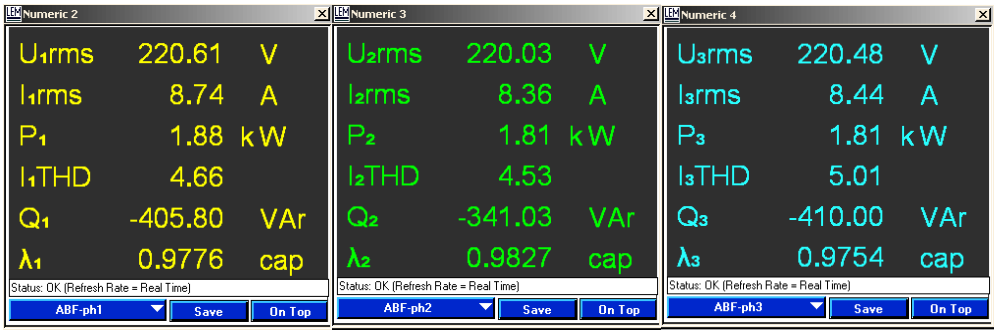

Fig. 5.42 Line side experimental data for phases 1, 2 and 3 at full-load for 5.5kW rated system employing ABF filter (voltage V, current I, real power P, current THDi%, reactive power Q, power factor ʎ).

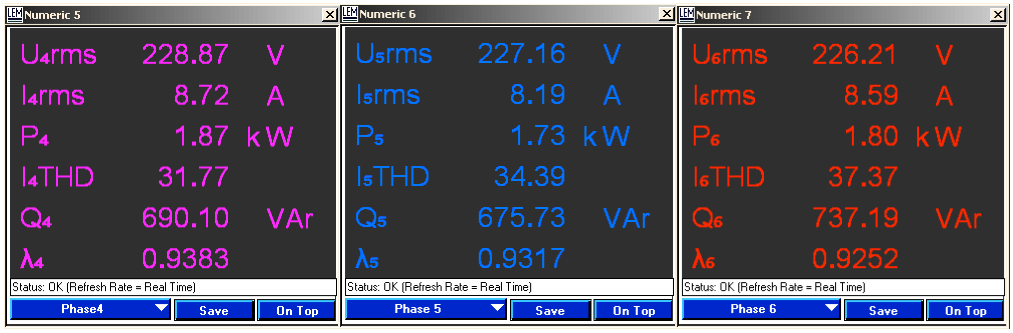

Fig. 5.43 Rectifier side experimental data for phases 4, 5 and 6 at full-load for 5.5kW rated system employing ABF filter (voltage V, current I, real power P, current THDi%, reactive power Q, power factor ʎ).

For the 5.5kW ASD designed system the three-phase experimental full-load line recorded current waveforms is shown in Fig. 5.44 and their analysed harmonic spectrum is shown in Fig. 5.45. It is apparent from the presented figures that the ASD designed system is practically drawing sinusoidal (distortion free) lines current waveforms. The fundamental current component is effectively the only existing component in the current spectrum illustrated. These results and figures are consistent with the simulation findings explained in section 5.6.2.

On the other hand, the distorted three-phase experimental full-load rectifier side current waveforms and the related harmonic spectrum are shown in Fig. 5.46 and Fig. 5.47, respectively. The distortion level, as presented, is significant and the ABF structure displays great effectiveness to block these rectifier current wide range harmonic components by the line reactor (L_i) and divert them through the single shunt filter (L_f and C_f). Meanwhile the fundamental current component is freely passing through the line.

As the power analyser figures indicate, the ABF filtering method dramatically decreases the rectifier current distortion and is able to attenuate a broad range of the harmonic components.

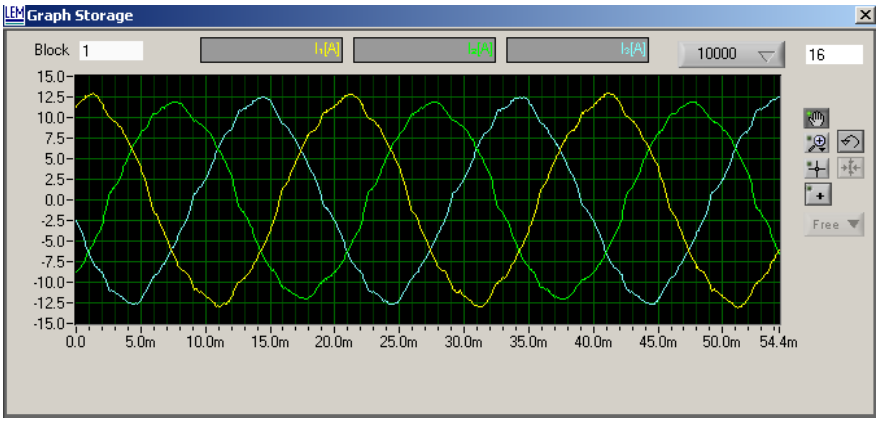

Fig. 5.44 Line side 3-phase current experimental waveforms at full-load for 5.5kW rated system employing ABF filter.

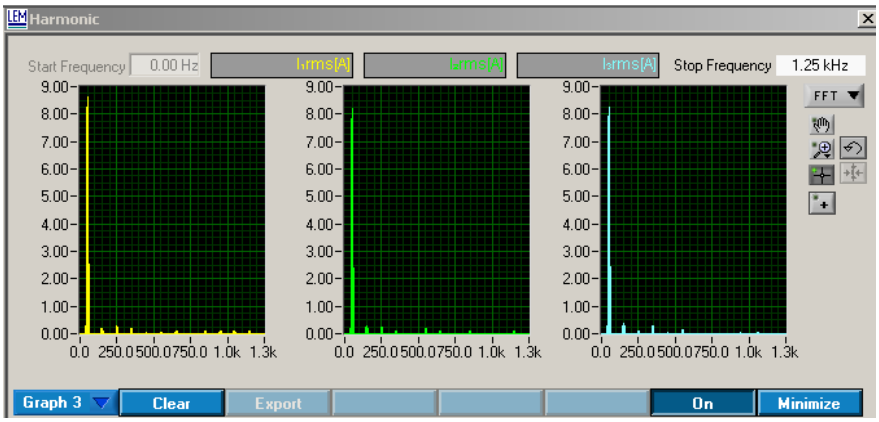

Fig. 5.45 Line side 3-phase current harmonic spectrum at full-load for 5.5kW rated system employing ABF filter.

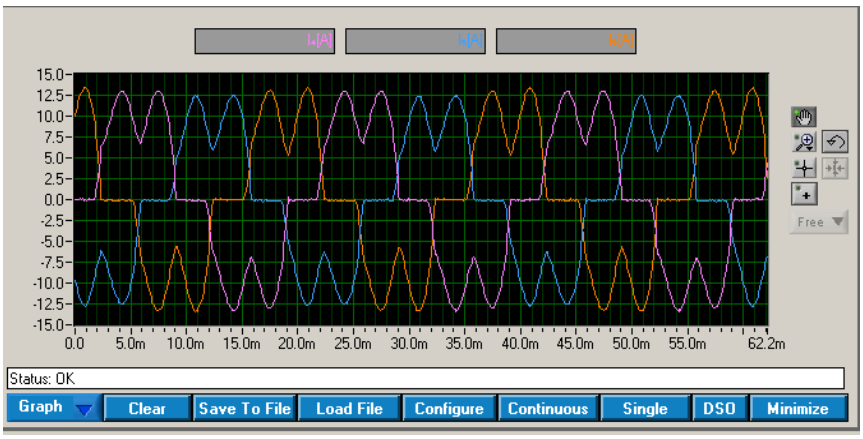

Fig. 5.46 Rectifier side 3-phase current experimental waveforms at full-load for 5.5kW rated system employing ABF filter.

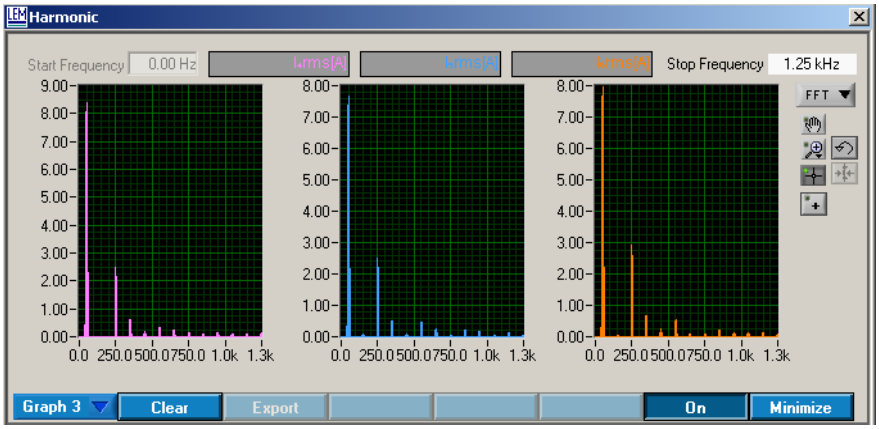

Fig. 5.47 Rectifier side 3-phase current harmonic spectrum at full-load for 5.5kW rated system employing ABF filter.

For the purpose of extra clarifying the ABF topology effect, the line and rectifier currents waveforms are extracted and shown in the same graph. Therefore, the phase 2 (green) line side current and phase 5 (blue) rectifier side current waveforms are shown overlapped in Fig. 5.48. Furthermore, for the same aim, the correlated current harmonic spectrums are zoomed-in and shown in Fig. 5.49.

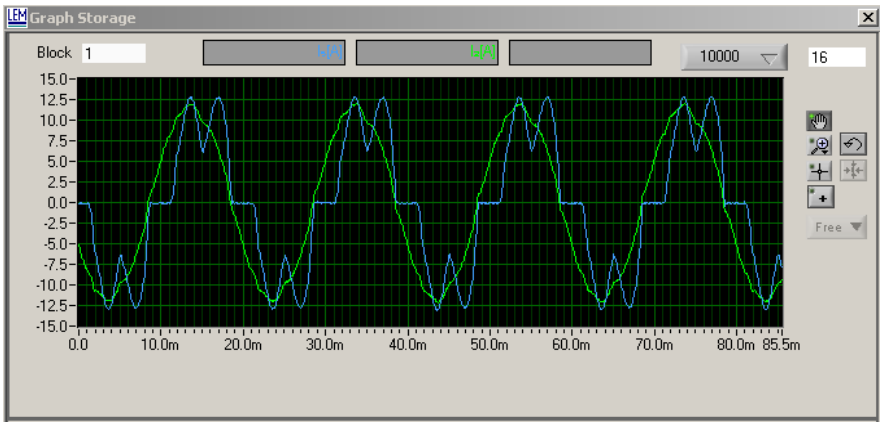

Fig. 5.48 Line and rectifier current experimental waveforms at full-load for 5.5kW rated system employing ABF filter.

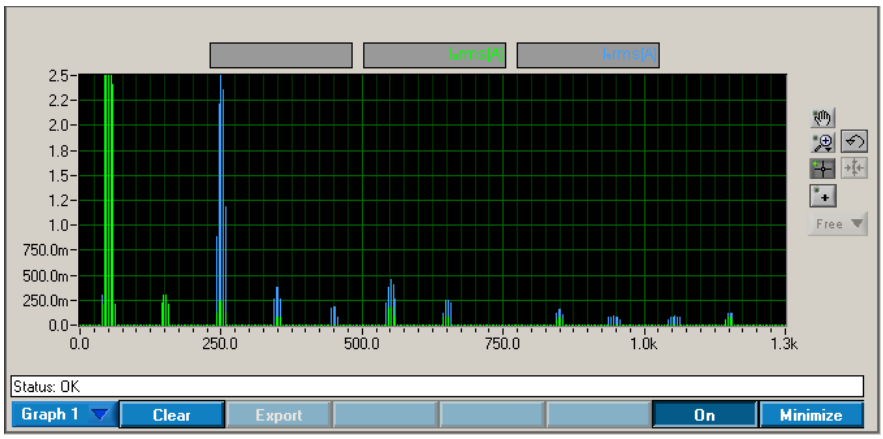

Fig. 5.49 Line and rectifier side current harmonic spectrum at full-load for 5.5kW rated system employing ABF filter (Zoomed).

Similarly, to confirm the line power factor obtained numerical results shown in Fig. 5.42 and to enhance results presentation, phase 1 full-load line current and supply voltage waveforms are shown in Fig. 5.50 and (with a zoomed-in view) in Fig. 5.51. As the presented figures reveals, the line current is slightly leading the phase voltage to confirm a total line power factor power analyser estimated value of 0.98 average ranges. Lastly, the harmonic spectrum analysis for the same phase 2 voltage and current waveforms shown in Fig. 5.50 combined with the rectifier side phase 4 current (brown) harmonic spectrums are all shown in Fig. 5.52. The clean line side supply voltage and drawn current are obviously clear in the figure whereas the rectifier side current is heavily polluted with harmonics. Regarding the rectifier side voltage recorded waveforms investigation; the phase 5 rectifier phase voltage and current experimental waveforms are shown in Fig. 5.53. The negative effect of the rectifier distorted current on the voltage is observed from the presented figure.

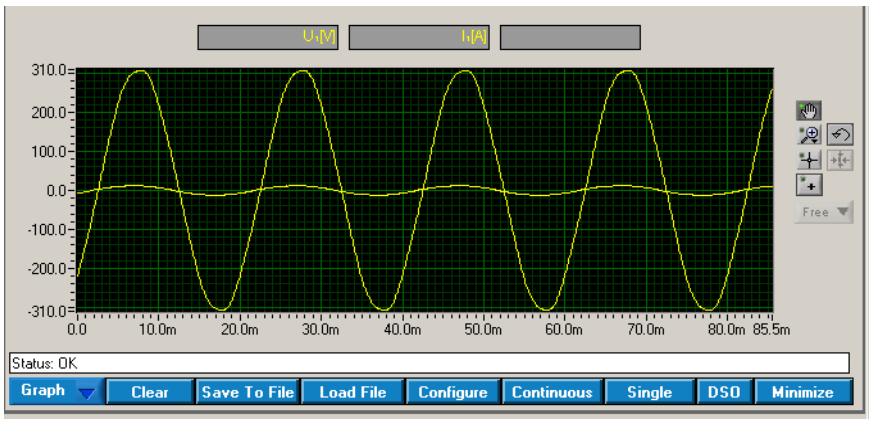

Fig. 5.50 Supply phase voltage and current experimental waveforms at full-load for 5.5kW rated system employing ABF filter.

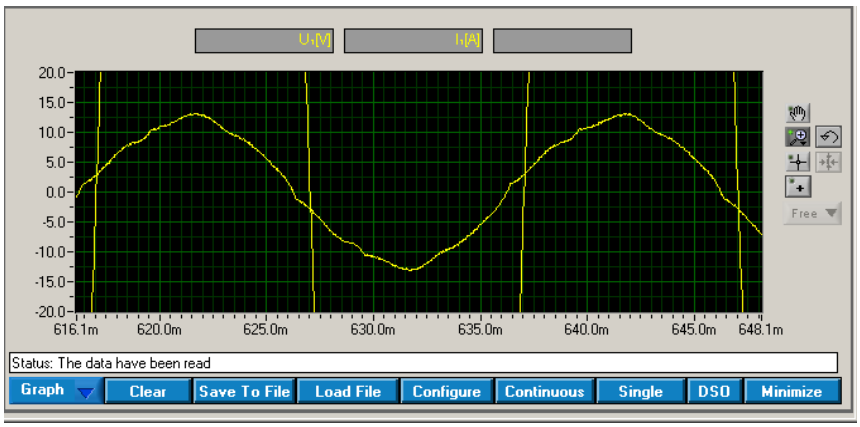

Fig. 5.51 Supply phase voltage and current experimental waveforms at full-load for 5.5kW rated system employing ABF filter (Zoomed).

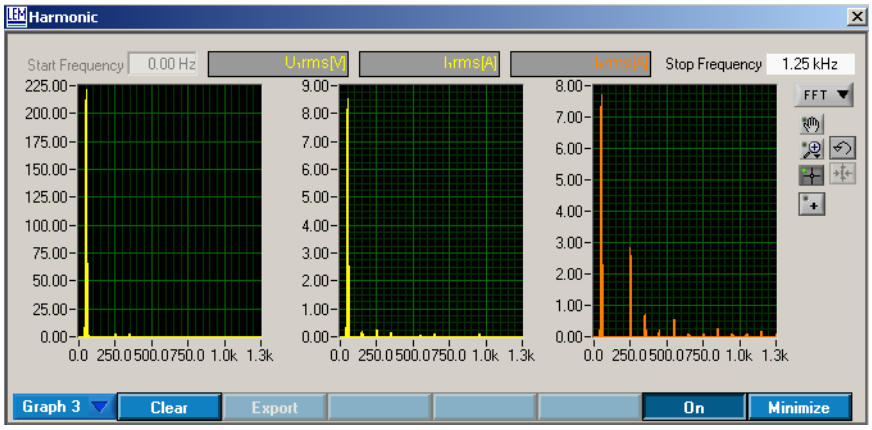

Fig. 5.52 Phase voltage, line current and rectifier current harmonic spectrum at full-load for 5.5kW rated system employing ABF filter.

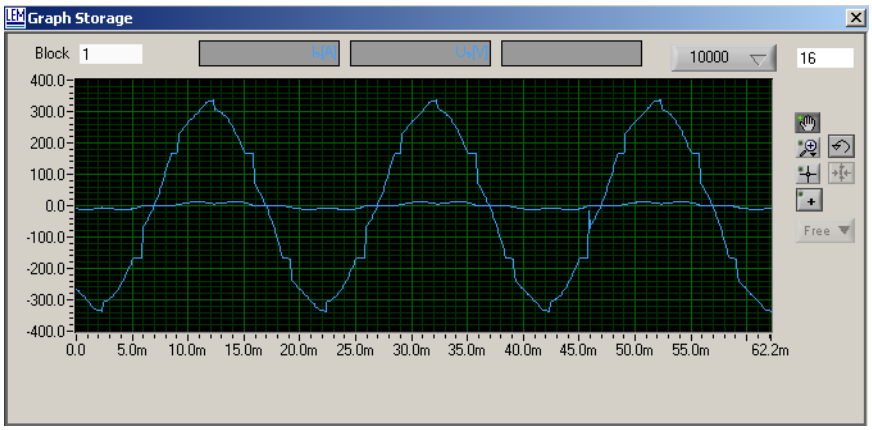

Fig. 5.53 Rectifier side phase voltage and current experimental waveforms at full-load for 5.5kW rated system employing ABF filter.

The experimental full-load condition presented results of this designed 5.5kW ASD system utilizing the ABF filter provides additional practical evidence (along with simulation results) of the overall satisfactory performance characteristics of the used filtering method. The ABF structure (with fewer components) succeeded to improve

the main power quality indices (THDi% and PF) in the proposed system to actual operating values that can comply with any international regulations. The only need for this progression is the use of the 6% DC-link inductor built-in the ASD (or an equivalent AC reactor at the rectifier side).

The rated load DC current and voltage experimental measured values are (10.4A and 519V). The next section will present the half-load operating condition experimental results for the same power rated ASD system.

5.7.3 ABF Half-Load Experimental Results

This section provides the half-load operating condition experimental results of the 5.5kW ASD designed system with the use of the ABF passive filter. The half-load power condition is similarly achieved by changing the variable load resistor to a higher equivalent resistance value that decreases the load current to approximately 50%.

The half-load situation experimental data of the supply and rectifier sides is presented in Fig. 5.54. The phase 2 supply voltage has an acceptable harmonic distortion value (2.00% THDv) and, as shown, the three-phase power delivered is 2.91kW. Due to the filter capacitance the line-to-line rectifier side voltage rms values have experienced stable minor increase range (397V – 403V) with respect to the full-load condition range (391V – 397V).

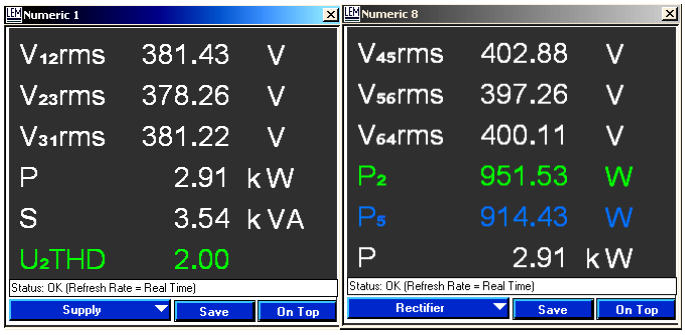

Fig. 5.54 Supply and rectifier side experimental data at 50% load for 5.5kW rated system employing ABF filter (line and rectifier line-to-line voltage, total real and apparent power and supply voltage THD_V%).

Phases 1, 2 and 3 supply side experimental data are shown in Fig. 5.55. On the other hand, phases 4, 5 and 6 rectifier side experimental data are shown in Fig. 5.56. By utilizing the ABF filtering method the three-phase lines current has low distortion level with THDi% range of 6.62% to 7.10%. On the contrary, the lines power factor estimated values have decreased to 0.82 – 0.83 leading values. This is obviously due to the additional reactive power that is provided by the filter capacitance with respect to the approximate 50% loading condition.

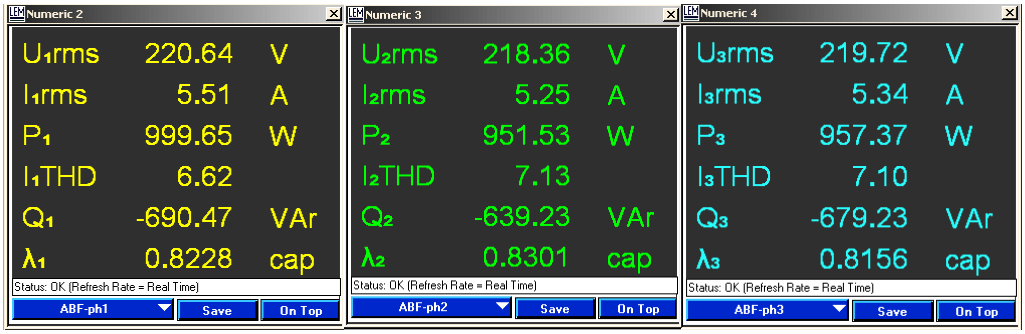

Fig. 5.55 Line side experimental data for phases 1, 2 and 3 at 50% load for 5.5kW rated system employing ABF filter (voltage V, current I, real power P, current THDi%, reactive power Q, power factor λ).

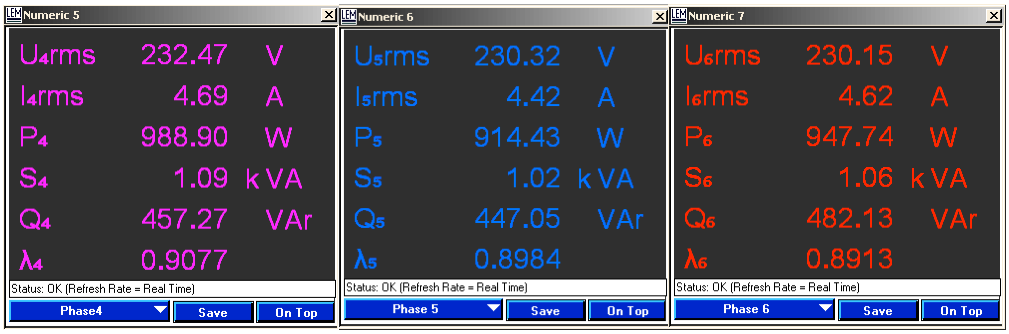

Fig. 5.56 Rectifier side experimental data for phases 4, 5 and 6 at 50% load for 5.5kW rated system employing ABF filter (voltage V, current I, real power P, apparent power S, reactive power Q, power factor λ).

The three-phase experimental line current waveforms and their harmonic spectrum for the 5.5kW ASD system at 50% loading operating condition are shown, respectively, in Fig. 5.57 and Fig. 5.58. Furthermore, for the same experiment, the three-phase rectifier side current waveforms are shown in Fig. 5.59 and the linked current harmonic spectrums are shown in Fig. 5.60. As these four figures indicate, the ABF filter structure maintain its ability to improve the rectifier side distorted non-continuous current waveforms to a smooth continuous sinusoidal waveform at

the line side with minimum total harmonic distortion levels (6.62% - 7.10%). Additionally, observing the current harmonic spectrum figures at both sides the ABF filter components are effective to block the rectifier current harmonic components at the line side and absorb them in the shunt filter path.

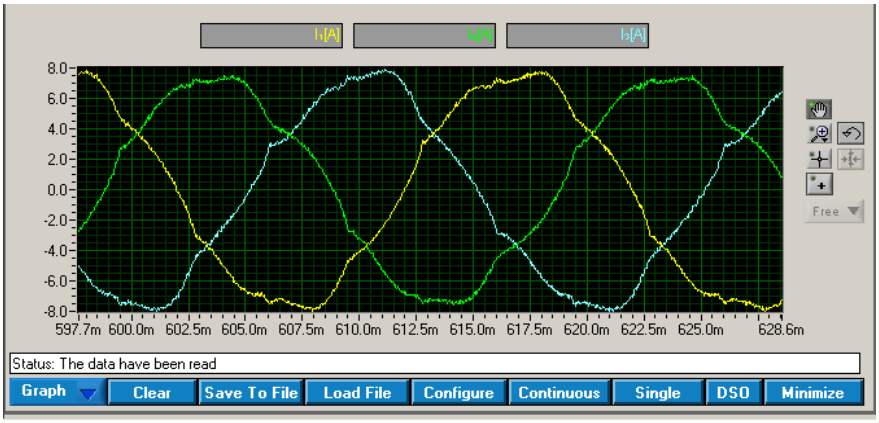

Fig. 5.57 Line side 3-phase current experimental waveforms at 50% load for 5.5kW rated system employing ABF filter.

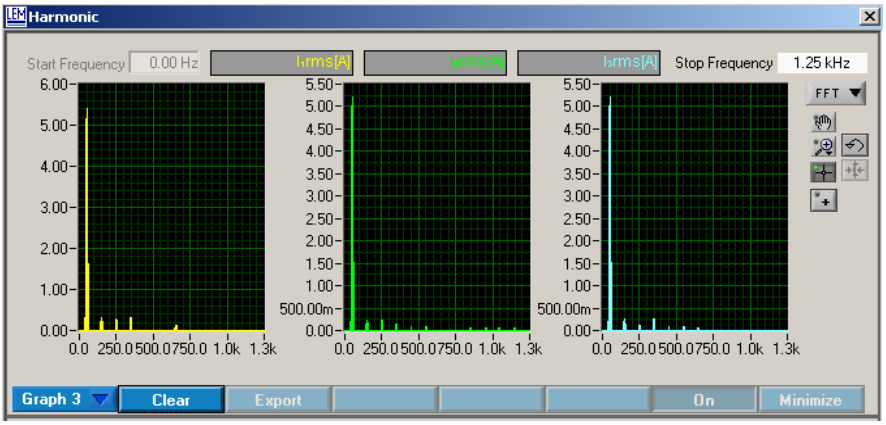

Fig. 5.58 Line side 3-phase current harmonic spectrum at 50% load for 5.5kW rated system employing ABF filter.

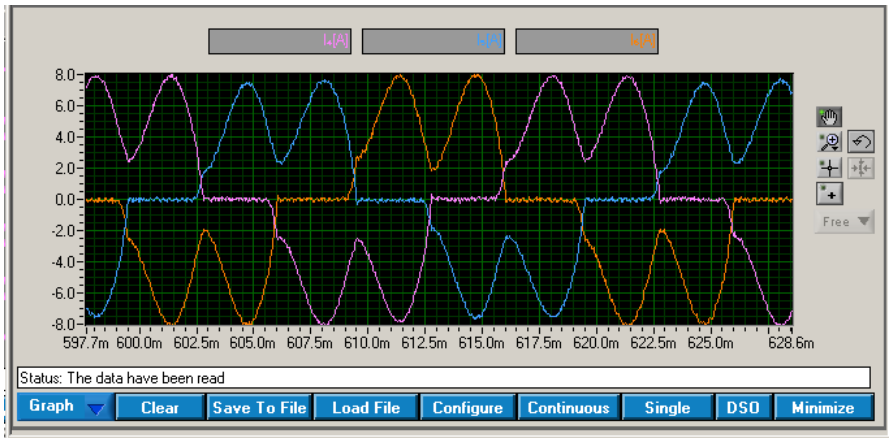

Fig. 5.59 Rectifier side 3-phase current experimental waveforms at 50% load for 5.5kW rated system employing ABF filter.

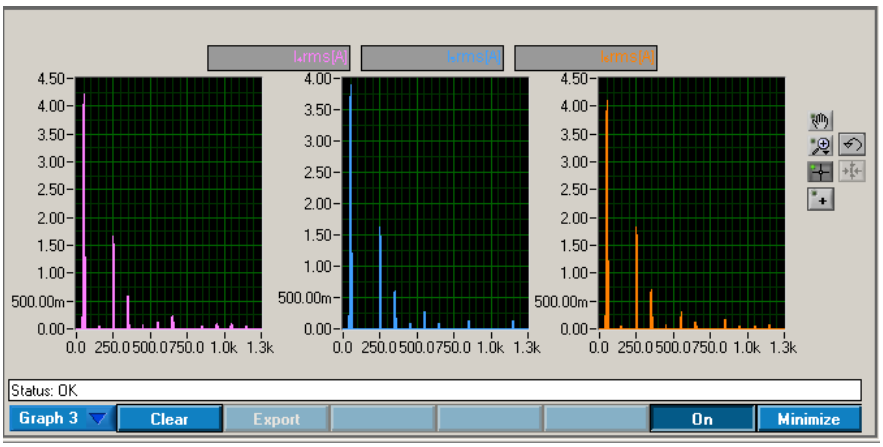

Fig. 5.60 Rectifier side 3-phase current harmonic spectrum at 50% load for 5.5kW rated system employing ABF filter.

Similar to the full-load condition extracted waveforms, the phase 2 (green) line side current and phase 5 (blue) rectifier side current waveforms, and their harmonic spectrums are shown overlaid in Fig. 5.61 and Fig. 5.62, respectively. This illustration method helps to compare both side's current waveforms and spectrum analysis. The results show superior performance of the tested filter in improving the current waveform at the line side and, therefore, reducing the harmonic distortion in the system to an acceptable levels.

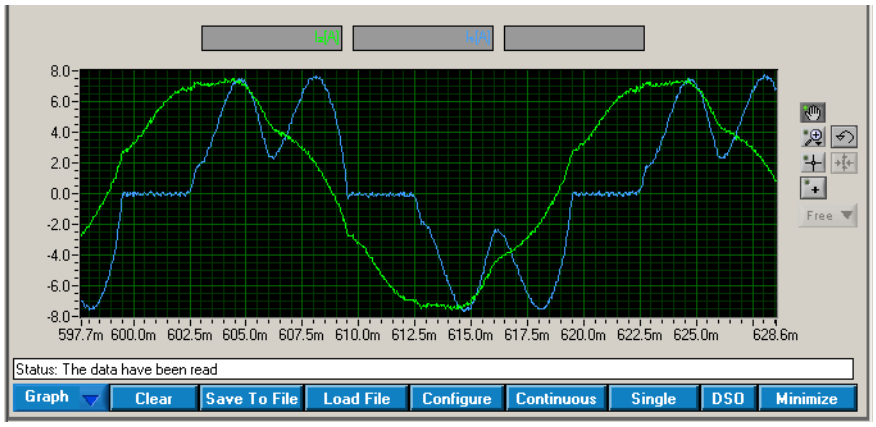

Fig. 5.61 Line and rectifier current experimental waveforms at 50% load for 5.5kW rated system employing ABF filter.

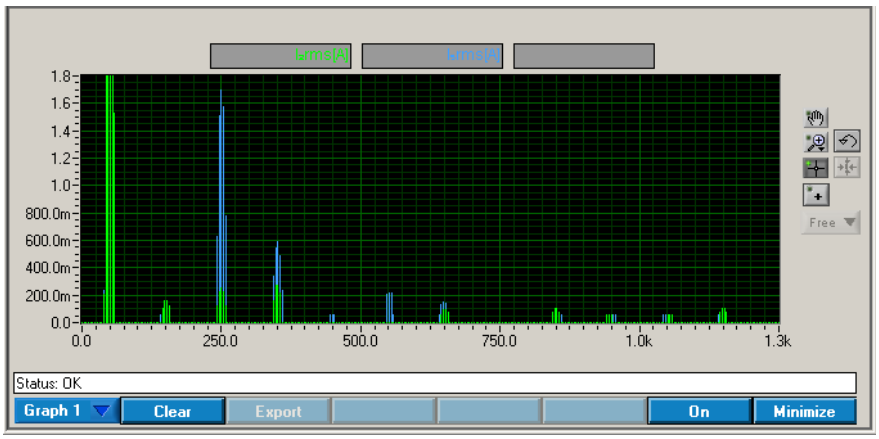

Fig. 5.62 Line and rectifier side current harmonic spectrum at 50% load for 5.5kW rated system employing ABF filter (Zoomed).

To observe the displacement angle between the line current and the supply voltage in a different form, phase 1 related waveforms are shown in Fig. 5.63. Specifically, a closer view to the same waveforms is shown in Fig. 5.64. The 0.822 leading power factor condition of the line current with the supply voltage is noticeable.

The rated load DC current and voltage experimental measured values are (5.4A and 532V).

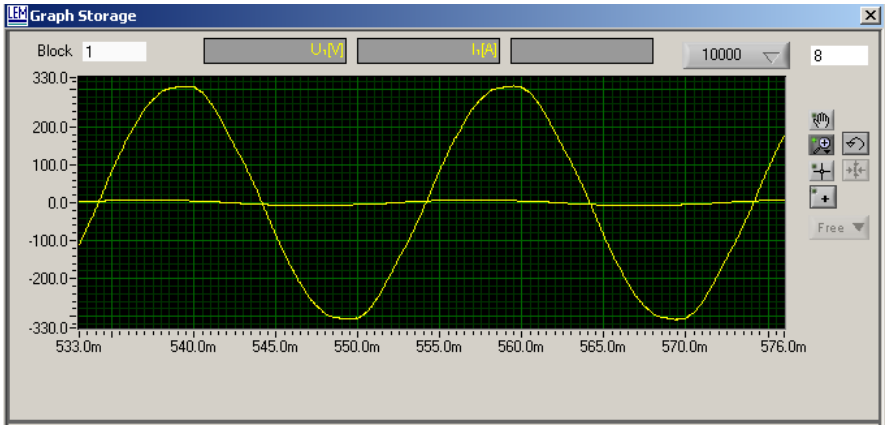

Fig. 5.63 Supply phase voltage and current experimental waveforms at 50% load for 5.5kW rated system employing ABF filter.

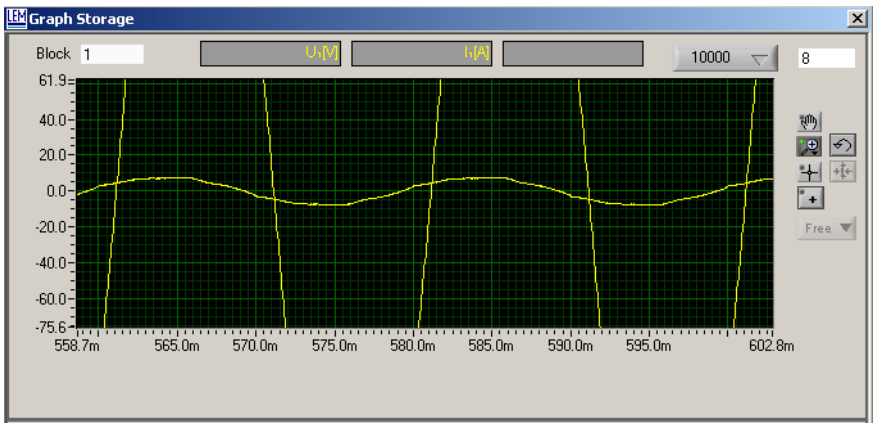

Fig. 5.64 Supply phase voltage and current experimental waveforms at 50% load for 5.5kW rated system employing ABF filter (zoomed).

5.7.4 ABF No-Load Experimental Results

The no-load experimental results of the 5.5kW ASD system utilizing the ABF are presented in this section. The variable resistance load is not connected to the DC-link capacitors by switching off the load contactor. Fig. 5.65 demonstrates the no-load supply and rectifier side's data. The line-to-line voltages at the rectifier side are increased to 404.86V rms average value. Referring back to full-load test data shown in Fig. 5.41, the line to line voltages at the rectifier side are increased to 393.88V rms average value. Therefore, the filter output voltage regulation from no-load to full-load (ΔV_o (%)) has a steady calculated value of 2.71%.

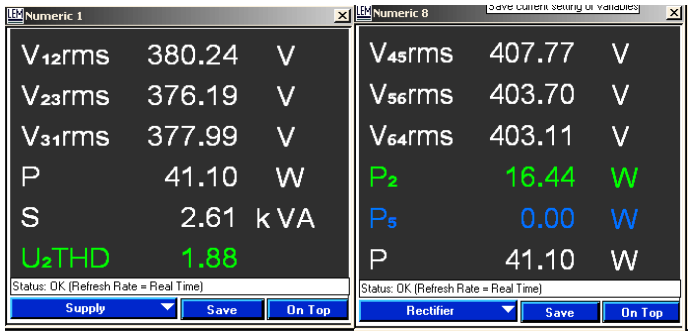

Fig. 5.65 Supply and rectifier side experimental data at no-load for 5.5kW rated system employing ABF filter (line and rectifier line-to-line voltage, total real and apparent power and supply voltage THD_V%).

Fig. 5.66 shows the no-load line side experimental data for phases 1, 2 and 3, while Fig. 5.67 shows the rectifier side results data for phases 4, 5 and 6 illustrating the no power consumption condition. The line side currents have a low current distortion

with THDi% range of 5.58% - 7.74%. Meanwhile the line power factor has a very high phase displacement angle with high capacitance reactive power provided to the system (0.02 max. leading power factor).

Fig. 5.66 Line side experimental data for phases 1, 2 and 3 at no-load for 5.5kW rated system employing ABF filter (voltage V, current I, real power P, current THDi%, reactive power Q, power factor ʎ).

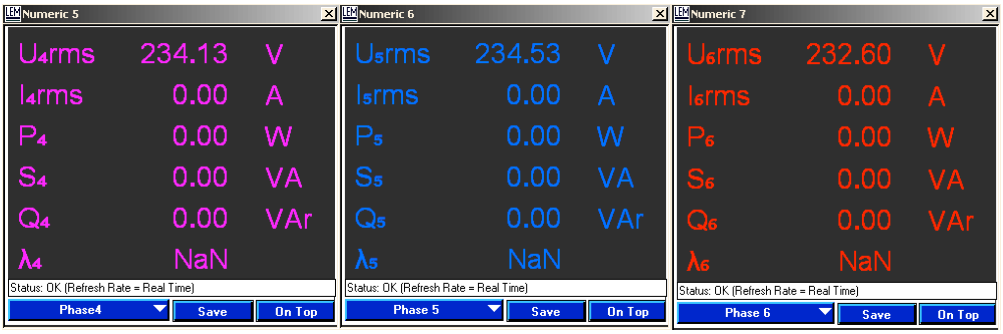

Fig. 5.67 Rectifier side experimental data for phases 4, 5 and 6 at no-load for 5.5kW rated system employing ABF filter (voltage V, current I, real power P, apparent power S, reactive power Q, power factor ʎ).

Similarly, the associated experimental no-load line current waveforms and their harmonic spectrums are shown in Fig. 5.68 and Fig. 5.69, respectively. Both figures show smooth sinusoidal waveforms with minimum harmonic components that confirm the power analyser estimated low current THDi% values (5.58% - 7.74%). Fig. 5.70 shows the no-load current at the rectifier side which is practically an open circuit path with no current existence.

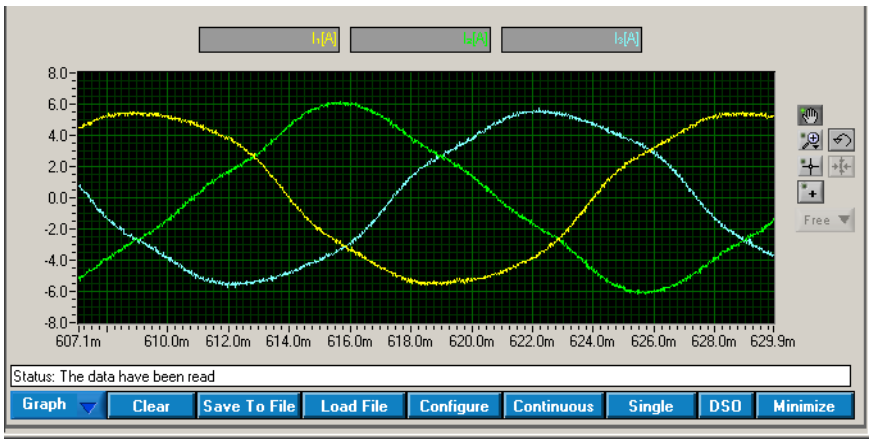

Fig. 5.68 Line side 3-phase current experimental waveforms at no-load for 5.5kW rated system employing ABF filter.

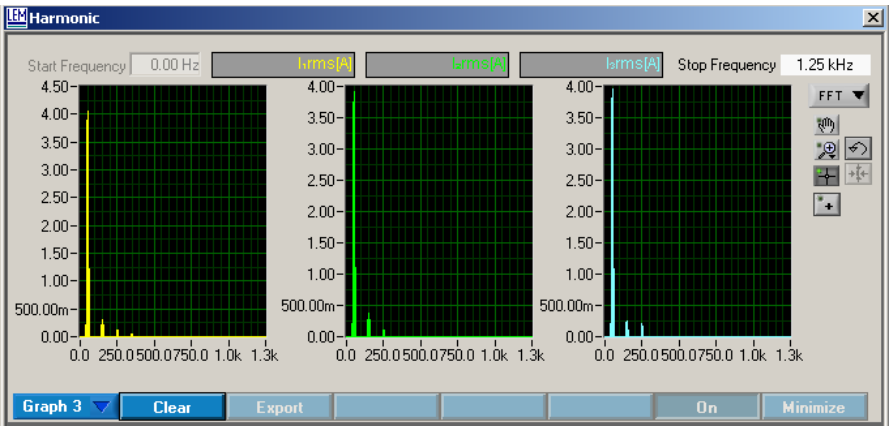

Fig. 5.69 Line side 3-phase current harmonic spectrum at no-load for 5.5kW rated system employing ABF filter.

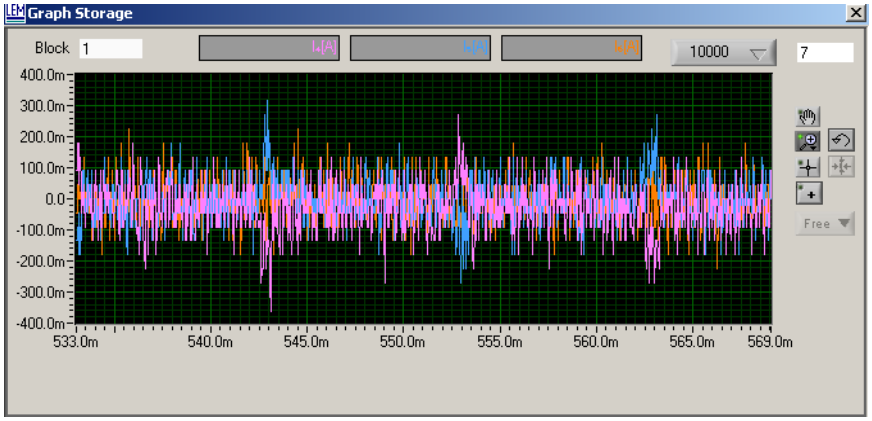

Fig. 5.70 Rectifier side 3-phase current experimental waveforms at no-load for 5.5kW rated system employing ABF filter.

Finally, the phase 2 (green) no-load line current and supply voltage harmonic spectrums combined with the phase 5 (blue) rectifier current harmonic spectrum are shown in Fig. 5.71. Essentially, both supply side voltage and current are clean and

will practically have no undesired interference with the distribution network. As the figure reveals a minor third harmonic component appears in the line current spectrum from the huge number of computers connected to the laboratory grid. However, the ABF parameters are designed to have minimum resonance risk with this 3rd harmonic component and are successful not to initiate any overvoltage condition during the experiment.

On the other hand, at no-load condition, the ASD system using the ABF filtering method has a major limitation of providing large amount of capacitive reactive power by its capacitor. As a result, the line current will lead the supply voltage by nearly 90 degrees, as shown in Fig. 5.72.

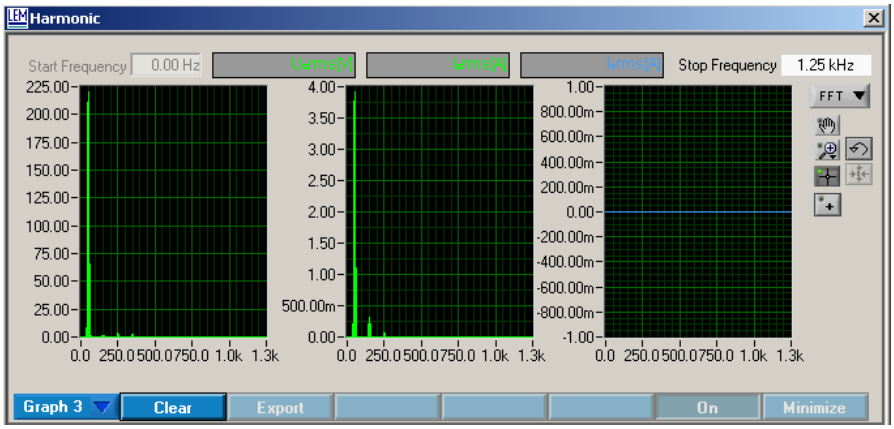

Fig. 5.71 Phase voltage, line current and rectifier current harmonic spectrum at no-load for 5.5kW rated system employing ABF filter.

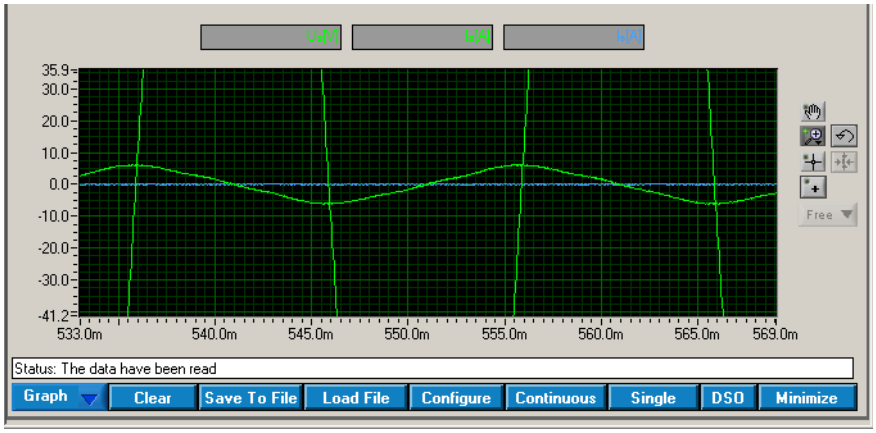

Fig. 5.72 Supply phase voltage and current experimental waveforms at no-load for 5.5kW rated system employing ABF filter (Zoomed).

Finally, the no-load current waveform at the rectifier side and the rectifier side smooth phase voltage are shown in Fig. 5.73. The rectifier side actually has no passing current and, therefore, the rectifier voltage is a sinusoidal waveform.

The rated load DC current and voltage experimental measured values are (0.0A and 560V).

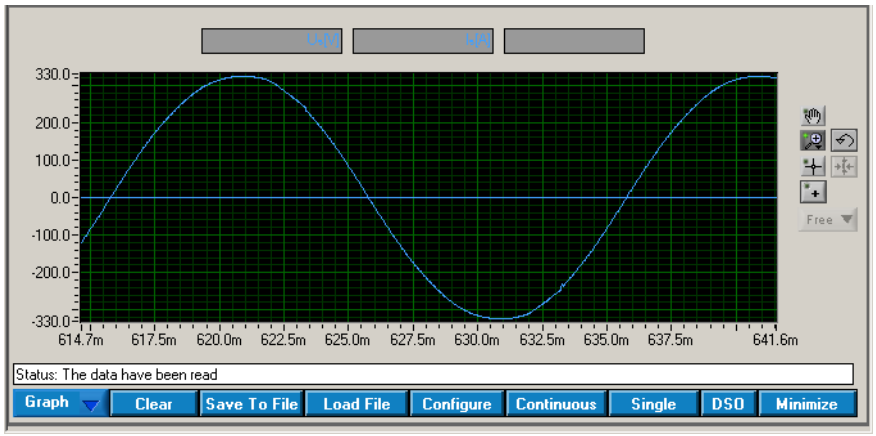

Fig. 5.73 Rectifier phase voltage and current experimental waveforms at no-load for 5.5kW rated system employing ABF filter.

5.7.5 Experimental Based Performance Evaluation of the ABF

In this section the advanced broadband filter (ABF) experimental performance specifications are obtained. Data collected from no-load to full-load (0%, 50%, 60%, 75% and 100%) operating conditions has been used to present the performance characteristic curves. The 0%, 50% and 100% loading conditions experimental results presented in the previous sections and the 75% and 60% loading conditions experimental results shown in Appendix G (sections G.1 and G.2) are all used.

As shown in Fig. 5.74, the designed 5.5kW ASD system utilizing the ABF structure has satisfactory low current THDi% values. This load dependent current THDi% performance can fulfil any power quality standards requirements in this current era.

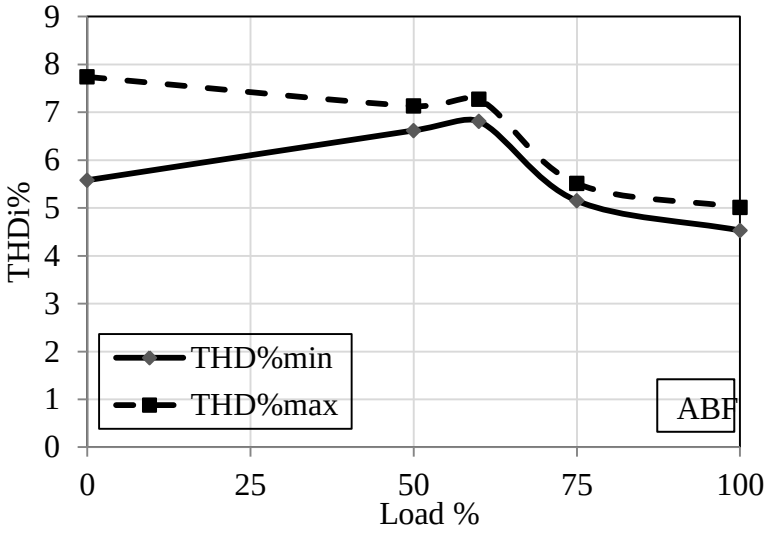

Fig. 5.74 The experimental line current THDi% range from no-load to full-load for a 5.5kW ASD system utilizing the ABF structure.

The line power factor performance characteristic is shown in Fig. 5.75. Parallel to the obtained simulation results, the experimentally tested system has unity line power factor at full-load condition and considerably high values down to the half-load operating condition. On the contrary, the line power factor decrease dramatically below 50% loading condition to reach very low leading values (0.02 - 0.80). Similar to the IBF performance conclusion, the ABF line power factor performance impose a practical limitation to the use of the proposed broadband filters under 50% loading condition. Therefore, either the used filter will be disconnected for this range of loading variation or used for ASD with high duty cycles applications.

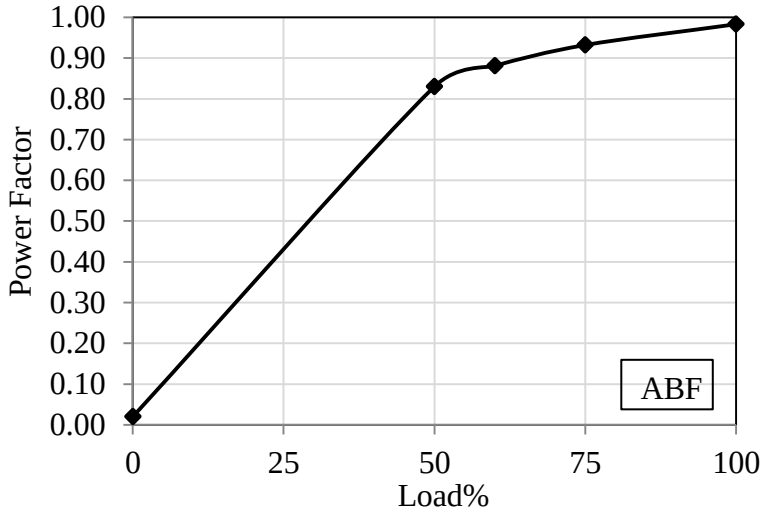

Fig. 5.75 The experimental line power factor from no-load to full-load for a 5.5kW ASD system utilizing the ABF structure.

The energy efficiency performance characteristic of the ABF including the power analyser shunt resistors (from 0% to 100% loading condition) is shown in Fig. 5.76. Comparatively, the tested ABF structure does not achieve high energy efficiency values (> 97%) as obtained from the simulation results. This resultant reduction in the lab is due to the use of the measuring shunt resistors associated with the power analyser equipment utilized for all measurements (explained earlier). Therefore, it is expected that the ABF structure, separately, will have much higher load dependent energy efficiency values (> 97%) that can be comparable with the simulation results presented in section 5.6.7.

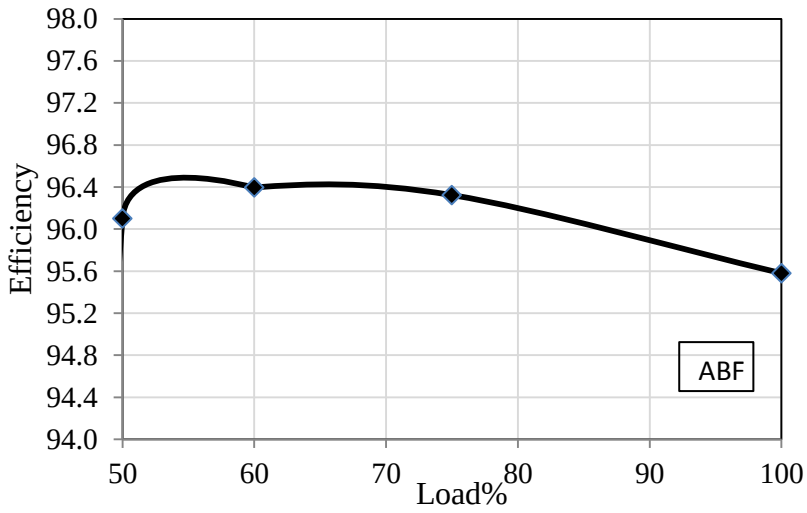

Fig. 5.76 The experimental ABF structure energy efficiency from half-load to full-load for a 5.5kW ASD system (including the power analyser shunt resistors).

Finally and similarly, the designed 5.5kW ABF laboratory prototype has been tested under 400V supply voltage. Table 5.8 summarizes and compares full-load experimental results of various illustrated passive filters designed and tested in the lab.

The 400V supply voltage full-load and no-load experimental results and waveforms are shown in Appendix G(sections G.3 and G.4). Comparable superior performances are preserved.

Table 5.8 Full-load experimental performance of various designed filters for 5.5kW ASD systems* (average values)

Filter Type	4% L_{ac} &2%L_{dc}	IBF 380V	IBF 400V	6% L_{dc}	ABF 380V	ABF 400V
Line THDi(%)	32.3	5.79	5.41	42.0	4.73	5.16
Line Power Factor**	0.921 (-)	0.991 (+)	0.981 (+)	0.915(-)	0.983(+)	0.964(+)
DC Voltage (V) mean	488	500	523	506	519	543

* Supply $THD_V\%$ = (1.72 -2.23)
** (+) leading and (-) lagging

5.8 **Summary**

In this chapter, a novel advanced broadband filter structure has been introduced. The new configuration is achieved by eliminating the IBF three-phase AC smoothing reactor and adding, instead, extra single-phase DC-link built-in inductor. The DC-link inductor selection method has been explained, then the ABF design process using the linear and the GA techniques has been described and results compared. The GA procedure in optimizing the choice of filter component values has shown a better ability to attain smaller filter values while maintaining the same and/or improve system power quality indices levels.

The designed ABF structure performance has been investigated. The steady-state performance characteristics at various loading conditions under balanced utility grid with voltage harmonic distortion operating situations were illustrated. Unbalanced utility grid with different voltage variation rates was also considered. The main power quality parameters (line current $THD_i\%$ and power factor, filter output voltage regulation ($\Delta V_o\%$)) and energy efficiency aspects have been studied.

The computer simulation based study confirms the theoretical performance prediction and proves the accuracy of the ABF filter parameter optimization method.

Lastly, the laboratory performance characteristics of a 5.5 kW ASD system power rated employing the 6% L_{dc} filter type and the designed ABF structure have been

considered and assessed. The ASD steady-state performance characteristics from no-load to full-load operating situations were extracted. Analysis of the main power quality constraints (line current THDi%, power factor, and filter output voltage regulation) and energy efficiency attributes have been shown.

The accomplished experimental results, similarly, approve the simulation results achieved and the superior comprehensive performance of ABF based ASD systems have been concluded including the defined minor limitations.

Additional detailed simulation and experimental results comparison will be presented in the conclusion chapter (final chapter).

The next sixth chapter involves testing the IBF and the ABF effectiveness in a standard IEEE distribution network at different stages of nonlinear penetration levels in the network. The simple 4% AC line reactor and 6% DC-link inductor filtering types are also included in the study for clarification enhancement and comparison purposes.

6 TESTING BROADBAND FILTERS IN A DISTRIBUTION NETWORK

6.1 Introduction

The previous chapters discussed the operating principles and the design methods of both the improved broadband filter (IBF) and the advanced broadband filter (ABF). In this chapter, the operating performance and effectiveness of the harmonic passive broadband filters, proposed in this thesis, are tested by connecting them in a standard IEEE distribution network that contains different levels of nonlinear loads (ASD system). The study will be conducted via detailed modelling of the distribution network and the connected nonlinear loads through computer simulations.

The analysis and evaluation will involve three different nonlinear load penetration levels (< 10%, < 50% and 70%) of the total overall network linear load. These three cases of distortion in the network with current harmonics (light, moderate and heavy) will help to have a better decision whether to use a harmonic filter or not, and in choosing the required type of filtering technique that can comply with the applied harmonic standards (IEEE 519) for each situation.

In these three main operating conditions, power quality indices such as; the network lines current THDi% and power factor values are monitored. Furthermore, the voltage THDv% and rms values at the network buses are under investigation for the various nonlinear loading conditions considered. The study will involve, in the first stage, the network performance including the ASD systems with no filters connected. In the second stage, the study will investigate these various network specifications with different types of filtering techniques utilization.

The low voltage harmonic filters can be connected either to the nonlinear load directly or to a common distribution PCC bus. Generally, the nonlinear load connected harmonic filter is more effective in reducing the line current harmonics and the bus voltage harmonics [63] and can be cost effective when a few nonlinear loads exist in the network. On the other hand, with many harmonic loads in the

network, the common bus connected filters can help in improving the overall network power factor and can reduce the installation cost of several harmonic filters at individual loads to one or two larger filters at the PCC [64]. This analysis will involve several types of only two nonlinear loads combinations connected (at a time) to the network. Therefore, for only two nonlinear loads existing in the network, the considered filters will be connected at the ASD system directly.

Finally, the IEEE 30-bus distribution network is selected to study the effectiveness of the harmonic broadband passive filters performance under different operation conditions. Simulation results are presented, analysed and compared for the three network harmonic distortion conditions before and after the installation of the assigned filters.

6.2 IEEE 30-bus Distribution Network with Nonlinear Loads

The IEEE 30-bus distribution network with two buses connected to nonlinear loads is shown in Fig. 6.1 [34], [65] and [66]. The proposed system under investigation includes three types of nonlinear loads (different polluting current harmonic spectrum) connected to bus 15 and bus 18, as shown in Table 6.1. The first type is the basic 6-pulse bridge rectifier system without installing any filters either at the AC side or the DC-link side. The second type is the same 6-pulse bridge rectifier system utilizing a typical three-phase 4% Lac (AC-reactor) and 2% Ldc (DC-link inductor). The final type involves utilizing a built-in 6% Ldc (DC-link inductor) filtering method only. In all cases, the harmonic contents of the injected current is known (simulation based method) and considered in the analysis.

The active power and reactive power data of the nonlinear load cases considered in the analysis are based on the previous chapter's information and given in Table 6.1 (KVar values are estimated using the total power factor known data for each load type, shown in Tables 6.2 to 6.4). These different load cases are connected to bus 15 and bus 18 in various combinations to perform three major nonlinear loading

conditions in the network (in percentage) with respect to the total load in the system (< 10%, < 50% and 70%).

For instance, a combination of a 55kW load connected to both buses 15 and 18, individually, will represent about 8% nonlinear load of the total network load value (1413.7kW). The second combination will be a 55kW connected to bus 18 and a 500kW connected to bus 15. This will increase the penetration level to about 40%. Finally, connecting two 500kW individual loads to bus 15 and bus 18 will bring the nonlinear load penetration level to the highest value of about 70%.

The 30-bus system network, bus data and the linear loads information (real and reactive power), line data specifications and shunt capacitors installed in the network data are given in Appendix H. As shown in Table H.1, most of the linear conventional industrial reactive loads connected to the network load buses have a lagging 0.95 total power factor at full-load condition.

Table 6.1 Nonlinear load types assigned in the study

Load type	Case no.	Non-linear load type	kW	kVar
Type 1	1	6-pulse bridge rectifier (no-filter)	55	73
	2	6-pulse bridge rectifier (no-filter)	500	666
Type 2	3	6-pulse bridge rectifier with 4%Lac+2%Ldc	55	22
	4	6-pulse bridge rectifier with 4%Lac+2%Ldc	500	200
Type 3	5	6-pulse bridge rectifier with 6%Ldc	55	22
	6	6-pulse bridge rectifier with 6%Ldc	500	200

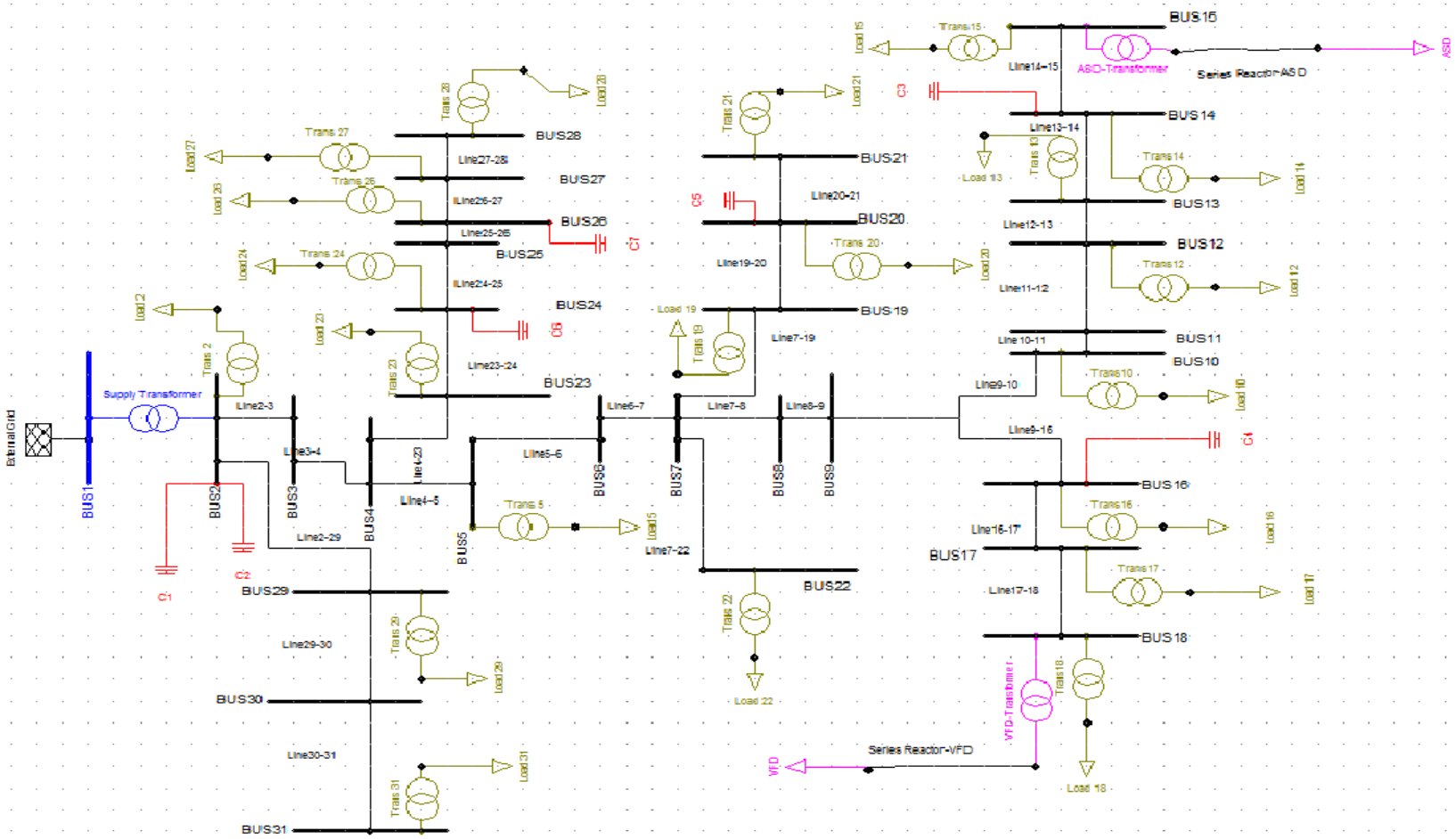

Fig. 6.1 IEEE 30-bus distribution network with nonlinear loads (6-pulse bridge rectifier front-end application) connected to bus 15 and bus 18 used for simulation.

6.3 Testing the Broadband Harmonic Filters in the IEEE 30 Bus Distribution Network

The two broadband passive filter topologies (IBF and ABF) will be connected via 400V step-down transformers to the 23kV IEEE 30-bus network at buses 15 and 18, as shown in Fig. 6.2. The filter components for the different ASD rated powers considered in each case study will be designed by the same methods explained in the preceding chapters. For comparison reasons, another two basic and conventional filtering methods will be considered for the same assigned operating conditions. The first one is adding a 4% three-phase AC reactor (Lac) and a 2% DC-link inductor (Ldc). The second method involves the use of a 6% DC-link (Ldc) only for smoothing the rectifier current as explained in section 5.2. These two filtering topologies added to the basic ASD structure (load type 1) will perform load type 2 and load type 3, respectively, as shown in Table 6.1.

Each nonlinear load type will draw a different line current waveform with its own current harmonic spectrum details. Table 6.2 shows the line current harmonic spectrum (simulation based) for basic three-phase 6-pulse bridge rectifier front-end 5.5kW ASD application (load type 1) including the fundamental component (I_1) and the first six harmonic components in the spectrum (I_5, I_7, I_{11}, I_{13}, I_{17} and I_{19}). The table shows the harmonic components magnitude in percentage with respect to the fundamental component and the phase angle of each component in radian and degrees values. These harmonic components magnitudes ratios are constant (independent on the load rating) for a medium range power rated ASD systems (5kW to 500kW).

Consequently, the rectifier drawn current will be modelled in the simulation using the current harmonic spectrum. Each component magnitude percentage and phase angle (referred to the fundamental component phase angle degrees) is implemented, for better accuracy levels, as shown in Fig. 6.3.

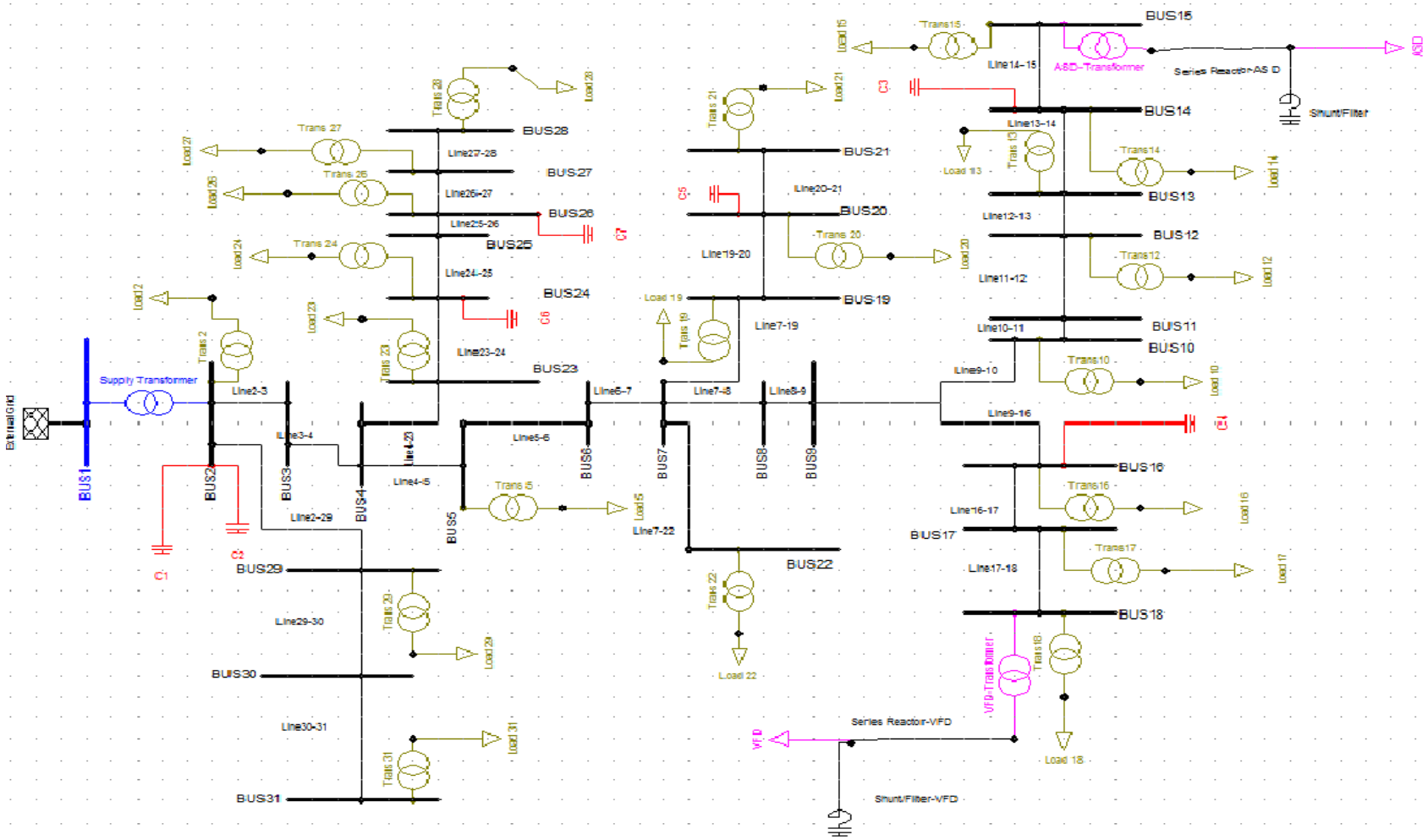

Fig. 6.2 IEEE 30-bus distribution network with nonlinear loads and harmonic filters connected to bus 15 and bus 18.

Table 6.2 Line current harmonic spectrum for basic 6-pulse bridge rectifier front-end ASD application (Load type 1)*

	f [Hz]	L1.I [A]	Phi [rad]	Phi [deg]	%(Max)
Minimum	50.001	0.14084	0.40957	23.467	1.1589
Maximum	2.75k	12.152	6.2579	0.35855k	0.1k
0	50.001	12.152	3.1374	0.17976k	0.1k
1	0.25k	10.688	6.2579	0.35855k	87.947
2	0.35k	9.3672	3.0995	0.17759k	77.082
3	0.55001k	6.1291	6.1775	0.35394k	50.436
4	0.65001k	4.4851	2.9736	0.17037k	36.907
5	0.85001k	1.7824	5.797	0.33214k	14.667
6	0.95001k	0.96321	2.1794	0.12487k	7.9262

*Line total power factor = 0.60

The Line current harmonic spectrum details for 6-pulse bridge rectifier front-end ASD application using 4%Lac+2%Ldc filters (Load type 2) are shown, in a similar approach, in Table 6.3. The huge reduction of the current harmonic components magnitudes percentage is very obvious. Therefore, the rectifier current waveform has a better smoothened shape and its total THDi% value will be dropped dramatically (more details is presented in the next section). Accordingly, the line power factor is improved from 0.6 lagging (load type 1) to 0.93 lagging (load type 2).

Similarly, Table 6.4 shows the Line current harmonic spectrum details for 6-pulse bridge rectifier front-end ASD application using 6%Ldc filter (Load type 3). As explained is section 5.2, the built-in single-phase 6% DC-link inductor has a special superior ability in suppressing the 5^{th} harmonic component (most dominant) magnitude percentage to the same level of utilizing the AC three-phase 4% reactor Lac and 2%Ldc filtering method in load type 2. However, it has less capability in reducing other current harmonic components magnitudes.

In all previously described load types three cases (1, 2 and 3), the simulation based estimated total line power factor information (shown under each table) is used to calculate the total three-phase reactive power (Q) in kVar for every case study shown in Table 6.1.

Table 6.3 Line current harmonic spectrum for 6-pulse bridge rectifier front-end ASD application using 4%Lac+2%Ldc filters (Load type 2)*

	f [Hz]	L1.I [A]	Phi [rad]	Phi [deg]	%(Max)
Minimum	50.001	0.14926	1.0701	61.311	1.2137
Maximum	1.25k	12.298	6.2627	0.35882k	0.1k
0	50.001	12.298	2.9301	0.16788k	0.1k
1	0.25k	3.7456	5.0567	0.28973k	30.457
2	0.35k	0.98886	6.2627	0.35882k	8.041
3	0.55001k	0.82711	1.0701	61.311	6.7257
4	0.65001k	0.44235	1.4071	80.622	3.597
5	0.85001k	0.36088	3.0911	0.17711k	2.9345
6	0.95001k	0.2519	3.3069	0.18947k	2.0484

*Line total power factor = 0.93

Table 6.4 Line current harmonic spectrum for 6-pulse bridge rectifier front-end ASD application using 6% Ldc filter (Load type 3)*

	f [Hz]	L1.I [A]	Phi [rad]	Phi [deg]	%(Max)
Minimum	50.001	0.12137	0.90892	52.077	1.0083
Maximum	3.25k	12.037	6.2438	0.35775k	0.1k
0	50.001	12.037	3.0687	0.17582k	0.1k
1	0.25k	3.658	5.6071	0.32126k	30.389
2	0.35k	1.875	0.90892	52.077	15.577
3	0.55001k	1.0074	2.9679	0.17005k	8.3692
4	0.65001k	0.75144	3.3958	0.19457k	6.2425
5	0.85001k	0.59918	6.0605	0.34724k	4.9777
6	0.95001k	0.52031	6.2438	0.35775k	4.3225

*Line total power factor = 0.93

For the purpose of the network modelling, a graphic computer simulation package program DigSilent (version, 13.2) has been utilized [67]. The name **DIgSILENT** stands for "**DIg**ital **SI**mu**L**ation and **E**lectrical **N**e**T**work calculation program". DIgSILENT Version 13.2 has power system analysis software with an integrated graphical one-line interface, as shown in Fig. 6.2. That interactive one-line diagram included drawing functions, editing capabilities and all relevant static and dynamic calculation features. The accuracy and validity of the results obtained with this package has been confirmed in a large number of implementations, by organizations involved in planning and operation of power systems [67].

The computer simulation software includes a data manager separate window that allows you to input and control your data. Also, the integrated graphical one-line interface window has a tool bar that can be used for all simulation requirements (filing options, editing, calculation, data, options, window and help).The load flow calculation uses the Newton Raphson iteration method (shown in Fig. 6.3a) and the harmonic load flow are done for a balanced network representation and for all frequencies. The harmonic source presentation is shown in Fig. 6.3b.

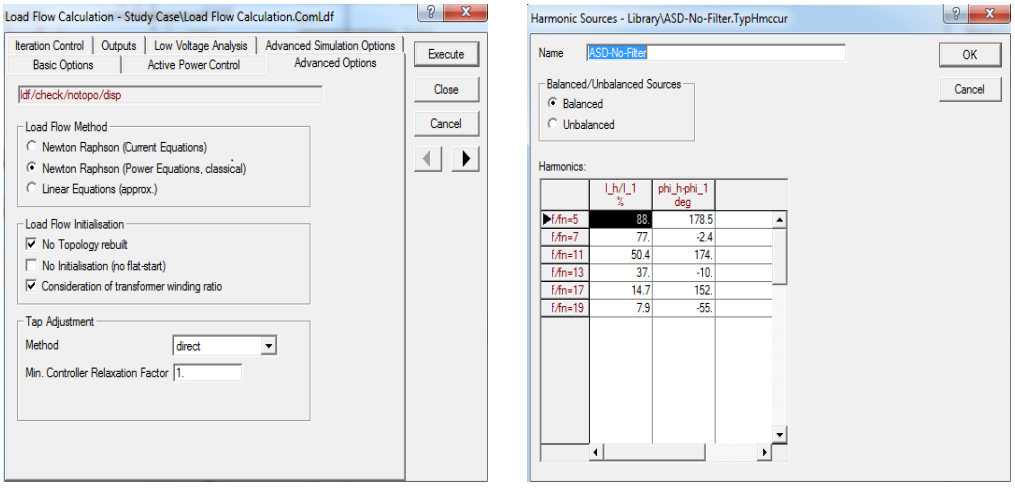

(a) (b)

Fig. 6.3 (a) Simulator integration method, (b) Harmonic load modelling method.

In order to validate the chosen testing system, a prototype 30-bus network is built and a given nonlinear loads in [34] are connected to examine the system under the same conditions presented in this paper. The network simulation harmonic analysis results obtained from this sample case study with no filter utilized are very similar to the results achieved in this reference to a high degree of accuracy providing the different simulation software and modelling method utilized in each attempt. For instance, system THDv values are 3.182% in the ref. paper and 3.189% in this study while the maximum THDv values are 6.51% at bus15 in the ref. paper and 6.737% at bus 14 in this study).

In the following sections, the performance analysis of the real IEEE 30-bus network considered is presented. Simulation results of selected power quality indices, such as; all lines current THDi%, voltage THDv% and rms (p.u.) values at the buses, and

lines power factor are illustrated and analysed. This will involve the selected three case studies for different nonlinear load (ASD systems) penetration levels of 70%, 40% and 8%, respectively.

6.3.1 IEEE 30-bus Distribution Network with 70% Nonlinear Load (ASD) Case Study

The first case study involves connecting a 2*500kW rated ASD systems, one to bus 15 and another to bus 18. This total nonlinear load of 1.0MW presents about 70% penetration level in the network that contains 1413.7kW total linear load. Furthermore, for the same power ratings, the analysis will involve different load types (current harmonic spectrum) connected to the same buses in order to compare the results. The three main load types shown in Table 6.1 are considered along with the installation of the two proposed harmonic broadband passive filters in this thesis (IBF and ABF) to appropriate ASD structure for each filter (i.e. IBF for load type 2 and ABF for load type 3). The simulation results of these five different cases are presented and analysed in the following:

a) Load type 1 simulation results and analysis:

The 30-bus network simulation results for the basic three-phase 6-pulse bridge rectifier load type utilizing none of the considered filtering techniques are illustrated. The lines current THDi% values are shown in Fig. 6.4. Most of the lines current are highly distorted with the current harmonics resulting in unacceptable corresponding THDi% values (> 100%) that exceed any standard limits for the distribution networks such as IEEE519. Fig. 6.5 shows the lines power factor values that can be interpreted by looking at the corresponding line current THDi% values shown in Fig. 6.4. The more harmonic distortion in the line, the poorer line power factor (lagging or leading) values can exist. For example, lines (10-11, 11-12, 12-13 and 13-14) have a very low lagging power factor values (< 0.3) even though with the use of the power factor correction capacitors. This is due to the enormous THDi% values in these lines that distort the line current waveforms shape and provide a huge amount of lagging reactive power (kVARs) to the system. On the other hand, lines having higher power

factor (> 0.92 lagging or leading), as shown, have matching very low current THDi% values (< 20%). Nevertheless, these higher power factor values are below the recommended standards due the high current harmonic distortion levels in the network. Lines (7-22, 20-21, 24-25) and all other higher buses numbers lines represent this situation.

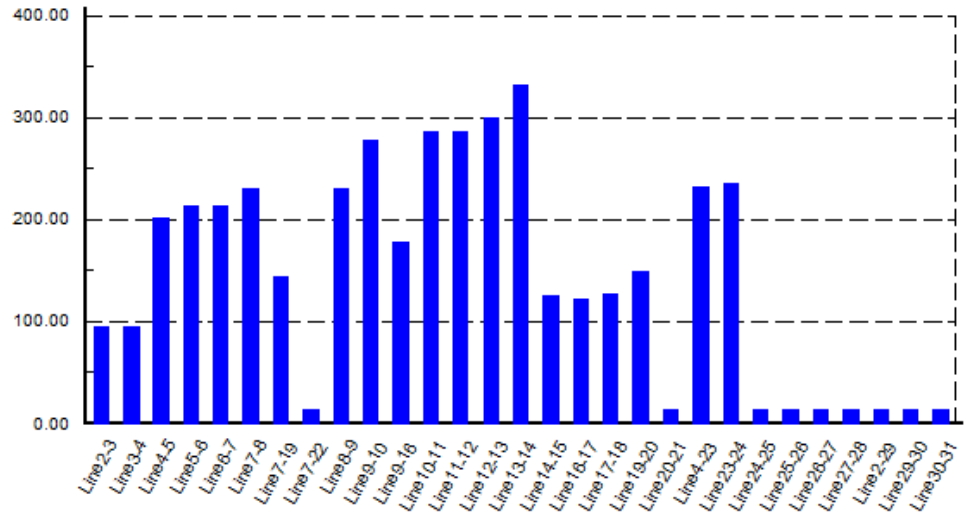

Fig. 6.4 Line current THDi% values for a 70% total nonlinear load (ASD) connected at buses 15 and 18 with no harmonic filter connected.

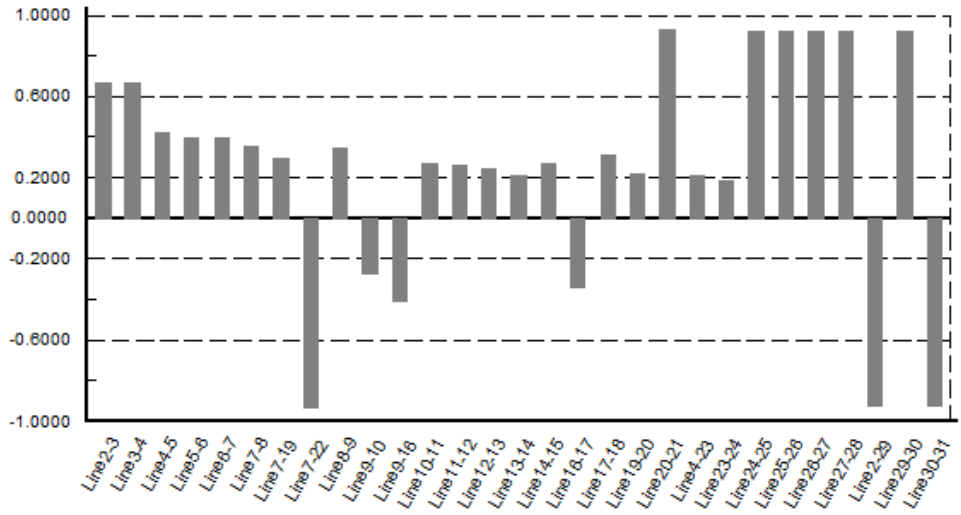

Fig. 6.5 Line power factor values for a 70% total nonlinear load (ASD) connected at buses 15 and 18 with no harmonic filter connected.

The voltage THDv% values at all buses in the network are shown in Fig. 6.6. All buses have a very high voltage THDv% values (more than 25%) with a maximum value of about 40%. These range of values are not acceptable as the IEEE519

harmonic standard puts a limit of 5% voltage THDv% for low voltage bus systems (<69kV). These THDv% high values are also due to the high current harmonic distortion levels in the network. Finally, the voltage rms (p.u.) values at all buses simulation results are shown in Fig. 6.7. The voltage rms values have a range of 1.045 to 1.078 in per unit system. According to the ANSI (American National Standard Institute) C84.1 which is the electric power systems and equipment – voltage ranges [68] the maximum limit to this network service voltage level is 105% of the nominal voltage value. Most of the buses voltage rms values in p.u. violate this standard.

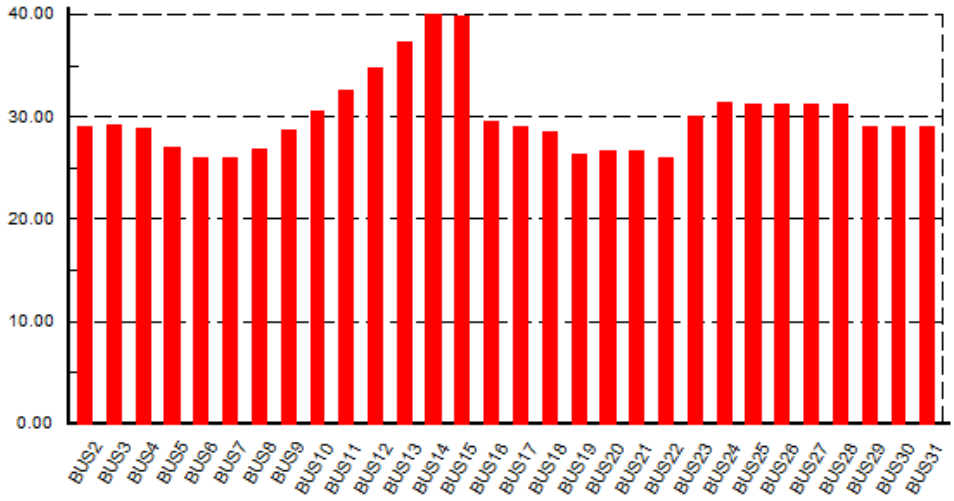

Fig. 6.6 Bus voltage THDv% values for a 70% total nonlinear load (ASD) connected at buses 15 and 18 with no harmonic filter connected.

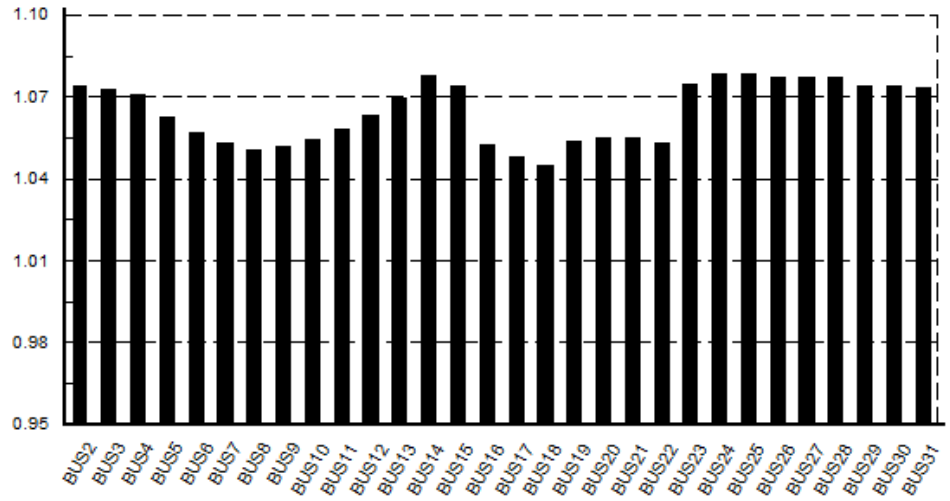

Fig. 6.7 Bus voltage rms values (p.u.) for a 70% total nonlinear load (ASD) connected at buses 15 and 18 with no harmonic filter connected.

b) Load type 2 simulation results and analysis:

The next illustrated 30-bus network simulation results involve the case study of introducing a basic filtering method (4%Lac+2%Ldc) to the ASD system connected to the buses 15 and 18 for the same power ratings. This is implemented in the modelling software [67] by modifying the load current harmonic specifications utilized according to the corresponding data shown in Table 6.3. Fig. 6.8 reveals that the simulation lines current waveforms have a smoother continuous shape. The THDi% values dropped very sharply (by a factor of 10) in most of the network lines compared to the previous case results shown in Fig. 6.4. As a result, the line power factor values, shown in Fig. 6.9, have improved at most of the network lines. However, many of the network lines (> 2/3) have a current total harmonic distortion values range of 12% to 30% THDi which is still not satisfactory. In contrast, the rest of the lines have a very low harmonic distortion levels with nearly sinusoidal line current waveforms that have minimum recommended THDi levels (< 5%). Similarly, the power factor values of some lines have increased to approximate 0.95 (lagging or leading) improving the overall situation.

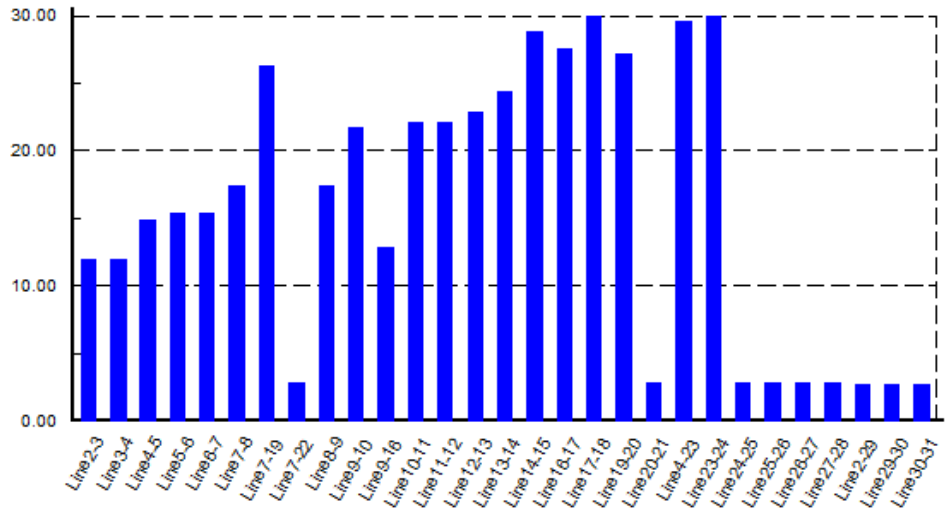

Fig. 6.8 Line current THDi% values for a 70% total nonlinear load (ASD) connected at buses 15 and 18 utilizing 4%Lac & 2%Ldc filters.

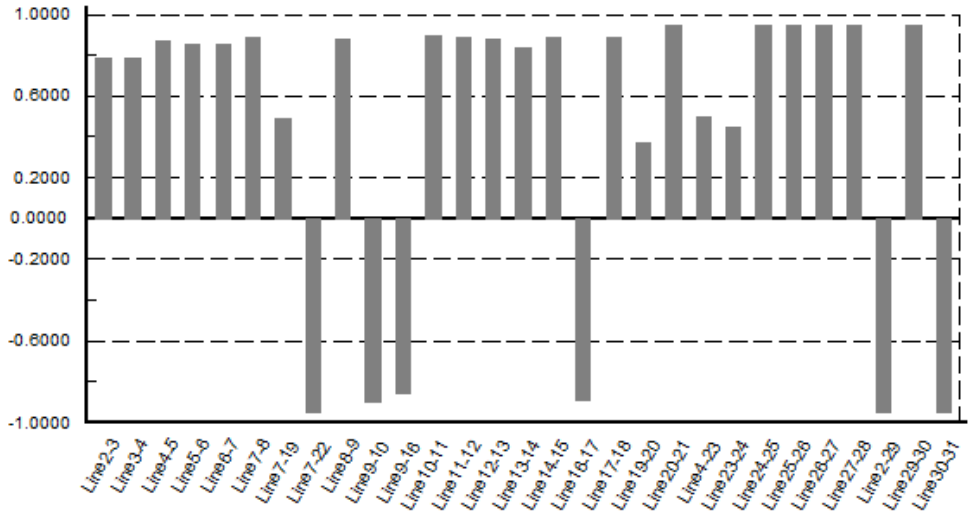

Fig. 6.9 Line power factor values for a 70% total nonlinear load (ASD) connected at buses 15 and 18 utilizing 4%Lac & 2%Ldc filters.

In the same approach, a great reduction in the voltage THDv% values at all buses in the network is achieved with a range of (5.02 to 5.73%), as shown in Fig. 6.10. This range violates the assigned limitations for such a network (THDv% < 5) by a very small amount. Moreover, Fig. 6.11 shows the reduced buses voltage rms normalized values (1.028 to 1.048 per unit) that comply with the regulations.

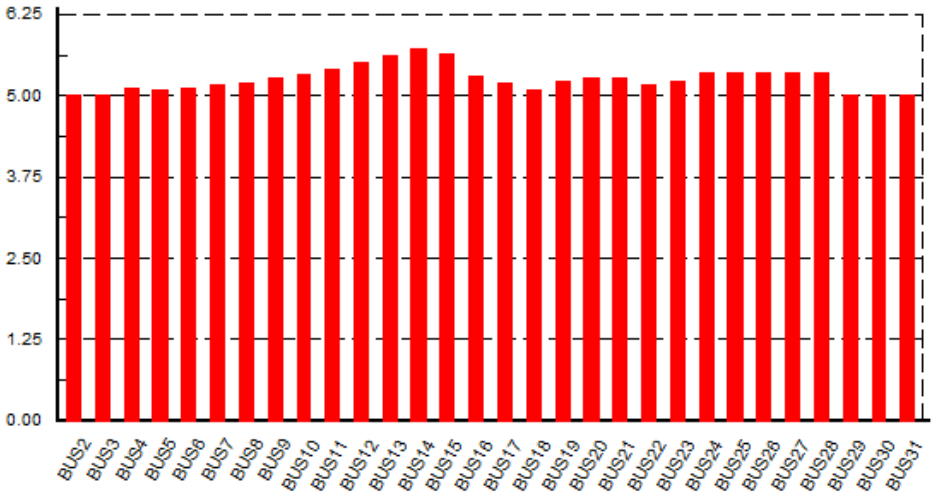

Fig. 6.10 Bus voltage THDv% values for a 70% total nonlinear load (ASD) connected at buses 15 and 18 utilizing 4%Lac & 2%Ldc filters.

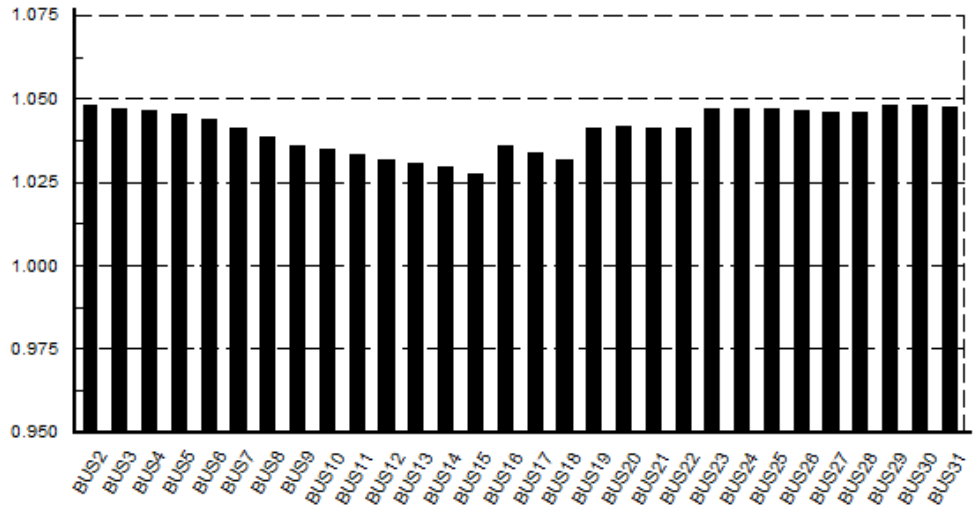

Fig. 6.11 Bus voltage rms values (p.u.) for a 70% total nonlinear load (ASD) connected at buses 15 and 18 utilizing 4%Lac & 2%Ldc filters

c) Load type 2 utilizing IBF simulation results and analysis:

In order to improve the overall operating performance for the power quality indices under investigation in this study (lines THDi% and PF, buses THDv% and Vrms), the developed improved broadband filter (IBF) is installed in the network and connected to the nonlinear load side, as shown in Fig. 6.2. To be tested, the IBF filter (shown in Fig. 2.1b) is designed for the existing 500kW power rating ASD system (Li = 0.121 mH, Lf = 0.0658 mH and Cf = 5666 µF star connection). It is practically assumed that the IBF rectifier side current harmonics have similar characteristics as the previous load type (section b) current harmonic spectrum data. These known data is implemented in the modelling system (shown in Fig. 6.3b) to obtain the simulation results. It is expected, according to the results in chapter 4, that the system overall performance will improve and have the ability to comply with the IEEE519 harmonic standards.

Figures 6.12 and 6.13 show the lines current THDi% and the resultant lines total power factor simulation values. All lines current have a very low THDi% values (< 5%) at full-load operating condition which reduce the overall harmonic distortion dramatically in the network w.r.t the previous cases simulation results. These lines low current distortion values (0.16 to 4.87 THDi%) can comply with any harmonic standards and are recommended by all electrical supply utilities. Furthermore, many

of the lines improved their power factor values (> 0.95 lagging and leading) and specific ones have a unity power factor values. However, even though with the network approximately sinusoidal lines current that contains practically negligible harmonic components, the associated line power factor values are affected by the installed power factor correction capacitors. Some of these capacitors provide extra leading reactive power (more than required) that degrade certain line power factor values. This may require redesigning the installed power factor correction capacitors in this standard IEEE 30-bus distribution network that contains such filters which is beyond the scope of this study.

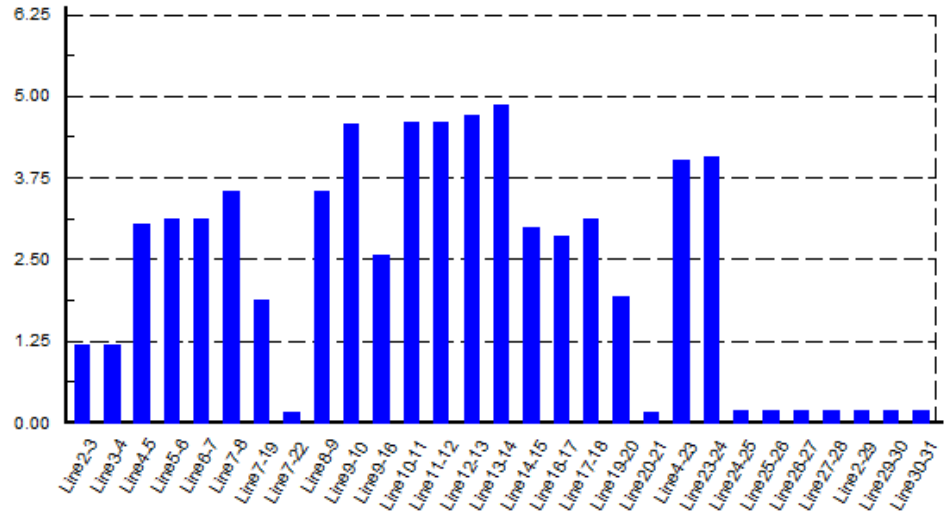

Fig. 6.12 Line current THDi% values for a 70% total nonlinear load (ASD) connected at buses 15 and 18 utilizing IBF harmonic filter.

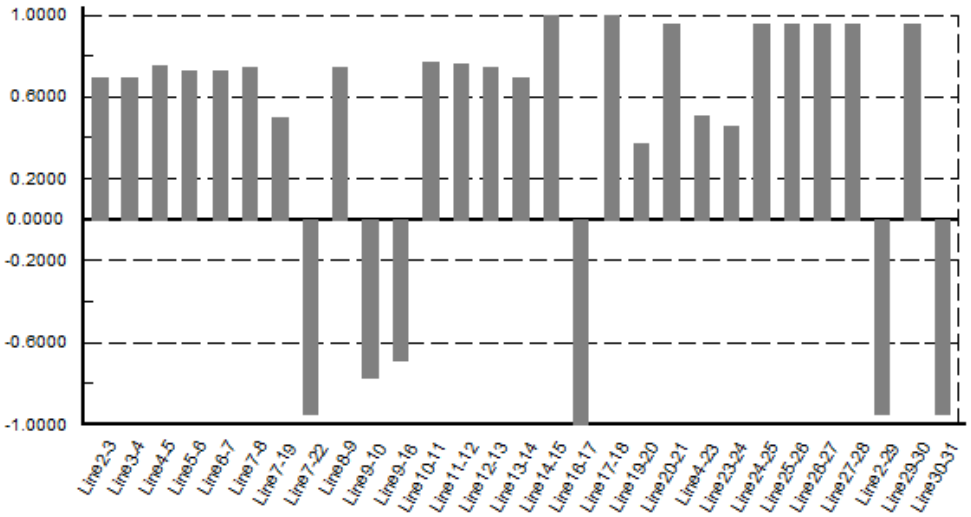

Fig. 6.13 Line power factor values for a 70% total nonlinear load (ASD) connected at buses 15 and 18 utilizing IBF harmonic filter.

The utilization of the IBF in the network is not only beneficial to reduce the line current THDi% values but also to decrease the voltage harmonic distortion THDv% at all the network buses. Fig. 6.14 shows the extremely low THDv% values (< 0.67%) at all buses of the 30-bus network. This will eliminate the undesirable effects of the current harmonics on the linear loads connected to the buses and enhance the overall operating conditions for all power consuming customers connected to the grid. Nevertheless, the voltage rms values at all buses for this simulation case study marginally exceed the standard limits (1.05%) with a range of 1.04 – 1.055 p.u, as shown in Fig. 6.15. This is due to the existing shunt capacitors in the network and, therefore, validates the necessity to reconsider their rated kVA requirements for such harmonic broadband passive filters topologies usage.

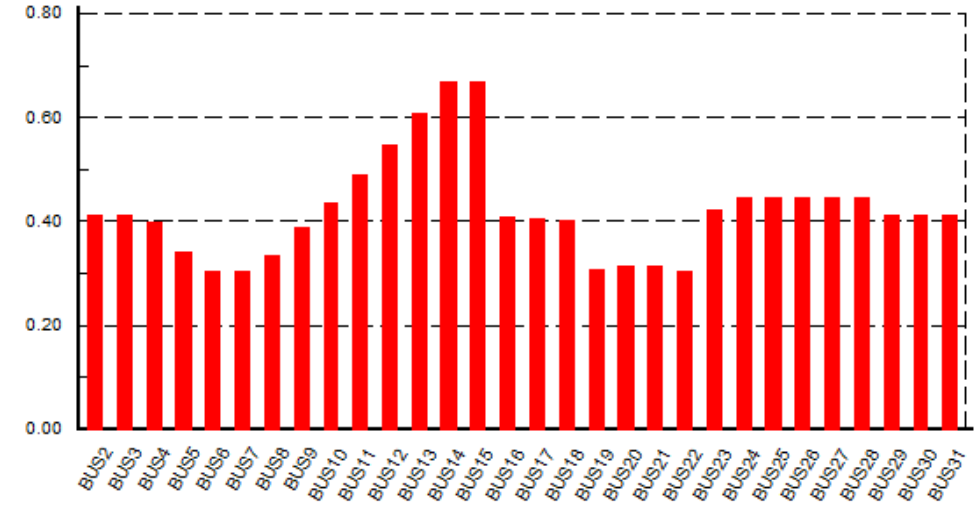

Fig. 6.14 Bus voltage THDv% values for a 70% total nonlinear load (ASD) connected at buses 15 and 18 utilizing IBF harmonic filter.

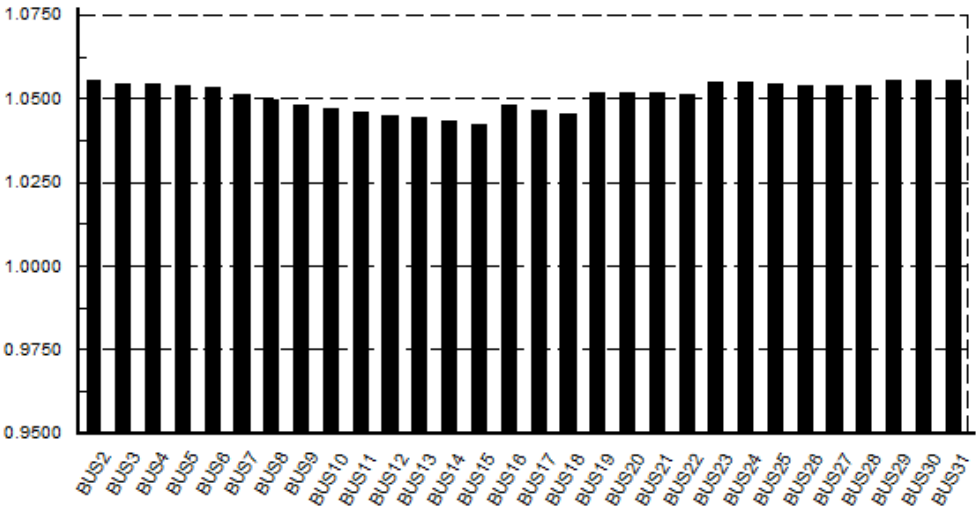

Fig. 6.15 Bus voltage rms values (p.u.) for a 70% total nonlinear load (ASD) connected at buses 15 and 18 utilizing IBF harmonic filter.

d) Load type 3 simulation results and analysis:

In this section, in order to examine the use of the commonly DC-link built-in inductors in a ASD, the 6% Ldc filtering method explained in section 5.2 is considered and assessed in a similar process method for the same nonlinear penetration level (70%). For this purpose the current harmonic spectrum shown in Table 6.4 (representing the fundamental component and the first six dominant harmonics components) is chosen and implemented in the modelling software DigSilent 13.2. Generally, the obtained results, to a large extend, are similar to section b (load type 2) with 4%Lac and 2%Ldc filtering technique simulation results. The lines current THDi% values are shown in Fig. 6.16 with a range of 2.7% to 33%. The ability of this simple and low-cost technique (6%Ldc method) is obvious in eliminating the current harmonic components in the system compared to Fig.6.4 results (no filter method). Yet, the majority of the lines THDi% values are >10%. Similarly, the interrelated line power factor values have improved (compared to Fig. 6.5 results) and achieved a maximum values of 0.95 lagging (lines 20-21, 24-25, 25-26, 26-27, 27-28 and 29-30) and 0.95 leading (lines 7-22, 2-29 and 30-31) as shown in Fig. 6.17 .

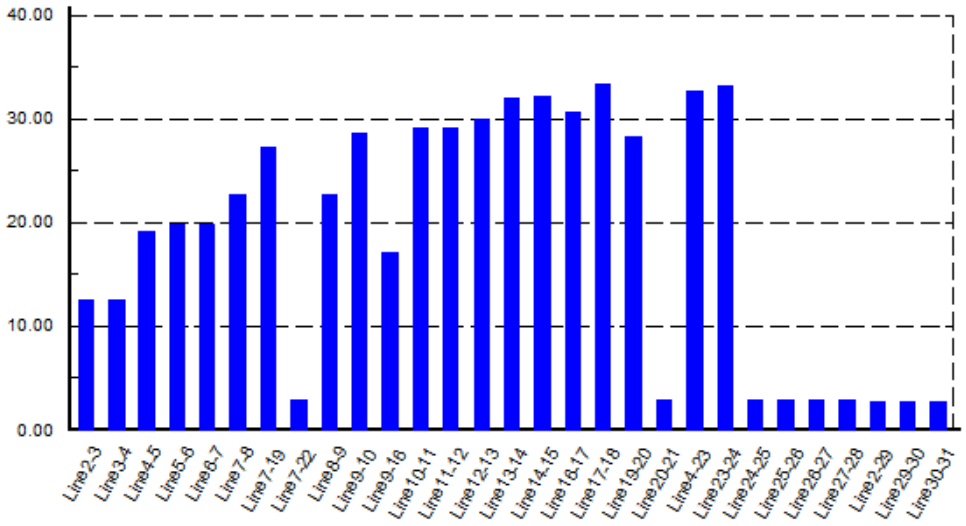

Fig. 6.16 Line current THDi% values for a 70% total nonlinear load (ASD) connected at buses 15 and 18 utilizing 6%Ldc filters.

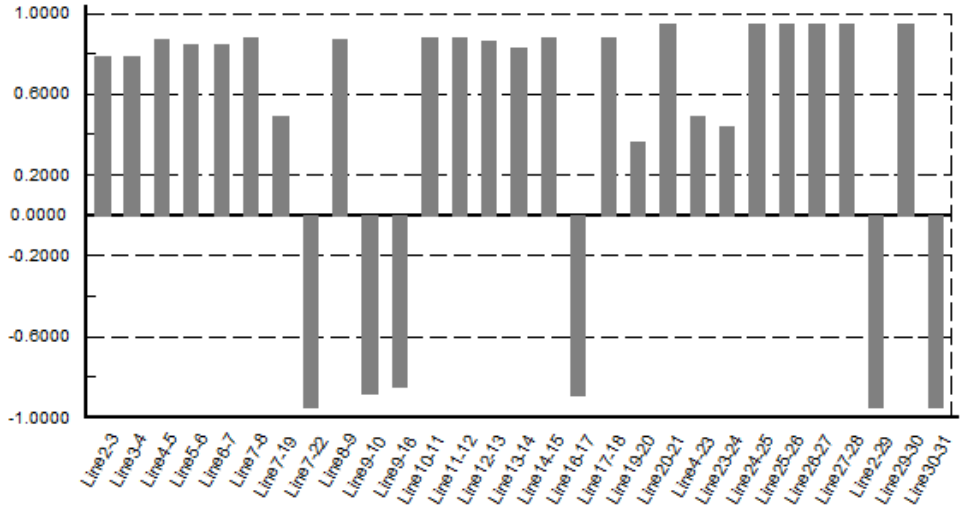

Fig. 6.17 Line power factor values for a 70% total nonlinear load (ASD) connected at buses 15 and 18 utilizing 6%Ldc filters.

The voltage THDv% values at all buses in the network are shown in Fig. 6.18. The results have a minimum value of 5.21% and a maximum value of 6.11%. In other words, all the network buses has a voltage total harmonic distortion levels just above the permitted boundary for <69kV systems (5% THDv) according to the IEEE519 harmonic standards. This situation might result in undesirable current harmonics effects (extra losses, heating and interference) for any load connected to the bus. However, the voltage rms (p.u.) values at all buses simulation results (shown in Fig. 6.19) do not exceed the limit of 1.05 p.u, similarly to the results shown in Fig. 6.11 with the 4%Lac and 2%Ldc filtering type.

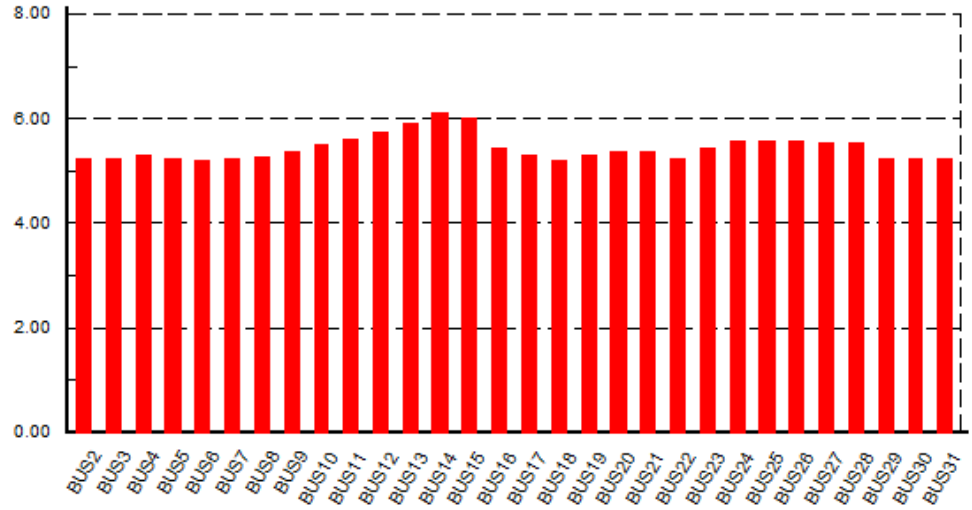

Fig. 6.18 Bus voltage THDv% values for a 70% total nonlinear load (ASD) connected at buses 15 and 18 utilizing 6%Ldc filters.

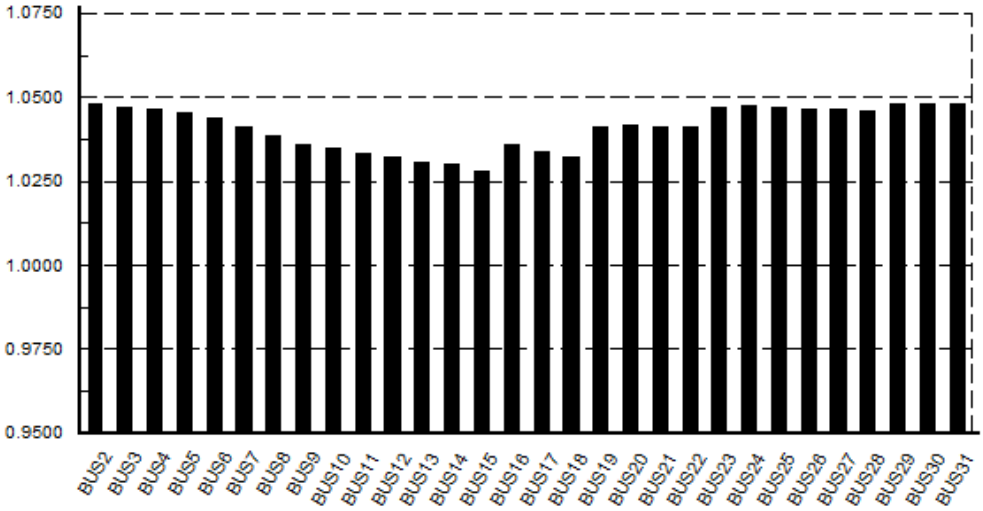

Fig. 6.19 Bus voltage rms values (p.u.) for a 70% total nonlinear load (ASD) connected at buses 15 and 18 utilizing 6%Ldc filters.

e) Load type 3 utilizing ABF simulation results and analysis:

From the preceding case study, lines current THDi% and buses voltage THDv% values need to be reduced in order to meet with the power quality assigned levels by the electrical power systems regulations. Therefore, in this new case study the use of the suggested advanced broadband filter presented in chapter 5 is considered (Fig. 5.1b). This type of passive filter utilizes the 6%Ldc DC-link inductor and is encountered to basically the same rectifier current harmonic contents (shown in Table 6.4) which are applied in the harmonic model shown in Fig. 6.3b. This advanced filter should have the capability to absorb most of the undesired current harmonic components while allowing the whole fundamental component to pass through the line. This will lead to a very low line current THDi% values and thus reduce the buses voltage THDv% results below its limits compared to the previous case study.

The advanced broadband filter (ABF) for both 500kW power rating ASD systems connected to the network is designed (Li = 0.142 mH, Lf = 0.066 mH and Cf = 5695 µF star connection). Figures 6.20 and 6.21 show the lines current THDi% and the lines total power factor simulation results values. All network lines current are smooth and clean having a very low THDi% values (< 6%) at full-load operating condition. This is a superior advantage of the new broadband structure that will help

in meeting the power quality requirements in such applications. Additionally, the power factor values in many lines have achieved high values (> 0.95 lagging and leading) and with unity power factor values in some other lines. Conversely, some other lines are affected by the installed power factor correction capacitors and have lower line power factor values than the permitted operating margins.

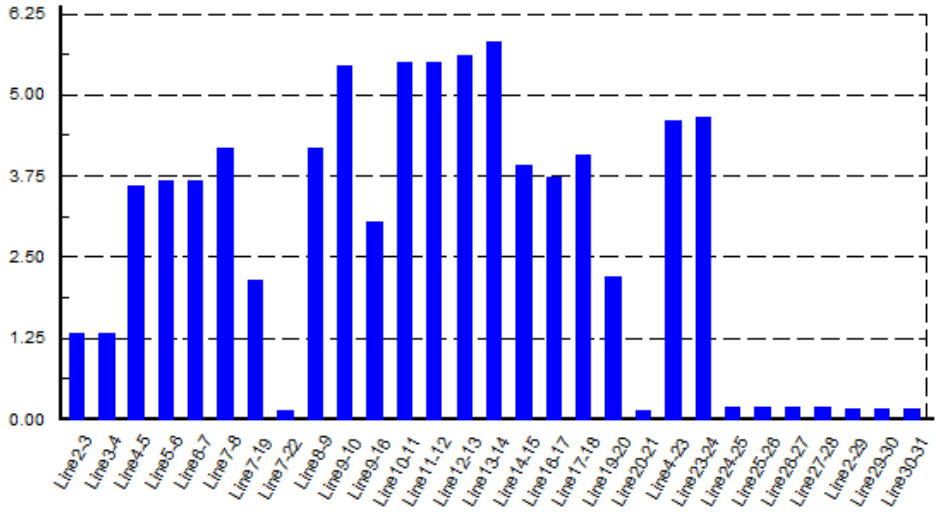

Fig. 6.20 Line current THDi% values for a 70% total nonlinear load (ASD) connected at buses 15 and 18 utilizing ABF harmonic filter.

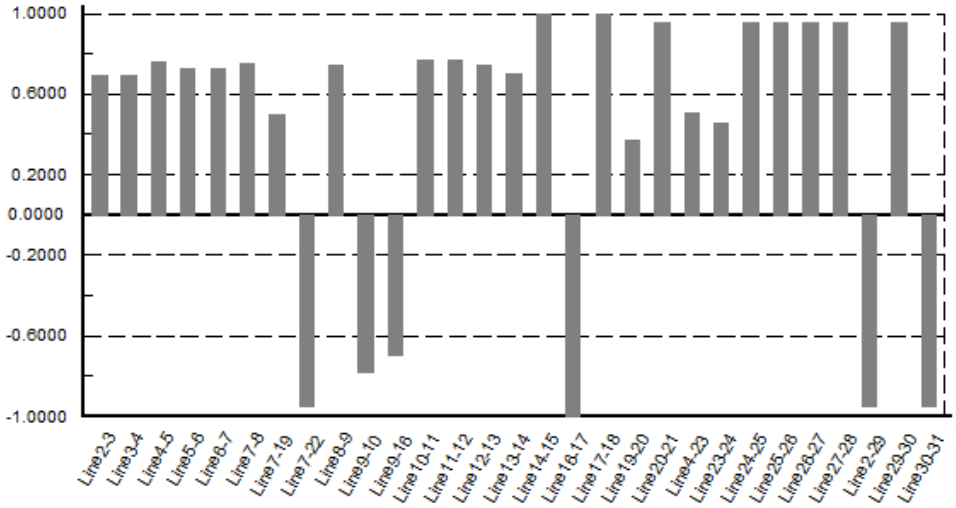

Fig. 6.21 Line power factor values for a 70% total nonlinear load (ASD) connected at buses 15 and 18 utilizing ABF harmonic filter.

Moreover the employment of the ABF in the network gives the opportunity to minimize the voltage harmonic distortion THDv% at all the network buses. The ideal case of the very low THDv% values (< 0.76%) at all buses of the 30-bus network is

shown in Fig. 6.22. These low voltage distortion levels at the load buses will essentially eliminate any possibility of any unwanted interaction with the connected loads. Furthermore, as shown in Fig. 6.23, nearly half of buses have an acceptable voltage rms values range (< 1.05 p.u.). On the other hand, the other buses have voltage rms values in per units that just violate the standard in different ratios with a maximum value of 1.055 p.u. (buses 2, 29, 30 and 31). For a restrict implementation of the voltage regulations in the power systems the design and installation of the boosting standalone capacitors may need to reconsidered.

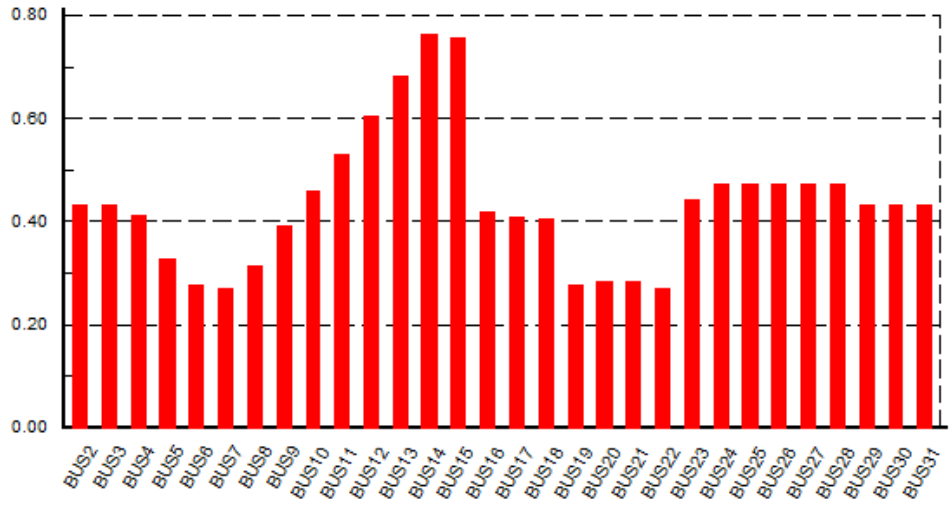

Fig. 6.22 Bus voltage THDv% values for a 70% total nonlinear load (ASD) connected at buses 15 and 18 utilizing ABF harmonic filter.

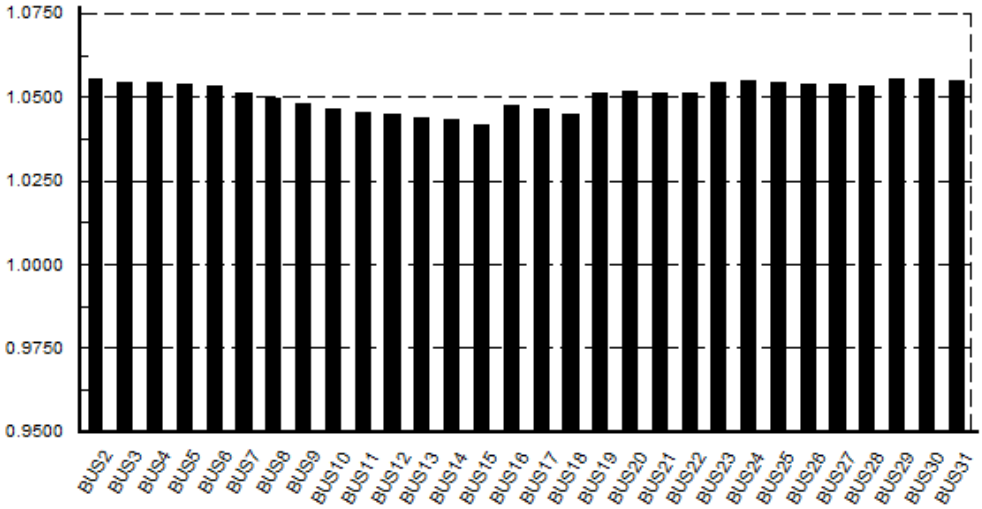

Fig. 6.23 Bus voltage rms values (p.u.) for a 70% total nonlinear load (ASD) connected at buses 15 and 18 utilizing ABF harmonic filter.

In summary, for this high penetration level (70%) of the nonlinear loads in the 30-bus distribution network, all different case studies results (minimum and maximum values) are presented in Table 6.4. It is obvious that the network might not be able to operate without using any filtering techniques as all power quality limitations are severely violated.

As presented in the table below, the several filter topologies used were capable of practically keeping the bus voltage rms values below or at the permitted margins (1.05 p.u.). Meanwhile, only the proposed IBF and ABF structures were able to maintain the voltage THDv% at the buses. Similarly, the line current THDi% values are kept below 6% through all the lines by using the same broadband passive filters IBF and ABF only. Exceptionally, the line power factor values have not improved and reached nearly unity in all lines by using these broadband filters structures. This is due to the existence of the power factor shunt capacitors that are already installed in this typical IEEE 30-bus distribution network. Therefore, this operating situation results may conclude to a strong recommendation for the distribution networks to re-examine the need and/or the design of such reactive power compensation capacitors when such broadband filters are installed.

Table 6.5 Summary of simulation results for IEEE 30-bus system with 70% nonlinear load penetration level before and after the installation of various harmonic passive filters

	No-Filter		4%Lac +2%Ldc		IBF		6%Ldc		ABF	
	Min	Max	Min	Max	Min	Max	Min	Max	Min	Max
Vrms (pu)	1.045 @bus 18	1.078 @bus 24	1.028 @bus 15	1.048 @bus 2,29,30	1.04 @bus 15	1.055 @bus 2	1.03 @bus 15	1.048 @bus 2,29,3	1.04 @bus 15	1.055 @bus 2,29,30
THDv	25.9% @bus 6&22	40% @bus 14	5.02% @bus 31,2,3	5.73% @bus 14	0.30% @bus 22	0.67% @bus 14	5.21% @bus 29	6.11% @bus 14	0.27% @bus 22	0.76% @bus 14
THDi	13.8% @line 30-31	330% @line 13-14	2.67% @line 30-31	29.9% @line 17-18	0.159% @line 7-22	4.87% @line 13-14	2.7% @line 30-31	33% @line 17-18	0.1% @line 7-22	5.8% @line 13-14
Power factor	0.18 @line 23-24	0.928 @line 7-22	0.36 @line 19-20	0.949 @line 7-22	0.37 @line 19-20	0.997 @line 16-17	0.36 @line 19-20	0.95 @line 7-22	0.375 @line 19-20	0.997 @line 16-17

For a better illustration of the data summary shown in Table 6.5, the maximum values of the different cases for the power quality 4-indices considered in the study are plotted in the Figures 6.24 and 6.25 (same scale parameters are joined). The lines

current THDi and buses voltage THDv% maximum achieved values are shown in Fig. 6.24. While the lines power factor and the buses voltage rms (p.u.) values are shown in Fig. 6.25.

The plotted diagrams clearly demonstrate and proof the previous mentioned conclusions. Remarkably, the performance of the single-phase 6%Ldc DC-link inductor filtering method is very similar to the use of three-phase 4%Lac AC line reactor joined with the 2%Ldc inductor. As the single-phase 6%Ldc is practically less in size and cost than the other used combination, it might be in favour of the designing engineers to be utilized.

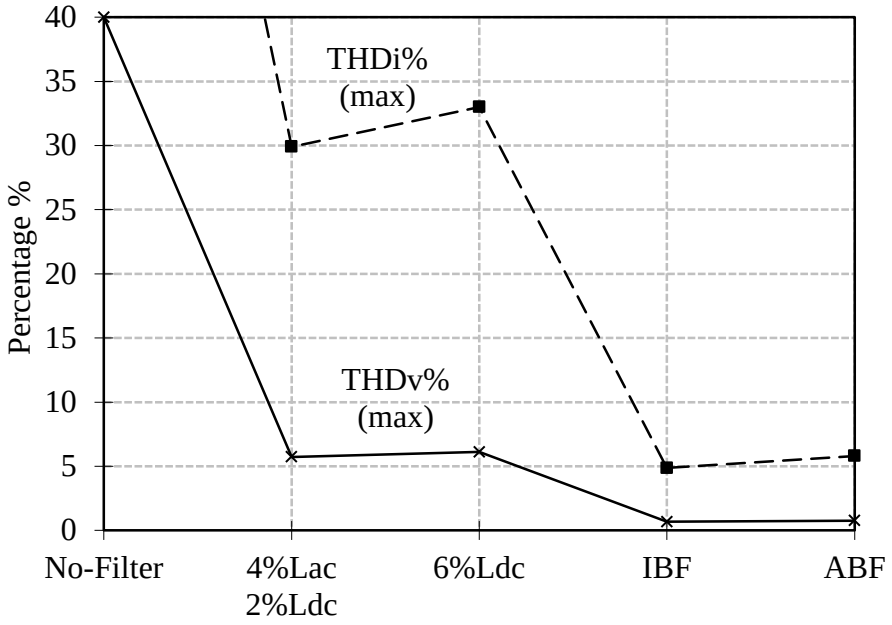

Fig. 6.24 IEEE-30 bus network line current and bus voltage maximum THD values utilizing various harmonic filtering methods for a 70% nonlinear load connected at buses 15 and 18.

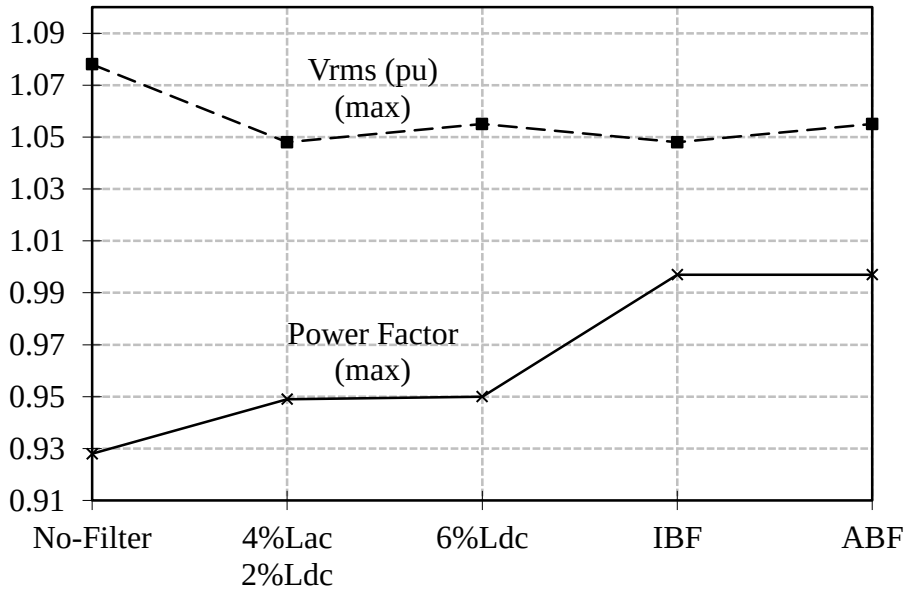

Fig. 6.25 IEEE-30 bus network line power factor and bus rms voltage (p.u.) maximum values utilizing various harmonic filtering methods for a 70% nonlinear load connected at buses 15 and 18.

6.3.2 IEEE 30-bus Distribution Network with 40% Nonlinear Load (ASD) Case Study

The second nonlinear load penetration case study involves connecting a 55kW rated ASD system to bus 18 and a 500kW rated ASD system to bus 15. This will decrease the total nonlinear load (555kW) in the network to about 40% level of the total connected load (1413.7kW). The less polluted 30-bus network will be assessed and performance analysed by the similar process presented in section 6.3.1. The simulation results of the network power quality indices without utilizing any filtering method and with the other four harmonic mitigation techniques are presented.

a) Load type 1 simulation results and analysis:

The filtering free 30-bus network simulation results connecting the three-phase 6-pulse bridge rectifier to buses 15 and 18 are clarified. As estimated, the lines current THDi% values, shown in Fig. 6.26, have lower values than resultant in Fig. 6.4 for 70% penetration case. However, the average line current THDi% value existing in the lines is far above the limits (>50%). Fig. 6.27 shows the lines power factor values

with negligible improvement in most of lines other than lines 16-17 and 17-18 compared to the values for the 70% penetration level, shown in Fig. 6.5.

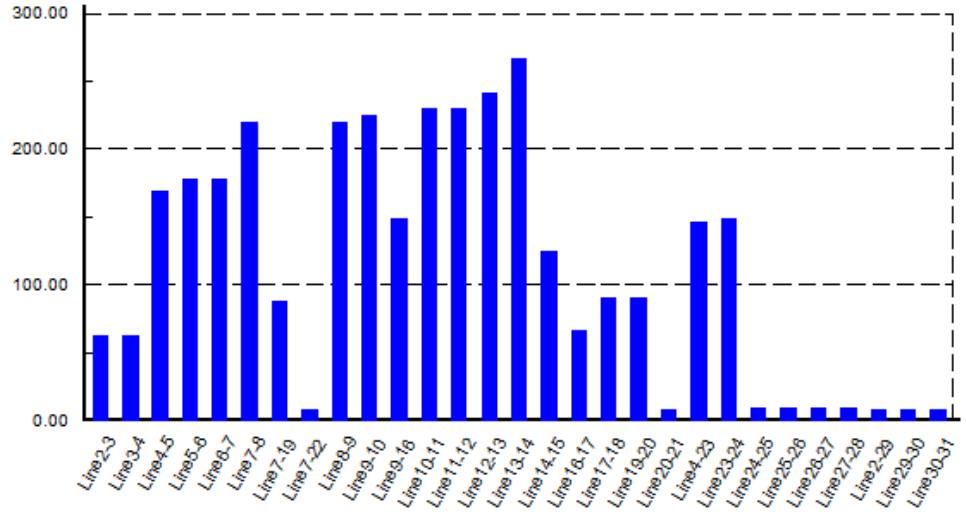

Fig. 6.26 Line current THDi% values for a 40% total nonlinear load (ASD) connected at buses 15 and 18 with no harmonic filter connected.

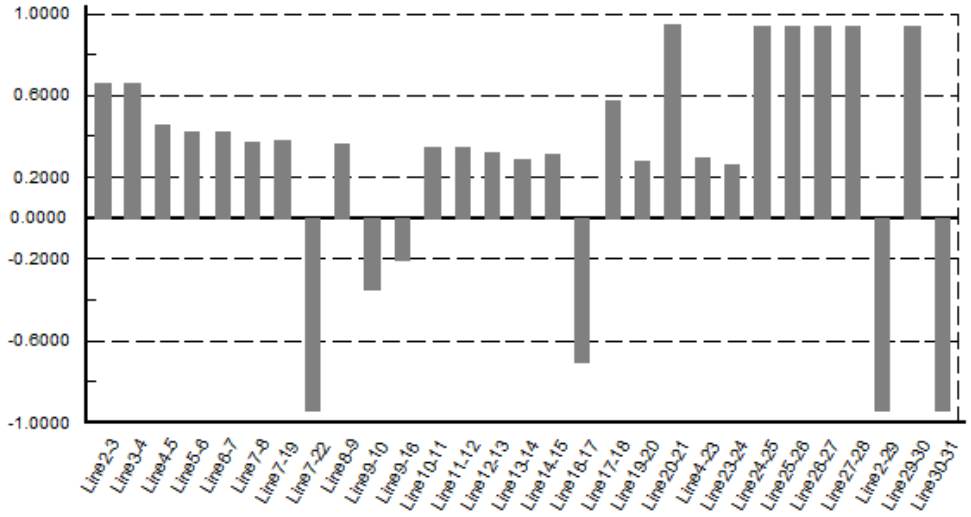

Fig. 6.27 Line power factor values for a 40% total nonlinear load (ASD) connected at buses 15 and 18 with no harmonic filter connected.

The voltage THDv% values at all buses in the network are shown in Fig. 6.28. Although the supply voltage distortion relatively reduced, buses still have a high voltage THDv% values with a range of 14% to 24%. Likewise section 6.3.1 (a) results, these range of values are not acceptable as the IEEE519 harmonic standard puts a limit of 5% voltage THDv% for low voltage bus systems (<69kV). Lastly, the

voltage rms (p.u.) values at all buses simulation results are shown in Fig. 6.29. The voltage rms values have a range of 1.046 to 1.058 in per unit system.

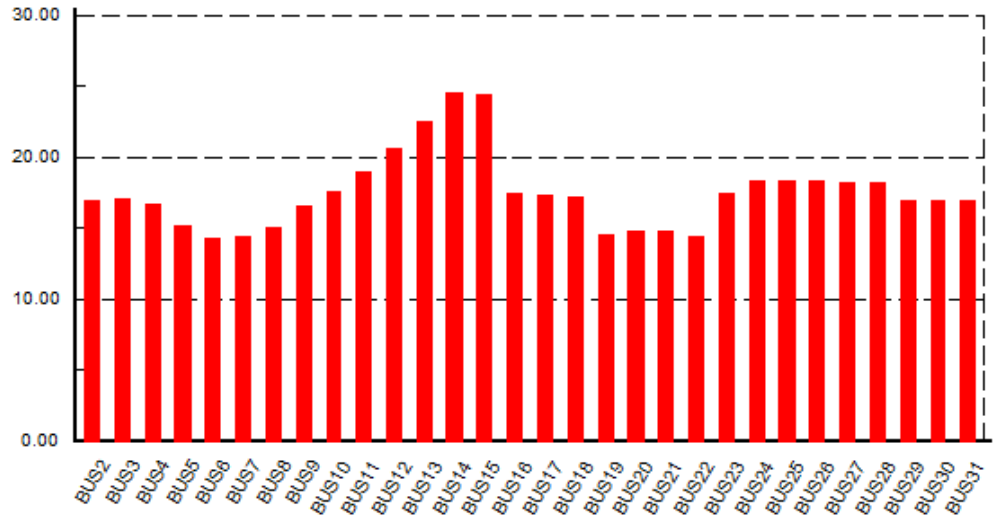

Fig. 6.28 Bus voltage THDv% values for a 40% total nonlinear load (ASD) connected at buses 15 and 18 with no harmonic filter connected.

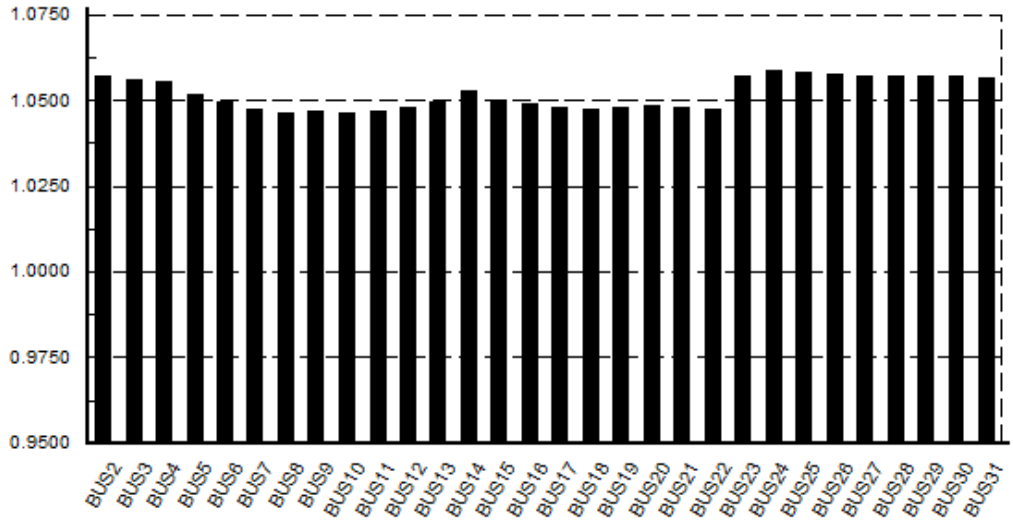

Fig. 6.29 Bus voltage rms values (p.u.) for a 40% total nonlinear load (ASD) connected at buses 15 and 18 with no harmonic filter connected.

b) Load type 2 simulation results and analysis:

The following explained 30-bus network simulation results includes the usage of 4%Lac+2%Ldc filters with the ASD system connected to the buses 15 and 18 for the same, respectively, 500kW and 55kW power ratings. Fig. 6.30 shows the simulation lines current waveforms results. Compared to the previous case simulation results without any filtering method, shown in Fig. 6.26, the THDi% values improved

intensely (decreased by a factor of 10) in most of the network lines. Meanwhile they also improved with respect to w.r.t the same filtering method connected with the higher penetration level (70%) earlier presented (Fig. 6.8). Nevertheless, line current THDi% values are generally recommended to be <10% which is not possible by utilizing only the given basic filtering combination (4%Lac+2%Ldc). Similar improvement in the lines power factor is achieved after installing this filtering type, as shown in Fig. 6.31. However, poor lagging and leading total power factor (< 0.9) exist. This will lead to the necessity of including better harmonic mitigation method in order to achieve line current THDi% and power factor limitations.

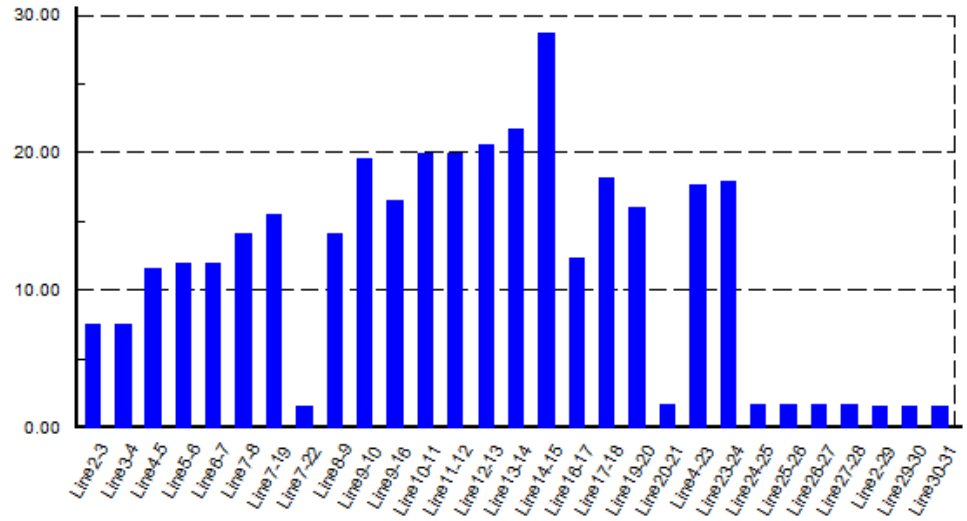

Fig. 6.30 Line current THDi% values for a 40% total nonlinear load (ASD) connected at buses 15 and 18 utilizing 4%Lac & 2%Ldc filters.

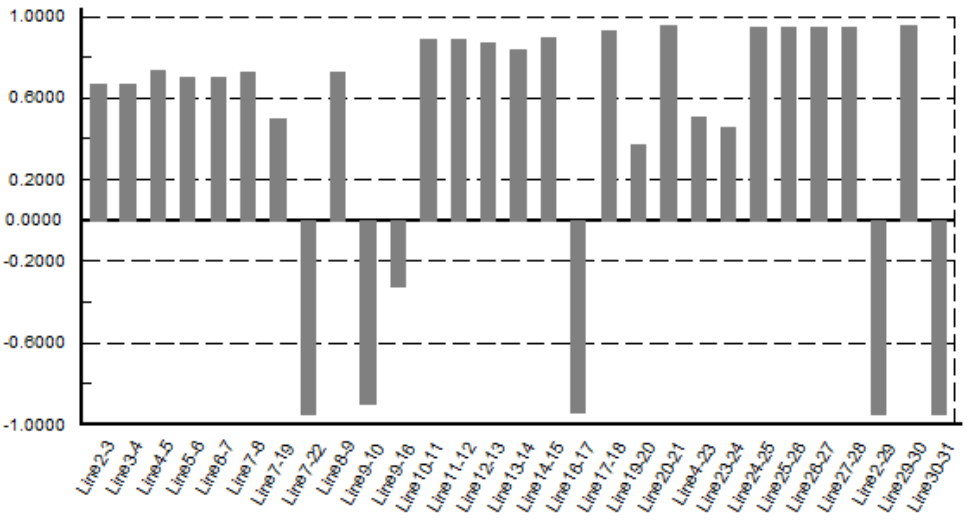

Fig. 6.31 Line power factor values for a 40% total nonlinear load (ASD) connected at buses 15 and 18 utilizing 4%Lac & 2%Ldc filters.

A full success has been achieved by this simple and conventional passive filter combination in decreasing the bus voltage THDv% and rms (p.u.) values to the permitted standards. The maximum THDv% in all buses is 3.15% which is well beyond the 5% limit, shown in Fig. 6.32. Meanwhile the buses voltage rms values in per unit have a maximum value of 1.05%, shown in Fig. 6.33. However, in order to reduce the lines current THDi% values to an acceptable margin the employment of IBF is introduced in the next section.

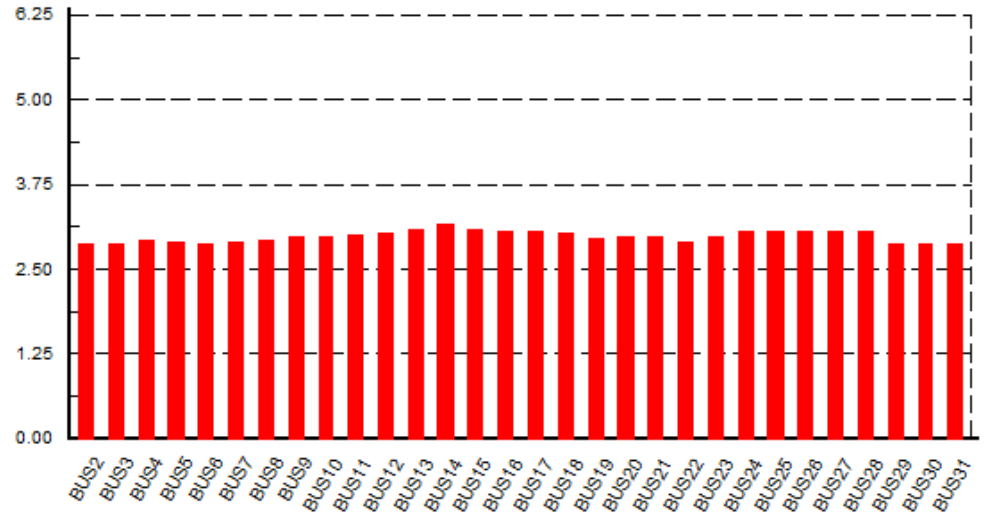

Fig. 6.32 Bus voltage THDv% values for a 40% total nonlinear load (ASD) connected at buses 15 and 18 utilizing 4%Lac & 2%Ldc filters.

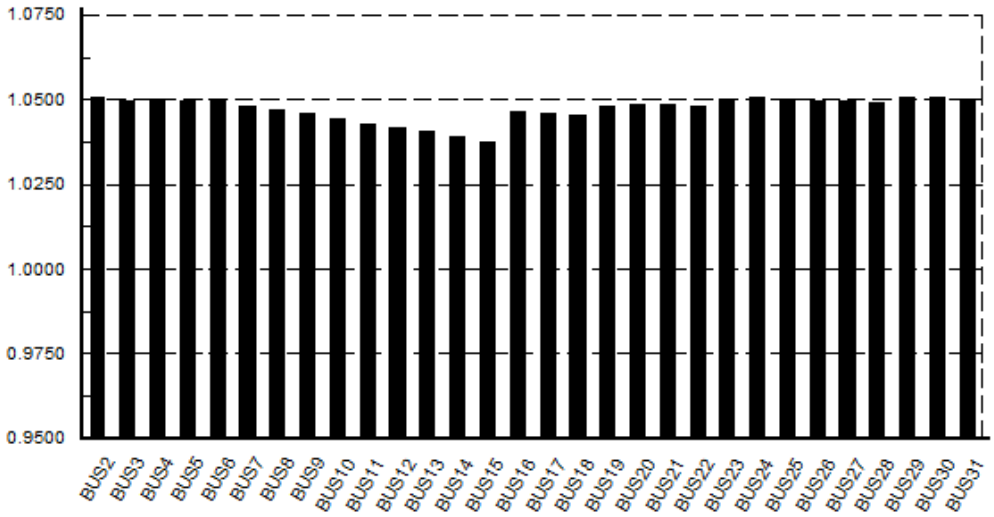

Fig. 6.33 Bus voltage rms values (p.u.) for a 40% total nonlinear load (ASD) connected at buses 15 and 18 utilizing 4%Lac & 2%Ldc filters.

c) Load type 2 utilizing IBF simulation results and analysis:

The developed improved broadband filter (IBF) is installed in the network and connected to the nonlinear load side of buses 15 and 18. The first IBF filter is designed for the 500kW power rating ASD system connected to bus 15 (Li = 0.121 mH, Lf = 0.0658 mH and Cf = 5666 µF star connection). The second IBF filter is designed for the 55kW power rating ASD system (Table 4.1) connected to bus 18 (Li = 0.99 mH, Lf = 0.75 mH and Cf = 540 µF star connection).

Figures 6.34 and 6.35 show the lines current THDi% and total power factor simulation values. A huge reduction in the line current THDi% values (< 4%) has been achieved. Furthermore, lines near to the filter connection point (lines 14-15, 16-17, 17-18) have achieved unity power factor values. Other lines (e.g. 2-3, 3-4 and 4-5) have been affected by the new filter capacitance added to the already installed shunt capacitors and their power factor values slightly decreased.

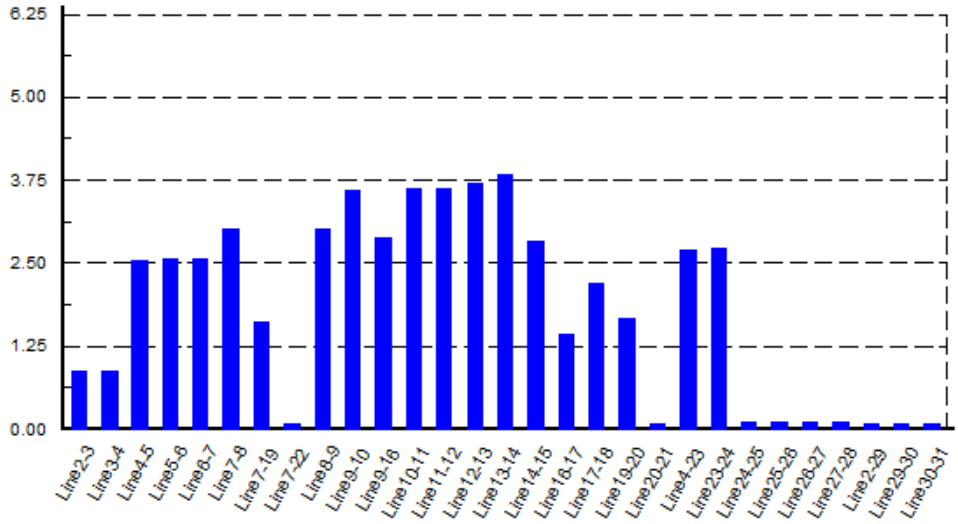

Fig. 6.34 Line current THDi% values for a 40% total nonlinear load (ASD) connected at buses 15 and 18 utilizing IBF harmonic filter.

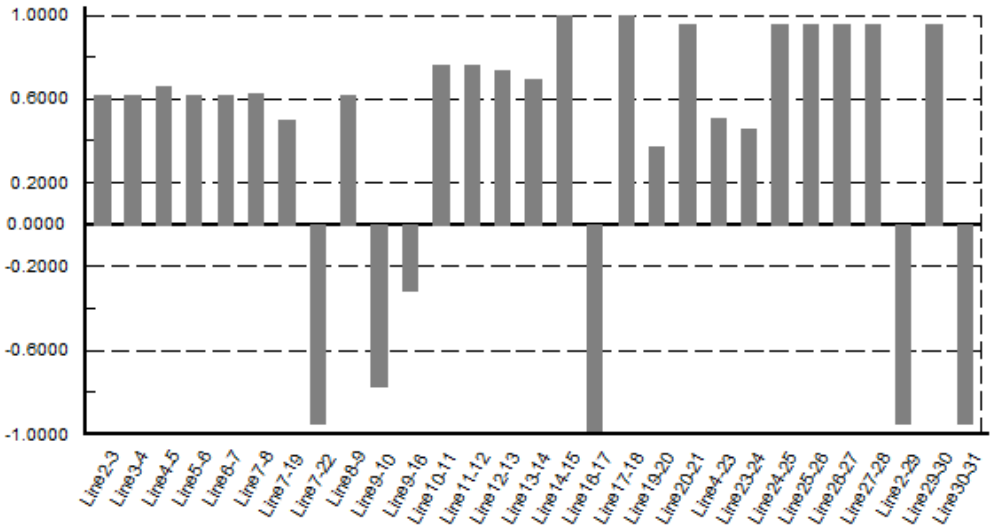

Fig. 6.35 Line power factor values for a 40% total nonlinear load (ASD) connected at buses 15 and 18 utilizing IBF harmonic filter.

Alternatively, the voltage THDv% at all buses has attained a very low range of voltage distortion values (0.15% – 0.45%) where the voltage rms (p.u.) values has been marginally boosted by the IBF capacitor component with its relatively high capacitance.

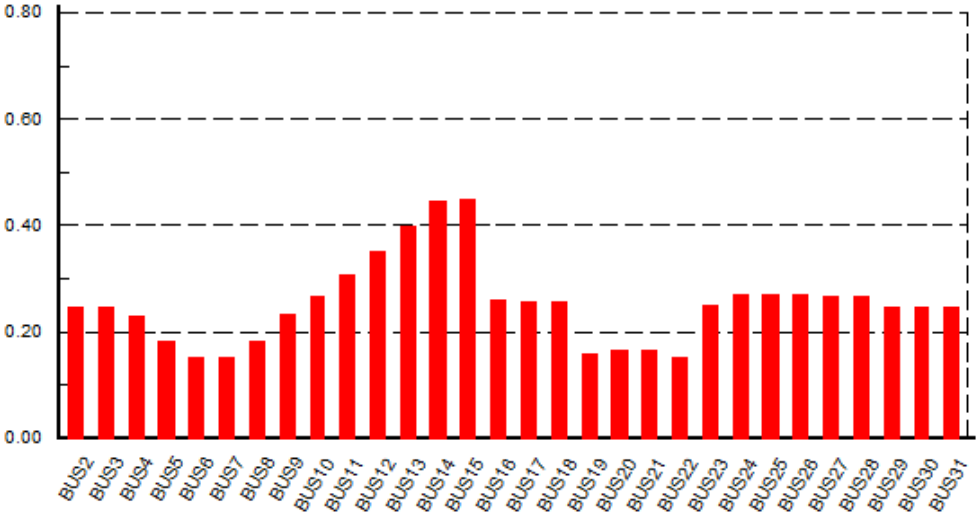

Fig. 6.36 Bus voltage THDv% values for a 40% total nonlinear load (ASD) connected at buses 15 and 18 utilizing IBF harmonic filter.

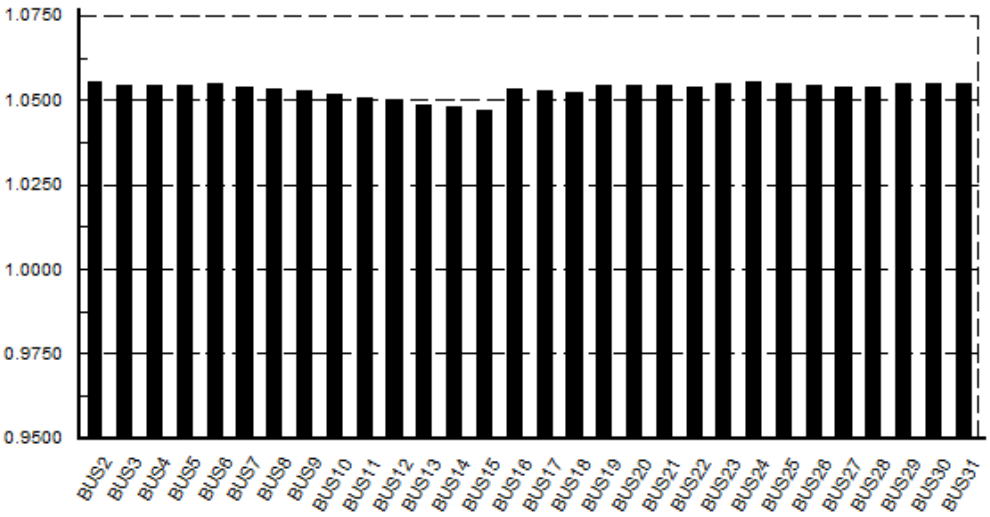

Fig. 6.37 Bus voltage rms values (p.u.) for a 40% total nonlinear load (ASD) connected at buses 15 and 18 utilizing IBF harmonic filter.

d) Load type 3 simulation results and analysis:

In this section, the load type 3 is connected to buses 15 and 18 for the same chosen power rating. This involves using only the 6%Ldc inductor implementing its obtained current harmonic distortion spectrum. With less polluted network it is expected that this simple filtering method will improve the 30-bus distribution network power quality parameters.

The lines current THDi% and total power factor simulation values are shown in Fig. 6.38 and Fig. 6.39, respectively. The utilized 6%Ldc filter type has been effective in mitigating current harmonic components when comparing its achieved line THDi% values with the case presented in Fig. 6.26 (no filter case) for the same distortion level. Similarly, and with same comparing conditions, the line power factor values results are advanced from the values illustrated in Fig. 6.27

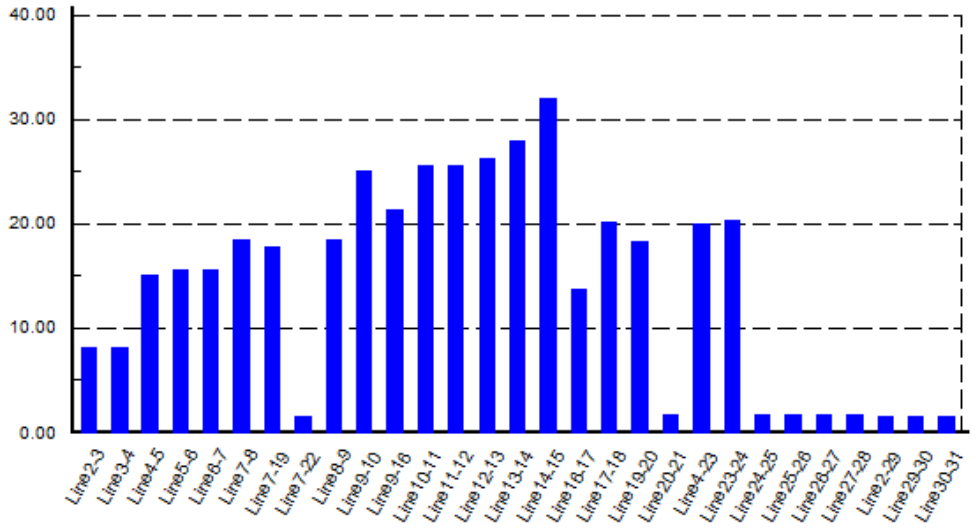

Fig. 6.38 Line current THDi% values for a 40% total nonlinear load (ASD) connected at buses 15 and 18 utilizing 6%Ldc filters.

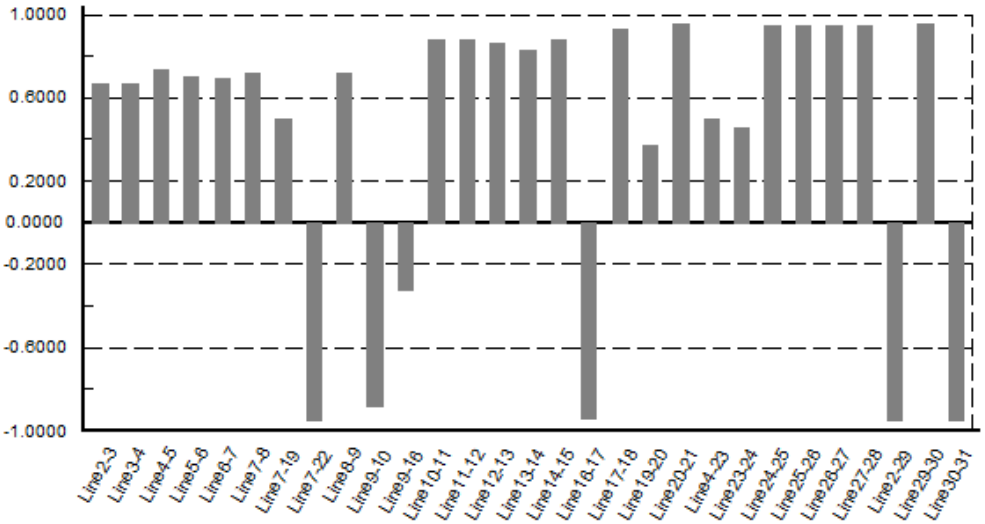

Fig. 6.39 Line power factor values for a 40% total nonlinear load (ASD) connected at buses 15 and 18 utilizing 6%Ldc filters.

The voltage THDv% values at all buses in the network have a maximum value of 3.45%, as shown in Fig. 6.40. Meanwhile the voltage rms (p.u.) values have a maximum value of 1.05%, as shown in Fig. 6.41. This situation will positively enhance the operating conditions in the network regarding the buses voltage harmonic interaction with connected loads and over voltage problems.

To conclude, mainly the line current THDi% values needed to be improved and, therefore, the utilization of an extra filtering type is necessary.

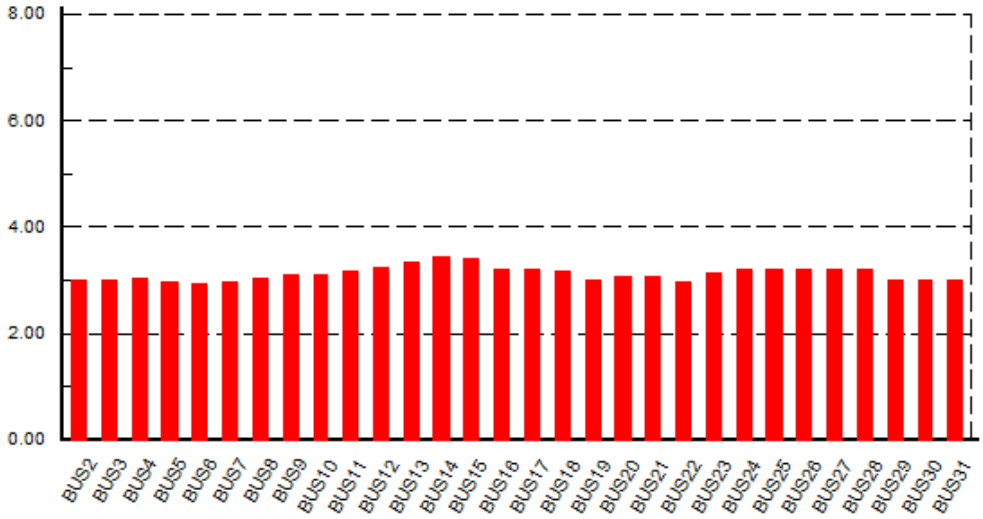

Fig. 6.40 Bus voltage THDv% values for a 40% total nonlinear load (ASD) connected at buses 15 and 18 utilizing 6%Ldc filters.

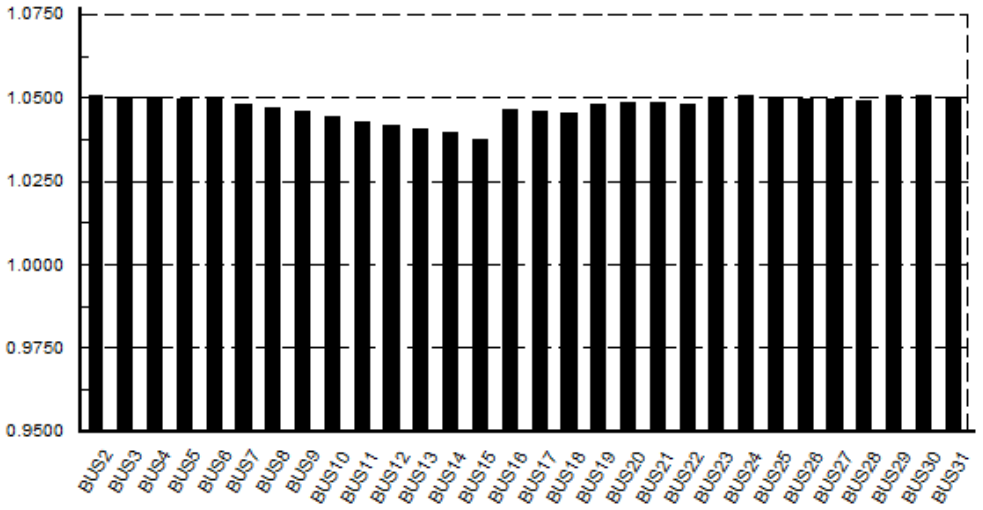

Fig. 6.41 Bus voltage rms values (p.u.) for a 40% total nonlinear load (ASD) connected at buses 15 and 18 utilizing 6%Ldc filters.

e) Load type 3 utilizing ABF simulation results and analysis:

In this final stage, the ABF is added to both nonlinear loads and network operating performance evaluated. The first ABF filter is designed for the 500kW power rating ASD system connected to bus 15 (Li = 0.142 mH, Lf = 0.066 mH and Cf = 5695 µF star connection). The second ABF filter is designed for the 55kW power rating ASD system (Table 5.1) connected to bus 18 (Li = 1.2 mH, Lf = 0.79 mH and Cf = 504 µF star connection).

Figures 6.42 and 6.43 show the lines current THDi% and the lines total power factor simulation results values. A set of lines current THDi% values with extremely low range of (0.07% - 4.6%) is achieved. These current's sinusoidal waveforms practically contain negligible harmonic components in their spectrum. Compared to the 70% penetration level for the similar installed ABF filter (Fig. 6.20), this lower distortion (40%) line THDi% results have lower values and consequently better current waveforms. The line power factor has a range of values between 0.31 and 0.996 (lagging and leading). Lines close to the ABF installation points achieved unity power factor while lines near to the shunt capacitors have less power factor values.

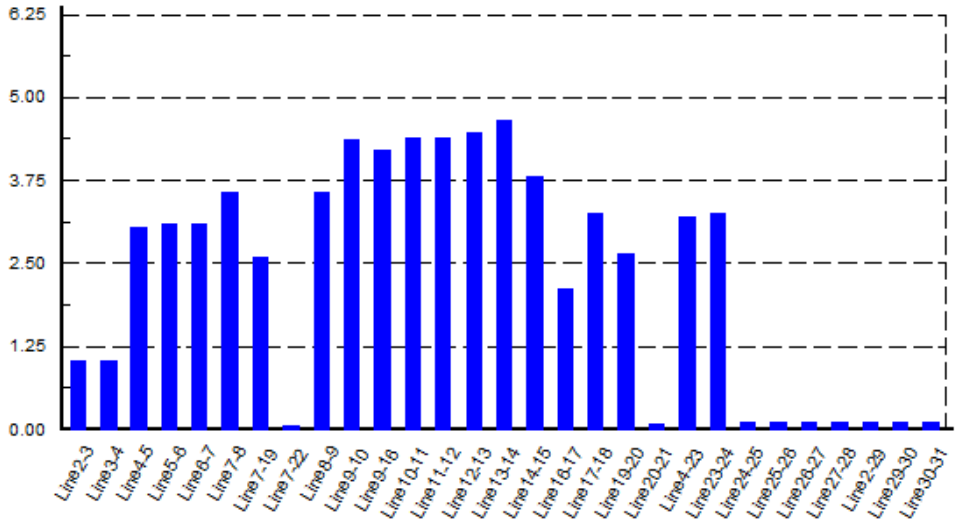

Fig. 6.42 Line current THDi% values for a 40% total nonlinear load (ASD) connected at buses 15 and 18 utilizing ABF harmonic filter.

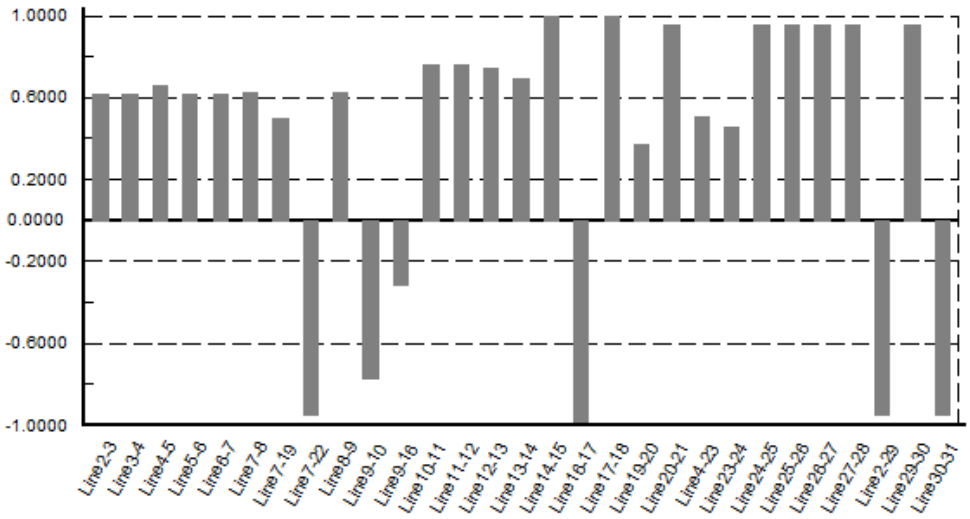

Fig. 6.43 Line power factor values for a 40% total nonlinear load (ASD) connected at buses 15 and 18 utilizing ABF harmonic filter.

Furthermore, as revealed, the ABF installation is very effective in mitigating the lines current THDi% and, therefore, the resultant THDv% at all buses are negligible (shown in Fig. 6.44). Buses voltage rms (p.u.) simulation results values at all buses are satisfactory with a maximum of 1.05%, (shown in Fig. 6.45). These results confirm the effectiveness of such type of passive filters that can be utilized in a distribution network.

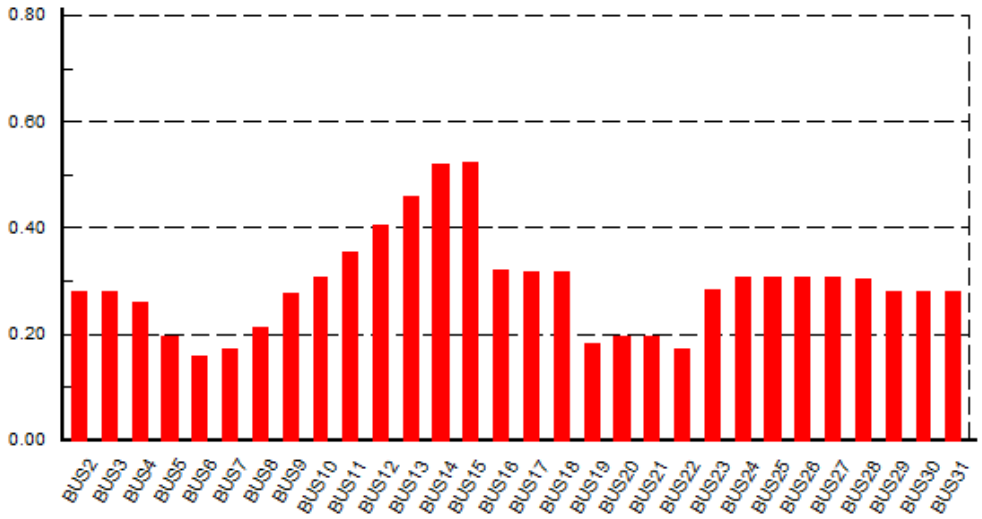

Fig. 6.44 Bus voltage THDv% values for a 40% total nonlinear load (ASD) connected at buses 15 and 18 utilizing ABF harmonic filter.

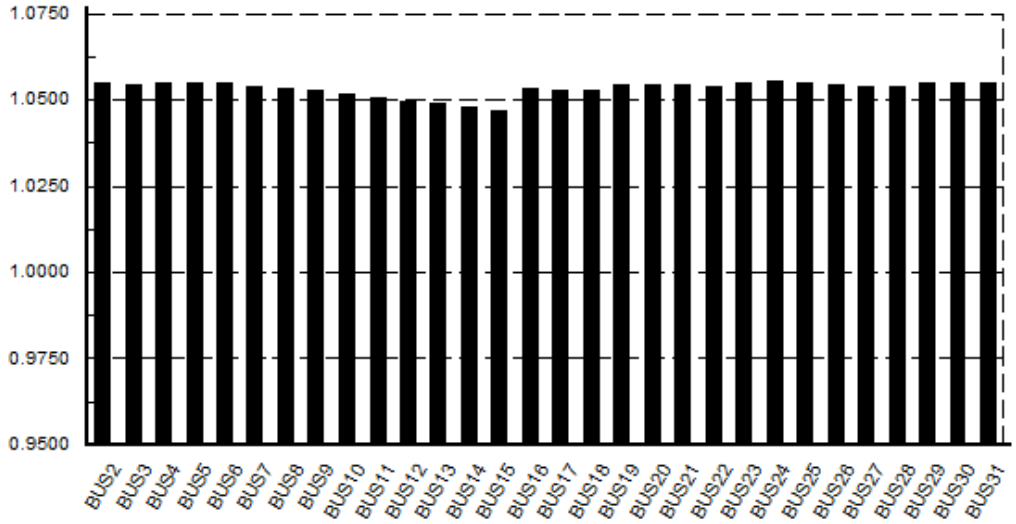

Fig. 6.45 Bus voltage rms values (p.u.) for a 40% total nonlinear load (ASD) connected at buses 15 and 18 utilizing ABF harmonic filter.

Table 6.6 summarizes the different case results and presents the minimum and maximum values for each situation. Fig. 6.46 shows the maximum achieved values only for the lines current THDi% joined with the buses voltage THDv%. Provided that the nonlinear loads penetration level decreased from 70% to 40%, it is clearly illustrated that only the IBF and ABF can reduce the THDi% to tolerable levels. However, all filtering structures were able to decrease the buses voltage THDv% below the mentioned value in the IEEE-519 voltage standard (max. 5%). Fig. 6.47 shows the maximum values of the buses voltage rms (p.u.) joined with the line power factor. All types of proposed filters can keep the buses voltage rms normalized values within the limits (max. 1.05%) while only IBF and ABF have the ability to achieve unity power factor conditions in the adjacent transmission lines.

Table 6.6 Summary of simulation results for IEEE 30-bus system with 40% nonlinear load penetration level before and after the installation of various harmonic passive filters

	No-Filter		4%Lac +2%Ldc		IBF		6%Ldc		ABF	
	Min	Max	Min	Max	Min	Max	Min	Max	Min	Max
Vrms (pu)	1.046 @bus 8,10	1.058 @bus 24	1.037 @bus 15	1.05 @bus 2,29,30	1.046 @ bus 15	1.05 @ most	1.037 @bus 15	1.05 @bus 2,24,29	1.046 @bus 15	1.055 @bus 2, 24
THDv	14.2 % @bus 6	24% @bus 14	2.87% @bus 29,30 ,31,2	3.15% @bus 14	0.15 % @bus 6	0.45 % @bus 15	2.9% @bus 6	3.45% @bus 14	0.15% @bus 6	0.52% @bus 15
THDi	7.5% @line 7-22	265% @line 13-14	1.5% @line 29-30, 30-31	28.6% @line 14-15	0.074 % @line 7-22	3.82 % @line 13-14	1.5% @line 30-31	32% @line 14-15	0.07% @line 7-22	4.6% @line 13-14
Power factor	0.25 @line 9-16	0.947 @line 7-22	0.326 @line 9-16	0.949 @line 7-22,	-0.31 @line 9-16	0.996 @line 17-18	0.32 @line 9-16	0.95 @line 7-22	-0.31 @line 9-16	0.996 @line 14-15

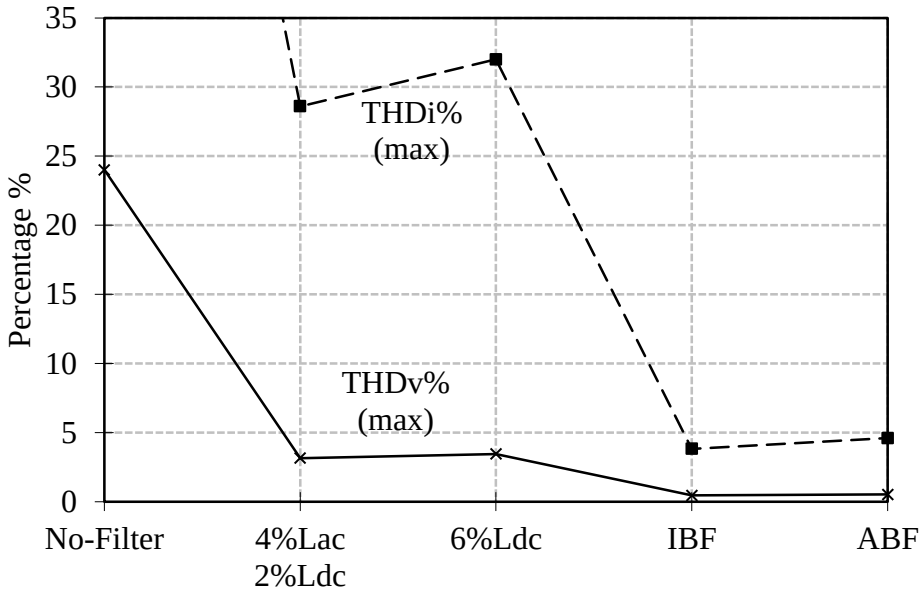

Fig. 6.46 IEEE-30 bus network line current and bus voltage maximum THD values utilizing various harmonic filtering methods for a 40% nonlinear load connected at buses 15 and 18.

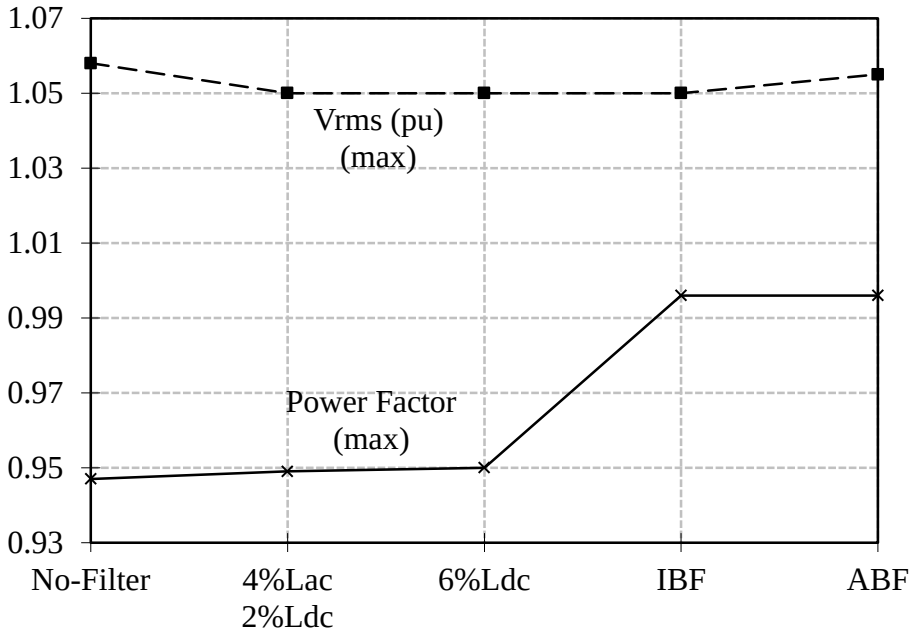

Fig. 6.47 IEEE-30 bus network line power factor and bus rms voltage (p.u.) maximum values utilizing various harmonic filtering methods for a 40% nonlinear load connected at buses 15 and 18.

6.3.3 IEEE 30-bus Distribution Network with 8% Nonlinear Load (ASD) Case Study

The final load penetration case study includes connecting two *5.5kW rated ASD system to the buses 15 and 18. This presents the minimum nonlinear load concentration in the network with approximate 8% (110kW) of the total network load (1413.7kW). This might reduce the overall impact of the current harmonic distortion in the network and enhance the effectiveness of the simple passive filters proposed in this study (AC & DC reactors). Similar to the previous sections 6.3.1 and 6.3.2, the proposed four different filtering topologies will be designed, implemented and assessed.

a) Load type 1 simulation results and analysis:

First, the basic 30-bus network without any filter connected simulation results are presented and analysed. These fundamental results are considered as a reference to compare with other filtering structure results cases. The lines current THDi% values of the least polluted network condition are shown in Fig. 6.48. The figure has a similar scale range use in Fig. 6.26 (showing THDi% for the 40% distortion) for comparison purpose. As shown in Fig. 6.48, most of the line current harmonic THDi% values have dropped by a factor of 3.0 with a range of (1.28% - 88%). Fig. 6.49 shows the lines power factor values with negligible improvement in most of lines with overall unsatisfactory condition.

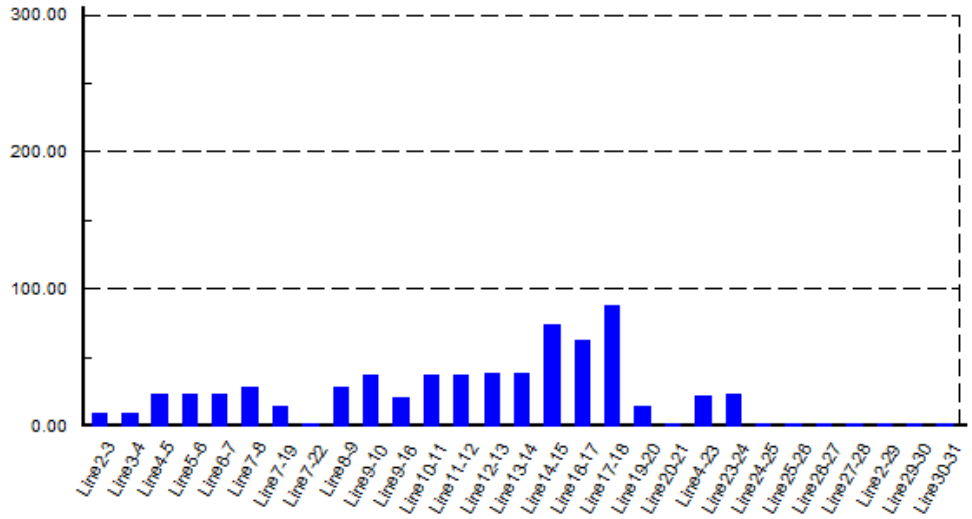

Fig. 6.48 Line current THDi% values for an 8% total nonlinear load (ASD) connected at buses 15 and 18 with no harmonic filter connected.

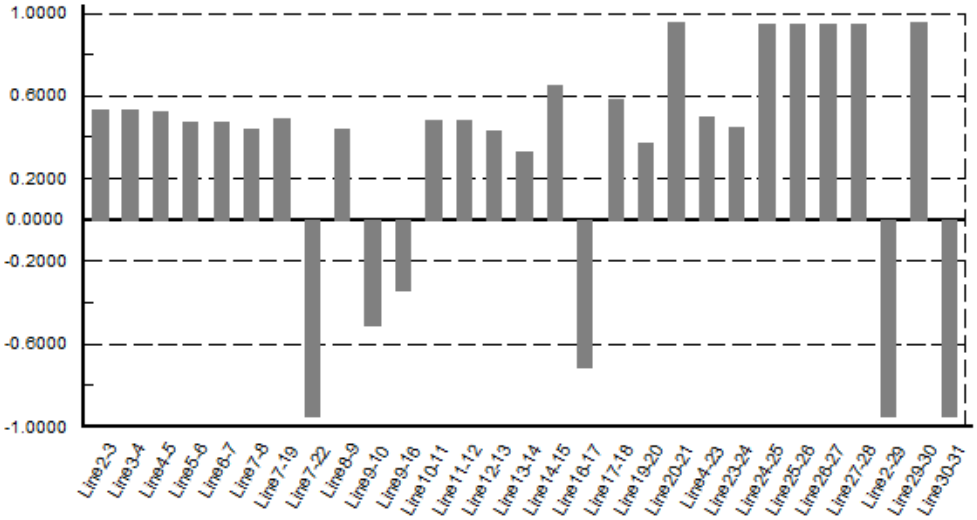

Fig. 6.49 Line power factor values for an 8% total nonlinear load (ASD) connected at buses 15 and 18 with no harmonic filter connected.

The voltage THDv% values at all buses in the network are shown in Fig. 6.50. The values are presented in the scale range of those presented in Fig. 6.28 (THDv% values of 70% penetration) for the same evaluation purposes. The reduction in the THDv% values is enormous. A voltage harmonic distortion range of (2.41 – 3.67) is achieved at all busses. This is an acceptable operation range that can comply with the considered power systems standards. Finally, the voltage rms (p.u.) values at all buses simulation results are shown in Fig. 6.50. The voltage rms values have a range of 1.052 to 1.055 in per unit system. The reduction in the nonlinear load

concentration level did not reduce the voltage rms values at the network buses in the existence of the boosting shunt capacitors.

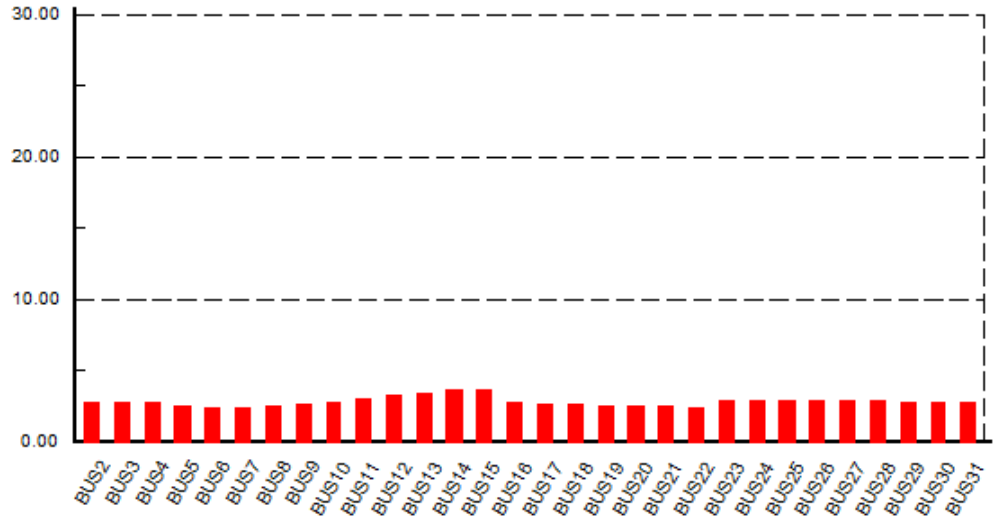

Fig. 6.50 Bus voltage THDv% values for an 8% total nonlinear load (ASD) connected at buses 15 and 18 with no harmonic filter connected.

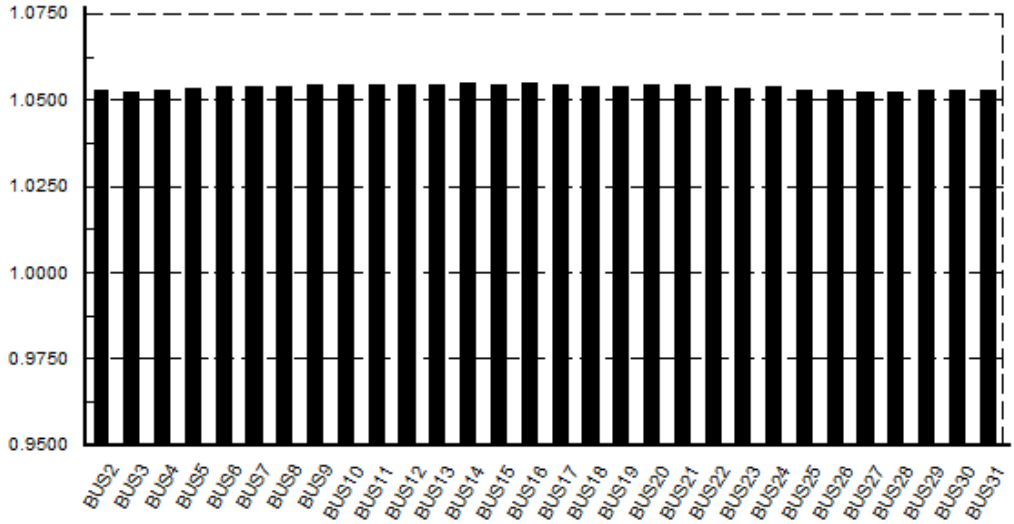

Fig. 6.51 Bus voltage rms values (p.u.) for an 8% total nonlinear load (ASD) connected at buses 15 and 18 with no harmonic filter connected.

In conclusion, mainly the line current THDi% values at most of the network transmission sections are beyond the permitted range. This implies the requirement of utilizing a harmonic mitigation technique to comply with the related standards.

b) Load type 2 simulation results and analysis:

The usage of 4%Lac+2%Ldc filters with the ASD system connected to the buses 15 and 18 is under focus in this section. Fig. 6.52 shows the line current THDi% in the network. Apart from the lines close to the distortion sources (lines 14-15, 16-17 and 17-18), the THDi% values in the rest of the network transmission lines are acceptable (THDi < 5%). The distorted lines have a maximum THDi of 17.0% in line 17-18. This maximum value can comply with the IEEE 519 harmonic current limits (Table 1.2) if the short circuit ratio (I_{SC}/I_L) at feeder is >1000. The lines power factor values are shown in Fig. 6.53. Compared to the previous case results shown in Fig. 6.49, extra lines have achieved high values (0.95). However, compared the 40% penetration level results shown in Fig. 6.31, considerable number of lines has experienced a lower power factor values.

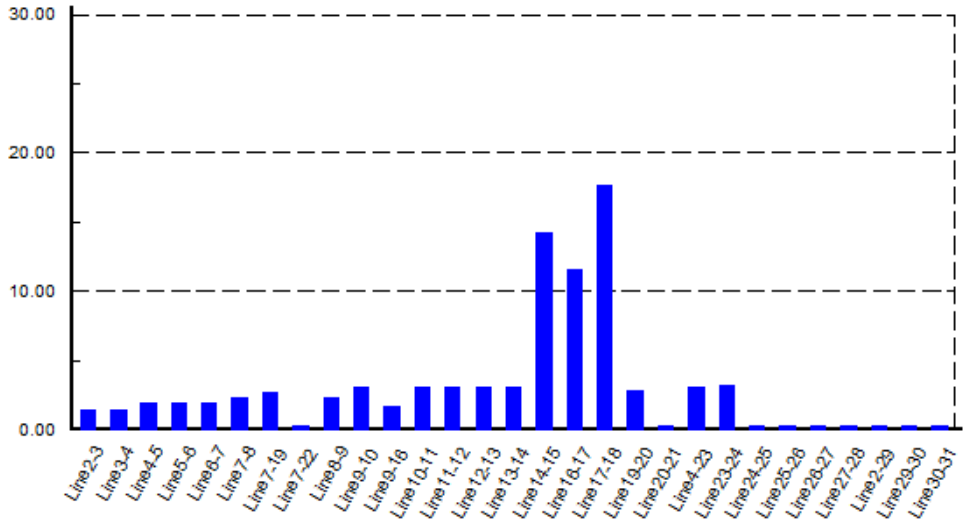

Fig. 6.52 Line current THDi% values for an 8% total nonlinear load (ASD) connected at buses 15 and 18 utilizing 4%Lac & 2%Ldc filters.

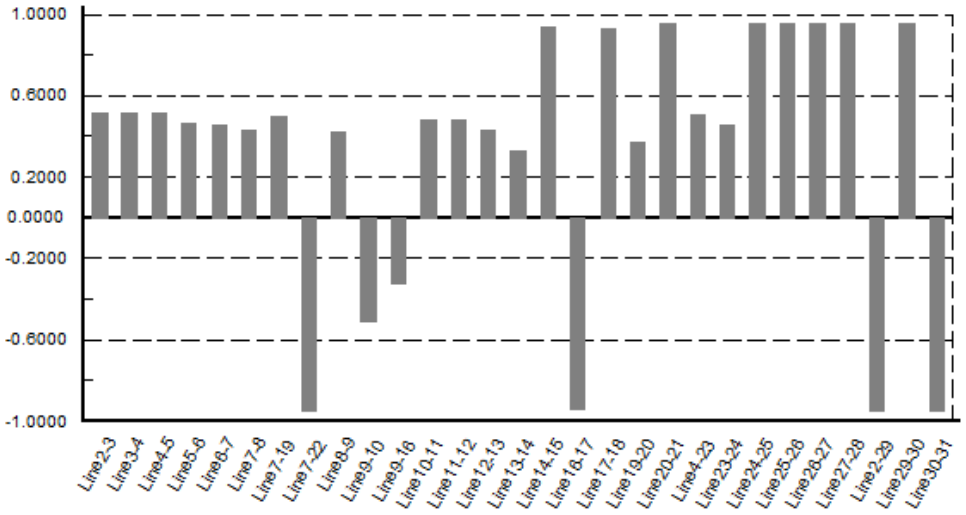

Fig. 6.53 Line power factor values for an 8% total nonlinear load (ASD) connected at buses 15 and 18 utilizing 4%Lac & 2%Ldc filters.

The buses voltage THDv% values continue to decrease and achieved a very low range of values with a maximum THDv of 0.58%, shown in Fig. 6.54. On the other hand, the buses voltage rms values in per unit have negligibly increased. The values range from (1.053 – 1.056) p.u.

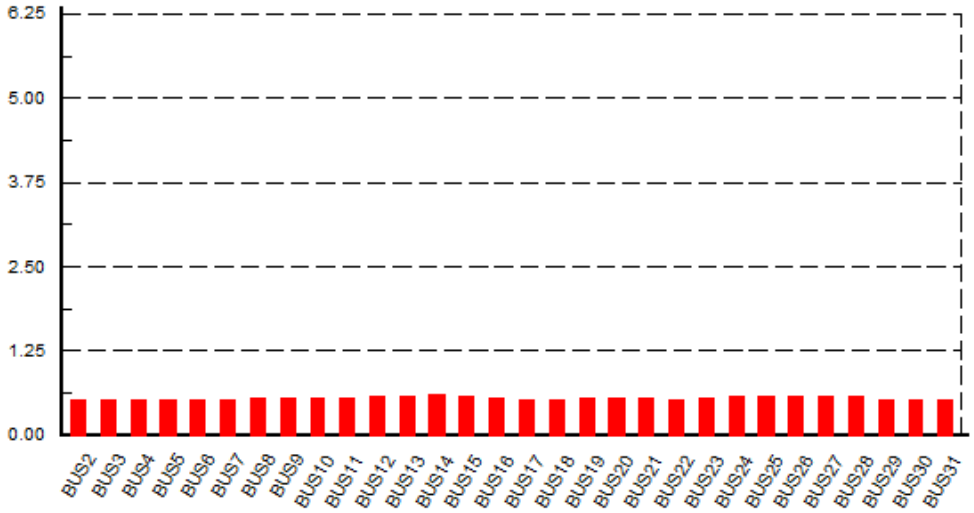

Fig. 6.54 Bus voltage THDv% values for an 8% total nonlinear load (ASD) connected at buses 15 and 18 utilizing 4%Lac & 2%Ldc filters.

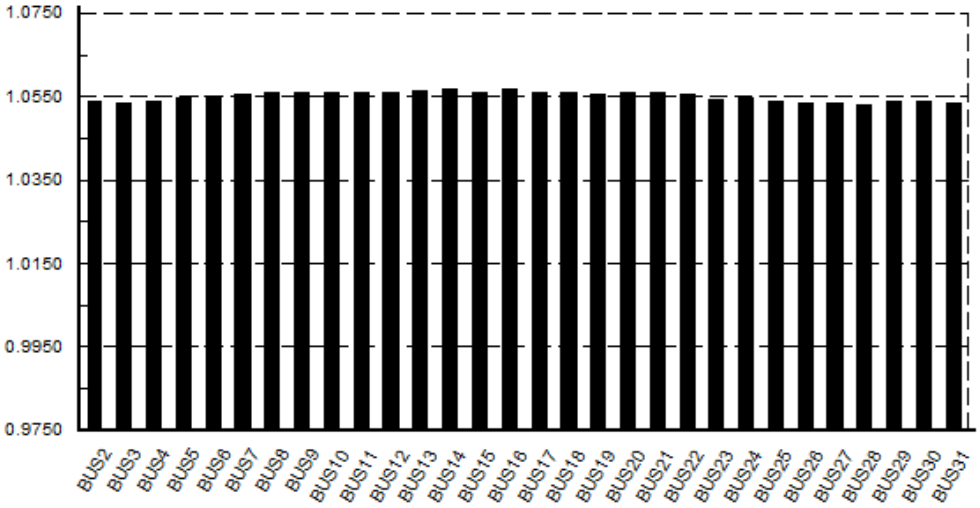

Fig. 6.55 Bus voltage rms values (p.u.) for an 8% total nonlinear load (ASD) connected at buses 15 and 18 utilizing 4%Lac & 2%Ldc filters.

c) Load type 2 utilizing IBF simulation results and analysis:

In this section, the IBF filter is designed for both the 55kW power rating ASD system (Table 4.1) connected to bus 15 and bus 18 (Li = 0.99 mH, Lf = 0.75 mH and Cf = 540 µF star connection). From the line current THDi% results shown in Fig. 6.56, the IBF is successful in reducing the three problematic lines in the previous case (Fig. 6.52) to a very low range of values (< 2.5%). Line power factor values are shown in Fig. 6.57. Lines close to the filters connection point (lines 14-15, 16-17, 17-18) have achieved unity power factor values. Other lines had a negligible effect compared with previous case study.

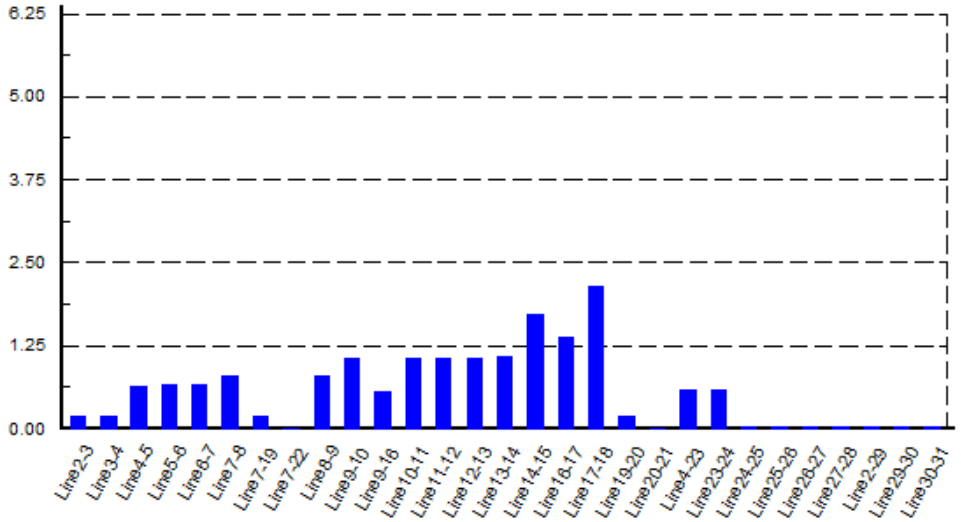

Fig. 6.56 Line current THDi% values for an 8% total nonlinear load (ASD) connected at buses 15 and 18 utilizing IBF harmonic filter.

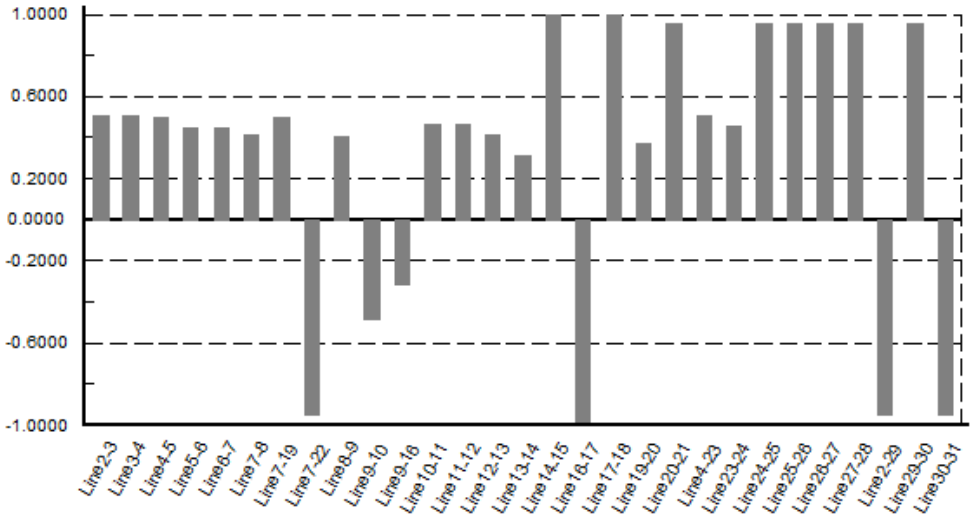

Fig. 6.57 Line power factor values for an 8% total nonlinear load (ASD) connected at buses 15 and 18 utilizing IBF harmonic filter.

The voltage THDv% at all buses has continued to decline to a very low range of values (< 0.1), whereas the voltage rms (p.u.) values has been slightly boosted to (1.054 – 1.058) p.u. range.

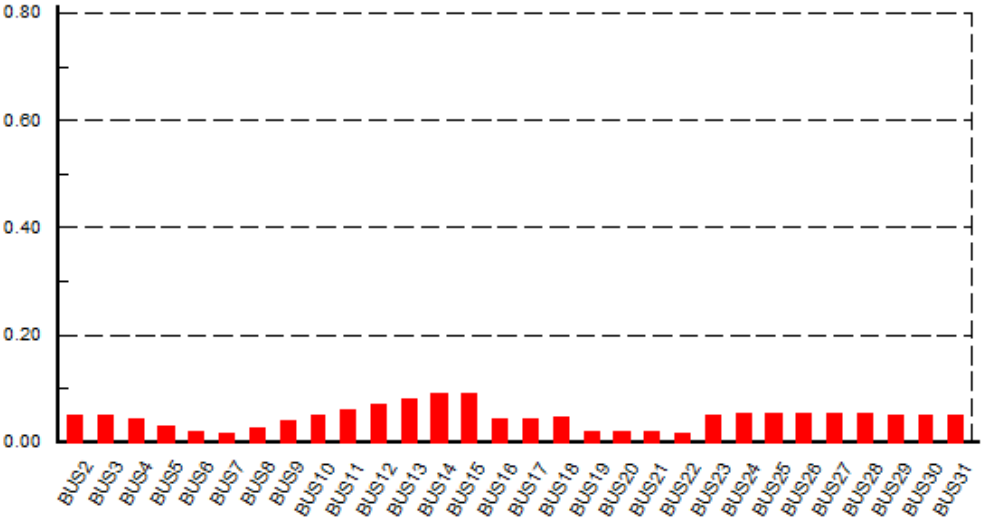

Fig. 6.58 Bus voltage THDv% values for an 8% total nonlinear load (ASD) connected at buses 15 and 18 utilizing IBF harmonic filter.

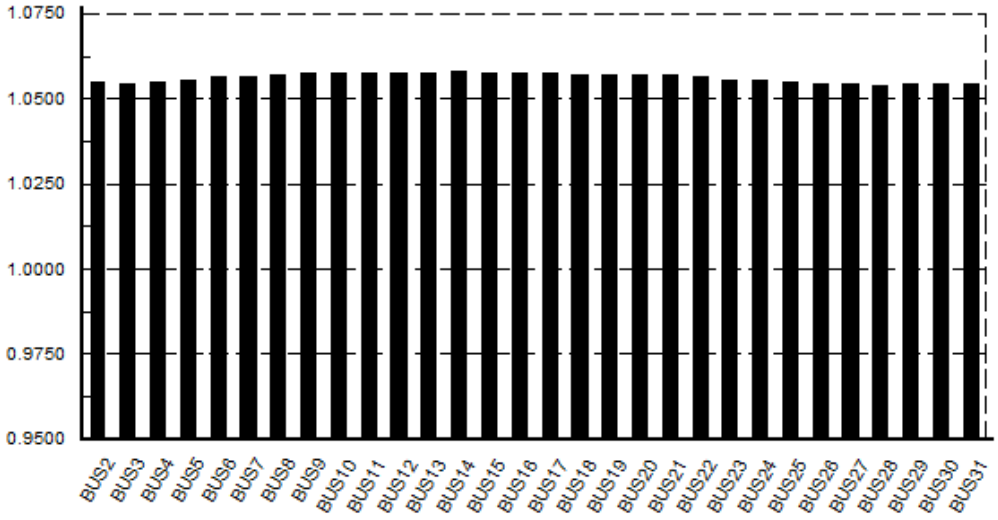

Fig. 6.59 Bus voltage rms values (p.u.) for an 8% total nonlinear load (ASD) connected at buses 15 and 18 utilizing IBF harmonic filter.

d) Load type 3 simulation results and analysis:

The 6%Ldc inductor is used in this section as a filtering method. The simulation results of the line current THDi% values are shown in Fig. 6.60. Similar to the use of 4%Lac+2%Ldc results is achieved (Fig. 6.52). Generally, apart from ASD systems feeding lines (14-15, 16-17 and 17-18), the distortion level in the network is negligible (THDi < 5%). In specific, line 17-18 has the maximum distortion value of 19.6% THDi. The lines power factor results are shown in Fig. 6.61. Compared to the presented results of the basic network in Fig. 6.49 (no filter case) the same ASD system feeding lines are affected by the 6%Ldc installed filter. The mentioned transmission lines have improved from about 0.6 to 0.95 lagging and leading values.

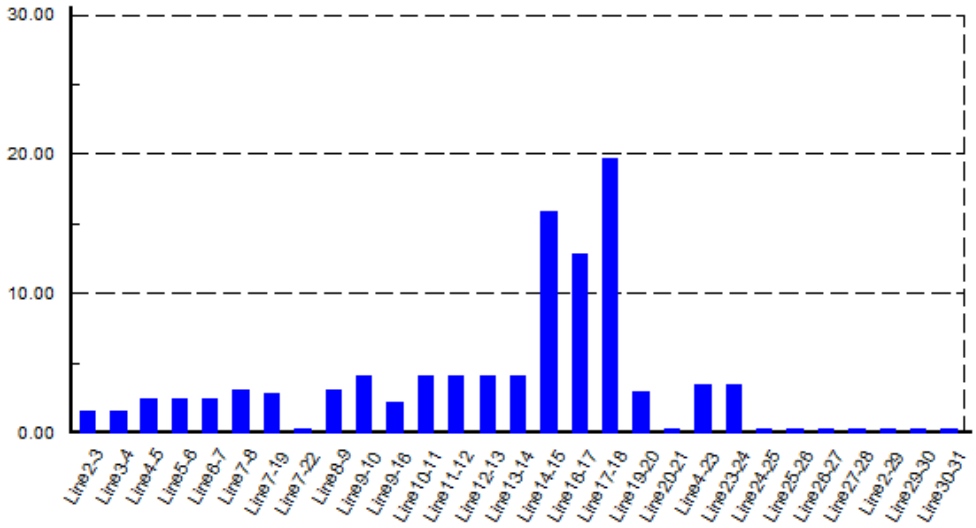

Fig. 6.60 Line current THDi% values for an 8% total nonlinear load (ASD) connected at buses 15 and 18 utilizing 6%Ldc filters.

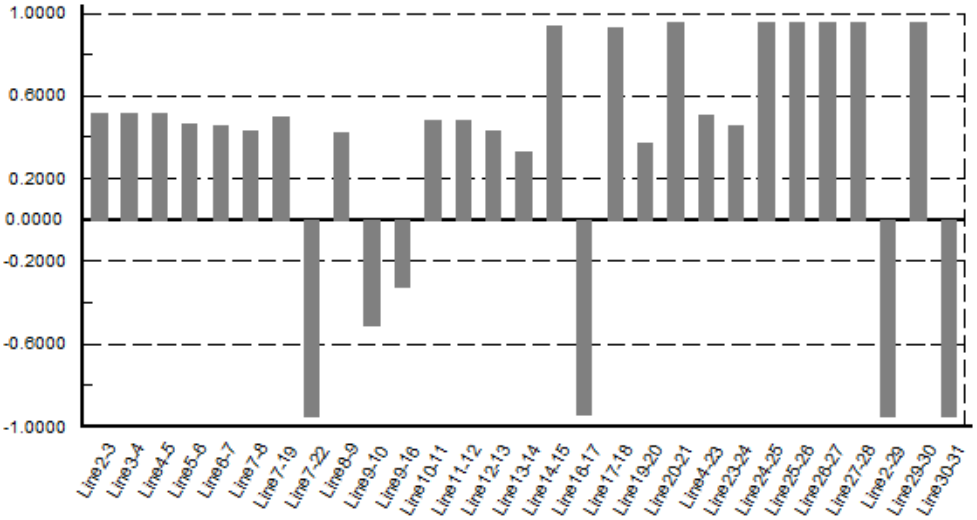

Fig. 6.61 Line power factor values for an 8% total nonlinear load (ASD) connected at buses 15 and 18 utilizing 6%Ldc filters.

The simulation results of the voltage distortion THDv% at all buses are shown in Fig. 6.62. Negligible service voltage distortion exists in the network which is a common outcome for the 8% nonlinear penetration level case study. Finally, the simulation results of the voltage rms value in per unit at all load buses are shown in Fig. 6.63. The results have a marginally acceptable range of values (1.053 to 1.056) p.u. which are similar to the use of 4%Lac+2%Ldc simulation results.

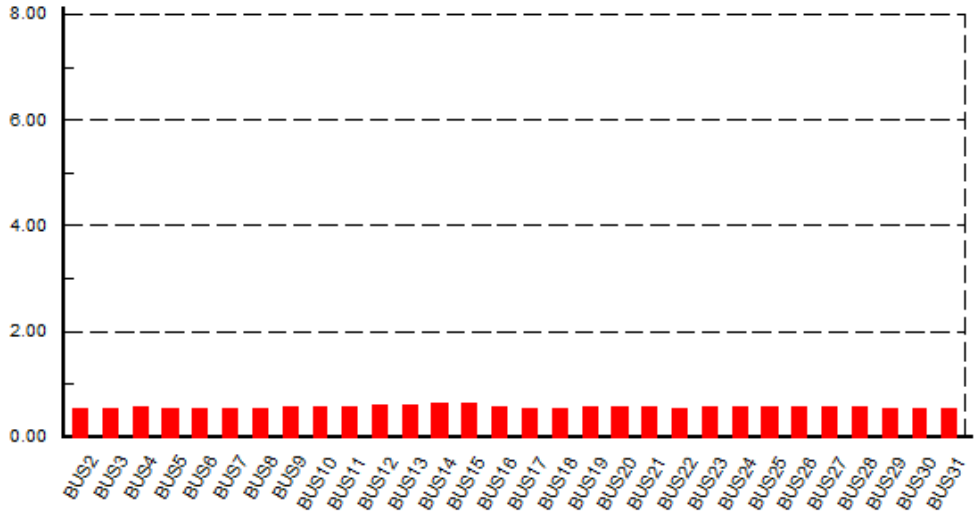

Fig. 6.62 Bus voltage THDv% values for an 8% total nonlinear load (ASD) connected at buses 15 and 18 utilizing 6%Ldc filters.

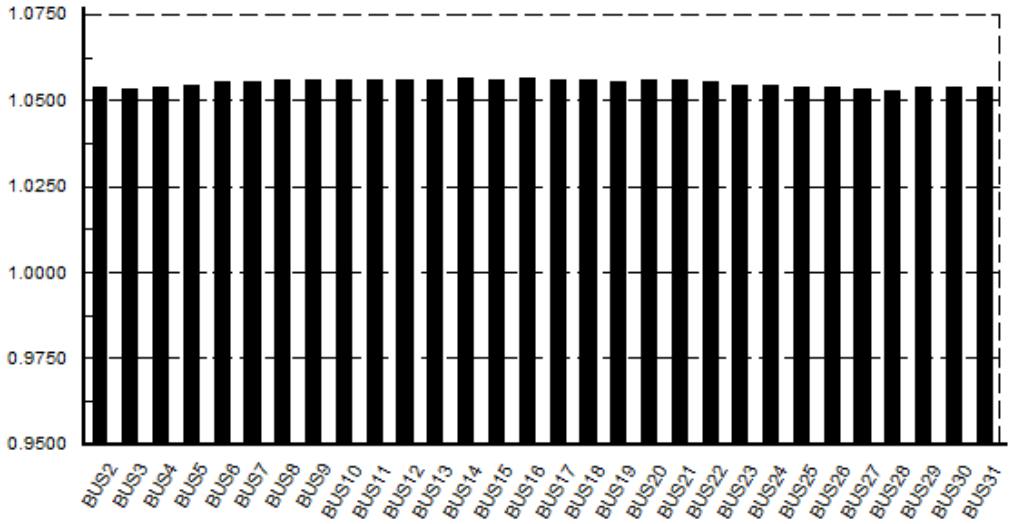

Fig. 6.63 Bus voltage rms values (p.u.) for an 8% total nonlinear load (ASD) connected at buses 15 and 18 utilizing 6%Ldc filters.

e) Load type 3 utilizing ABF simulation results and analysis:

In this last step, the IBF filter is designed for the 55kW power rating ASD system connected (Table 5.1) to bus 15 and bus18 (Li = 1.2 mH, Lf = 0.79 mH and Cf = 504 µF star connection). Figures 6.64 and 6.65 show the simulation results of the lines current THDi% and the lines total power factor values. The lines current are practically free of distortion with a maximum THDi value of 3.2%. The line power factor has a range of values between 0.31 and 0.993 (lagging and leading). Lines

transmitting electrical power to the ABF installation points reached unity power factor while lines close to the shunt capacitors have less power factor values.

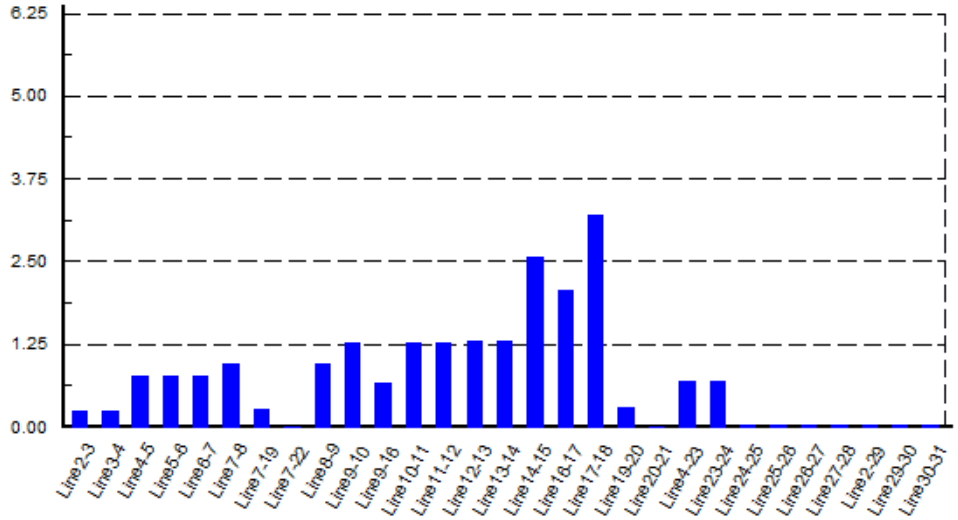

Fig. 6.64 Line current THDi% values for an 8% total nonlinear load (ASD) connected at buses 15 and 18 utilizing ABF harmonic filter.

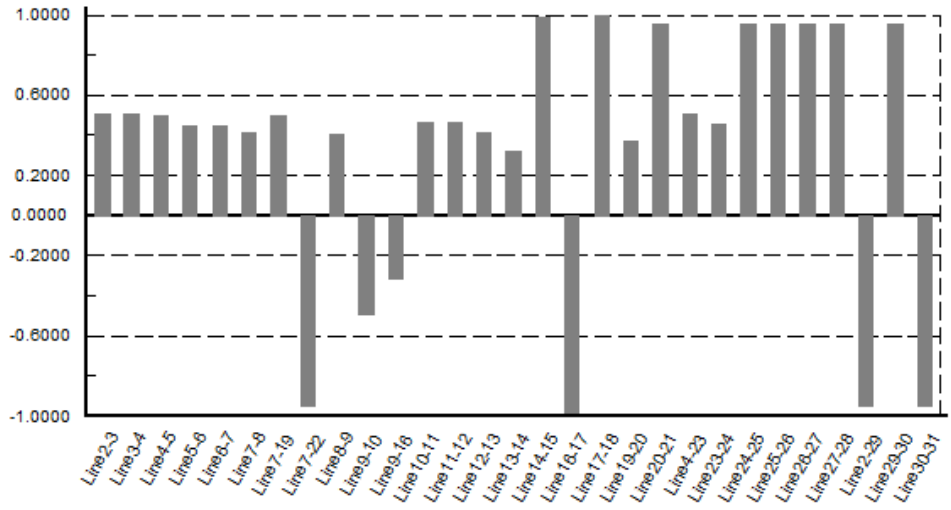

Fig. 6.65 Line power factor values for an 8% total nonlinear load (ASD) connected at buses 15 and 18 utilizing ABF harmonic filter.

As a result of the low current harmonics emission in the network the voltage distortion at the buses is negligible (shown in Fig. 6.66). The network voltage rms estimated values at all bus are shown in Fig. 6.67 with a range of 1.053% to 1.057%.

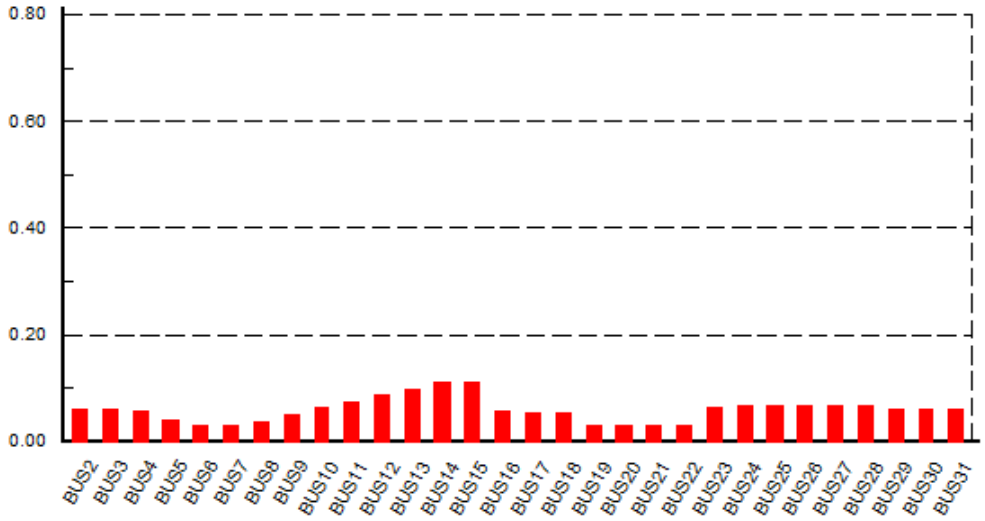

Fig. 6.66 Bus voltage THDv% values for an 8% total nonlinear load (ASD) connected at buses 15 and 18 utilizing ABF harmonic filter.

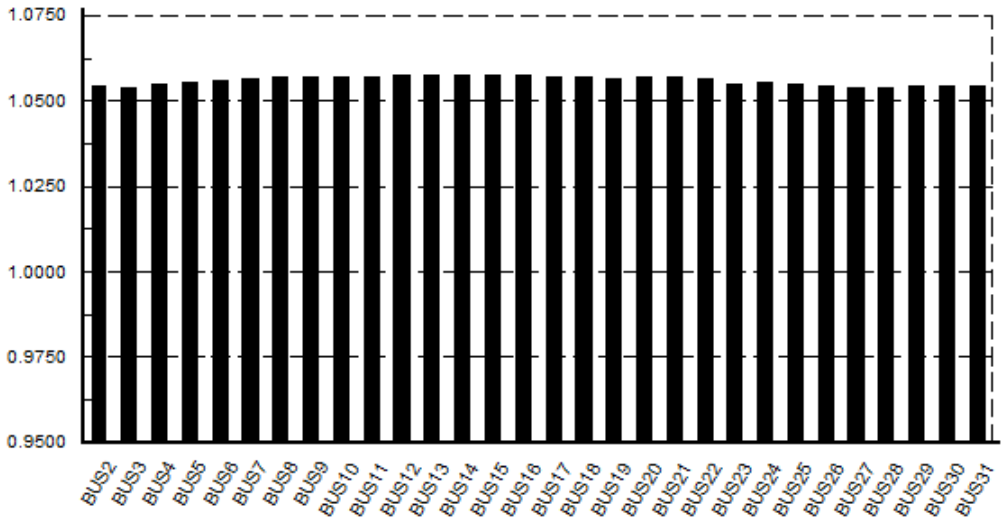

Fig. 6.67 Bus voltage rms values (p.u.) for an 8% total nonlinear load (ASD) connected at buses 15 and 18 utilizing ABF harmonic filter.

Table 6.7 presents the minimum and maximum values for the different cases results. Furthermore, Fig. 6.68 shows the maximum achieved values only for the lines current THDi% combined with the buses voltage THDv%. With this low nonlinear penetration level (8%) all used filtering types were relatively able to reduce the line current THDi% values to an acceptable range. The simple two filtering methods (4%Lac+2%Ldc) and (6%Ldc) are capable to reduce the THDi% values to a range of (17% - 20%). These results are only valid when the nonlinear load is connected to a large feeding transformer and the short circuit ratio (SCR) is >1000, as shown in Table 1.2. On contrary, both broadband passive filters designed in this study are

capable to reduce the THDi% to a very low level (< 5%) that can comply with any SCR loading conditions in the network.

Similarly, the maximum values of the voltage rms in per unit system at all buses and the maximum values of lines power factor are illustrated in the Fig. 6.69. The buses voltage maximum results are relatively levelled for all different cases to a marginally range of 1.052 p.u. to 1.057 p.u. that might be accepted. On the other hand, the line power factor maximum values can be satisfactory (> 0.95) only at specific lines with the utilization of the IBF and ABF structures.

Table 6.7 Summary of simulation results for IEEE 30-bus system with 8% nonlinear load penetration level before and after the installation of various harmonic filters

	No-Filter		4%Lac +2%Ldc		IBF		6%Ldc		ABF	
	Min	Max	Min	Max	Min	Max	Min	Max	Min	Max
Vrms (pu)	1.052 @bus 28	1.055 @bus 14,16	1.053 @bus 28	1.056 @bus 14,16	1.054 @bus 28	1.058 @ bus 14	1.053 @bus 3,28	1.056 @bus 16,14	1.053 @bus 28	1.057 @bus 14
THDv	2.41% @bus 6, 7,22	3.67% @bus 14	0.52% @bus 18	0.58% @bus 14	0.016% @bus 7,22	0.09% @bus 15	0.53% @bus 18	0.62% @bus 14	0.027% @bus 7,22	0.11% @bus 14
THDI	1.28% @line 7-22	88% @line 17-18	0.27% @line 29-30, 30-31	17% @line 17-18	0.00% @line 7-22	2.15% @line 17-18	0.3% @line 30-31	19.6% @line 17-18	0.01% @line 7-22	3.2% @line 17-18
Power factor	-0.34 @line 9-16	-0.949 @line 7-22	0.326 @line 9-16	0.95 @line 7-22	-0.31 @line 9-16	0.996 @line 17-18	0.32 @line 9-16	0.95 @line 7-22	-0.31 @line 9-16	0.993 @line 17-18

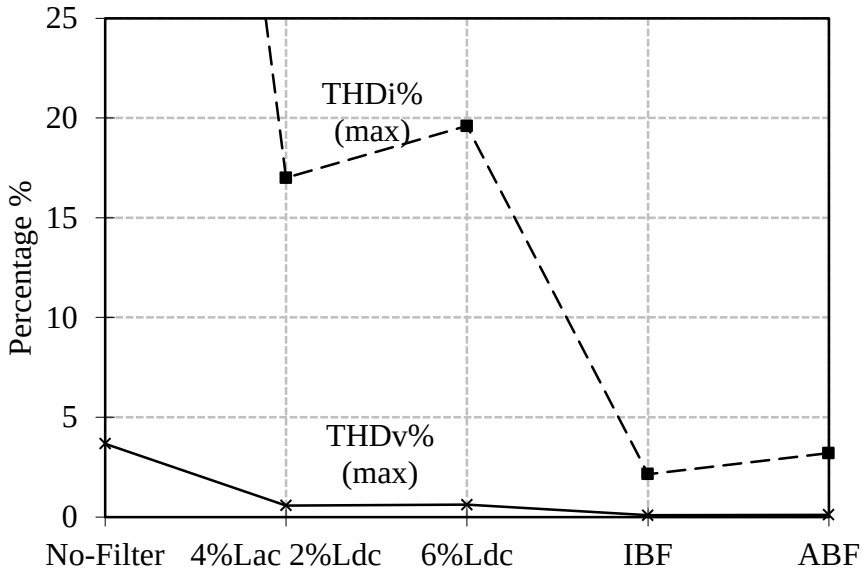

Fig. 6.68 IEEE-30 bus network line current and bus voltage maximum THD values utilizing various harmonic filtering methods for a 8% nonlinear load connected at buses 15 and 18.

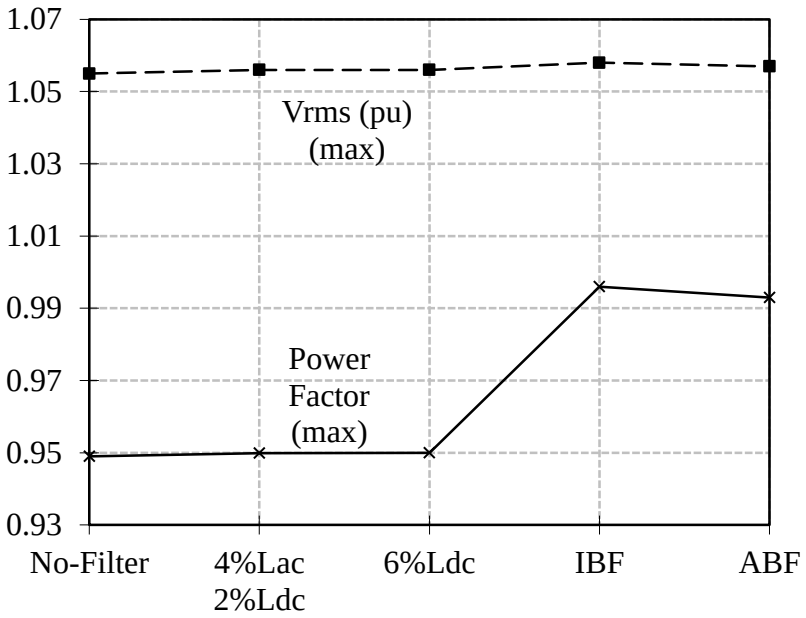

Fig. 6.69 IEEE-30 bus network line power factor and bus rms voltage (p.u.) maximum values utilizing various harmonic filtering methods for a 8% nonlinear load connected at buses 15 and 18.

6.4 **Performance Evaluation and Comparison**

In this section the simulation results of the different harmonic mitigation methods for the three main penetration nonlinear load (ASD systems) levels in the IEEE 30-bus distribution network (8%, 40% and 70%) are summarized, evaluated and compared. Fig. 6.70 shows the maximum lines current THDi% values for the basic network without the application of any filtering method and with the implementation of the other four proposed mitigation techniques. Generally, the high harmonic distortion in the network (> 80% THDi) for all nonlinear load concentration cases is not allowable by the harmonic control regulations. Therefore, the use of any suitable filtering method is a mandatory for such a distribution network.

In order to have a closer look at the performance comparison between the various utilized filtering techniques, the related line current THDi% results are zoomed-in and shown in Fig. 6.71. The first observation includes the results similarity of each two filtering methods couple, the (4%Lac+2%Ldc, 6%Ldc) and (IBF, ABF). Each couple has nearly the same harmonic mitigation ability in the network for the three different penetration level. Secondly, the first simple filtering couple is not able to

comply with the recommended THDi% limitations for the 70% and 40% concentration level. On the other hand, the IBF and ABF are effective in reducing the current distortion to a very low values (THDi < 5%) for any penetration level. Finally, for the 8% nonlinear load share in the network, the simple filtering solution might be more practical choice with less cost and size.

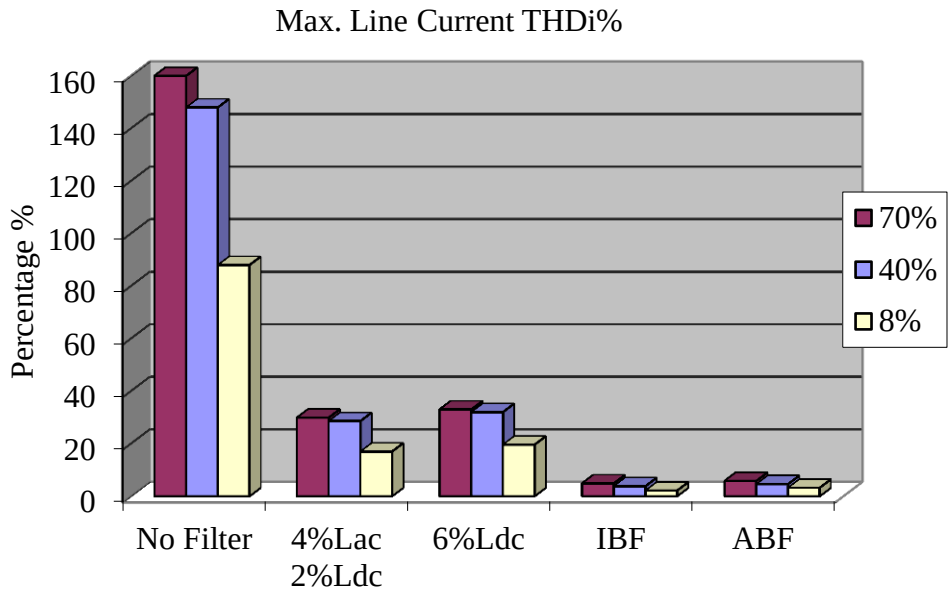

Fig. 6.70 IEEE-30 bus network line current THD maximum values for a 70%, 40% and 8% total nonlinear load connected at buses 15 and 18 utilizing various harmonic filtering methods.

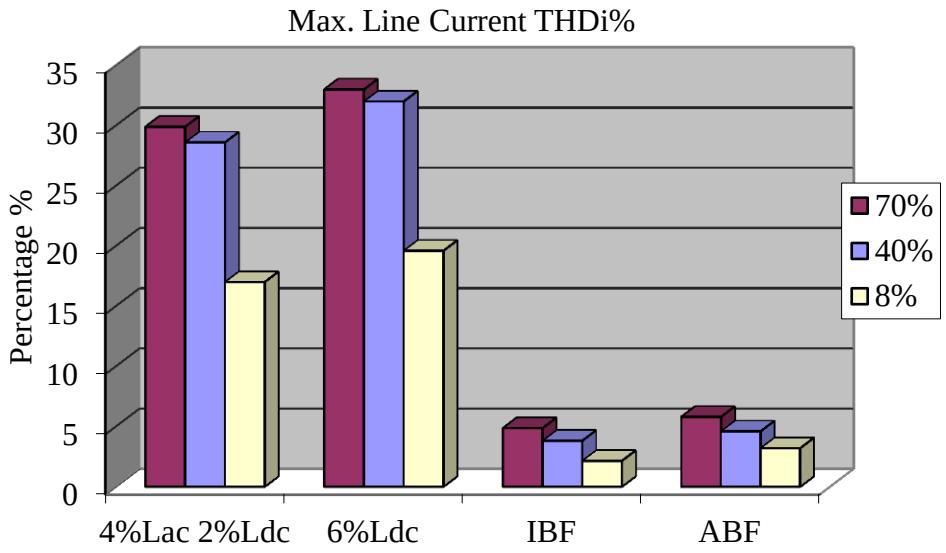

Fig. 6.71 IEEE-30 bus network line current THD maximum values for a 70%, 40% and 8% total nonlinear load connected at buses 15 and 18 utilizing various harmonic filtering methods (Zoomed).

The maximum achieved values of the lines power factor, in the study results, for the different operating conditions and filtering methods are shown in Fig. 6.72. The first couple of the simple filtering methods do not have a recognizable effect in the network compared to the first case results shown in the Figure (No Filter). On the other hand, the second filtering couple (IBF and ABF) can improve the line power factor to unity (≥ 0.99) in nearly all penetration levels. However, these levels of power factor are gained mainly in the lines that are close to the filters connection point and not at all lines as explained in the previous sections. The presence of the different seven shunt capacitors in the network interact with IBF and ABF structure affecting the other lines power factor results. This may recommend for the power systems engineers the requirement of re-designing and relocating the conventional power factor shunt capacitors when harmonic control filters are utilized.

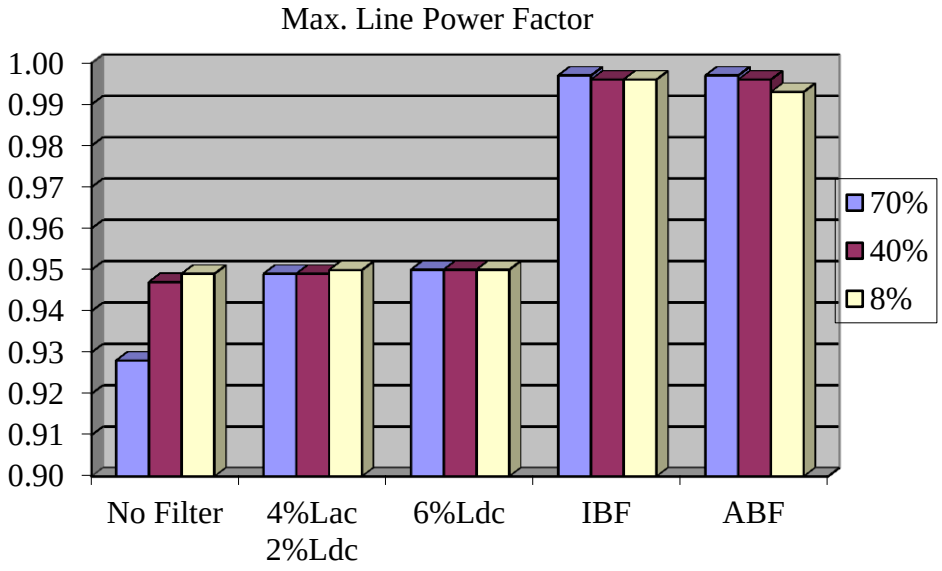

Fig. 6.72 IEEE-30 bus network line power factor maximum values for a 70%, 40% and 8% total nonlinear load connected at buses 15 and 18 utilizing various harmonic filtering methods.

Fig. 6.73 shows simulation results of the IEEE-30 bus network voltage THDv% maximum values for a 70%, 40% and 8% total nonlinear load connected at buses 15 and 18 utilizing the chosen harmonic filtering methods. From the results presented, the penetration level in the network is a major factor that helps in selecting the suitable filtering technique. In other words, according to this figure, only the heavily

penetrated network condition requires adding a filter to the ASD system to reduce the THDv% values at the buses to an acceptable level (5% max.).

The voltage rms (pu) maximum value for the different harmonic source loads concentration with the implementation of the various filtering methods are shown in Fig. 6.74. For the 70% concentration level, remarkably, only the simple filters structures were able to firmly comply with the assigned limit (1.05 p.u. max.). The IBF and ABF implementation results in slightly higher maximum value. Regarding the 40% concentration level all filtering methods succeed to keep the voltage rms normalized values at all buses below and/or marginally above the 1.05% limit. Finally, the 8% penetration low level of the nonlinear load (less inductive reactive power) causes the rise of the voltage rms maximum p.u. values to exceed the limits in with or without filters operation condition. This reduction in the harmonic distortion and, therefore, the inductive reactive power makes the capacitive reactive power provided by the connected shunt capacitors dominating the network and resulting in the shown overvoltage condition. This rise can be increased by the use of the IBF and the ABF filtering topology due to relatively large designed capacitors.

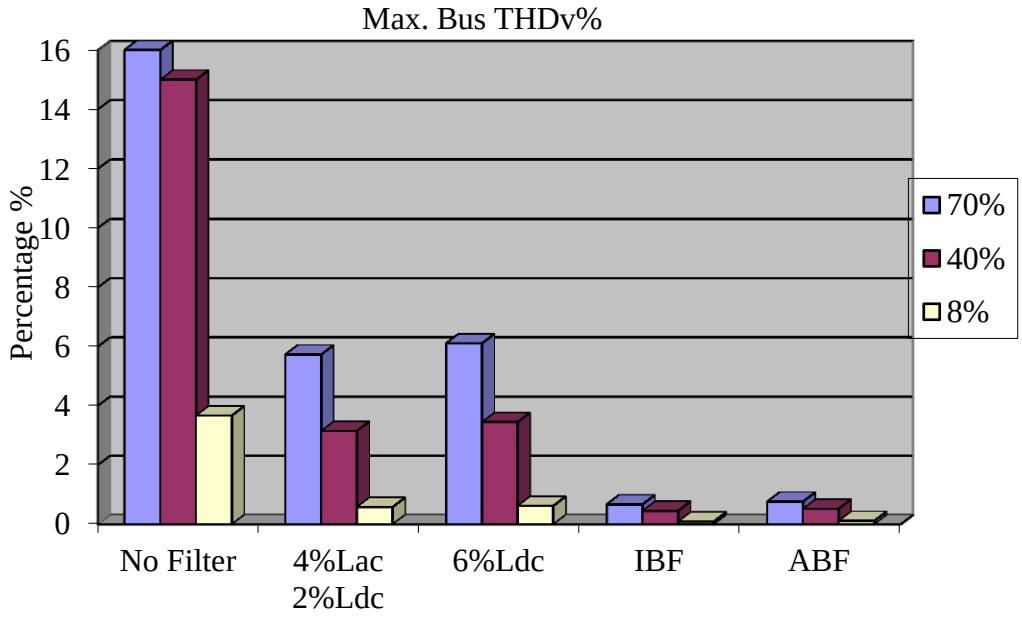

Fig. 6.73 IEEE-30 bus network voltage THD maximum values for a 70%, 40% and 8% total nonlinear load connected at buses 15 and 18 utilizing various harmonic filtering methods.

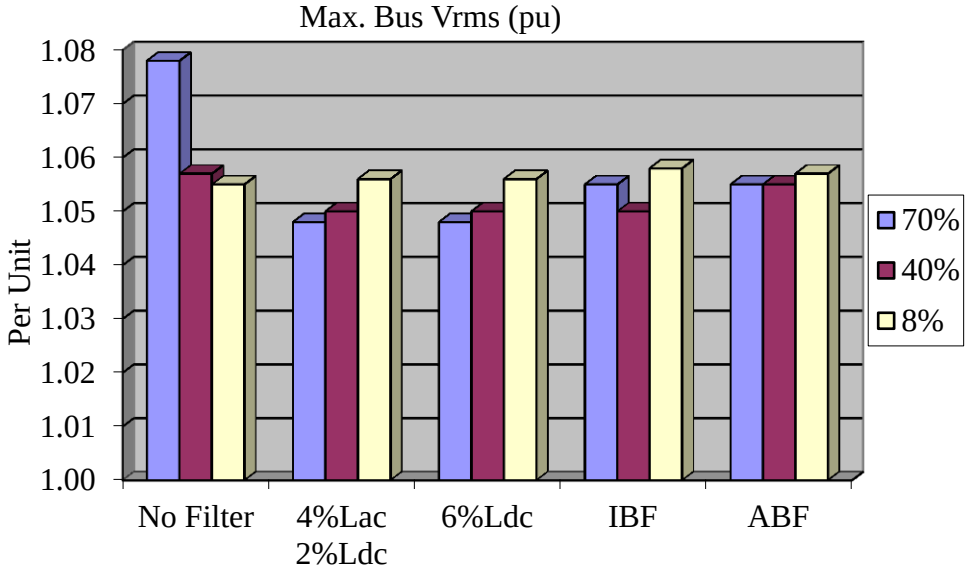

Fig. 6.74 IEEE-30 bus network rms voltage (p.u.) maximum values for a 70%, 40% and 8% total nonlinear load connected at buses 15 and 18 utilizing various harmonic filtering methods.

In conclusion, it has been clarified that several factors can be considered before selecting the suitable filtering structure in the network. The level of nonlinear load existing in the network is a major aspect as well as the number and the size of shunt capacitors connected to the network. Overall, the utilization of the IBF or the ABF broadband filters for the proposed network conditions can be a satisfactory decision.

6.5 **Summary**

In this chapter the performance of various filter topologies with the emphasis on the developed IBF and ABF filters have been discussed. The performance assessment of the discussed filters connected to a standard IEEE 30-bus distribution network was presented and a detailed comparison illustrated. The steady-state performance characteristics of the distribution network utilizing the proposed filters at various nonlinear load penetration levels were in focus. The main power quality indices (lines current THDi% and power factor values, buses voltage THDv% and rms values) have been considered.

The IEEE 30-bus distribution network computer simulation based study support the theoretical performance expectation of the IBF and ABF filtering structures and their parameters design method. The superior overall performance the proposed broadband passive filters configuration has been validated. The following chapter reviews and summarizes the research outcomes of this work.

7 CONCLUSIONS AND FUTURE WORK

The focus of this study is on the design and development of the low-pass passive harmonic broadband filters for ASD applications. In order to comply with modern power quality standards for such common applications in industry, this broadband filtering technique is implemented to limit the current harmonic components of the nonlinear converters (AC/DC) used in AC motor drives.

7.1 Thesis Summary

This thesis includes several stages; the first stage of the thesis demonstrated the continuous need of cost effective AC/DC and DC/AC power converter circuits in all industry applications. Specifically, the rapid growth of the world market for ASD systems and the related current harmonic distortion issues in such three-phase diode bridge rectifier front-end applications has been clarified. Consequently, the common harmonic mitigation methods that are utilized for ASD systems have been reviewed and discussed.

The three-phase rectifier ASDs system harmonic mitigation techniques illustration has involved passive filters, phase multiplication systems, active filters, hybrid systems and PWM rectifiers. The various techniques performance advantages, practical limitations and cost indices indication have been demonstrated. Due to the topology's relative simplicity and lower cost benefits, the passive harmonic filters methods are commonly selected and utilized by engineers for smoothing the line current of the three-phase 6-pulse front-end diode rectifier applications.

In this research project, within the various common passive harmonic filtering methods discussed, the emphasis has been put in the improved broadband passive filter (IBF) topology. The method superior overall performance (line current THDi < 10% and practically unity power factor at full-load) along with the fast gained commercial attention favour the IBF topology. Hence, for recent power quality

agreement filter, the improved broadband filter (IBF) has been selected as one of the main candidates.

In the second stage of the thesis, the IBF filter construction, operating principle and behaviour analysis are reviewed and described. The modelling method of filter-ASD system, using a frequency domain equivalent circuits approach, has been detailed. Finally, in this second stage, the IBF filter component values linear searching approach (used in my M.Sc. project) is briefly described. This method has been the basis to the new design method studied, utilizing the genetic algorithm approach, in an attempt to reduce the IBF filter components size and cost while improving its good performance.

The third stage of the thesis has provided an overview on several optimization methods used in a power system correlated issues. Mathematical Optimization main advantages and major disadvantages have been shown. Different Artificial Intelligence Optimization techniques have been discussed. This involves the Expert System (ES), Artificial Neural Network (ANN), Simulated Annealing (SA) and Genetic Algorithm (GA) methods. More details of the GA method and a comparison with the other optimization techniques have been presented. Finally, advantages and limitations of GA technique are detailed.

The fourth stage of the thesis has involved GA implementation details in designing the improved broadband filter for given operating conditions and power quality constraints. The design is conducted for 5.5 and 55 power ratings. The filter employs 4% L_o in all power ratings and the three main filter components, L_i, L_f, C_f are first calculated by means of linear searching technique using the accurate computational method. Utilizing the linear method parameters as initial values, the genetic algorithm approach further optimizes the three filter component values with high accuracy leading to optimal parameters in terms of reducing the size, cost and meeting performance criteria. A comparison of the different filter component values searching methods results has been discussed.

Moreover, in this fourth thesis stage, the performance of the new optimized filter component values design of the IBF has been under focus. The study is conducted by computer simulations through detailed modelling of the ASD system. Steady-state performance characteristics are assessed from light-load to full-load operating conditions. ASD system utilizing the IBF operating under balanced and unbalanced supply voltage with practical voltage harmonic distortion is considered. Input power quality (input current THDi and power factor), energy efficiency filter output voltage regulation are evaluated. Finally, a 5.5kW IBF prototype has been built and the experimental performance characteristics of the ASD system using the GA designed IBF under various operating conditions have been extracted.

Overall, in the fourth stage, the accuracy of the new IBF design method has been proven and its success in reducing the filter size and cost has been shown. In addition, the improved performance characteristics of the optimized IBF filter has been presented and compared to other common passive filters. Meanwhile, the application practical limitations have been described.

The fifth stage of the thesis has included a study that proposes, based on the IBF structure, a new advanced broadband filter (ABF) design which further reduces filter components, size and cost while maintaining similar satisfactory performance for ASD applications. The modified IBF structure has been developed by eliminating the smoothing AC reactor (4% Lac), normally connected at the rectifier side, which gives a novel advanced broadband filter (ABF) structure. Similarly, the ABF design has been performed using genetic algorithm (GA) at different power ratings to optimize the frequency-domain model of the system. In order to validate the effectiveness of the GA design method in sizing components, a comparison of the filter components given by a linear design method has been presented. Finally, the steady-state performance of an ABF filter implemented to an ASD system at various operating points has been evaluated, and ASD system successful performance has been confirmed by analytical means, detailed computer simulations and laboratory experiments. The main power quality parameters (line current THDi%, line power factor, and filter output voltage regulation) and energy efficiency attributes have

been investigated. Moreover, unbalanced supply voltage ABF filter sensitivity has been considered.

The sixth and final stage of the thesis has involved testing the operating performance and effectiveness of the both harmonic passive broadband filters, designed in this study (IBF and ABF) by connecting them in a standard IEEE distribution network that contains different penetration levels of nonlinear loads (ASD system). The study has been conducted via detailed modelling of the distribution network and the connected nonlinear loads through computer simulations.

The analysis and evaluation has involved three different nonlinear load penetration levels (8%, 40% and 70%) of the total overall network linear load. These three cases of harmonic distortion in the network with current harmonics (light, moderate and heavy) has helped in providing a better decision as to whether to use a harmonic filter or not and in choosing the required type of filtering technique that can comply with the harmonic standards (IEEE 519) for each situation.

In these three main operating conditions, power quality indices such as; the network lines current THDi% and power factor values are monitored. Furthermore, the voltage THDv% and rms values at the network buses are under investigation for the various loading conditions considered. The study has involved, in the first step, the network performance including the ASD systems with no filters connected. In the second step, the study has investigated these various network specifications with different types of filtering techniques utilization.

7.2 **Conclusions and Contributions**

As a whole, a new and simple frequency-domain equivalent-circuit-based analytical method for the improved broadband filter (IBF) and advanced broadband filter (ABF) design was developed by using GAs. The genetic algorithm design method, which has been described in this thesis, can play an important role in the optimization of IBFs and ABFs for industrial motor drives. The genetic algorithm optimization process

used was capable in achieving better power quality indices and reducing the filter components values .

The method is efficient, accurate, and results in reduced filter size and cost along with considerably less risk of harmonic-excited resonance problems. It allows a high standard of power-quality indices to be achieved with a set of filter components likely to have minimal bulk and overall cost. As summarized and shown in Table 7.1 (based on Table 4.2 and Table 5.2 results), the presented analytical results of the design case-studies have shown that the method is robust and has produced advanced designs with lower filter size and cost. A reduction of 7% - 10% in Li and 17.5% - 18.5% in Cf has been achieved when compared to the results obtained by linear searching technique for the same power quality system requirements. The analytical performance characteristics has illustrated that the IBF and ABF had very low input current THDi (< 7%) and near unity power factor at full-load.

Table 7.1 Analytically estimated power quality indices, components size, and components achieved reduction of IBF and ABF 5.5/55kW filters by GA algorithm

Filter structure	Searching method	THDi (%) (avg.)	PF≈ Cosφ (avg.)	ΔV_o (%) (avg.)	Li (mH) 5.5/55kW	Cf_Δ (µF) 5.5/55kW	Components size reduction (avg.)
IBF	Linear	6.60	0.955	3.75	10.6/ 1.138	21/ 208	-10% Li -17.5% Cf
	GA	6.25	0.985	3.10	10.1/ 0.99	16.6/ 180	
ABF	Linear	6.50	0.950	3.90	12.94/ 1.290	20.9/ 208.8	-6.75% Li -18.5% Cf
	GA	6.90	0.985	3.40	12.10/ 1.20	17.3/ 168	

Moreover, the IBF and ABF simulation and experimental results supports the estimated analytical results presented. Both filters are effective in reducing the line current THDi% to an acceptable low range that can comply with harmonic standards. For comparative illustration, the IBF performance results presented in sections 4.4.7 and 4.5.6 are recalled and utilized. Fig. 7.1 shows the 5.5kW ASD system line current THDi% simulation and experimental values (overlaid in the same graph)

from light-load to full-load operating range utilizing the designed IBF filter, while Fig. 7.2 shows line power factor values under equivalent conditions.

Similarly, for the same purpose, the 5.5kW ASD system utilizing the ABF filter simulation and experimental results (presented in sections 5.6.7 and 5.7.5) are superimposed in the same diagram and shown in Fig. 7.3 and Fig. 7.4. The load current dependency of the ABF line current THDi% is illustrated in Fig. 7.3 and the load current dependency of the ABF line leading power factor is shown in Fig. 7.4.

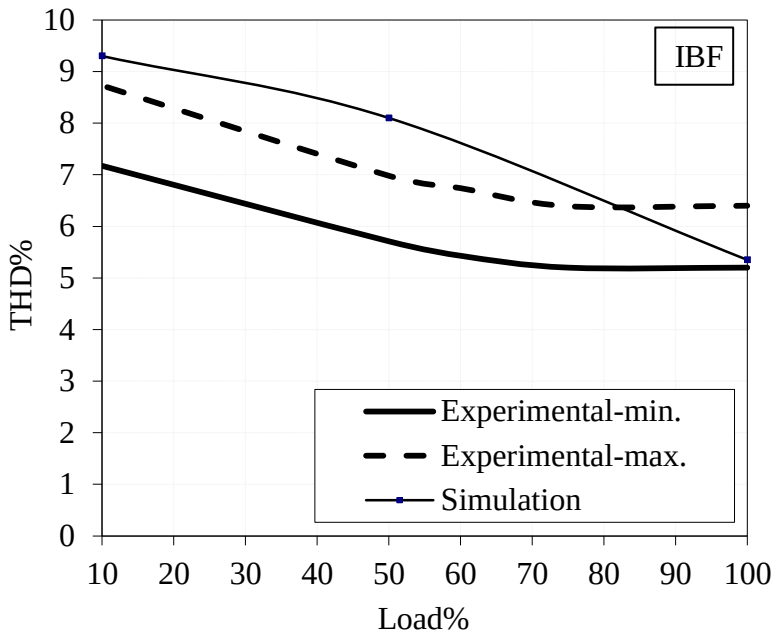

Fig. 7.1 The load current dependency of the IBF line current THDi% (simulation Vs experimental results).

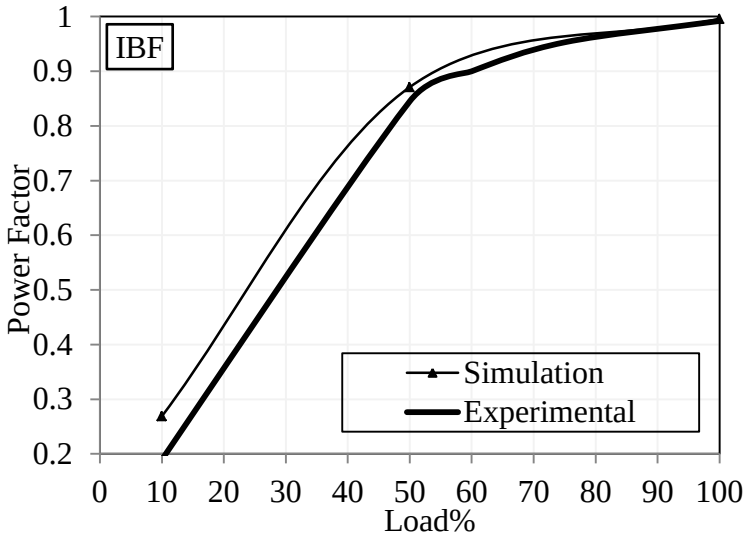

Fig. 7.2 The load current dependency of the IBF line leading power factor (simulation Vs experimental results).

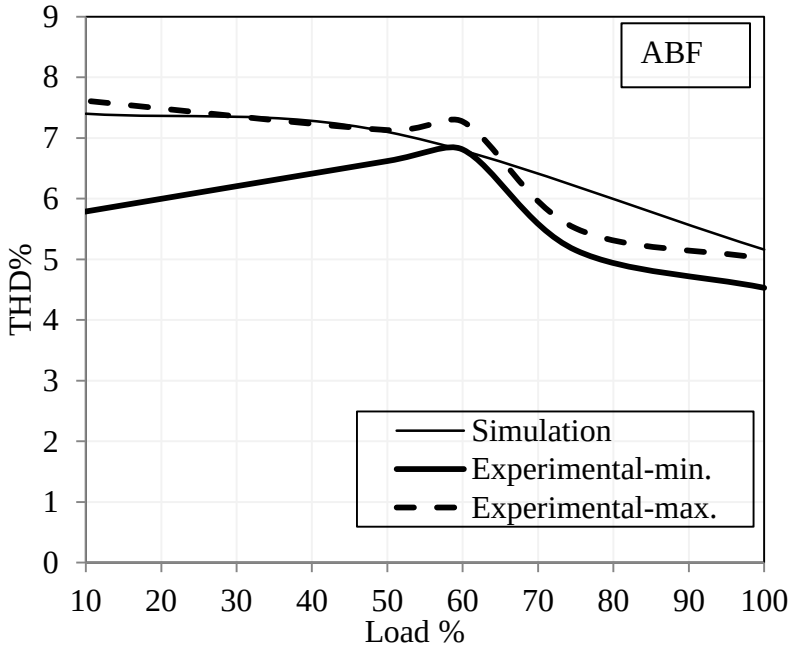

Fig. 7.3 The load current dependency of the ABF line current THDi% (simulation Vs experimental results).

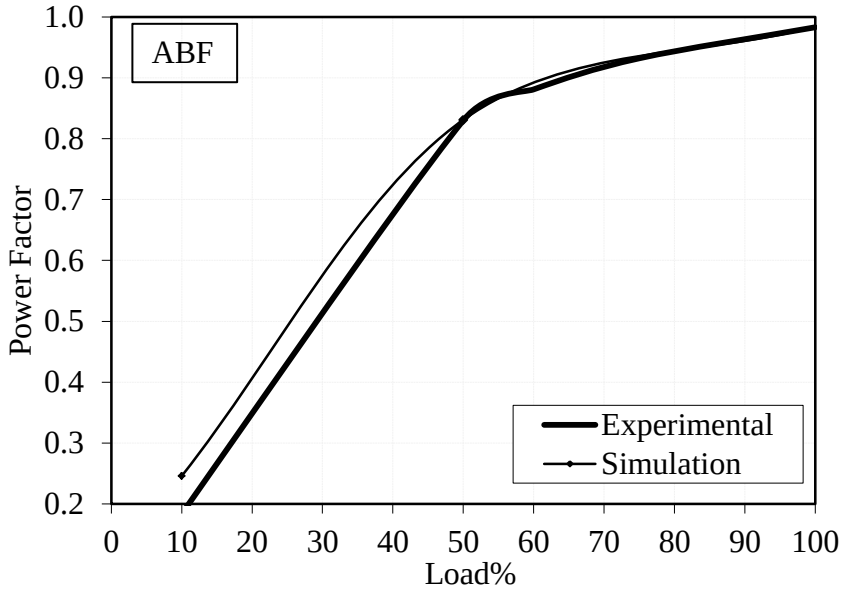

Fig. 7.4 The load current dependency of the ABF line leading power factor (simulation Vs experimental results).

In general, it is noticed, from the previous comparison figures, that the laboratory built setup of the 5.5kW ASD system using the IBF and ABF filters has slightly better performance. This is due to the lower supply voltage harmonic distortion existed in the laboratory experiments, shown in sections 4.5 and 5.7, (≤ 2.24% THDv) than the practical assumption implemented in the simulation model (3% THDv). Moreover, the available DC-link inductor in the laboratory experiments has an extra inductance (5% - 7%) than the actual designed value in the simulation model. Finally, the power analyser measurement accuracy level may also affect the results.

Overall, as the Fig. 7.1 and Fig. 7.3 reveals, the IBF and ABF based ASD system delivers high power quality performance along the various loading operating conditions. Over the wide loading range the line current THDi% has a satisfying spectrum of values (<10%) and very low value at full-load (< 6.5%). This will allow the ASD system, using the IBF or ABF filters, to have a negligible effect on the distribution network and specifically to other loads connected at the same PCC point. The IBF and ABF based drive does not emit any harmonics to the environment, making the drive environment friendly and a strong candidate for extremely low

harmonic emission system. This might be considered as a major improvement in terms of polluting the network.

Moreover, as the curves in the Fig. 7.2 and Fig. 7.4 specify, the IBF and ABF based ASD systems has a unity power factor at full-load condition and high values over the 50% loading situations. This will help in minimizing the reactive power requirement of the drive. However, from no-load to about half-load operating range the line power factor has a limited range of values. As a result, it is practically recommended that these proposed filtering structures are used for ASD systems with high duty cycles applications which are widely implemented in industry. For instance, a typical combustion fan in a power plant boiler runs > 90% of its operation time over 60% range of its full speed. Similarly, for pump usage in several applications (sewage systems, irrigation systems, and refinery and waste water systems) the effective power savings (according to Affinity law) by using ASDs will occur when the pumps operate from the half-load to the full-load operating conditions. At lower loading conditions the Affinity law breaks down and no major energy savings is increased as other variables emerge in the system (e.g. static pressure existence).

The low power factor performance below 50% loading condition is considered as the major limitation of such filters topology that should be considered in practical implementations. Therefore, ASD drives with relatively low duty cycle range operation should recommend disconnecting the IBF or ABF utilized filter during the specified low loading condition. On the other hand, for highly frequent light-load ASD drives applications the passive filtering approach (including IBF and ABF) is not effective and implementing other active filtering techniques become compulsory.

Finally, a qualitative assessment of the proposed IBF and ABF filters, three-phase typical AC reactor and STSF passive filters were considered and results are summarized in Table 7.2. As the table indicates, in terms of meeting modern power quality requirements (< 10% line current THDi and near unity PF) simply adding AC in-line reactors is not effective. Therefore, using a passive filtering approach to achieve higher power quality desires, the application must consider either the conventional single tuned shunt filters or the low-pass broadband filters structures.

The STSF can be comparable to the IBF and ABF size, cost and complexity. However, the voltage unbalance sensitivity and harmonic resonance risk factors (shown in Table 7.2) strongly support the superiority of the IBF and ABF methods. Finally, the broadband filters effectiveness is less sensitive to components preferred values or manufacturing tolerance as the convention STSF. Unlike the STSF that has to be tuned to a specific frequency for each shunt filter designed, the IBF and ABF are tuned to a single cut-off frequency that makes the filter shunt any harmonic component above this frequency and prevent these harmonic components from passing through the line.

In total, IBF and ABF utilize fewer components with higher current ratings than the conventional single tuned shunt filter. However, they have better performance than all harmonic filters presented. Therefore, typical single tuned shunt filter (STSF) and low-pass broadband filters (IBF and ABF) can be considered comparable in size and cost, but not in performance. Consequently, the IBF and ABF systems are a strong candidate for improving power quality of demanding applications.

The major novelty in this thesis involves:

1. Contributing in providing a theoretical background and design analysis of the IBF and ABF broadband harmonic filters. (Presented in chapter 2, sections 4.1 to 4.3 and sections 5.1 to 5.5 and meeting the first thesis objective).

2. Providing a novel design method using the GA searching technique to optimize the size (cost) of the existing IBF structure filter components. (Presented in sections 4.1 to 4.3 and meeting the second thesis objective).

3. Investigating the new design of the optimized IBF topology performance characteristics via a comprehensive analysis, detailed simulation and experimental studies. (Presented in sections 4.4 to 4.5and meeting the third thesis objective).

4. Developing a new ABF structure by reducing the number of the IBF filter components utilized in conjunction with optimizing the size. (Presented in sections 5.1 to 5.2 and meeting the fourth thesis objective).

5. Providing a new design method using the GA searching technique to optimize the size (cost) of the novel ABF structure filter components. (Presented in sections 5.3 to 5.5 and meeting the fifth thesis objective).

6. Investigating the new design of the optimized ABF topology performance characteristics via a comprehensive analysis, detailed simulation and experimental studies. . (Presented in sections 5.6 to 5.7 and meeting the sixth thesis objective).

7. Providing a detailed quantitative and qualitative performance comparison of the proposed broadband filters with the conventional passive filters. . (Presented in sections 4.4.7, 5.6.7 and 7.2, and meeting the seventh thesis objective).

8. Investigating the designed broadband filters effectiveness under different harmonic distortion levels in power system distribution networks. (Presented in chapter 7 and meeting the eighth thesis objective).

Table 7.2 Qualitative comparison of various common passive filters (AC line reactors, single tuned shunt filter, IBF and ABF)

Filter type	Line THDi%	Line PF	Harmonic resonance risk	Voltage regulation	Size	Structure complexity	DC-link inductor requirement	Cost***	Energy efficiency	Voltage unbalance sensitivity	Filter effectiveness sensitivity w.r.t. components tolerance
Typical AC line reactor	High	Low	N/A**	N/A**	Small	Simplest	Min.	Low	High	High	**N/A****
Tuned filter	Low	High*	High	Low	Large	Complex	Min.	High	Medium	Medium	High sensitivity
IBF	**Very low**	**High***	**N/A****	Low	Large	Simpler	Min.	Medium	Medium	**Very low**	**Low sensitivity**
ABF	**Very low**	**High***	**N/A****	Low	**Medium**	Simpler	Max.	Medium	Medium	**Very low**	**Low sensitivity**

*For > 50% loading conditions

**Not an issue (N/A)

***With respect to active harmonic mitigation solutions (Fig. 1.17)

7.3 **Future Work**

The designed low-pass improved and advanced broadband filters, for three-phase 6-pulse diode bridge rectifier front-end applications, in this thesis has been successful in current harmonic mitigation and complying with the overall harmonic regulations. Therefore, other front-end rectifier applications types can be investigated and similar harmonic solutions can be considered. This may involve the 6-pulse thyristor bridge rectifier applications and the multi-pulse (12-pulse and 18-pulse) rectifier front-end applications.

For such new proposed applications, the filter design principles and its parameters selection optimal method will become another challenge. However, based on this thesis methodology and the new application rectifier current harmonic components ratio (with respect to its fundamental value) knowledge, a new related filter design contribution can be achieved.

Accordingly, the consideration of the 6-pulse thyristor rectifier, 12-pulse diode/thyristor rectifier systems application in a comprehensive power quality study may be extended based on this study. The harmonic mitigation issue using passive filters for such systems may be investigated and filters design rules defined depending on the method established in this research.

Furthermore, in the design process, the modelling of the ASD system can be improved for better accuracy levels while the three-phase magnetic coupling and the nonlinearity of the inductance effects can be explored and implemented in future broadband filter studies.

Finally, as the related commercial information indicates, the passive filtering techniques will remain on the market. This is due to the fact that active rectifiers and stand-alone active harmonic filters are still complex, costly and challenging. Therefore, development of the passive filter along with hybrid systems to comply with the continuous power quality demand in electrical power systems is always

required. On the other hand, improving the active solutions systems to achieve lower cost and reduced structure complexity is also a necessity of the modern power quality era.

Appendices

A. Rectifier commutation effect and output voltage drop representation in ASD equivalent circuits

Since the generally large DC bus capacitor used in the DC-link of the ASD system (shown in Fig. 1.3) decouples the high PWM frequency switching ripples and drive dynamics from the rectifier side, the motor drive and inverter can be represented with an equivalent DC side resistor when investigating the low frequency behavior. Therefore, it is possible to study the ASD system behavior by representing the whole inverter drive system by an equivalent DC resistance R_{dc} and calculate R_{dc} from the power balance equation. Assuming a lossless system, the rated ASD power P_R is equal to the DC link power P_{dc}.

$$P_{dc} = \frac{V_{dc}^2}{R_{dc}} = P_R \tag{A1}$$

$$R_{dc} = \frac{V_{dc}^2}{P_R} = \frac{\left(\frac{3\sqrt{2} \times V_{LL}}{\pi}\right)^2}{P_R} \tag{A2}$$

Given the R_{dc} value, the next issue involves the representation of the rectifier DC side quantities on the AC side that is reflection of the DC side circuit to the AC side circuit. Assuming that the diode rectifier has unity displacement power factor and the rectifier is lossless, the fundamental component power AC and DC sides can be equated.

$$P_{ac} = \frac{3 \times V_{LN}^2}{R_{ac}} = \frac{V_{LL}^2}{R_{ac}} = P_{dc} = \frac{V_{dc}^2}{R_{dc}} = \frac{(\frac{3\sqrt{2} \times V_{LL}}{\pi})^2}{R_{dc}} \tag{A3}$$

where V_{LN} is the line-to-neutral voltage at the input to the three phase rectifier. From the above equation, R_{ac} can be obtained in terms of R_{dc}, in the following

$$R_L = R_{ac} = \frac{R_{dc}}{1.823} \tag{A4}$$

These extra assumptions used and details explained lead to the use of the simple Equation of 2.20. In the fundamental component full load model (Fig. 2.4), for highly accurate representation of the rectifier; a load inductor (L_L) should be added and connected to L_o in attempt to represent the rectifier commutation effect and the output voltage drop. The L_L empirical value is assumed to be the sum of L_i and L_o.

$$L_L = (L_i + L_o) \tag{A5}$$

It has been found that including the load inductor (L_L) in the equivalent circuit improves the accuracy of the method. To test the accuracy of the full load fundamental component equivalent circuit model of the system, the model was compared to the computer simulation based full system simulation for 5.5 kW, 380V, 50 Hz rating system. The initial filter component values of Table 2.3 were used in the study. In the computer simulation, the rectifier line-to-line voltage V_{ab} and line current I_a are measured at full load in an attempt to find the accurate equivalent AC impedance that represents the rectifier. V_{ab} and I_a have a phasor form peak values of $547\angle 138°$V and $12\angle 158°$A, respectively. To find the AC equivalent impedance Z_{ac} in the star connection configuration, V_{ab} is shifted by $+30^o$ and converted to the phase voltage value. Utilizing the I_a value, the equivalent AC rectifier side impedance is given by

$$Z_{ac} = R_{ac} + jX_{ac} = 25.9 + j4.57\Omega \tag{A6}$$

where Z_{ac} is the equivalent rectifier impedance at the AC rectifier side, R_{ac} and X_{ac} are the corresponding AC side resistance R_L and reactance ($\omega_e L_L$) values that are implemented in the full-load fundamental equivalent circuit (Fig. 2.4). The R_{dc}

estimated utilizing Equation (A2) for the 5.5 kW system result in a resistance value of 47 Ω which is very close to the simulation value (48 Ω). Employing (A4) the equivalent resistance can be found as 26.3 Ω, which is close to 25.9 Ω in (A6). The load inductor L_L value is 14.5 mH, which is a close value to the summation of L_i initial filter parameter (Table 2.3) and the utilized 4 % L_o (17.3 mH). The 50 Hz load reactance is therefore 5.4 Ω which is close to 4.57 Ω of (A6).

B. Damping Resistance (Rd) Selection Method

The IBF system along with the rectifier, involve switching transients during turn-on and turn-off of the drive. In an ASD system, the voltage and current over stresses due to the switching transients are manipulated by a DC bus pre-charge circuit. Generally, this circuit is made of a resistor in parallel with a contactor (or any switch) and the switching transients can be manipulated by controlling this switch according to the DC bus voltage level. If the DC bus voltage is below a pre-set threshold value, the switch remains off. Otherwise, the switch is turned on and remains on throughout, bypassing the pre-charge resistor. Therefore, the DC bus voltage capacitor does not experience major overvoltage stress during start-up and line voltage transients. As a result the inverter does not experience any significant overvoltage stress and the DC bus capacitor does not experience either overvoltage or overcurrent stress, leading to economical design. Presence of the broadband filter in the system involves introduction of additional dynamics to the system.

An IBF can be directly connected to the ASD terminals with no additional switches. However, a three-phase switch or contactor must be placed between the AC line and the IBF terminals. When turning this three-phase switch on or off, additional dynamics are excited. Considering that the pre-charge circuit manipulates the rectifier and drive side dynamics, the only problematic transients remaining would be on the AC side and related to the IBF components. Therefore the IBF structure and damping characteristics are important in determining the system behaviour.

In order to have a high efficiency system, the IBF components are designed and built with high efficiency characteristics (typically 97-99% efficient) and this implies very low damping filter structure. As a result, when enabling the input contactors, the filter experiences voltage and current overstress. Specifically, the capacitor voltage and filter output voltage can become excessively large. In order to damp the switching over-voltages, a damping resistor is necessary. In the IBF structure, as shown in Fig. 2.1, the damping resistor R_d is located across the L_i and L_f total system. Its duty is to specifically damp the turn-on transient over-voltages (reduce the voltage overshoot) across the AC filter capacitors and the rectifier terminals. The choice of R_d involves two criterions, low filter capacitor voltage overshoot and low energy dissipation. While the filter energy efficiency criteria requires high energy efficiency corresponding to large R_d, the voltage overshoot criteria requires low overshoot corresponding to small R_d (high damping). Therefore, a trade-off exists between steady-state and dynamic performance, and a computer simulation approach has been utilized through a detailed procedure to optimize its value.

An ASD system with IBF structure has been considered for the detailed system simulation. Two power ratings, 5.5 kW and 55 kW have been investigated. The filter component values selected are those listed in Table 4.1. Computer simulations have been conducted via Simplorer Student Version (Version 7). In the computer simulations, the inverter drive was modelled with an equivalent DC load in order to simplify the simulations. The simulation involves the start-up transient where the IBF input switch is turned-on and the filter is pre-charged followed by the DC bus capacitor charging. Further details of the simulation model and simulation software program have been provided in chapter 4. At this stage the damping resistor related results are presented.

For 5.5 kW, as Fig. B.1 indicates the AC filter capacitor is sensitive to line voltage switching transients, while the DC bus capacitor and the rectifier terminal voltages do not experience major voltage overshoot. Therefore, the voltage overshoot on C_f is what requires attention. The figure illustrates that the capacitor voltage overshoot has a saturation curve, indicating an R_d greater than 300 Ω does not have any damping effect and significant damping is achieved at 100 Ω or less. However, as

Fig. B.2 indicates, when R_d is near 100 Ω the input current THDi and filter losses increase (system efficiency decreases) significantly. Therefore, a damping resistor with a value less than 100 Ω is prohibitive from the efficiency and THDi point of view, while a value greater than 300 Ω is prohibitive from the capacitor voltage overshoot point of view. Depending on whether efficiency or component oversizing related cost is more emphasized in the design, a value in this range must be selected. Similarly for 55 kW ratings, computer simulations have been conducted and the results are shown in Fig. B.3 and Fig. B.4. As a summary the R_d parameter for each power rating can be chosen within the range shown in Table A.1.

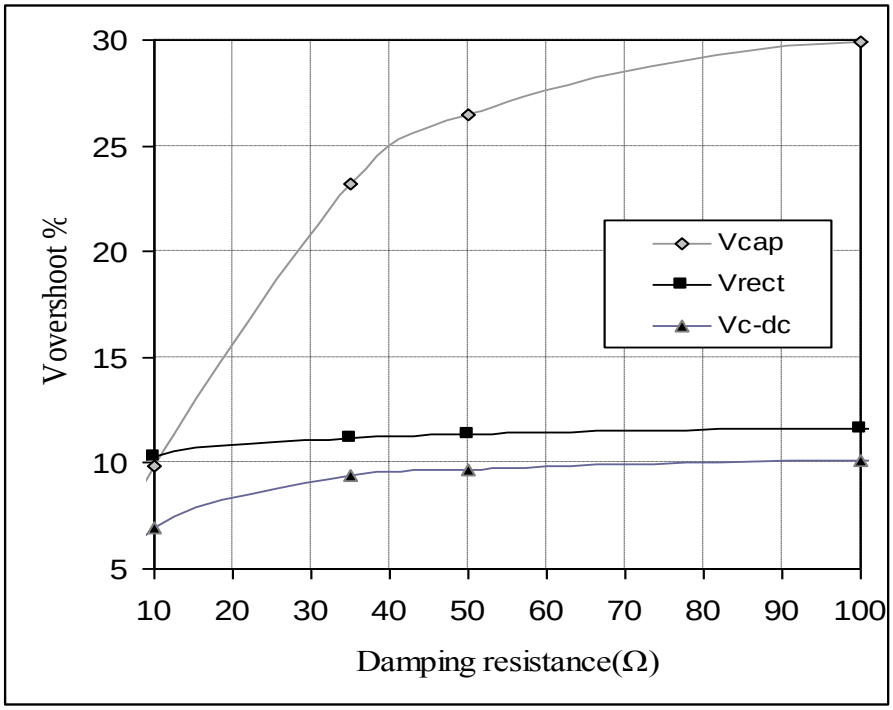

Fig. B.1 Voltage overshoot for various R_d values (5.5kW system).

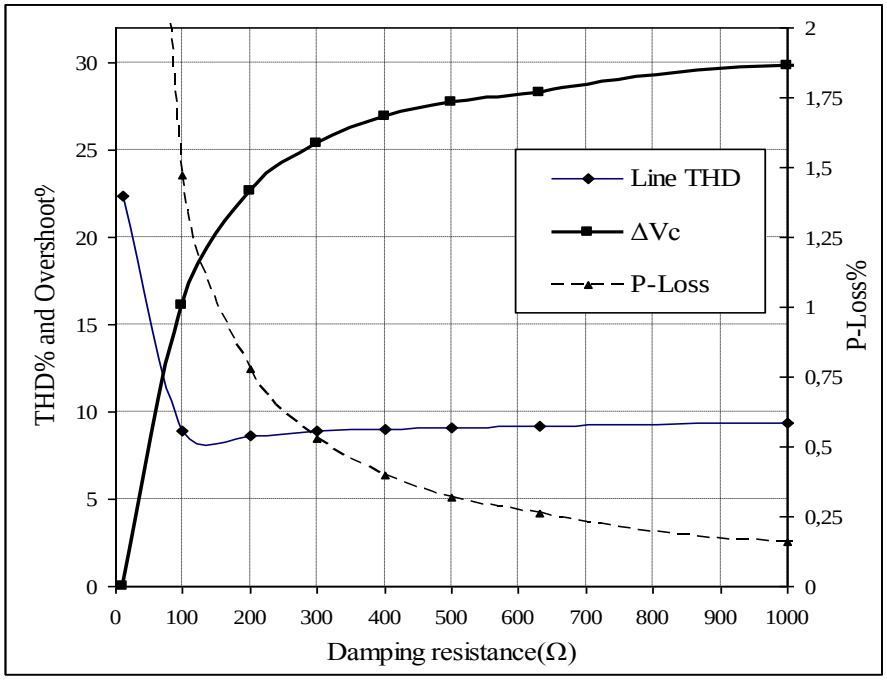

Fig. B.2 Voltage overshoot, line THDi and R_d losses for various R_d (5.5kW system).

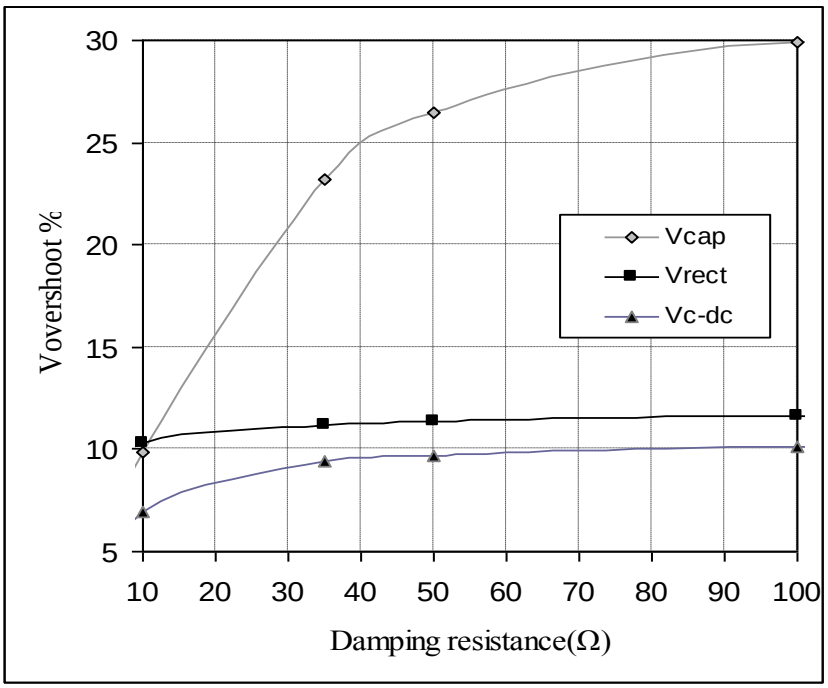

Fig. B.3 Voltage overshoot for various Rd values (55kW system).

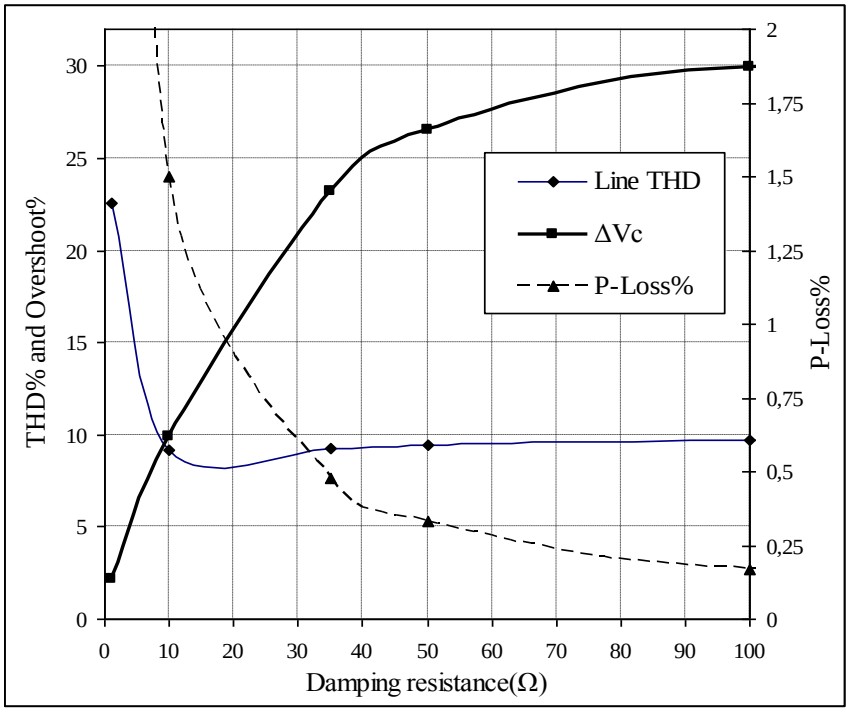

Fig. B.4 Voltage overshoot, line THDi and R_d losses for various R_d (55kW system).

C. Fundamental and rms stiffness factors (β_1 and β_{rms}) simulation based values estimation

Table C.1 Stiffness factors β_1 and β_{rms} values for various passive filtering topologies for 5.5 kW ASD system

Filter Type	Rectifier Current Waveform	THD_I (%)	I_{dc} Mean (A)	I_1 rms (A)	β_1	β_{rms}
L_{dc} (∞)		24	10.57	8.23	0.779	0.801
6% L_{ac}	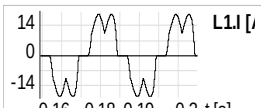	31	11.30	8.86	0.784	0.820
TF 5^{th},7^{th}	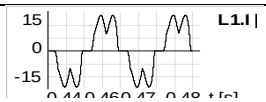	33	11.05	8.67	0.785	0.825
4% L_{ac}	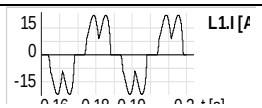	36	11.16	8.79	**0.787**	**0.837**
3% L_{ac}	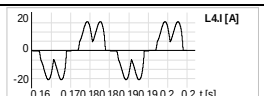	41	11.14	8.79	0.789	0.854
IBF	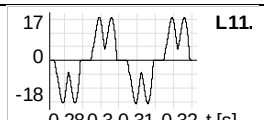	44	10.65	8.43	0.791	0.893
0% L_{ac}	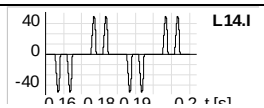	135	10.38	8.44	0.813	1.369

D. Extra IBF Simulation Results

D.1 BF Half-Load Simulations of 5.5 kW ASD System

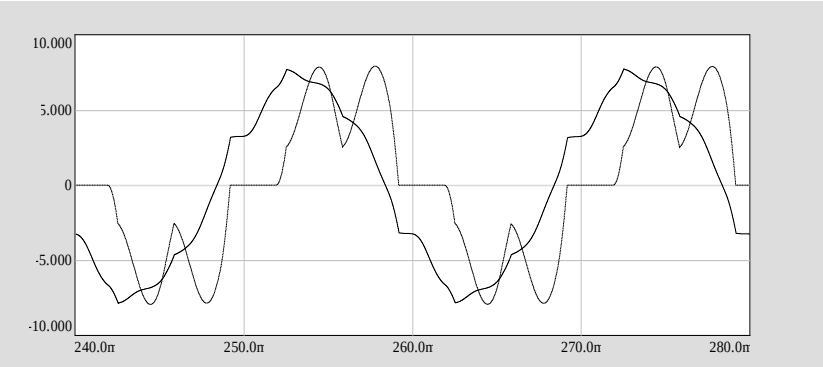

Fig. D.1 Line and rectifier (doted) current simulation waveforms at half-load for 5.5kW rated system employing IBF.

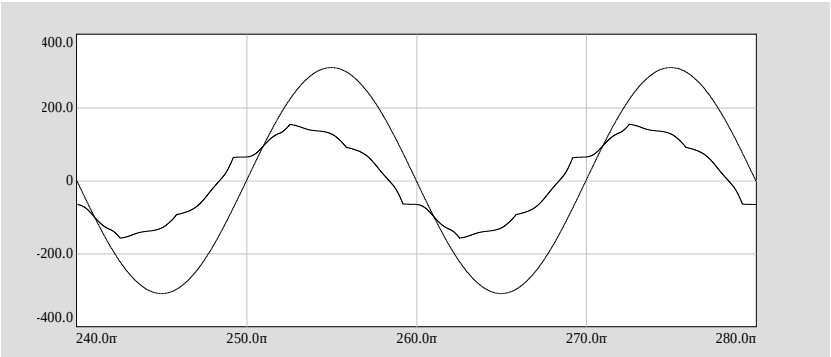

Fig. D.2 Line current and supply voltage (doted) simulation waveforms at half-load for 5.5kW rated system employing IBF (current scale: 20x).

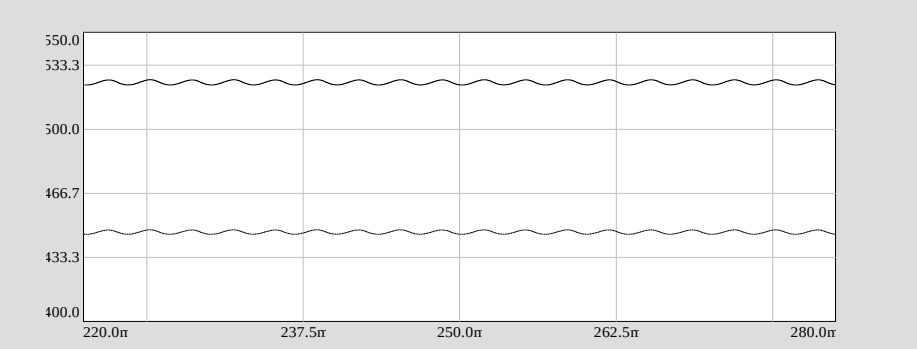

Fig. D.3 DC load current (doted) and voltage 524V simulation waveforms at Half-load for 5.5kW rated system employing IBF (current scale: 80x5.58).

D.2 IBF Half-Load Simulations of 55 kW ASD System

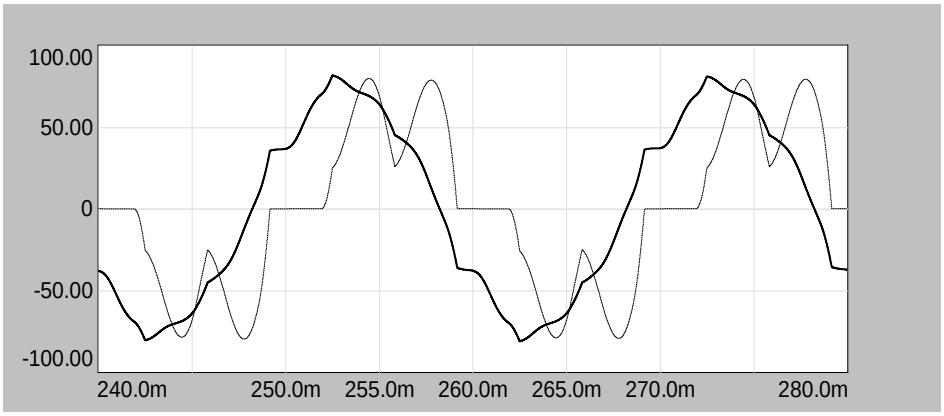

Fig. D.4 Line and rectifier (doted) current simulation waveforms at half-load for 55kW rated system employing IBF.

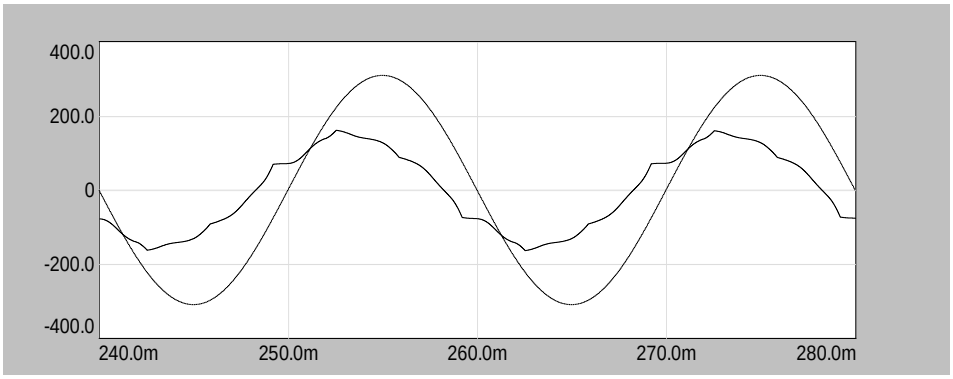

Fig. D.5 Line current and supply voltage (doted) simulation waveforms at half-load for 55kW rated system employing IBF (current scale: 2x).

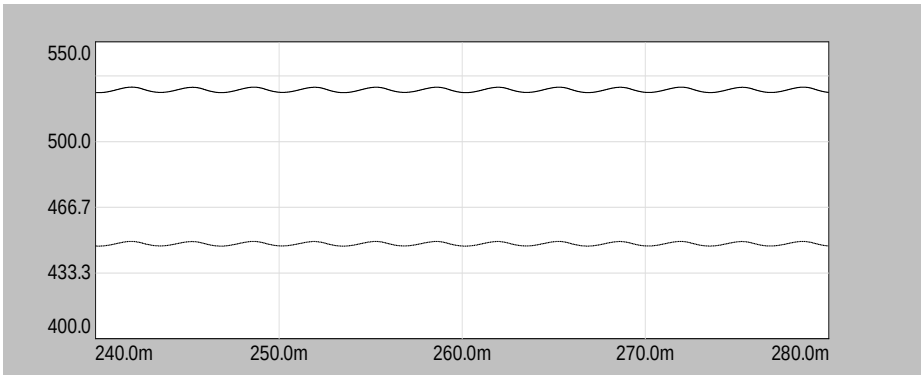

Fig. D.6 DC load current (doted) and voltage simulation waveforms at Half-load for 55kW rated system employing IBF (current scale: 8x).

E. Extra IBF Experimental Results of 5.5kW ASD System

E.1. IBF 75% Load Experimental Results

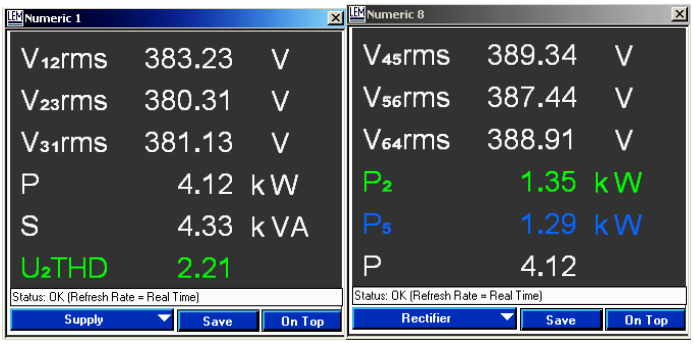

Fig. E.1 Supply and rectifier side experimental data at 75% load for 5.5kW rated system employing IBF filter (line and rectifier line-to-line voltage, total real and apparent power and supply voltage THD_V%).

Fig. E.2 Line side experimental data for phases 1, 2 and 3 at 75% load for 5.5kW rated system employing IBF filter (voltage V, current I, real power P, current THDi%, reactive power Q, power factor ʎ).

Fig. E.3 Rectifier side experimental data for phases 4, 5 and 6 at 75% load for 5.5kW rated system employing IBF filter (voltage V, current I, real power P, current THDi%, reactive power Q, power factor ʎ).*

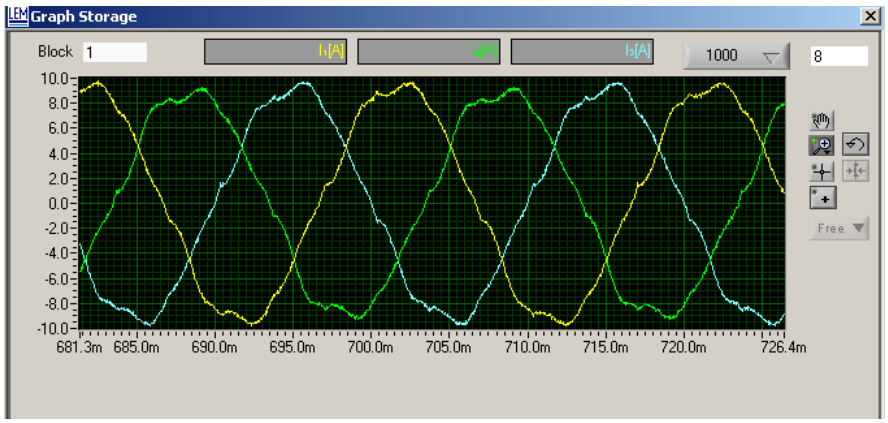

Fig. E.4 Line side 3-phase current experimental waveforms at 75% load for 5.5kW rated system employing IBF filter.

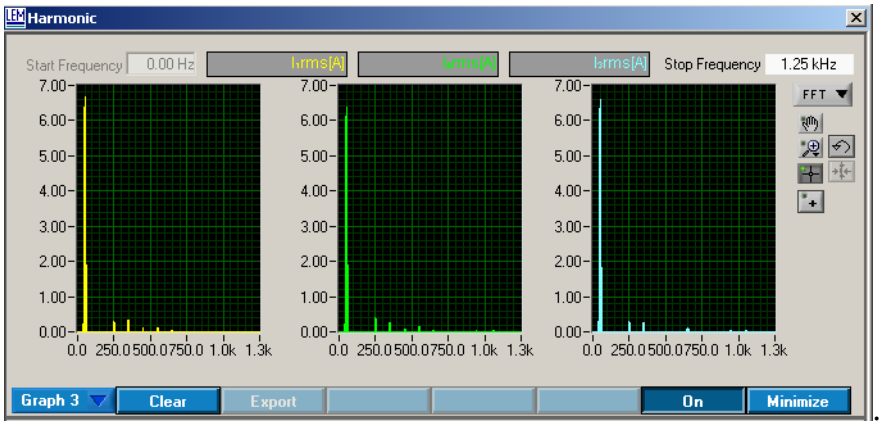

Fig. E.5 Line side 3-phase current harmonic spectrum at 75% load for 5.5kW rated system employing IBF filter.

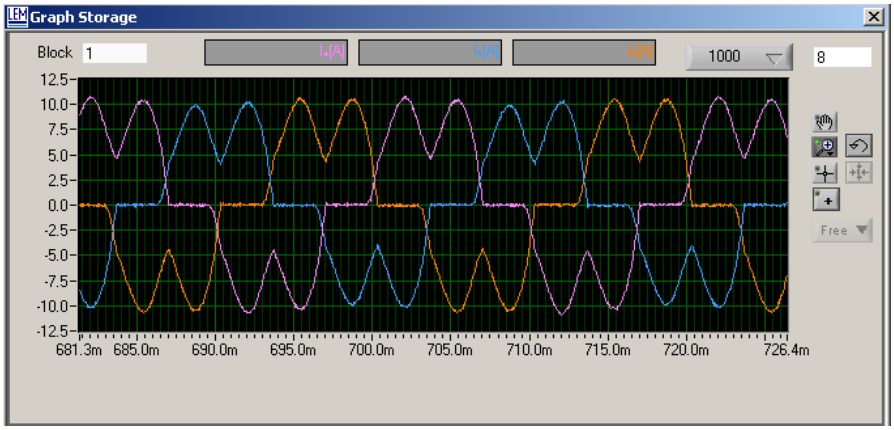

Fig. E.6 Rectifier side 3-phase current experimental waveforms at 75% load for 5.5kW rated system employing IBF filter.

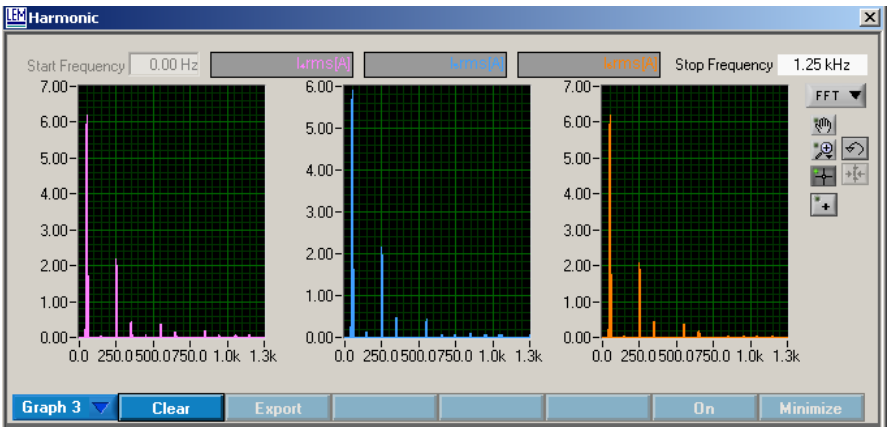

Fig. E.7 Rectifier side 3-phase current harmonic spectrum at 75% load for 5.5kW rated system employing IBF filter.

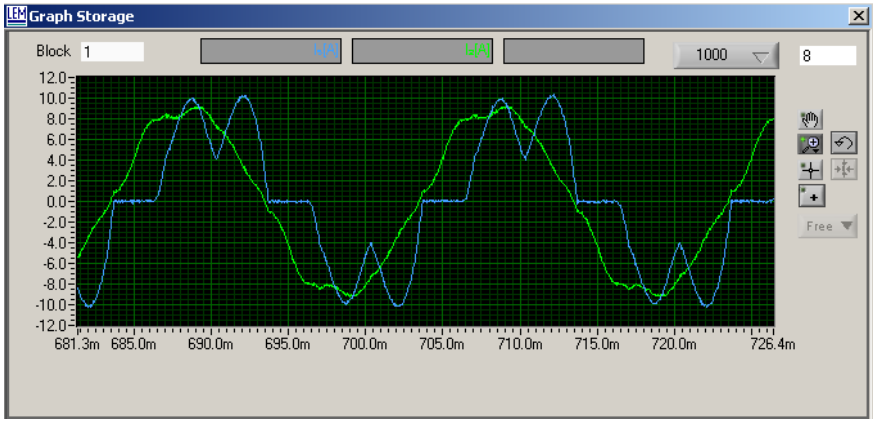

Fig. E.8 Line and rectifier current experimental waveforms at 75% load for 5.5kW rated system employing IBF filter.

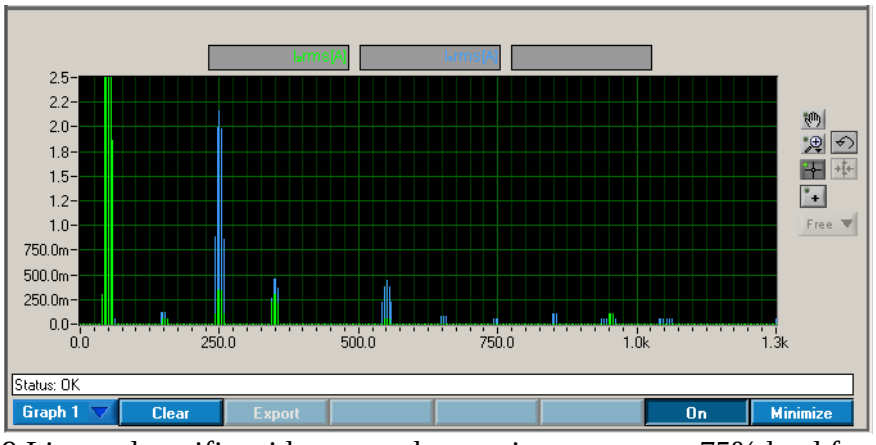

Fig. E.9 Line and rectifier side current harmonic spectrum at 75% load for 5.5kW rated system employing IBF filter (Zoomed).

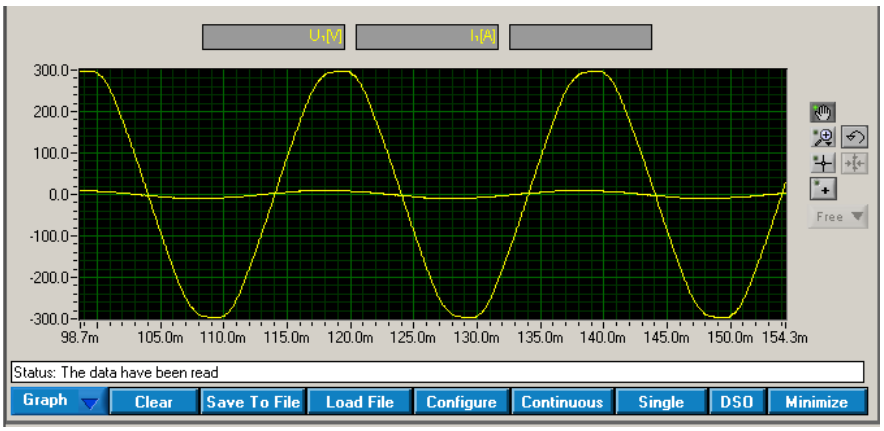

Fig. E.10 Supply phase voltage and current experimental waveforms at 75% load for 5.5kW rated system employing IBF filter.

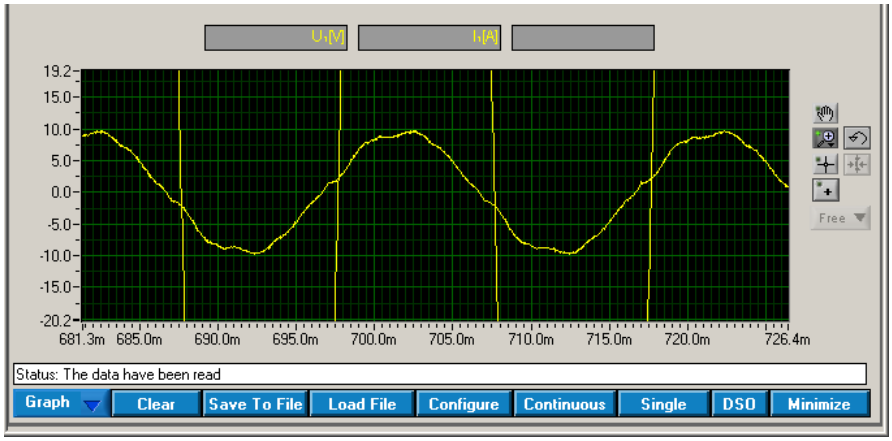

Fig. E.11 Supply phase voltage and current experimental waveforms at 75% load for 5.5kW rated system employing IBF filter (Zoomed).

E.2 IBF 60% Load Experimental Results

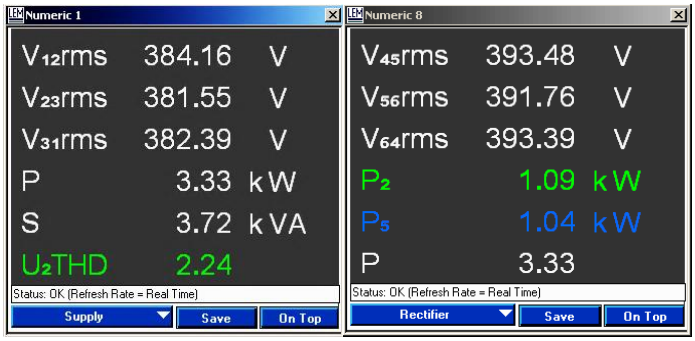

Fig. E.12 Supply and rectifier side experimental data at 60% load for 5.5kW rated system employing IBF filter (line and rectifier line-to-line voltage, total real and apparent power and supply voltage THD_V%).

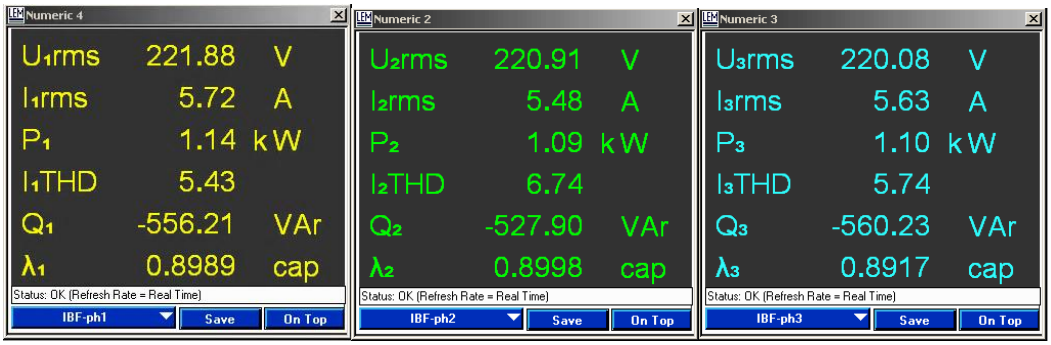

Fig. E.13 Line side experimental data for phases 1, 2 and 3 at 60% load for 5.5kW rated system employing IBF filter (voltage V, current I, real power P, current THDi%, reactive power Q, power factor ʎ).

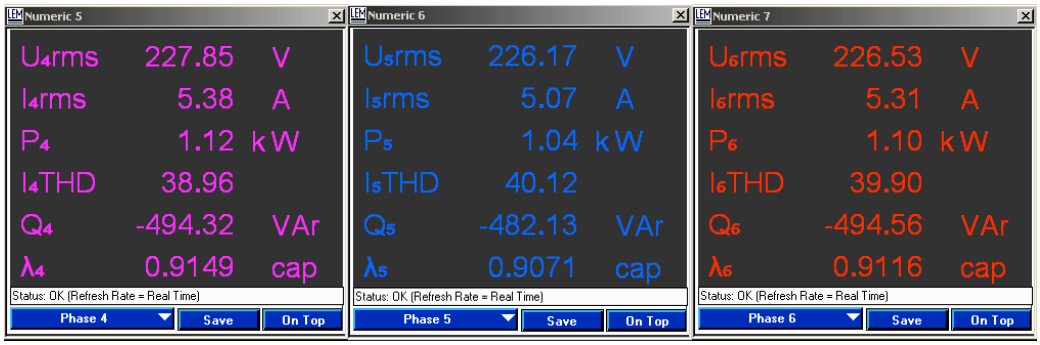

Fig. E.14 Rectifier side experimental data for phases 4, 5 and 6 at 60% load for 5.5kW rated system employing ABF filter (voltage V, current I, real power P, current THDi%, reactive power Q, power factor ʎ).*

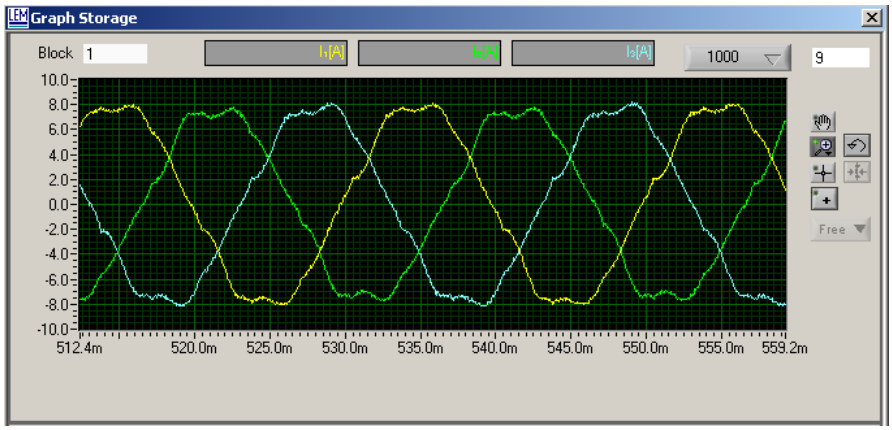

Fig. E.15 Line side 3-phase current experimental waveforms at 60% load for 5.5kW rated system employing IBF filter.

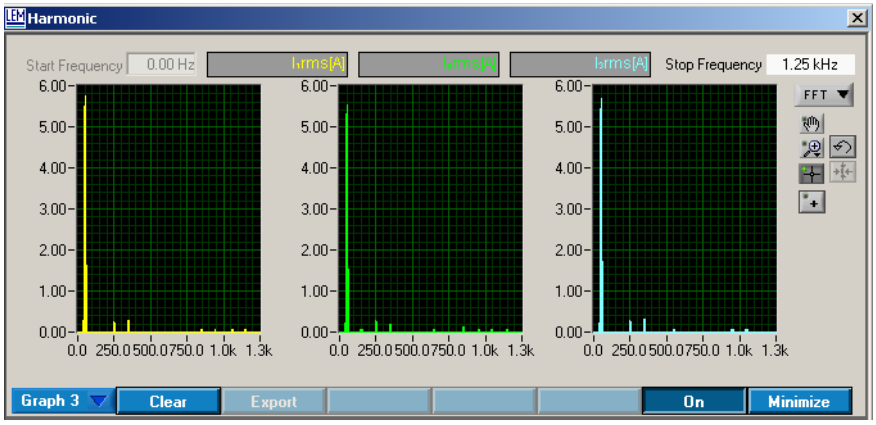

Fig. E.16 Line side 3-phase current harmonic spectrum at 60% load for 5.5kW rated system employing IBF filter.

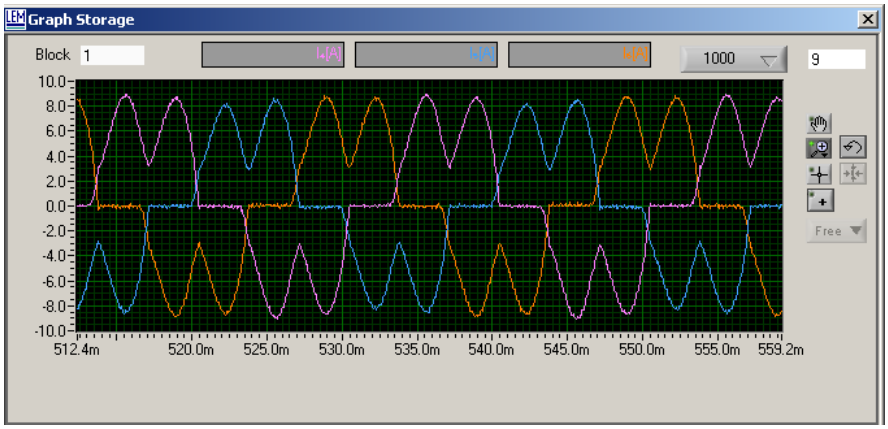

Fig. E.17 Rectifier side 3-phase current experimental waveforms at 60% load for 5.5kW rated system employing IBF filter.

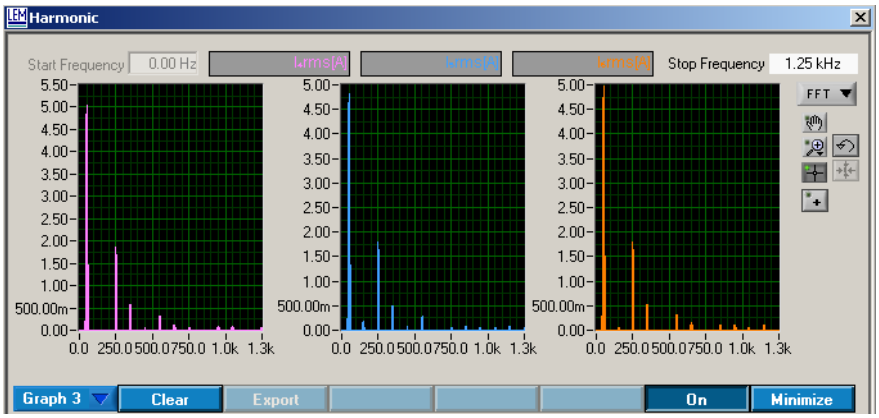

Fig. E.18 Rectifier side 3-phase current harmonic spectrum at 60% load for 5.5kW rated system employing IBF filter.

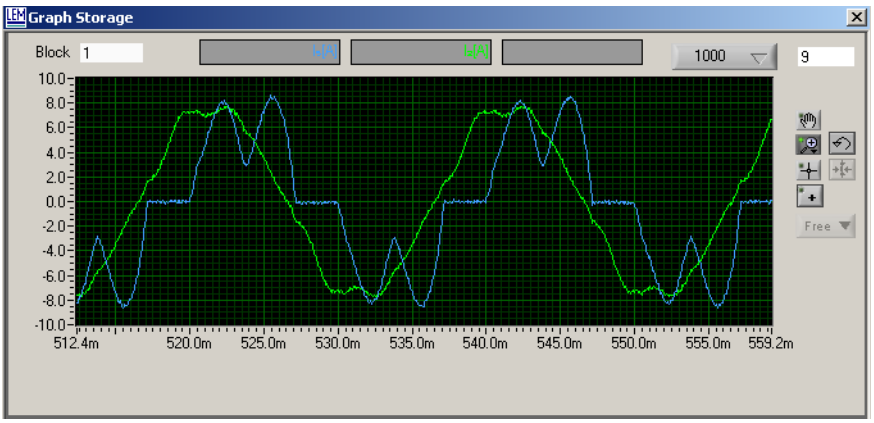

Fig. E.19 Line and rectifier current experimental waveforms at 60% load for 5.5kW rated system employing IBF filter.

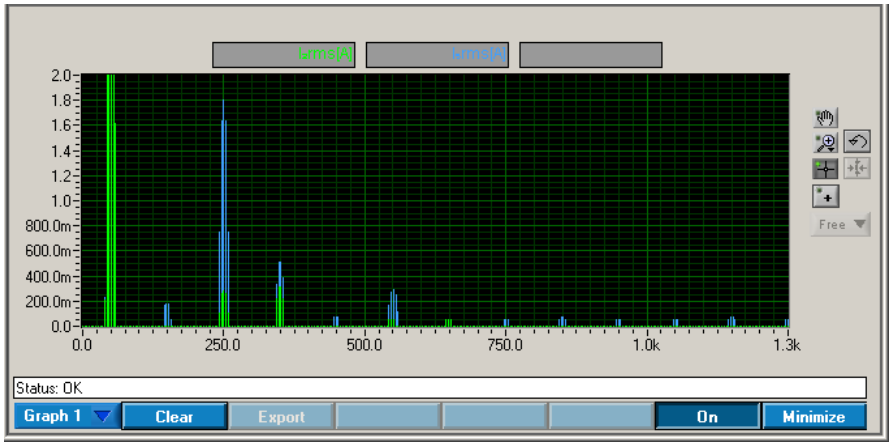

Fig. E.20 Line and rectifier side current harmonic spectrum at 60% load for 5.5kW rated system employing IBF filter (Zoomed).

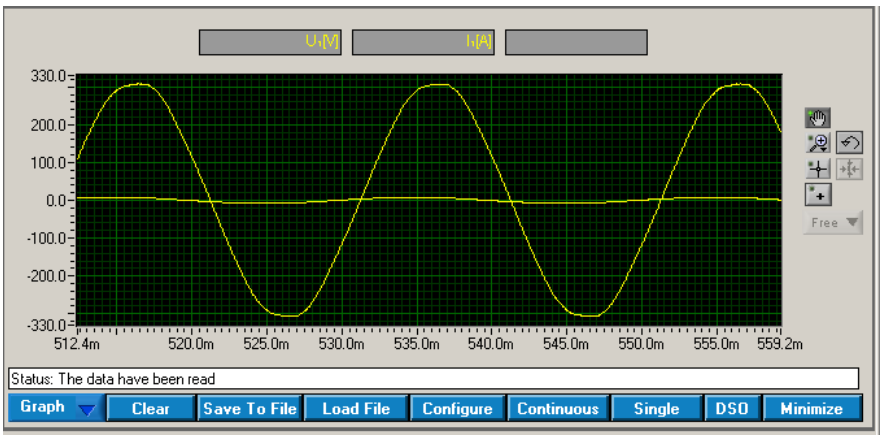

Fig. E.21 Supply phase voltage and current experimental waveforms at 60% load for 5.5kW rated system employing IBF filter.

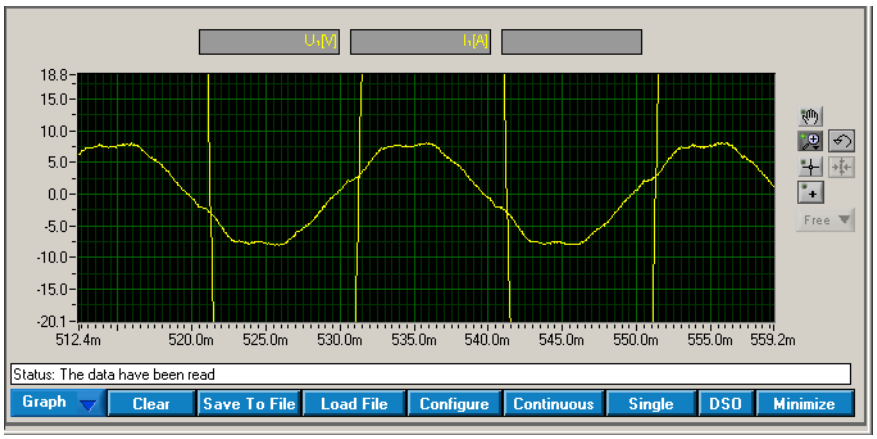

Fig. E.22 Supply phase voltage and current experimental waveforms at 60% load for 5.5kW rated system employing IBF filter (Zoomed).

E.3 IBF 400V Full-load Experimental Results

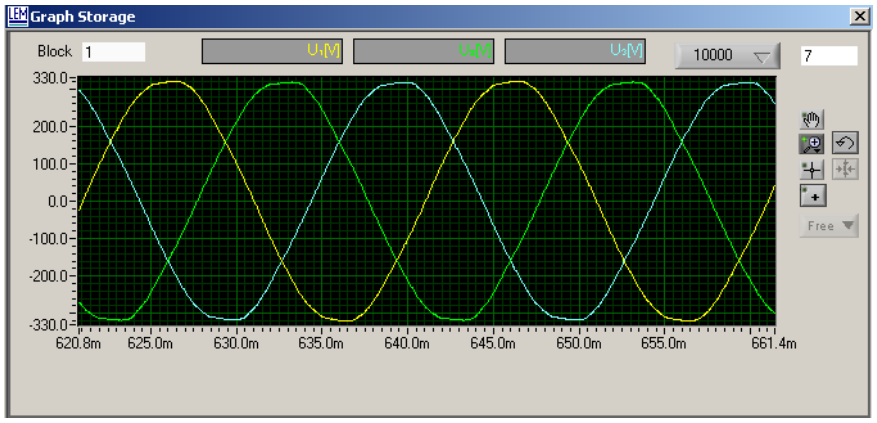

Fig. E.23 Line side 3-phase voltage experimental waveforms at full-load for 5.5kW rated system employing IBF filter (400 V_{LL}).

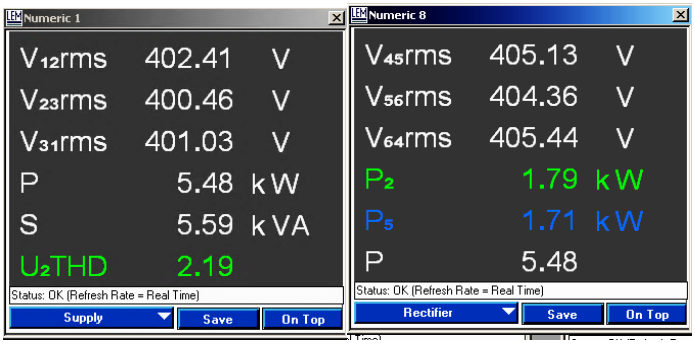

Fig. E.24 Supply and rectifier side experimental data at full-load for 5.5kW rated system employing IBF filter (line voltage, real power, apparent power and supply voltage THD_V%).

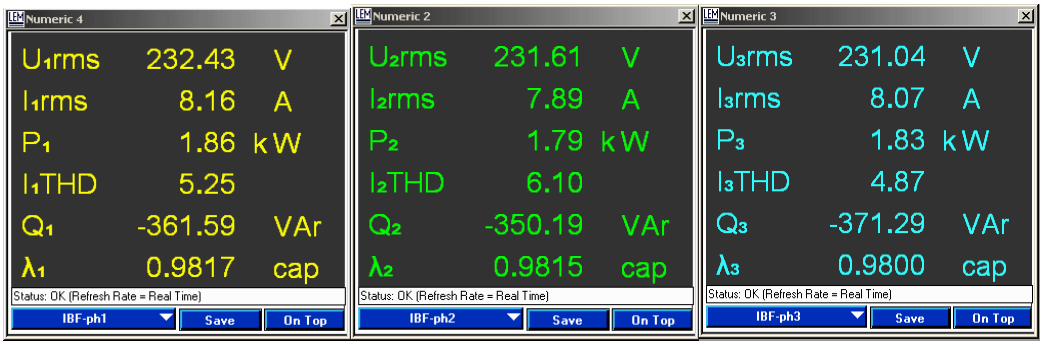

Fig. E.25 Line side experimental data for phases 1, 2 and 3 at full-load for 5.5kW rated system employing IBF filter (voltage V, current I, real power P, current THDi%, reactive power Q, power factor ʎ).

Fig. E.26 Rectifier side experimental data for phases 4, 5 and 6 at full-load for 5.5kW rated system employing IBF filter (voltage V, current I, real power P, current THDi%, reactive power Q, power factor ʎ).*

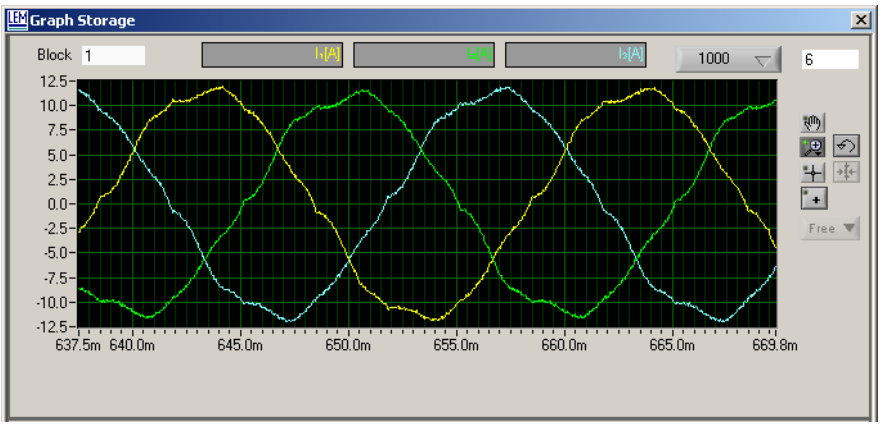

Fig. E.27 Line side 3-phase current experimental waveforms at full-load for 5.5kW rated system employing IBF filter.

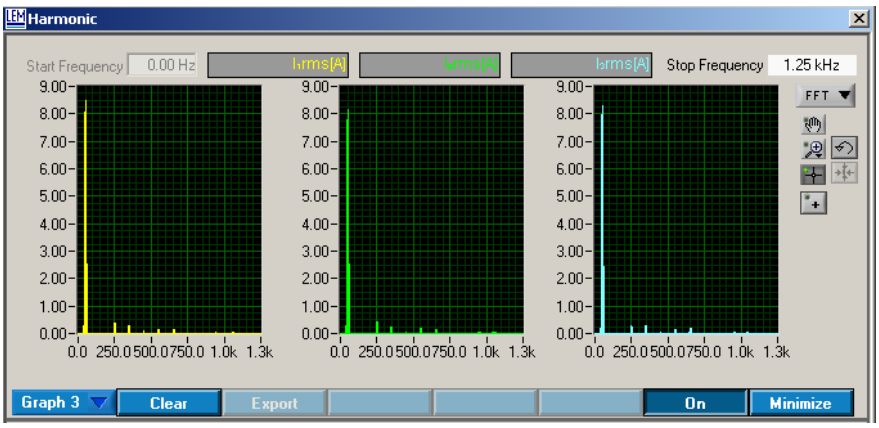

Fig. E.28 Line side 3-phase current harmonic spectrum at full-load for 5.5kW rated system employing IBF filter.

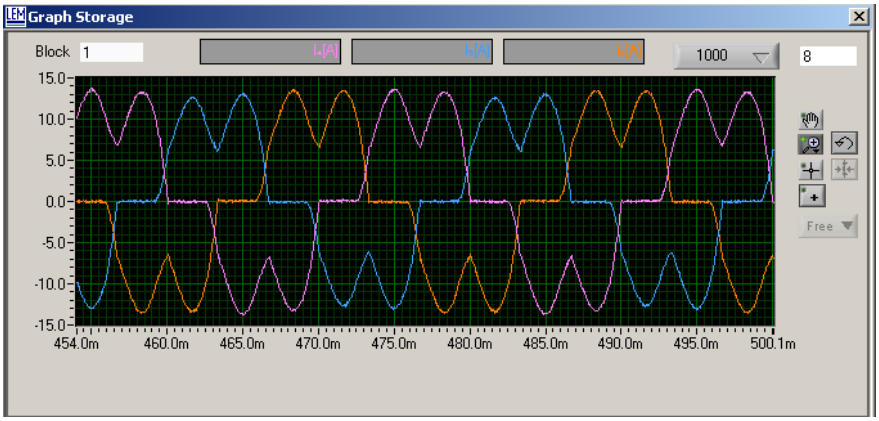

Fig. E.29 Rectifier side 3-phase current experimental waveforms at full-load for 5.5kW rated system employing IBF filter.

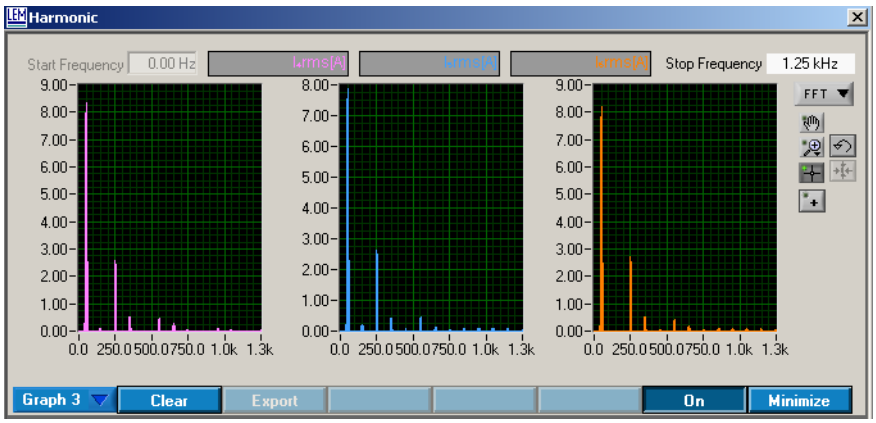

Fig. E.30 Rectifier side 3-phase current harmonic spectrum at full-load for 5.5kW rated system employing IBF filter.

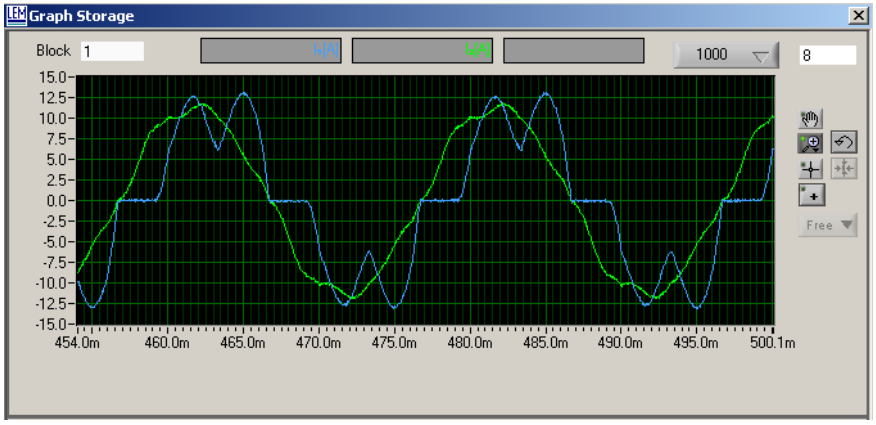

Fig. E.31 Line and rectifier current experimental waveforms at full-load for 5.5kW rated system employing IBF filter.

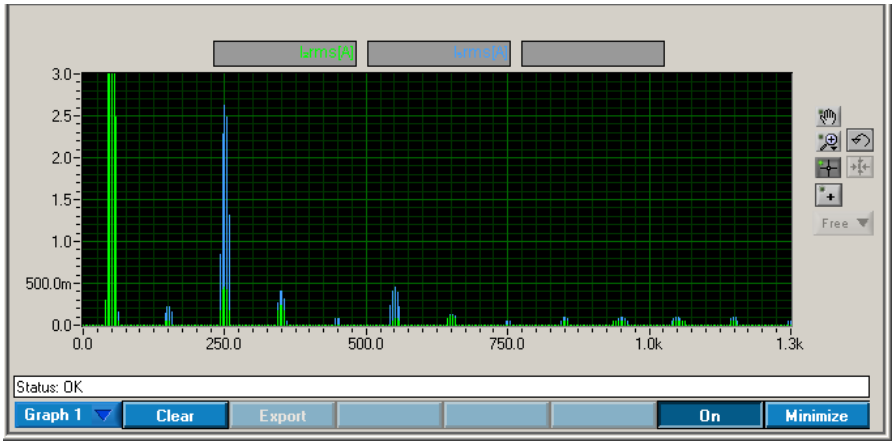

Fig. E.32 Line and rectifier side current harmonic spectrum at full-load for 5.5kW rated system employing IBF filter (Zoomed).

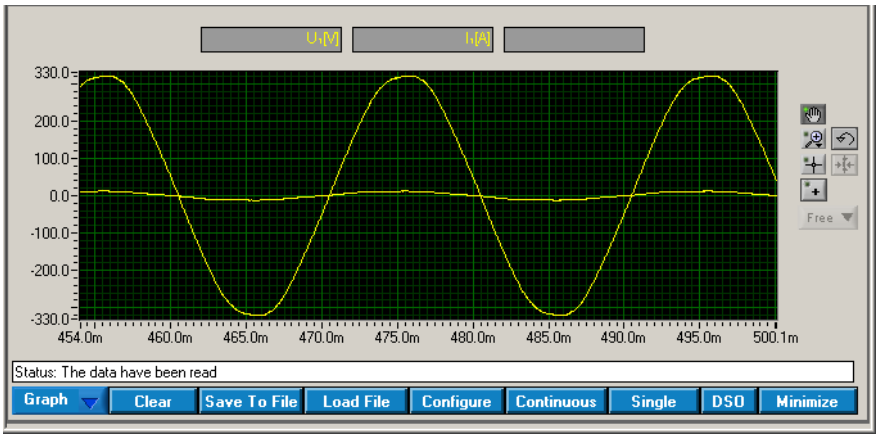

Fig. E.33 Supply phase voltage and current experimental waveforms at full-load for 5.5kW rated system employing IBF filter.

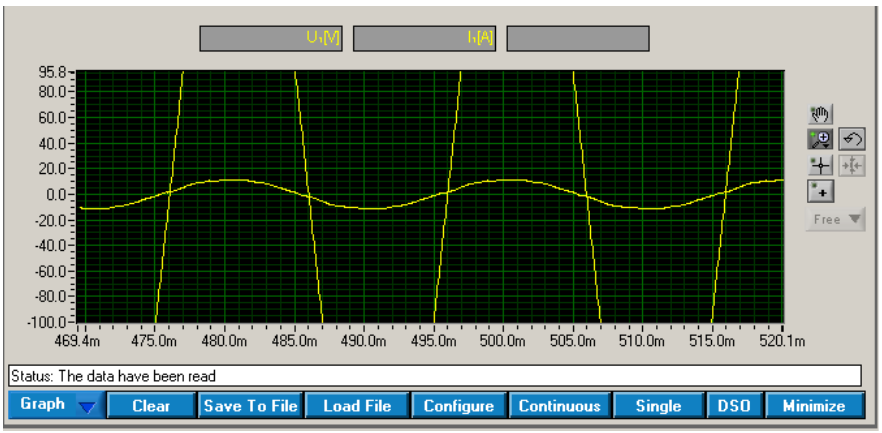

Fig. E.34 Supply phase voltage and current experimental waveforms at full-load for 5.5kW rated system employing IBF filter (Zoomed).

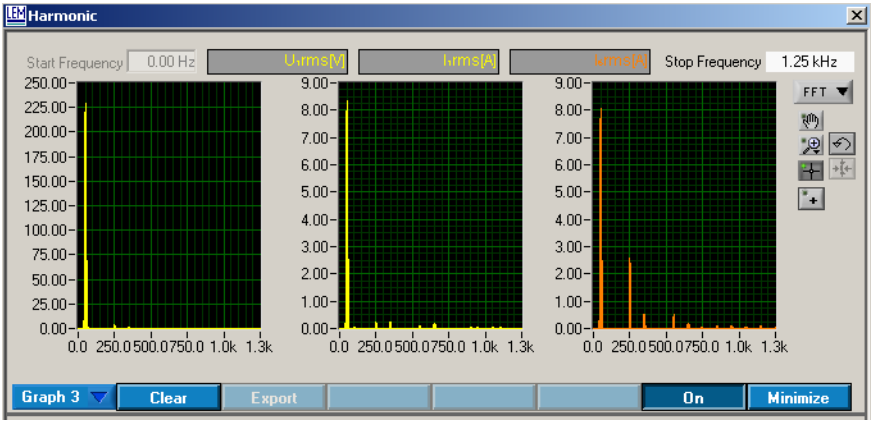

Fig. E.35 Phase voltage, line current and rectifier current harmonic spectrum at full-load for 5.5kW rated system employing IBF filter.

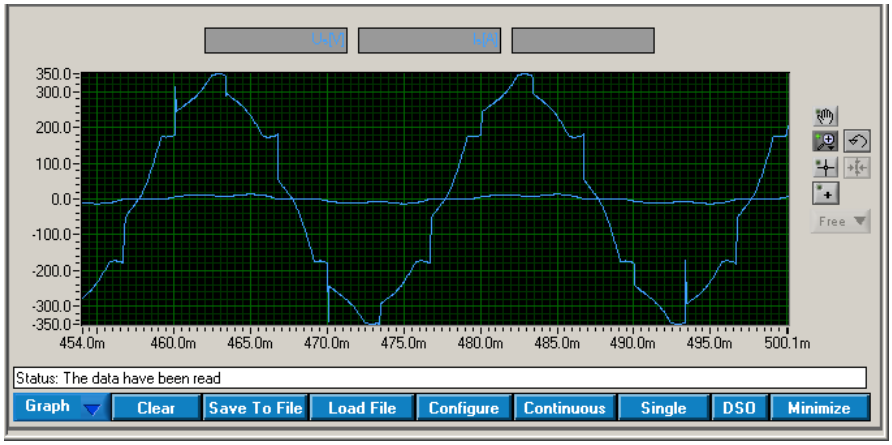

Fig. E.36 Rectifier side phase voltage and current experimental waveforms at full-load for 5.5kW rated system employing IBF filter.

E.4 IBF 400V No-Load Experimental Results

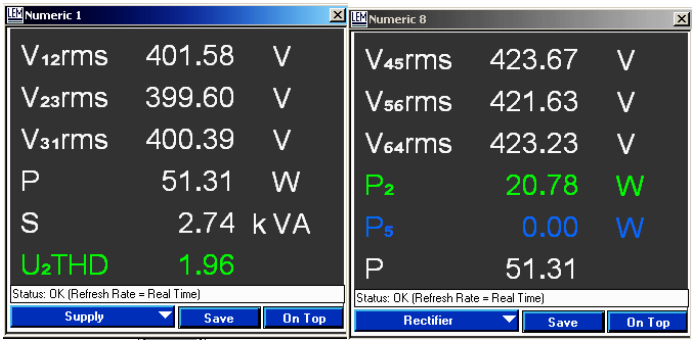

Fig. E.37 Supply and rectifier side experimental data at no-load for 5.5kW rated system employing IBF filter (line and rectifier line-to-line voltage, total real and apparent power and supply voltage THD_V%).

Fig. E.38 Line side experimental data for phases 1, 2 and 3 at no-load for 5.5kW rated system employing IBF filter (voltage V, current I, real power P, current THDi%, reactive power Q, power factor ʎ).

Fig. E.39 Rectifier side experimental data for phases 4, 5 and 6 at no-load for 5.5kW rated system employing IBF filter (voltage V, current I, real power P, current THDi%, reactive power Q, power factor ʎ).

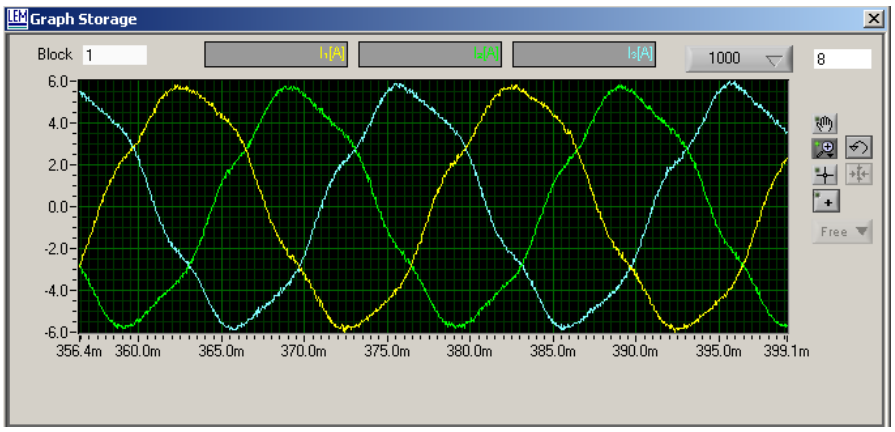

Fig. E.40 Line 3-phase current experimental waveforms at no-load for 5.5kW rated system employing IBF filter.

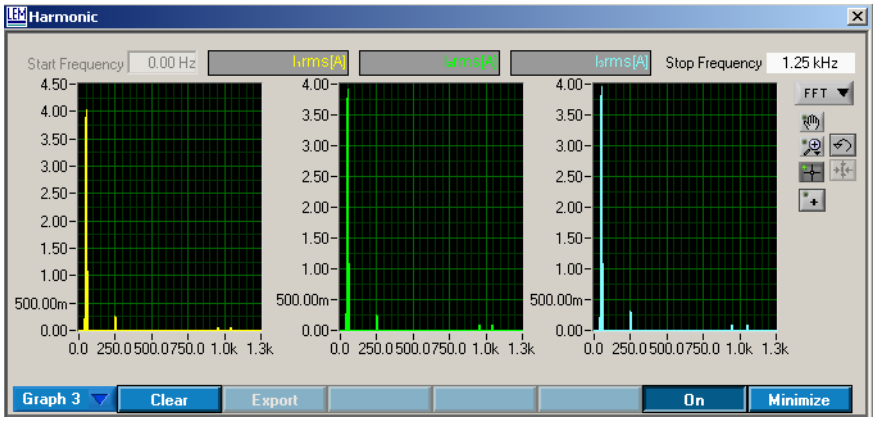

Fig. E.41 Line side 3-phase current harmonic spectrum at no-load for 5.5kW rated system employing IBF filter.

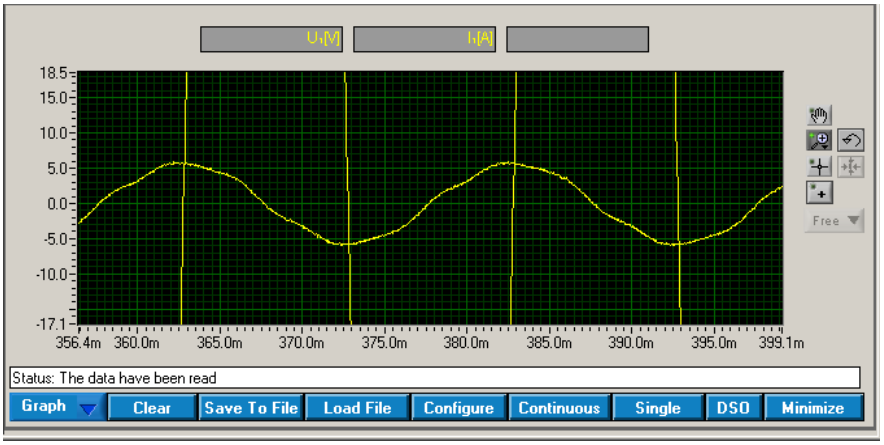

Fig. E.42 Supply phase voltage and current experimental waveforms at no-load for 5.5kW rated system employing IBF filter (Zoomed).

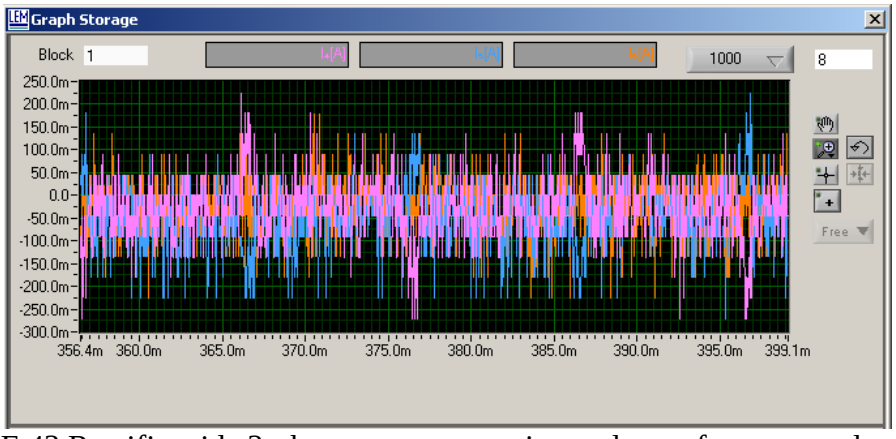

Fig. E.43 Rectifier side 3-phase current experimental waveforms at no-load for 5.5kW rated system employing IBF filter.

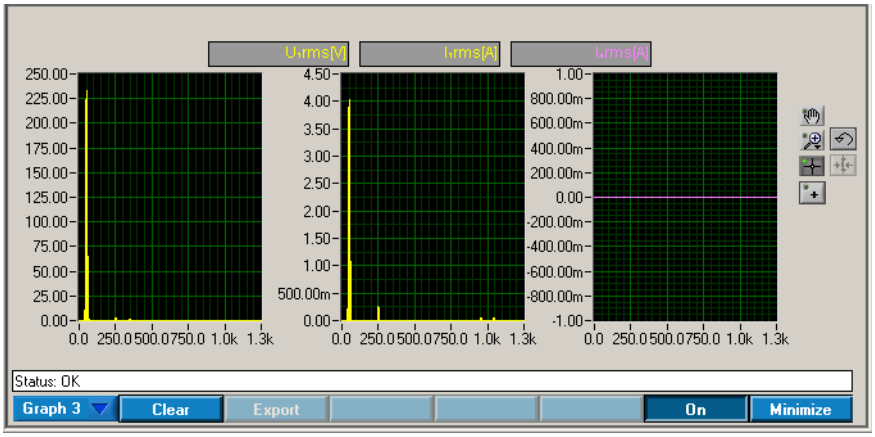

Fig. E.44 Phase voltage, line current and rectifier current harmonic spectrum at no-load for 5.5kW rated system employing IBF filter.

F. Extra ABF Simulation Results

F.1 ABF Half-Load Simulations of 5.5 kW ASD System

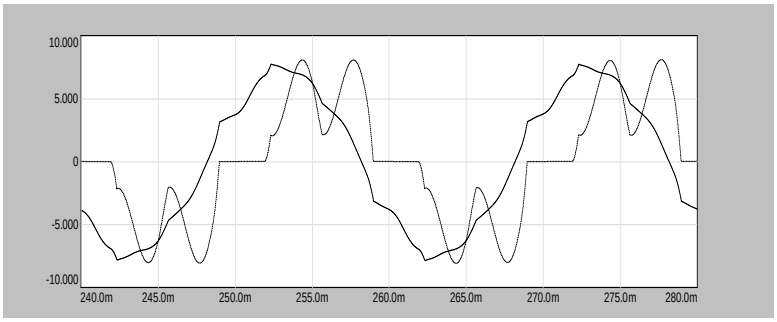

Fig. F.1 Line and rectifier (doted) current simulation waveforms at half-load for 5.5kW rated system employing IBF.

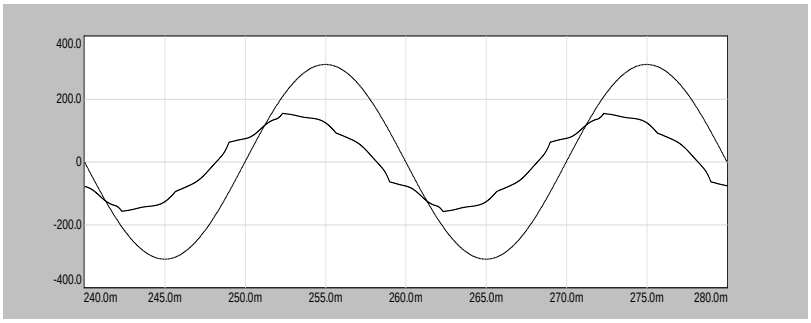

Fig. F.2 Line current and supply voltage (doted) simulation waveforms at half-load for 5.5kW rated system employing IBF (current scale: 20x).

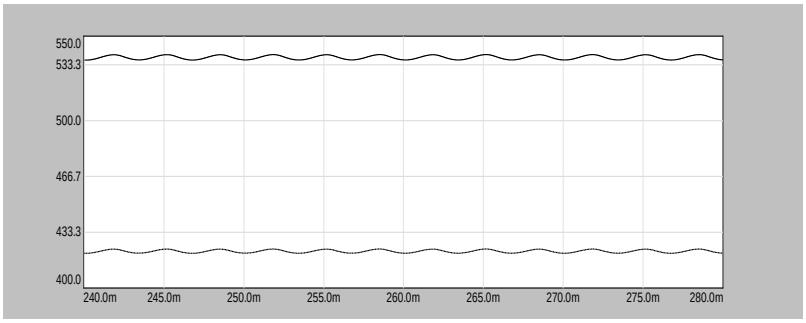

Fig. F.3 DC load current (doted) and voltage simulation waveforms at Half-load for 5.5kW rated system employing IBF (current scale: 80).

F.2 ABF Half-Load Simulations of 55 kW ASD System

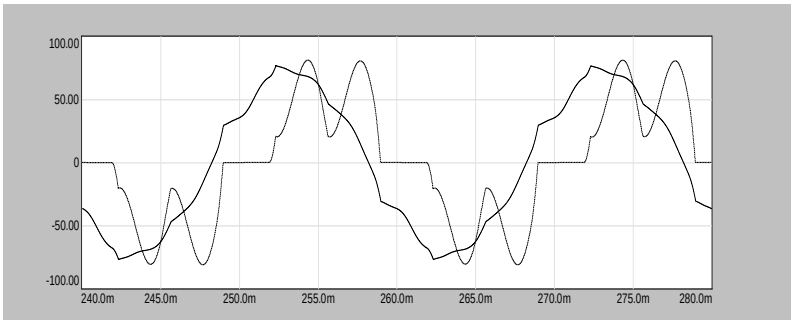

Fig. F.4 Line and rectifier (doted) current simulation waveforms at half-load for 55kW rated system employing IBF.

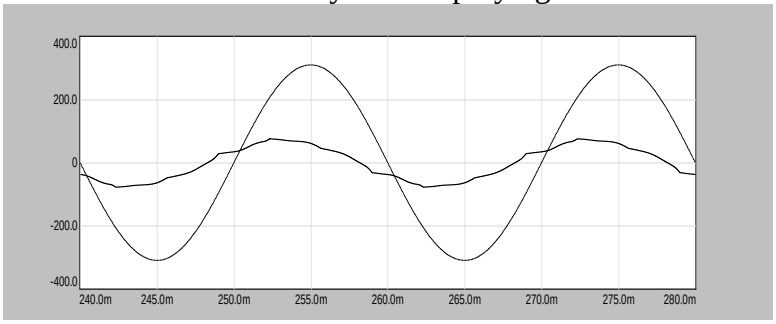

Fig. F.5 Line current and supply voltage (doted) simulation waveforms at half-load for 55kW rated system employing IBF.

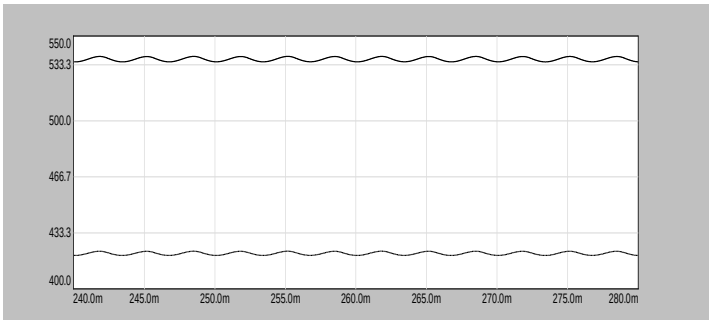

Fig. F.6 DC load current (doted) and voltage simulation waveforms at Half-load for 55kW rated system employing IBF (current scale: 8x52.6).

G. Extra ABF Experimental Results of 5.5kW ASD System

G.1 ABF 75% Load Experimental Results

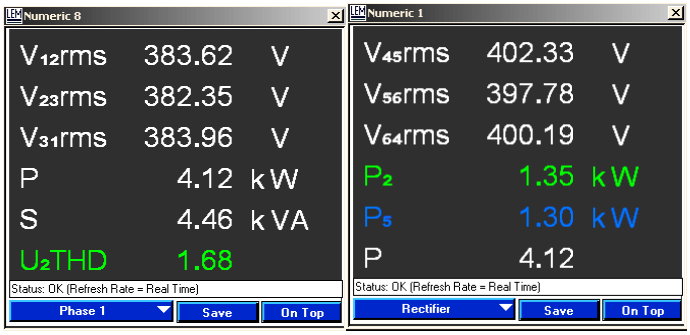

Fig. G.1 Supply and rectifier side experimental data at 75% load for 5.5kW rated system employing ABF filter (line voltage, real power, apparent power and supply voltage THD_V%).

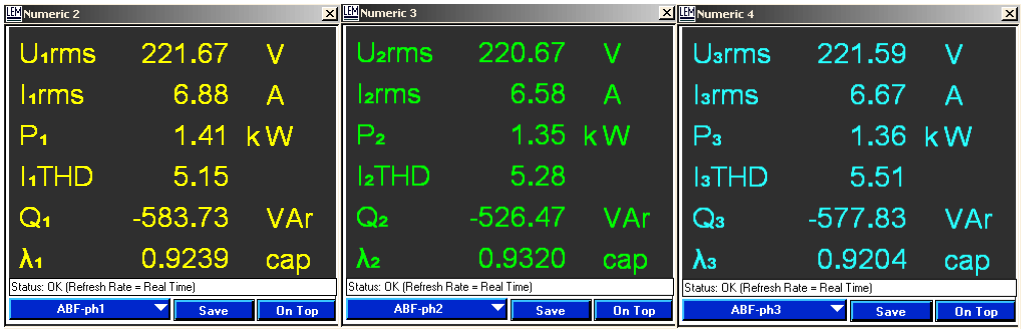

Fig. G.2 Line side experimental data for phase 1, 2 and 3 at 75% load for 5.5kW rated system employing ABF filter (voltage V, current I, real power P, current THDi%, reactive power Q, power factor λ).

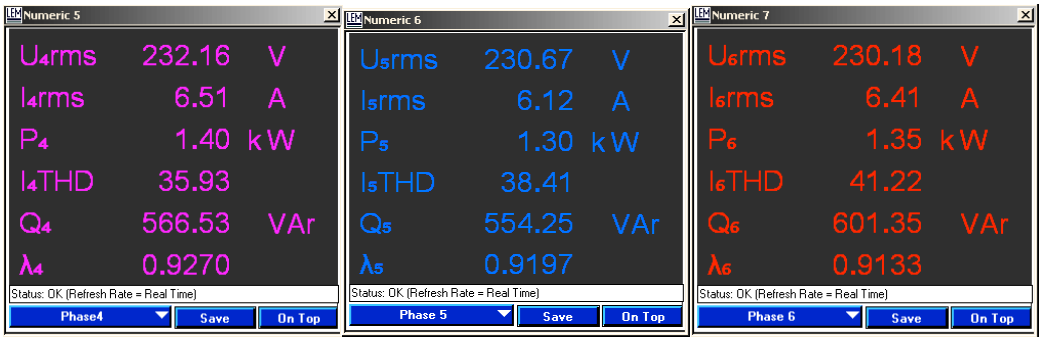

Fig. G.3 Rectifier side experimental data for phase 4, 5 and 6 at 75% load for 5.5kW rated system employing ABF filter (voltage V, current I, real power P, current THDi%, reactive power Q, power factor ʎ).

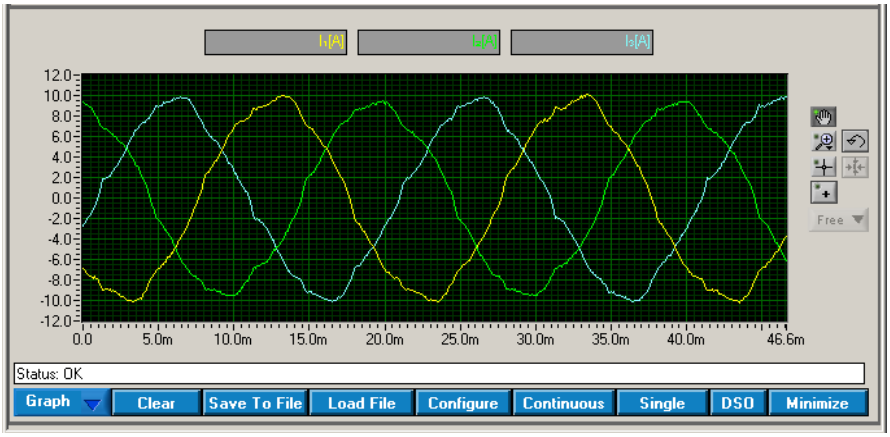

Fig. G.4 Line side 3-phase current experimental waveforms at 75% load for 5.5kW rated system employing ABF filter.

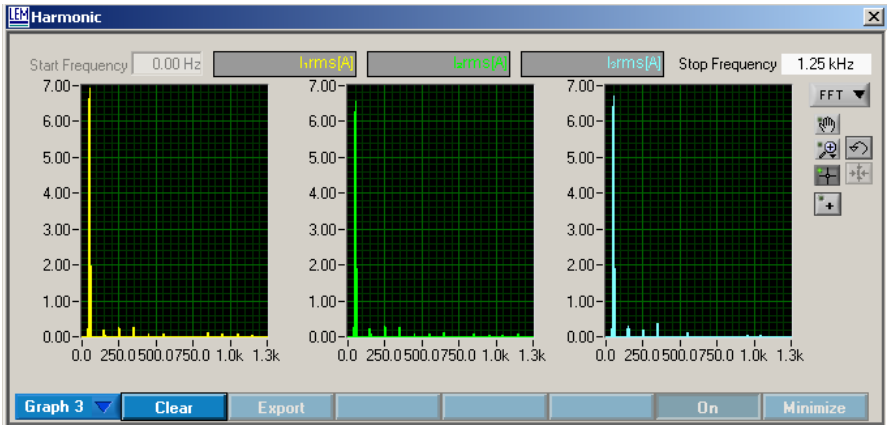

Fig. G.5 Line side 3-phase current harmonic spectrum at 75% load for 5.5kW rated system employing ABF filter.

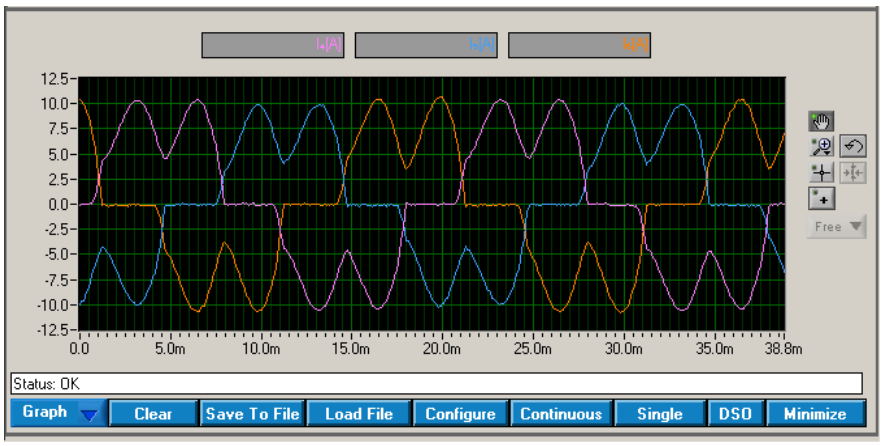

Fig. G.6 Rectifier side 3-phase current experimental waveforms at 75% load for 5.5kW rated system employing ABF filter.

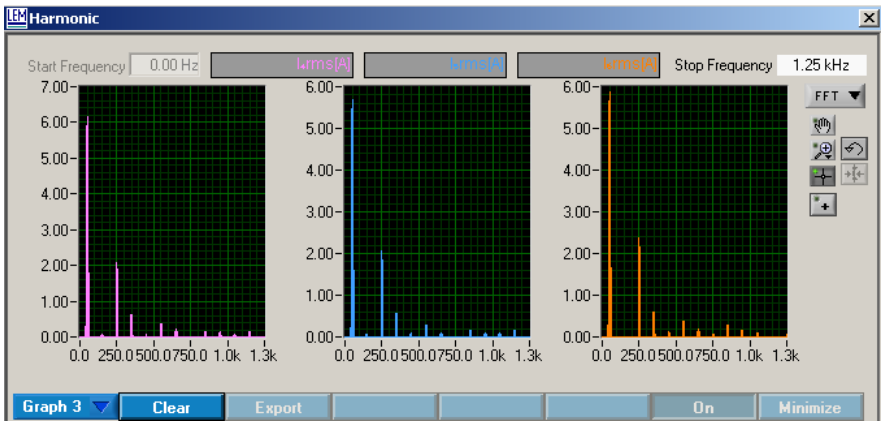

Fig. G.7 Rectifier side 3-phase current harmonic spectrum at 75% load for 5.5kW rated system employing ABF filter.

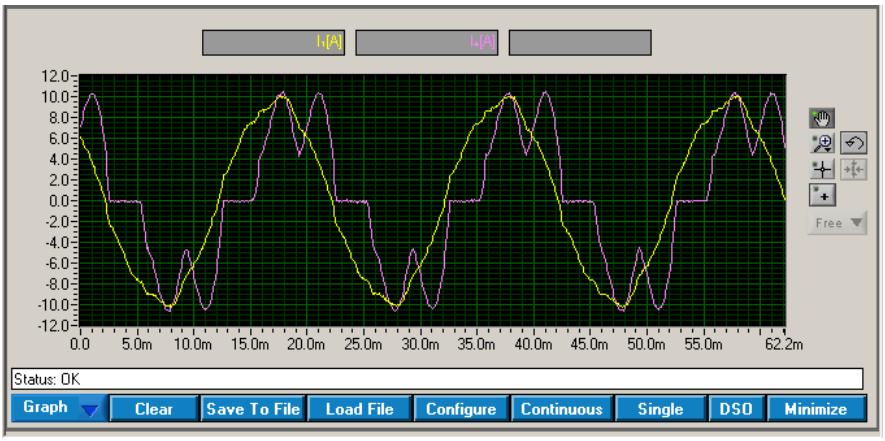

Fig. G.8 Line and rectifier current experimental waveforms at 75% load for 5.5kW rated system employing ABF filter.

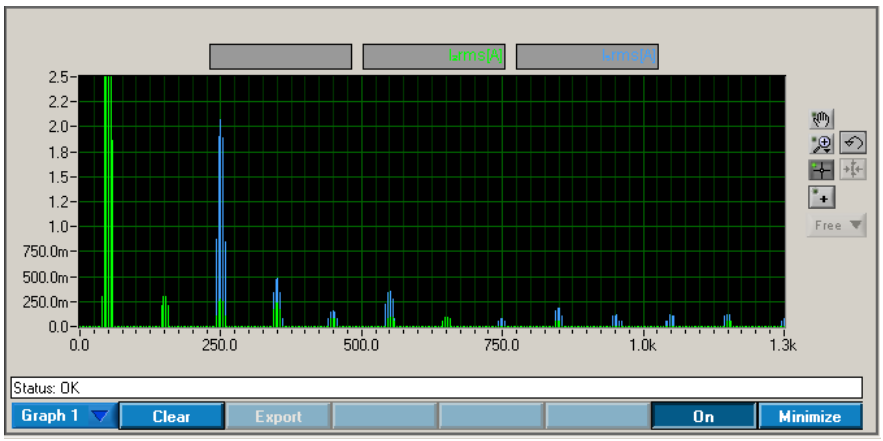

Fig. G.9 Line and rectifier side current harmonic spectrum at 75% load for 5.5kW rated system employing ABF filter (Zoomed).

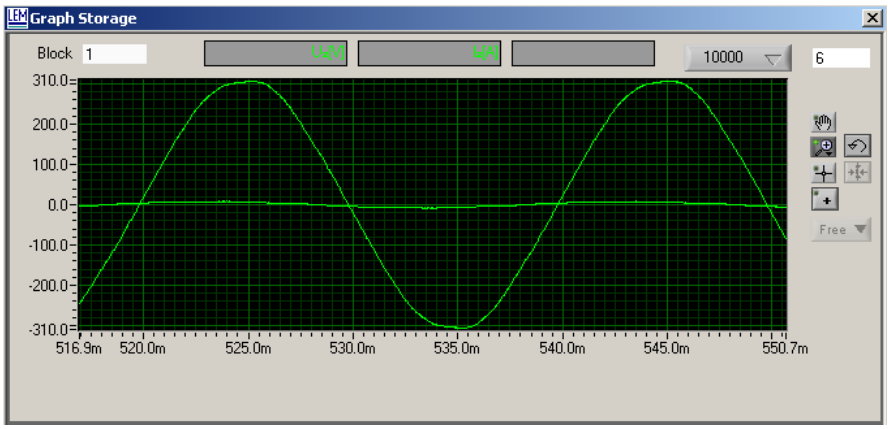

Fig. G.10 Supply phase voltage and current experimental waveforms at 75% load for 5.5kW rated system employing ABF filter.

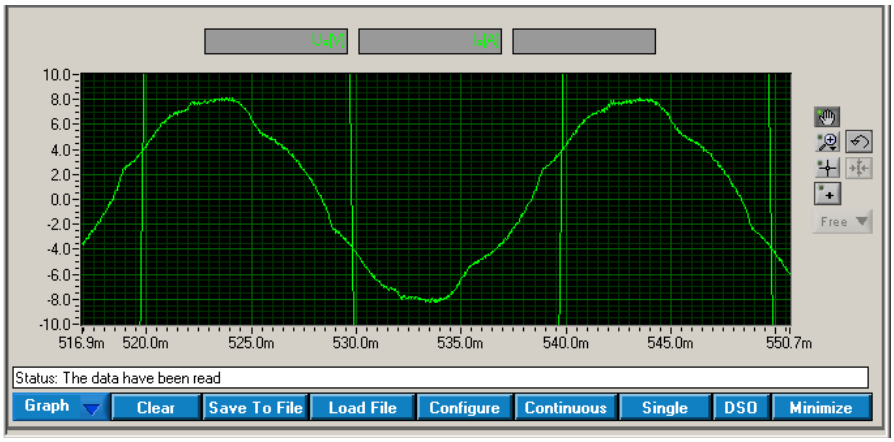

Fig. G.11 Supply phase voltage and current experimental waveforms at 75% load for 5.5kW rated system employing ABF filter (Zoomed).

G.2 ABF 60% Load Experimental Results

Fig. G.12 Line side experimental data for phase 1, 2 and 3 at 60% load for 5.5kW rated system employing ABF filter (voltage V, current I, real power P, current THDi%, reactive power Q, power factor ʎ).

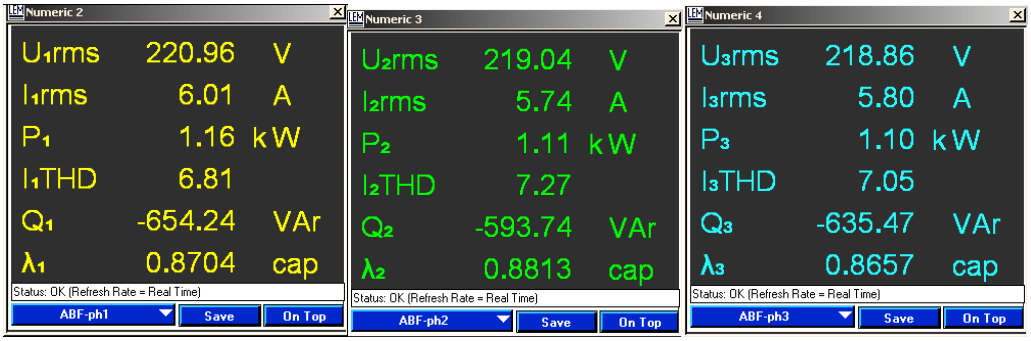

Fig. G.13 Line side experimental data for phase 1, 2 and 3 at 75% load for 5.5kW rated system employing ABF filter (voltage V, current I, real power P, current THDi%, reactive power Q, power factor ʎ).

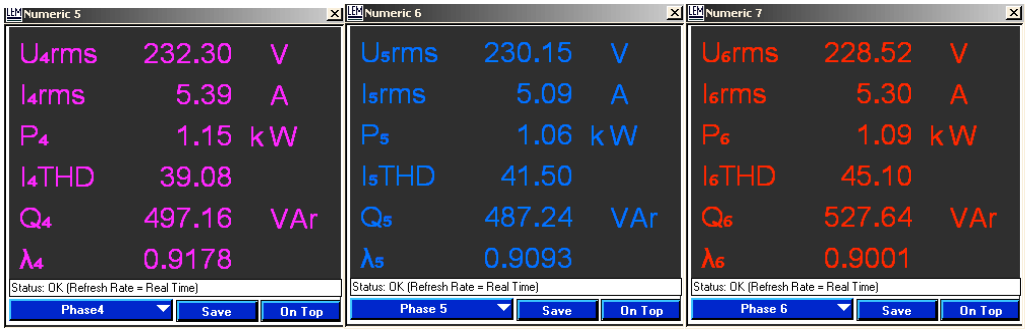

Fig. G.14 Rectifier side experimental data for phase 4, 5 and 6 at 75% load for 5.5kW rated system employing ABF filter (voltage V, current I, real power P, current THDi%, reactive power Q, power factor ʎ).

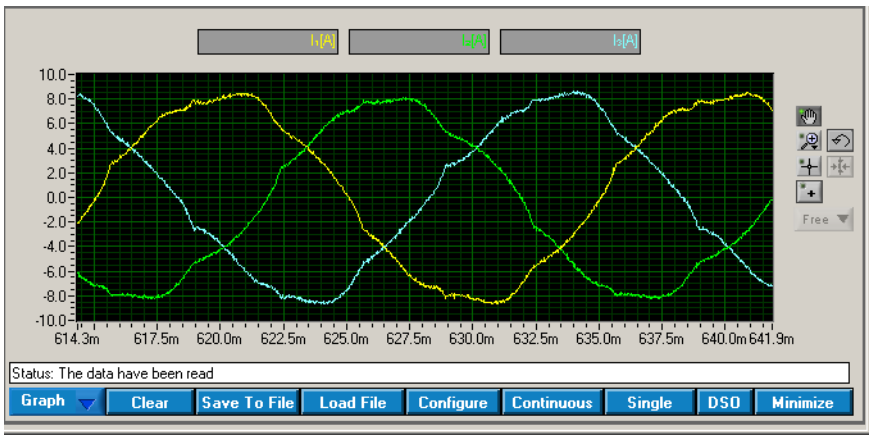

Fig. G.15 Line side 3-phase current experimental waveforms at 60% load for 5.5kW rated system employing ABF filter.

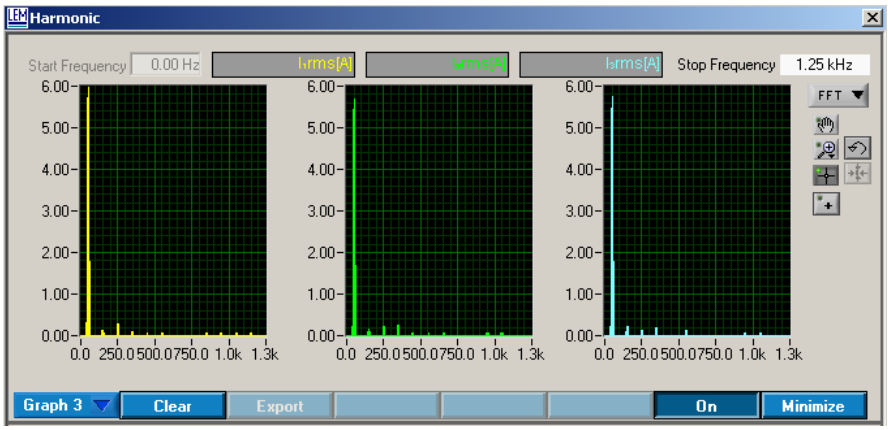

Fig. G.16 Line side 3-phase current harmonic spectrum at 60% load for 5.5kW rated system employing ABF filter.

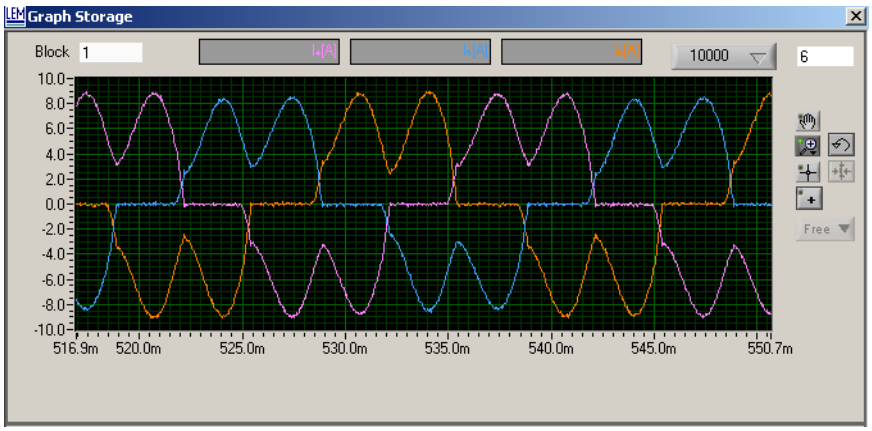

Fig. G.17 Rectifier side 3-phase current experimental waveforms at 60% load for 5.5kW rated system employing ABF filter.

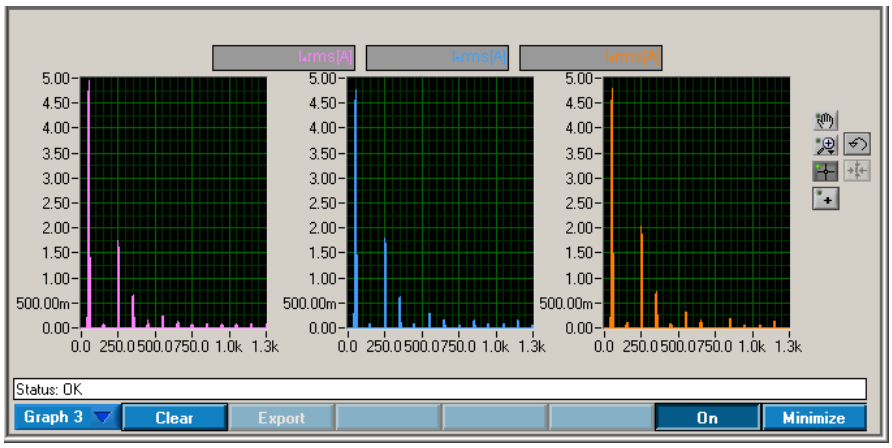

Fig. G.18 Rectifier side 3-phase current harmonic spectrum at 60% load for 5.5kW rated system employing ABF filter.

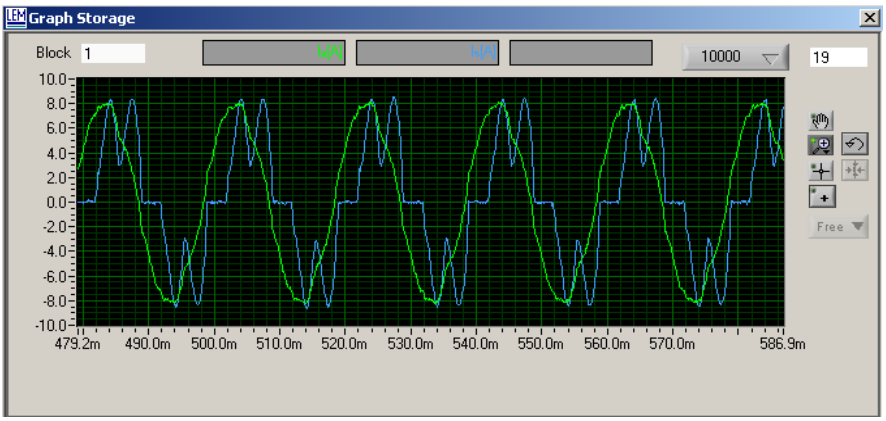

Fig. G.19 Line and rectifier current experimental waveforms at 60% load for 5.5kW rated system employing ABF filter.

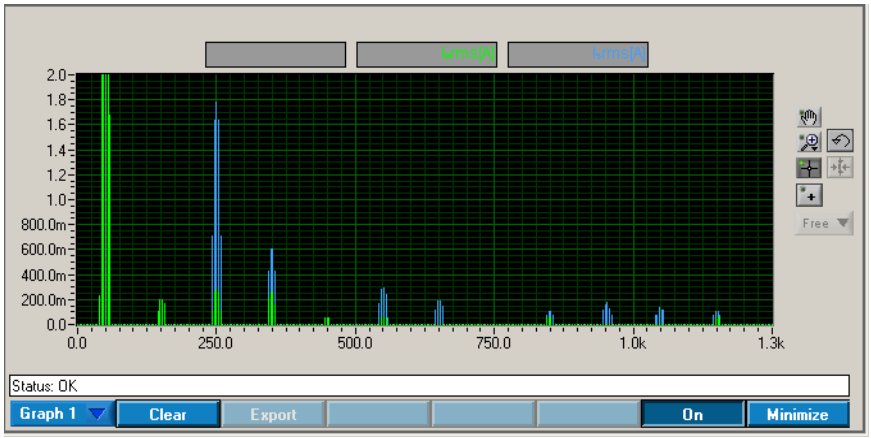

Fig. G.20 Line and rectifier side current harmonic spectrum at 60% load for 5.5kW rated system employing ABF filter (Zoomed).

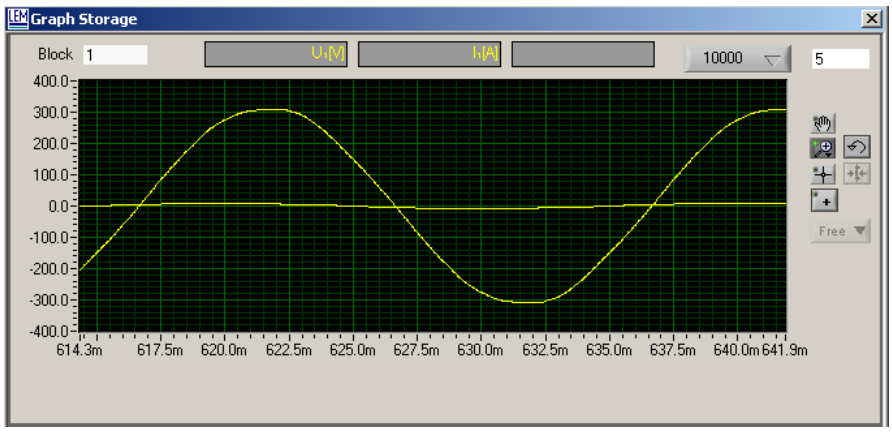

Fig. G.21 Supply phase voltage and current experimental waveforms at 60% load for 5.5kW rated system employing ABF filter.

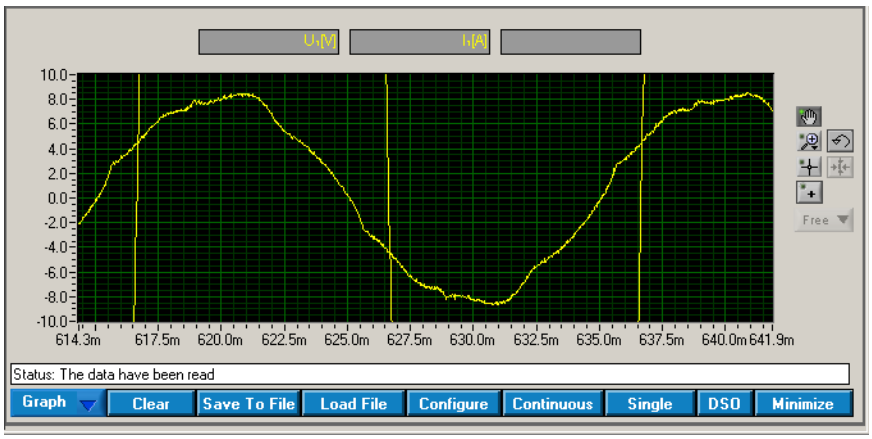

Fig. G.22 Supply phase voltage and current experimental waveforms at 60% load for 5.5kW rated system employing ABF filter (Zoomed).

G.3 ABF 400V Full-Load Experimental Results

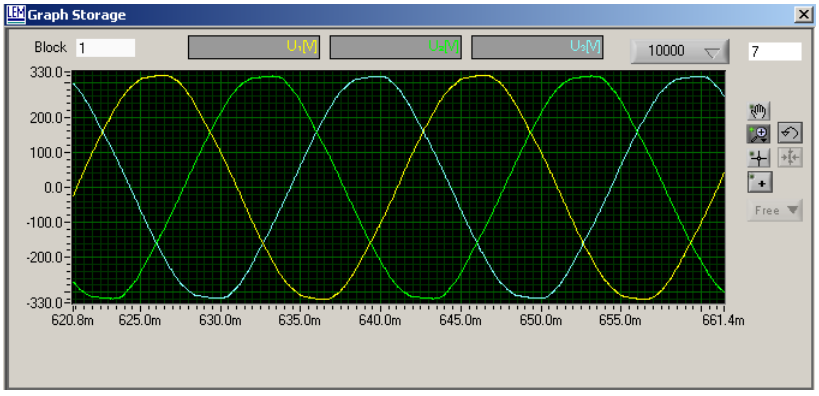

Fig. G.23 Line side 3-phase voltage experimental waveforms at full-load for 5.5kW rated system employing ABF filter (400 V_{LL}).

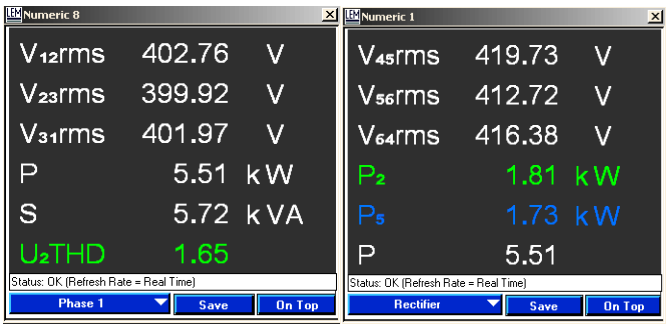

Fig. G.24 Supply and rectifier side experimental data at full-load for 5.5kW rated system employing ABF filter (400V line and rectifier line-to-line voltage, total real and apparent power and supply voltage THD_V%).

Fig. G.25 Line side experimental data for phases 1, 2 and 3 at full-load for 5.5kW rated system employing ABF filter (voltage V, current I, real power P, current THDi%, reactive power Q, power factor ʎ).

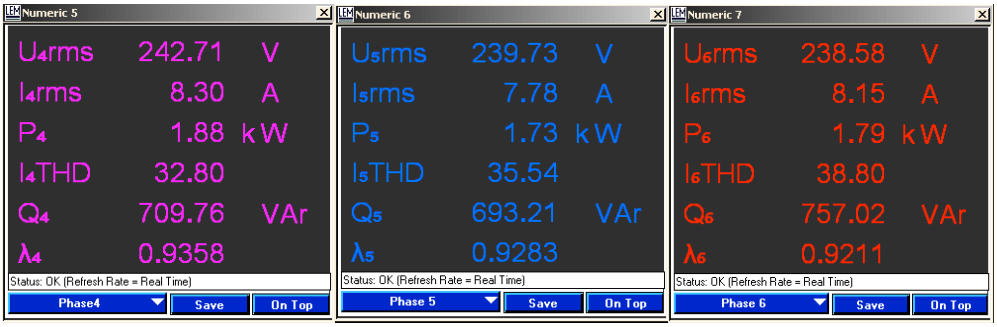

Fig. G.26 Rectifier side experimental data for phases 4, 5 and 6 at full-load for 5.5kW rated system employing ABF filter (voltage V, current I, real power P, current THDi%, reactive power Q, power factor ʎ).

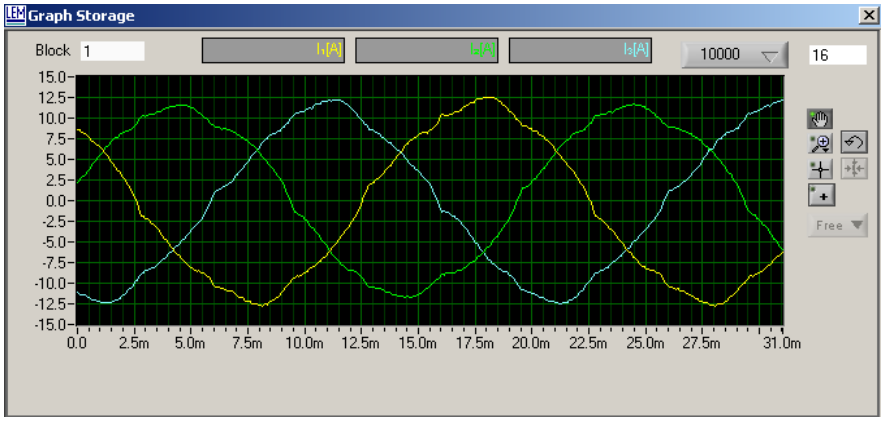

Fig. G.27 Line side 3-phase current experimental waveforms at full-load for 5.5kW rated system employing ABF filter.

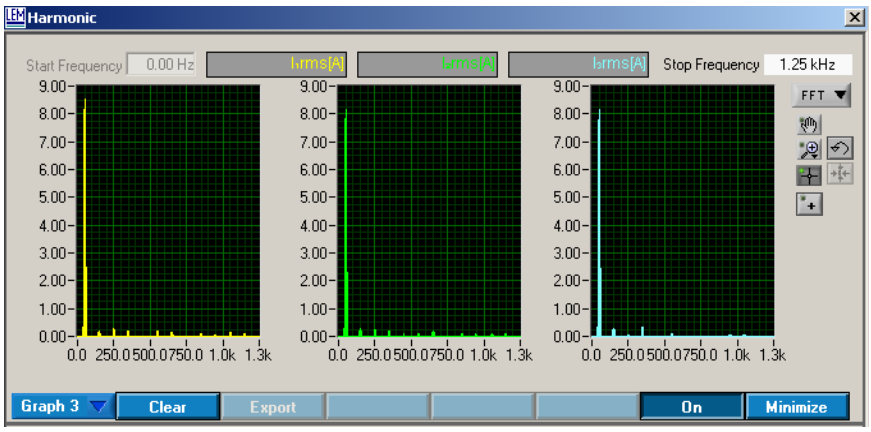

Fig. G.28 Line side 3-phase current harmonic spectrum at full-load for 5.5kW rated system employing ABF filter.

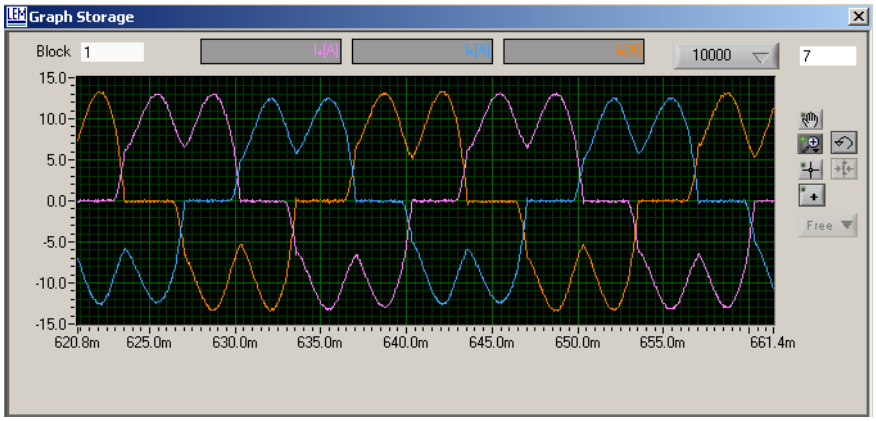

Fig. G.29 Rectifier side 3-phase current experimental waveforms at full-load for 5.5kW rated system employing ABF filter.

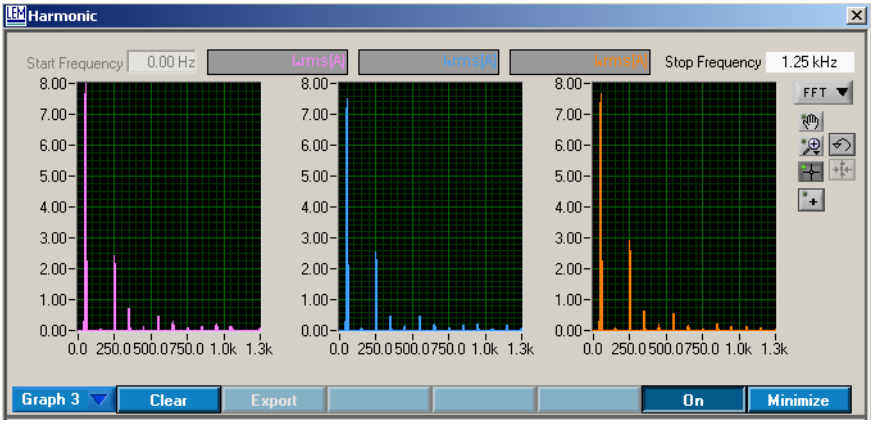

Fig. G.30 Rectifier side 3-phase current harmonic spectrum at full-load for 5.5kW rated system employing ABF filter.

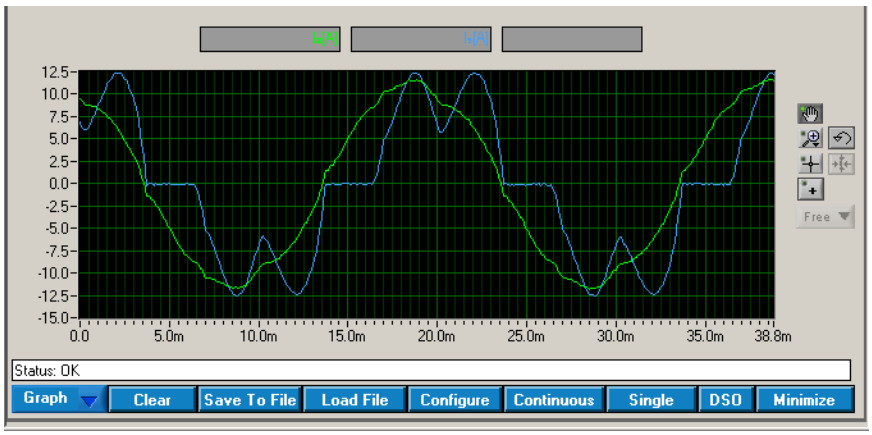

Fig. G.31 Line and rectifier current experimental waveforms at full-load for 5.5kW rated system employing ABF filter.

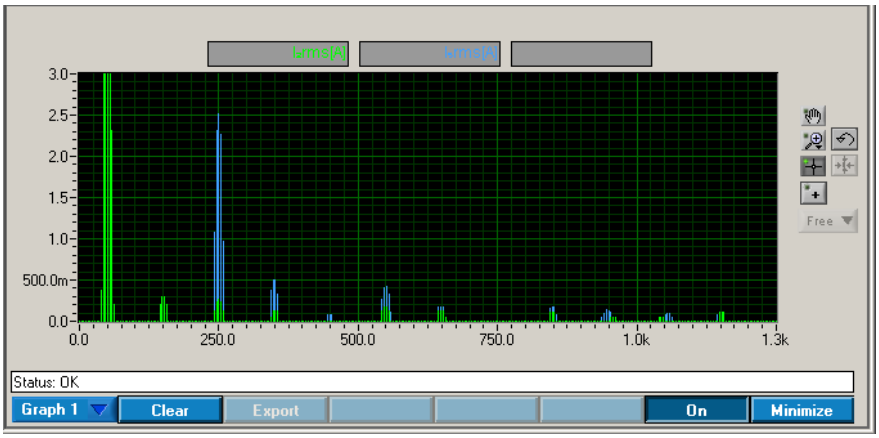

Fig. G.32 Line and rectifier side current harmonic spectrum at full-load for 5.5kW rated system employing ABF filter (Zoomed).

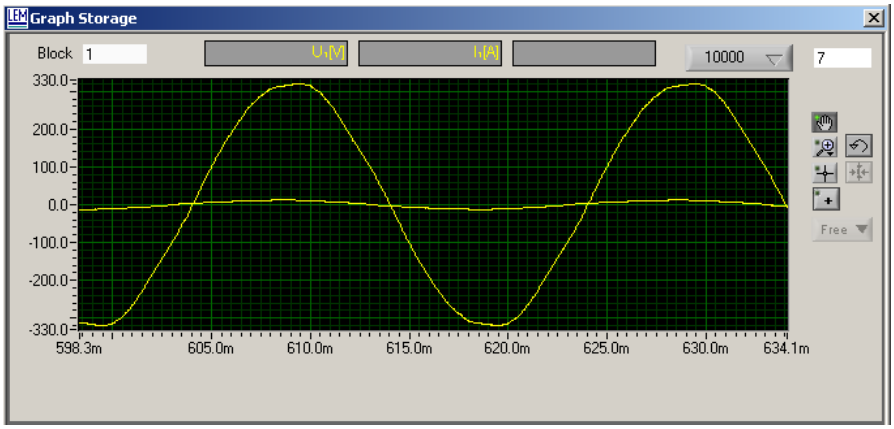

Fig. G.33 Supply phase voltage and current experimental waveforms at full-load for 5.5kW rated system employing ABF filter.

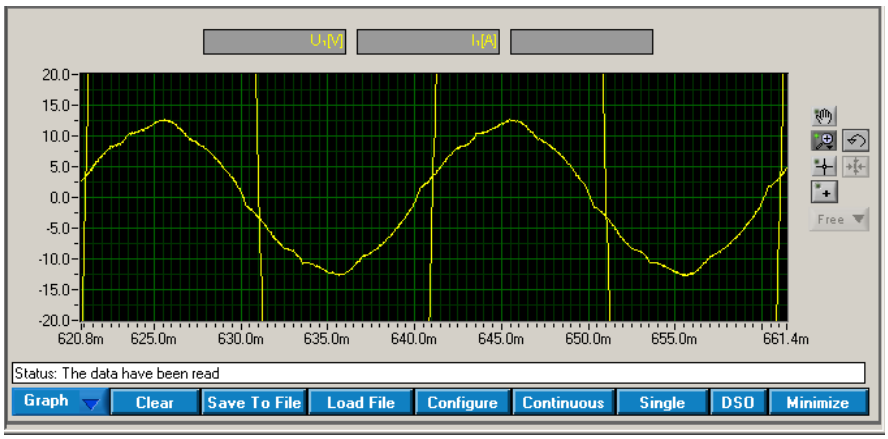

Fig. G.34 Supply phase voltage and current experimental waveforms at full-load for 5.5kW rated system employing ABF filter (Zoomed).

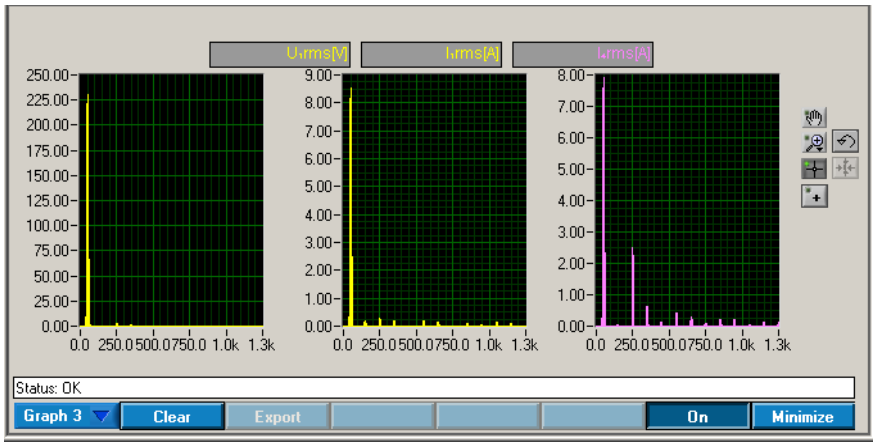

Fig. G.35 Phase voltage, line current and rectifier current harmonic spectrum at full-load for 5.5kW rated system employing ABF filter.

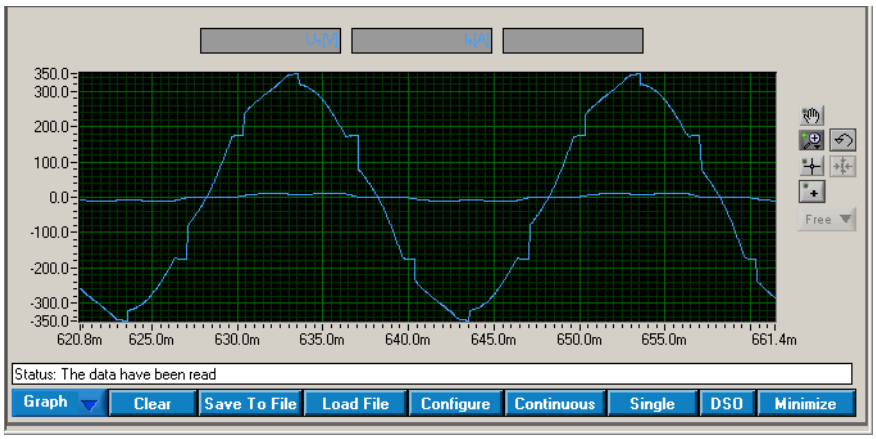

Fig. G.36 Rectifier side phase voltage and current experimental waveforms at full-load for 5.5kW rated system employing ABF filter.

G.4. ABF 400V No-Load Experimental Results

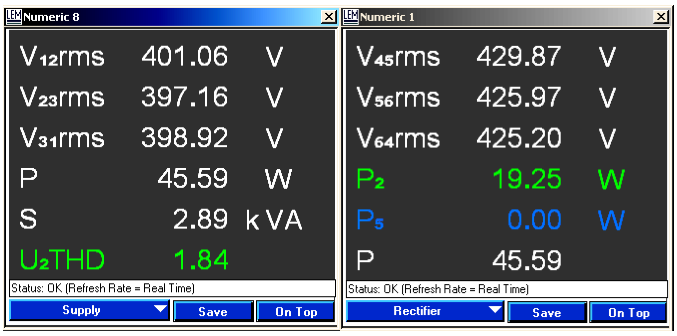

Fig. G.37 Supply and rectifier side experimental data at no-load for 5.5kW rated system employing ABF filter (line and rectifier line-to-line voltage, total real and apparent power and supply voltage THD_V%).

Fig. G.38 Line side experimental data for phases 1, 2 and 3 at no-load for 5.5kW rated system employing ABF filter (voltage V, current I, real power P, current THDi%, reactive power Q, power factor ʎ).

Fig. G.39 Rectifier side experimental data for phases 4, 5 and 6 at no-load for 5.5kW rated system employing ABF filter (voltage V, current I, real power P, apparent power S, reactive power Q, power factor ʎ).

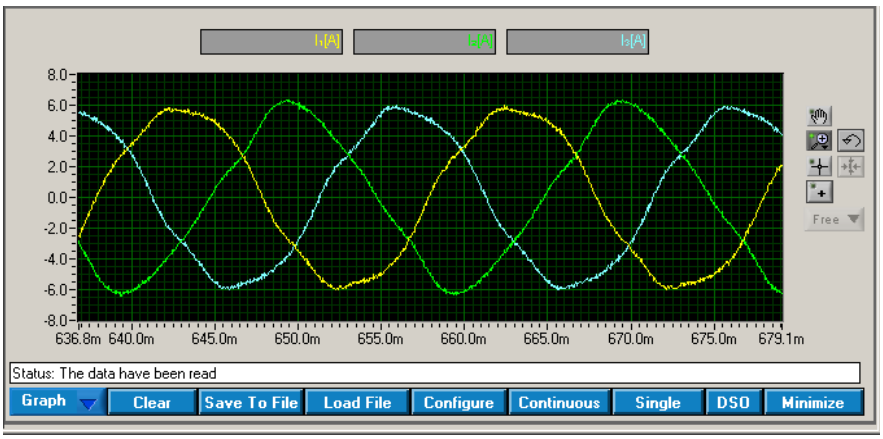

Fig. G.40 Line 3-phase current experimental waveforms at no-load for 5.5kW rated system employing ABF filter.

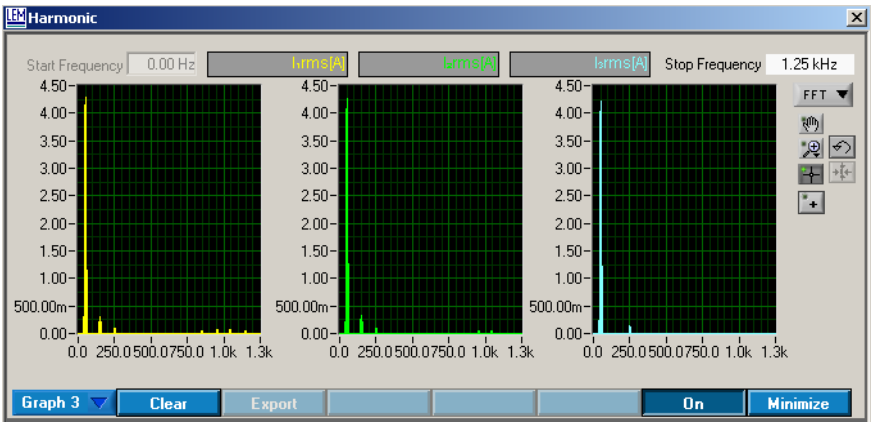

Fig. G.41 Line side 3-phase current harmonic spectrum at no-load for 5.5kW rated system employing ABF filter.

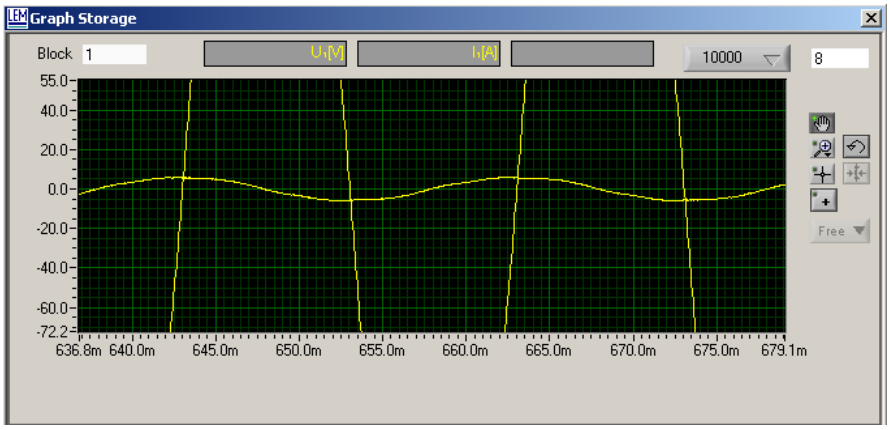

Fig. G.42 Supply phase voltage and current experimental waveforms at no-load for 5.5kW rated system employing ABF filter (Zoomed).

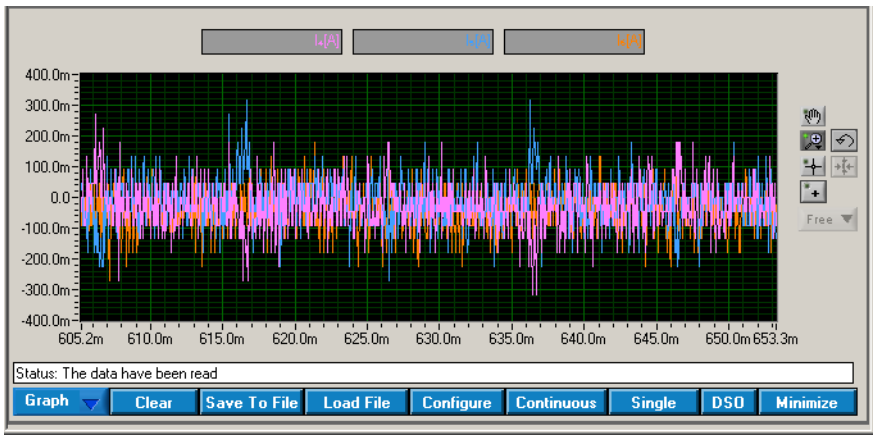

Fig. G.43 Rectifier side 3-phase current experimental waveforms at no-load for 5.5kW rated system employing ABF filter.

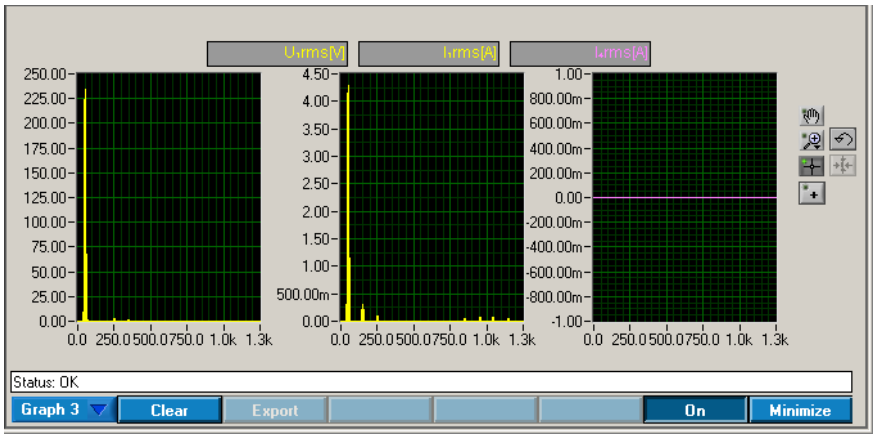

Fig. G.44 Phase voltage, line current and rectifier current harmonic spectrum at no-load for 5.5kW rated system employing ABF filter.

H. IEEE 30-Bus Distribution Network Data

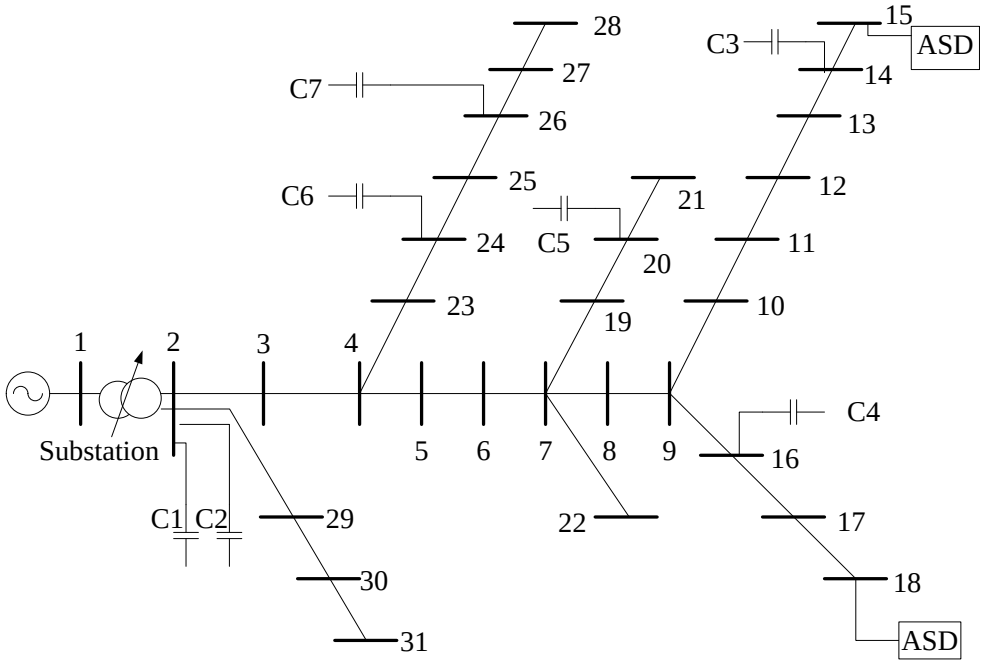

Fig. H.1IEEE 30-bus system utilized for simulation

Table H.1 Bus data for the IEEE 30-bus distribution system
(Base kV = 23 kV, Base MVA = 100 MVA)

Bus number	P (kW)	Q (kVAr)	P (pu)	Q (pu)
1*	0	0	0	0
2	52.52	17.2	0.522	0.172
3	0	0	0	0
4	0	0	0	0
5	93.8	30.8	0.938	0.308
6	0	0	0	0
7	0	0	0	0
8	0	0	0	0
9	0	0	0	0
10	18.9	6.2	0.189	0.062
11	0	0	0	0
12	33.6	11	0.336	0.11
13	65.8	21.6	0.658	0.216
14	78.4	25.8	0.784	0.258
15	73	24	0.73	0.24
16	47.8	15.7	0.478	0.157
17	55	18.1	0.55	0.181

Bus number	P (kW)	Q (kVAr)	P (pu)	Q (pu)
18	47.8	15.7	0.478	0.157
19	43.2	14.2	0.432	0.142
20	67.3	22.1	0.673	0.221
21	49.6	16.3	0.496	0.163
22	20.7	6.8	0.207	0.068
23	52.2	17.2	0.522	0.172
24	192	63.1	1.92	0.631
25	0	0	0	0
26	111.7	36.7	1.117	0.367
27	55	18.1	0.55	0.181
28	79.3	26.1	0.793	0.261
29	88.3	29	0.833	0.29
30	0	0	0	0
31	88.4	29	0.884	0.29

*swing bus

Table H.2 Line data for the IEEE 30-bus distribution system
(Base kV = 23 kV, Base MVA = 100 MVA)

From bus	To bus	R (ohm)	X (ohm)	R (pu)	X (pu)
1	2	0.0021	0.0365	0.0004	0.0069
2	3	0.2788	0.0148	0.0527	0.0028
3	4	0.4438	0.4391	0.0839	0.0830
4	5	0.8639	0.7512	0.1633	0.1420
5	6	0.8639	0.7512	0.1633	0.1420
6	7	1.3738	0.7739	0.2597	0.1463
7	8	1.3738	0.7739	0.2597	0.1463
8	9	1.3738	0.7739	0.2597	0.1463
9	10	1.3738	0.7739	0.2597	0.1463
10	11	1.3738	0.7739	0.2597	0.1463
11	12	1.3738	0.7739	0.2597	0.1463
12	13	1.3738	0.7739	0.2597	0.1463
13	14	1.3738	0.7739	0.2597	0.1463
14	15	1.3738	0.7739	0.2597	0.1463
9	16	0.8639	0.7512	0.1633	0.1420
16	17	1.3738	0.7739	0.2597	0.1463

From bus	To bus	R (ohm)	X (ohm)	R (pu)	X (pu)
17	18	1.3738	0.7739	0.2597	0.1463
7	19	0.8639	0.7512	0.1633	0.1420
19	20	0.8639	0.7512	0.1633	0.1420
20	21	1.3738	0.7739	0.2597	0.1463
7	22	0.8639	0.7512	0.1633	0.1420
4	23	0.4438	0.4391	0.0839	0.0830
23	24	0.4438	0.4391	0.0839	0.0830
24	25	0.8639	0.7512	0.1633	0.1420
25	26	0.8639	0.7512	0.1633	0.1420
26	27	0.8639	0.7512	0.1633	0.1420
27	28	1.3738	0.7739	0.2597	0.1463
2	29	0.2788	0.0148	0.0527	0.0028
29	30	0.2788	0.0148	0.0527	0.0028
30	31	1.3738	0.7739	0.2597	0.1463

Table H.3 Capacitor data for the 30-bus distribution network

Capacitor	C1	C2	C3	C4	C5	C6	C7
Bus location	2	2	14	16	20	24	26
KVar	900	600	600	600	300	900	900

I. Presented and Published Articles from the Current Work

- **Presentations:**

1. A poster (A1 sized) showing the project proposal has been presented in the 2009 Great Western Research Sustainability Exchange Conference, September, 2009, Exeter, UK.

- **Conferences Papers:**

2. A technical paper "Passive Filter Design Using Genetic Algorithms for Adjustable Speed Drives" had published in the proceedings at the 2010 IEEE PES General Meeting, July, 2010, Minnesota, USA.
3. A technical paper "Comparison of Different Common Passive Filters Topologies for Harmonic Mitigation" had been published in the proceedings at the 2010 UPEC Conference, Aug., 2010, Cardiff, Wales, UK.
4. A technical paper "Optimizing Broadband Harmonic Filter Design for Adjustable Speed Drive Systems" had published in the proceedings at the IEEE-EPE 2011 Conference August, 2011, Birmingham, UK.

- **Journal Papers:**

5. A technical paper "Advanced Passive Harmonic Filter Design and Assessment for Adjustable Speed Drives Applications" under submission process in IEEE Industry Applications Transaction.

- **Proposed papers:**

6. A technical paper "Harmonic distortion control on distribution systems with various penetration levels of non-linear loads" for near future follow-up.

REFRENCES

1. Singh, G.K., *Power system harmonics research: a survey.* European Transaction On Electrical Power 2009. 19: p. 151–172.
2. Cavallini, A., *Power electronics and electrical insulation systems - Part 1: Phenomenology overview.* IEEE electrical insulation magazine, 2010. 26(3): p. 7-15.
3. Bose, B.K., *Energy, environment, and advances in power electronics.* IEEE Transactions on Power Electronics, 2000. 15(4): p. 688-701.
4. Savolainen, A., *" Driving towards a better future,"* World Pumps, Elsevier, 2005(463): p. 56-59.
5. Hoevenaars, A.H., *Design considerations when applying various LV ASD topologies to meet harmonic compliance.* Ieee Transactions on Industry Applications, 2011. 47(4): p. 1578-1585.
6. (IEA), *TRACKING INDUSTRIAL ENERGY EFFICIENCY AND CO2 EMISSIONS*, 2007, The International Energy Agency France, p224.
7. Blaabjerg, F. and P. Thoegersen. *Adjustable speed drives - Future challenges and applications*. in *4th International Power Electronics and Motion Control Conference (IPEMC)*. 2004. Xian, PEOPLES R CHINA.
8. ABB, *ABB drives -Technical guide book.* 2011. No. 4: p. 26.
9. Hanigovszki, N., J. Landkildehus, and F. Blaabjerg. *Output filters for AC adjustable speed drives*. in *Applied Power Electronics Conference, APEC - Twenty Second Annual IEEE*. 2007.
10. Hansen, S., *Harmonic Distortion of Rectifier Topologies for Adjusrable Speed Drives*, in *Institute of Energy Technology*2000, Aalborg University: Denmark. p. 242.
11. IEEE, *Recommended Practices and Requirements for Harmonics Control in Electric Power Systems*, IEEE, Editor 1992.
12. Wang, F., et al., *Analysis and Design Optimization of Diode Front-End Rectifier Passive Components for Voltage Source Inverters.* Ieee Transactions on Power Electronics, 2008. 23(5): p. 2278-2289.
13. R. C. Dugan, M.F.M., *Electrical Power Systems Quality*, 2002, McGraw-Hill, p 252.
14. Chang, G.W., et al., *Passive Harmonic Filter Planning in a Power System With Considering Probabilistic Constraints.* Ieee Transactions on Power Delivery, 2009. 24(1): p. 208-218.
15. Das, J.C., *Passive filters - Potentialities and limitations.* Ieee Transactions on Industry Applications, 2004. 40(1): p. 232-241.
16. Ginn, H.L., *An optimization based method for selection of resonant harmonic filter branch parameters.* Ieee Transactions on Power Delivery, 2006. 21(3): p. 1445.
17. Swamy, M.M., et al., *Passive Harmonic Filter System for Variable Frequency Drives, U.S.Patent no: 5,444,609,*, 1995.
18. Swamy, M.M., et al. *Case Studies on Mitigating Harmonics in ASD Systems to Meet IEEE519-1992 Standards*. in *Conf. Rec. IEEE-IAS Annual Meeting*. 1994. Denver, vol.1 , pp. 685 - 692.
19. Hava, A.M. and H. Zubi. *Improved broadband harmonic filter design for adjustable speed drives*. in *IEEE PEDS*. 2005. Kuala Lumpur, Malaysia.

20. Corporation, M. *http://www.mtecorp.com/matrix.html*. 2005; Matrix filter product literature].
21. A.M.Munoz, *Power Quality, Mitigation Technologies in a Distributed Enviroment.* 2007: Springer-Verlag London Limited. pp.152-153.
22. Asiminoaei, L., S. Hansen, and F. Blaabjerg, *Evaluation of an Advanced Harmonic Filter for Adjustable Speed Drives using a Toolbox Approach.* Proc. of NORPIE, 2004. 4.
23. Singh, B., et al., *Multipulse AC-DC Converters for Improving Power Quality: A Review.* Power Electronics, IEEE Transactions on, 2008. 23(1): p. 260-281.
24. Grigsby, L.L., *The Electronic Power Engineering Handbook,* 2000, CRC Press, pp 358-366.
25. Akagi, H., *Modern active filters and traditional passive filters.* Bulletin of the Polish Academy of Sciences: Technical Sciences, 2006. 54(3): p. 255-269.
26. Lee, K., et al., *Input Harmonic Estimation and Control Methods in Active Rectifiers.* Power Delivery, IEEE Transactions on, 2010. 25(2): p. 953-960.
27. Singh, B., K. Al-Haddad, and A. Chandra, *A review of active filters for power quality improvement.* Ieee Transactions on Industrial Electronics, 1999. 46(5): p. 960-971.
28. Akagi, H. *Active and hybrid filters for power conditioning*. in *IEEE Industrial Electronics Conf. Proc*. 2000.
29. Bhattacharya, S. and D. Divan. *Active filter solutions for utility interface of industrial loads*. in *Conf. Proc., Power Electronics, Drives and Energy Systems for Industrial Growth, vol.2, pp 1078-1084,* . 1996.
30. Yin, B., et al. *Performance comparison of voltage mode control and current mode control of a three-phase PWM rectifier based on a dual SISO model*. in *32nd Annual Conference of the IEEE-Industrial-Electronics-Society*. 2006. pp. 2220-2226.
31. Rodriguez, J.R., et al., *PWM regenerative rectifiers: State of the art.* Ieee Transactions on Industrial Electronics, 2005. 52(1): p. 5-22.
32. Hansen, S., et al. *Line Side Harmonic Reduction Techniques of PWM Adjustable Speed Drives-A Cost-Benefit Analysis*. 2001. Intertec International Inc., 39-422.
33. Kampen, D., et al. *Comparative evaluation of passive harmonic mitigating techniques for six pulse rectifiers*. in *Optimization of Electrical and Electronic Equipment, OPTIM. 11th International Conference.* 2008.
34. Masoum, M.A.S., et al., *Hybrid passive filter design for distribution systems with adjustable speed drives.* 2007 International Conference on Power Electronics and Drive Systems, Vols 1-4, 2007: p. 1834-1839.
35. Au, M.T. and J.V. Milanovic, *Planning approaches for the strategic placement of passive harmonic filters in radial distribution networks.* Ieee Transactions on Power Delivery, 2007. 22(1): p. 347-353.
36. Chang, Y.-P., *Integration of SQP and PSO for optimal planning of harmonic filters.* Expert Systems with Applications, 2010. 37(3): p. 2522-2530.
37. Arteche *Harmonic Distortion Wastes Energy*. Technical report, 2011.
38. Gonzalez, D.A. and J.C. McCall, *Design of Filters to Reduce Harmonic Distortion in Industrial Power Systems.* Industry Applications, IEEE Transactions on, 1987. IA-23(3): p. 504-511.

39. Kun-Ping, L., L. Ming-Hoon, and L. Tung-Ping, *An advanced computer code for single-tuned harmonic filter design.* Industry Applications, IEEE Transactions on, 1998. 34(4): p. 640-648.
40. McGranaghan, M.F., *Designing harmonic filters for adjustable-speed drives to comply with IEEE-519 harmonic limits.* Ieee Transactions on Industry Applications, 1999. 35(2): p. 312.
41. Peeran, S.M., *Application, design, and specification of harmonic filters for variable frequency drives.* Ieee Transactions on Industry Applications, 1995. 31(4): p. 841.
42. Chen, Y.M., *Passive filter design using genetic algorithms.* Ieee Transactions on Industrial Electronics, 2003. 50(1): p. 202-207.
43. Berizzi, A. and C. Bovo. *The use of genetic algorithms for the localization and the sizing of passive filters*. in *Harmonics and Quality of Power, Proceedings of Ninth International Conference.* . 2000.
44. Zubi, H., *"Design of Broadband Harmonic Filters for Power Rectifiers," M.Sc. dissertation,*, in *Dept. Elec. Eng.*2005, Univ. Middle East Technical: Ankara. p. 192.
45. Inc., M., *MATLAB* 2008.
46. Verma, V. and B. Singh, *Genetic-algorithm-based design of passive filters for offshore applications.* Ieee Transactions on Industry Applications, 2010. 46(4): p. 1295-1303.
47. Bansal, R.C., *Optimization methods for electric power systems: An overview.* International journal of emerging electric power systems, 2005 March. Vol. 2(Iss.1, Article 1021).
48. Warwick, K., R. Aggarwal, and A. Ekwue, *Artificial Intelligence Techniques in Power Systems*. 1997, IEE, London, UK, p113.
49. Wasserman, P.D., *Neural computing: theory and practice*. 1989: Van Nostrand Reinhold Co., New York.
50. Thompson, D.R. and G.L. Bilbro, *Sample-sort simulated annealing.* Systems, Man, and Cybernetics, Part B: Cybernetics, IEEE Transactions on, 2005. 35(3): p. 625-632.
51. Sivanandam, S.N., *Introduction to genetic algorithms*. 2007: Springer. pp 27-35.
52. Mitchell, M., *An Introduction to Genetic Algorithms*. 1998: Massachusetts Institute of Technology Press.
53. Goldberg, D.E., *Genetic Algorithm in Search, Optimization and Machine Learning*, 1989, Addison-Wesly.
54. Lee, K., G. Venkataramanan, and T.M. Jahns, *Source current harmonic analysis of adjustable speed drives under input voltage unbalance and sag conditions.* Power Delivery, IEEE Transactions on, 2006. 21(2): p. 567-576.
55. Ansoft, *Simplorer*, 2004.
56. Zubi, H.M., R.W. Dunn, and F.V.P. Robinson. *Comparison of different common passive filter topologies for harmonic mitigation*. in *Universities Power Engineering Conference (UPEC), 2010 45th International*. 2010.
57. Drury, B., *Control Techniques Drives and Controls Handbook (2nd Edition)*, 2009, Institution of Engineering and Technology. p. 326-328.
58. V. Gosbell, S.P., V. Smith, , *Voltage Unbalance.* Integral Energy Power Quality & Reliability Centre, , 2002. Oct (Technical Note no.6).
59. LEM, *Three-Phase Power Analyzer User Manual*, in *Norma 5000*2005.

60. Zubi, H.M., et al., *Passive filter design using genetic algorthims for adjustable speed drives*, in *IEEE Power and Energy Society General Meeting 2010*. 2010, IEEE: New York.
61. Zubi, H.M., R.W. Dunn, and F.V.P. Robinson. *Optimizing broadband harmonic filter design for adjustable speed drive systems*. in *Power Electronics and Applications (EPE 2011), Proceedings of the 2011-14th European Conference on*. 2011.
62. Vrankovic, Z., et al. *The influence of the DC link inductor design on the rectifier voltage stress in an adjustable speed drive during a mains voltage surge*. in *Energy Conversion Congress and Exposition, 2009. ECCE 2009. IEEE*. 2009.
63. *IEEE Guide for Application and Specification of Harmonic Filters.* IEEE Std 1531-2003, 2003: p. 0_1-60.
64. IEEE-PES, *IEEE Guide for Application and Specification of Harmonic Filters.* IEEE Std 1531-2003, 2003: p. 0_1-60.
65. Baghzouz, Y. and S. Ertem, *Shunt capacitor sizing for radial distribution feeders with distorted substation voltages.* Power Delivery, IEEE Transactions on, 1990. 5(2): p. 650-657.
66. Civanlar, S. and J.J. Grainger, *Volt/Var Control on Distribution Systems with Lateral Branches Using Shunt Capacitors and Voltage Regulators Part III: The Numerical Results.* Power Apparatus and Systems, IEEE Transactions on, 1985. PAS-104(11): p. 3291-3297.
67. Manual, P.F., *DIgSILENT Power Factory*, 2007: GmbH, Germany.
68. ANSI, *American National Standard for Electric Power Systems & Equipment* in *Voltage Ratings*1989.